DISSERTATION

POLYMERIZATION CATALYSIS FOR THE PRECISION SYNTHESIS OF CHIRAL AND SUSTAINABLE POLYMERS

Submitted by

Garret M. Miyake

Department of Chemistry

In partial fulfillment of the requirements

For the Degree of Doctor of Philosophy

Colorado State University

Fort Collins, Colorado

Spring 2011

Doctoral Committee:

Advisor: Eugene Chen

Travis Bailey
Amy Prieto
Steven Strauss
David Wang

ABSTRACT

POLYMERIZATION CATALYSIS FOR PRECISION SYNTHESIS OF CHIRAL AND SUSTAINABLE POLYMERS

Polymerization catalysis for the precision synthesis of chiral and sustainable polymers is described in this dissertation. The central theme of chiral polymers has revolved around the employment of newly synthesized enantiomeric zirconocenium ester enolate catalysts. These catalysts have been utilized in the asymmetric coordination polymerization of prochiral functionalized vinyl monomers towards optically-active, solution stable, one-handed helical polymers. These enantiomeric catalysts have also been used in the successful kinetic resolution polymerization of a racemic methacrylamide monomer. The stereospecific polymerization of chiral oxazolidinone functionalized alkenes has been performed, producing highly isotactic polymers that assume helical or random-coil secondary conformations, dictated by the proximity of the chiral oxazolidinone to the main-chain of the polymer. Investigating applications of helical polymers, two pseudo-enantiomeric helical poly(phenyl acetylene)s bearing chiral organocatalyst side-groups have been synthesized and the effects of the helix-sense and helicity on the enantioselectivity of these catalysts was subsequently examined.

Towards sustainable polymers, renewable butyrolactone-based vinylidene monomers are of particular interest in exploring the prospects of substituting the petroleum-based methacrylate monomers for specialty chemicals production. The polymerization of such monomers by group

III and IV transition metal catalysts has been investigated resulting in the synthesis of sustainable polymers with controlled molecular weights. These butyrolactone-based monomers have also been successfully polymerized in a rapid and living fashion, using ambiphilic silicon propagating species.

TABLE OF CONTENTS

CHAPTER 1

Introduction

This dissertation is written in a "journals-format" style that is accepted by the Graduate School at Colorado State University and is based on six peer-reviewed publications that have appeared in *Journal of the American Chemical Society*, *Macromolecules*, and *Dalton Transactions*, as well as one manuscript that has been prepared for future submission. The principal theme of this dissertation is to develop and utilize advanced polymerization catalyst systems for the precision synthesis of chiral and sustainable polymers, which is composed of two major sections: the synthesis and application of chiral polymers and the polymerization of naturally renewable monomers to sustainable polymers. The author has studied six topics in chiral polymers as well as the polymerization of biorenewable monomers, which are discussed in detail in the proceeding chapters:

2.) Metallocene-Mediated Asymmetric Coordination Polymerization of Polar Vinyl Monomers to Optically Active, Stereoregular Polymers

3.) Coordination-Addition Polymerization and Kinetic Resolution of Methacrylamides by Chiral Metallocene Catalysts

4.) Stereospecific Polymerization of Chiral Oxazolidinone-Functionalized Alkenes

5.) Helix-Sense Control and Effects on Enantioselectivity of Helical Poly(Cinchona Phenyl Acetylene) Organocatalysts

6.) Coordination Polymerization of Renewable Butyrolactone-Based Vinyl Monomers by Lanthanide and Early Metal Catalysts

7.) Living Polymerization of Naturally Renewable Butyrolactone-Based Vinylidene Monomers by Ambiphilic Silicon Propagators

In Chapter 2, the synthesis and application of enantiomeric zirconocenium catalysts for the synthesis of chiral polymers are described. These optically active, chiral catalysts were utilized for the asymmetric coordination polymerization of bulky *N,N*-diaryl acrylamides to solution stable, static, optically active one-handed helical polymers. An investigation on the necessity of the diaryl side-groups to render solution stable helical polymers was also carried out, which led to the fundamental study on the relationship between polymer MW of helical or non-helical polymers and optical activity. The ability of non-helical block copolymers to be optically active was also discussed.

Chapter 3 reports the first successful coordination polymerization of a methacrylamide monomer, 2-methacryloyl aziridine (MAz), employing chiral zirconocenium catalysts for the isospecific polymerization of MAz. Being a racemic monomer, enantiomeric zirconocenium catalysts were used in the first successful kinetic resolution polymerization of a methacrylamide monomer.

Chapter 4 deals with the stereospecific polymerization of chiral oxazolidinone-functionalized alkenes and the ability of these isotactic polymers to form helical secondary structures. The acryloyl monomers, *N*-acryloyl-(*R* or *S*)-4-phenyl-2-oxazolidinone [(*R* or *S*)-AOZ] were successfully polymerized by chiral zirconocenium catalysts to afford isotactic polymers, however, through a series of experiments it was concluded that PAOZ does not form a helical secondary structure. Vinyl derivatives *N*-vinyl-(*R*)-4-phenyl-2-oxazolidinone (VOZ) and its *para*-hexyloxy-phenyl derivative (*R*)-HVOZ were not polymerizable by such metallocene catalysts, but a novel chiral auxiliary controlled polymerization, intitiated by various acids was developed, resulting in polymers with quantitative isotacticity that adopt solution stable helical conformations.

In Chapter 5, novel helical poly(phenyl acetylene)s bearing cinchona alkaloid organocatalyst side-groups were synthesized. These polymers showed a unique property in that the helix-sense could be controlled through interactions with achiral solvents, and the effect on the enantioselectivity of the organocatalyst side-groups by the helicity and helix-sense was determined.

Both Chapters 6 and 7 explore the polymerization of the biorenewable butyrolactone based monomers, α-methylene-γ-butyrolactone (MBL) and γ-methyl-α-methylene-γ-butyrolactone (MMBL). Specifically, Chapter 6 discusses the polymerization of (M)MBL mediated by early metal catalysts. Most notably, the polymerization of (M)MBL by decamethyl samarocene is rapid, efficient, living, and controlled, producing well-defined homo and copolymers with each other and methyl methacrylate (MMA). The catalytic production of polymer chains was achieved by the addition of external chain-transfer reagents. Chapter 7 utilizes Si^{+} metalloid catalysts for the polymerization of (M)MBL in rapid and living fashion, using an ambiphilic silicon propagating species consisting of both the nucleophilic silyl ketene acetal (SKA) initiating moiety and the electrophilic silylium catalyst.

Chapter 8 contains a brief summary of the work presented within. The majority of the work conducted by the author during the course of graduate studies has been included in this dissertation, but to maintain a level of consistency, work that has been published but not directly pertaining to the central theme of this dissertation have been excluded. For reference, a list of all the work that has resulted in a publication during the course of this dissertation can be found in Appendix I.

Chapter 2

Metallocene-Mediated Asymmetric Coordination Polymerization of Polar Vinyl Monomers to Optically Active, Stereoregular Polymers

Abstract

Asymmetric coordination polymerization of 13 acrylamide and methacrylate monomers of four different classes has been investigated using chiral *ansa*-zirconocenium ester enolate catalyst (*S,S*)-(EBI)Zr^{+}(THF)[OC(O^{i}Pr)=CMe_2][$MeB(C_6F_5)_3$]$^{-}$ [(*S,S*)-**1**), EBI = $C_2H_4(\eta^5\text{-Ind})_2$] and its enantiomer (*R,R*)-**1**. This polymerization system is built upon four advanced features of polymerization including living, stereospecific, coordination and asymmetric core elements, thus efficiently converting prochiral *N,N*-diaryl acrylamides at ambient temperature to optically active, stereoregular polymers with solution-stable, single-handed helical secondary structures. Kinetic studies show that the polymerization of *N,N*-diaryl acrylamides by **1** proceeds via a monometallic, coordination-conjugate addition mechanism. Investigation into polymer chain-length effects on optical activity of the chiral polymers reveals two opposite trends, depending on the polymer secondary structure (i.e., helical vs. random coil conformation). Examination of the polymerization scope shows that the formation of optically active poly(acrylamide)s due to solution-stable helical conformations with an excess of one-handed helicity is dictated by the sterics and rigidity of the monomer repeat units; while diaryl acrylamides can readily achieve such conformations, unsymmetrically substituted diaryl acrylamides give the chiral polymers with much higher optical activity than the symmetrically substituted ones. It is also possible for *N,N*-dialkyl acrylamides to lead to chiral helical polymers. Extensive asymmetric block

copolymerization studies of MMA with acrylamides and other methacrylates have also been carried out, producing optically active, high molecular weight methacrylate-*b*-acrylamide block copolymers in which the acrylamide block can be either helical or nonhelical; in sharp contrast, all high molecular weight methacrylate-*b*-methacrylate di- or triblock copolymers produced by the enantiomeric catalysts **1** are optically inactive.

Introduction

Optically active chiral polymers are not only fundamentally interesting, due to the rich and complex architecture of macromolecular chirality as compared to that of small molecules, but also technologically important because their unique chiral arrays give rise to a number of potential, and in some cases commercially implemented, applications.[1] In the case of stereoregular vinyl polymers[2] with configurational main chain chirality derived from 1-substituted or nonsymmetric 1,2-disubstituted vinyl monomers (i.e., technologically most important polymers) without chiral side groups, such enantiomerically pure or enriched polymers cannot be optically active because the entire polymer chain (by the infinite chain model) contains a mirror plane (for isotactic polymers) or a glide mirror plane and translational mirror planes perpendicular to the chain axis (for syndiotactic polymers), and thus are achiral.[1] Low molecular weight (MW) isotactic oligomers of propylene,[3] 1-butene,[4] and other α-olefins[5] produced by optically active *ansa*-zirconocene catalysts showed measurable optical activity, but high MW isotactic polypropylene (*it*-PP) produced by the similar enantiomeric chiral catalyst did not have a detectable optical activity in solution and in the melt.[6] As a polymer chain becomes long enough its chain-end groups impose negligible effects on the chiroptical properties of the polymer; thus, an enantiomerically pure or enriched polymer of low enough MW and containing nonequivalent chain-end groups can be optically active, as shown by the above oligomeric α-olefin examples. Wulff et al. determined at which degree of polymerization (P_n) the optical activity of enantiomerically pure or enriched isotactic poly(methyl methacrylate), P(MMA), in a random-coil conformation with different chain ends, is still observable ($[\alpha]^{20}_{546}$ = −3.0° to −0.5 for M_n = 3050 to 26050) as a result of elimination of the mirror plane by the chain-end groups;[7] only at a very high P_n (>300) the optical activity becomes negligible, and the polymer then becomes *cryptochiral*. On the other hand, Okuda and coworkers recently employed enantiomerically pure nonmetallocene titanium catalysts for the asymmetric polymerization of styrene and found that P_n at which optically active isotactic oligomeric styrenes (($[\alpha]^{23}_{D}$ = ±5.9 to 1.5°) became cryptochiral

with no measurable optical activity in solution is rather low (<45).[8] In short, it appears that polar functionalized vinyl polymers such as P(MMA) develop the cryptochiral phenomenon at a considerably higher degree of polymerization than that for nonpolar polyolefins.

Three major strategies that do not rely on chain-end groups or chiral auxiliaries to eliminate reflection elements of symmetry of stereoregular vinyl polymers have been developed for the synthesis of *high MW, chiral polymers* derived from prochiral vinyl monomers. First, chiral template-mediated polymerization utilizes styrene derivatives carrying optically active, removable mannitol template groups at the 4-position to radically copolymerize with styrene and subsequently convert the copolymer to an optically active polystyrene ($[\alpha]^{30}_{365} = -0.5$ to $-3.5°$).[9] The optical activity was attributed to the presence of chiral diads (in this case, the diad has a (*S,S*)-configuration) separated by atactic sequences, and other optically active vinyl polymers and copolymers of complex configurational architectures can be prepared in a similar manner.[10] Second, asymmetric cyclopolymerization of 1,5-pendadiene with enantiomerically pure zirconocene[11] or Salan-zirconium[12] catalysts produces optically active poly(methylene-1,3-cyclopentane), the optical activity of which is due to the presence of predominantly *trans*-isotactic structures devoid of mirror plans of symmetry.[11] Third, asymmetric anionic polymerization of functionalized vinyl monomers containing bulky side groups (e.g., triarylmethyl methacrylates[13] and *N,N*-diaryl acrylamides[14]) with chiral organolithium initiators affords optically active polymers with rigid one-handed, solution-stable helical conformations rendered by steric repulsion of the bulky side groups of the highly isotactic polymers accessible through the helix-sense-selective polymerization.[15] This strategy of using such bulky vinyl monomers has also been extended to asymmetric radical polymerization leading to optically active isotactic helical polymers.[16] Many stereoregular vinyl polymers can have a secondary structure of helical conformations in the solid state (e.g., *it*-PP); however, they adopt on-average random-coil conformations in solution due to the fast solution dynamics of the polymer chain with low helix inversion barriers. Thus, *it*-PP produced by an optically active zirconocene catalyst

exhibits a large optical rotation in suspension, but the optical activity is lost when the polymer is completely dissolved or heated.[6] Likewise, the large optical activity of helical poly(trityl methacrylate) almost vanishes with only a very small residual rotation when the bulky trityl groups are replaced with the methyl groups to give random-coil cryptochiral P(MMA).[13] Although the optical activity is lost, the enantiomeric nature of the polymer is maintained; thus, treatment of enantiomeric *it*-P(MMA) with achiral syndiotactic P(MMA) forms a double-stranded helical stereocomplex,[17] a chiral superstructure.[18]

We have recently developed the *living, stereospecific, and coordination* polymerization of functionalized vinyl monomers such as methacrylates utilizing the highly active racemic (*R,R*)/(*S,S*) *ansa*-zirconocenium catalyst, *rac*-(EBI)Zr^{+}(THF)[OC(O^{i}Pr)=CMe_2][$MeB(C_6F_5)_3$]$^{-}$ [*rac*-**1**; EBI = $C_2H_4(\eta^5\text{-Ind})_2$], under ambient conditions.[19] The polymers produced were highly isotactic (> 95% *mm* for P(MMA); >99% *mm* for P(*n*-butyl methacrylate), P(BMA), and had narrow molecular weight distributions (MWD = M_w/M_n = 1.03). The polymerization of methacrylates by *rac*-**1** is enantiomorphic-site controlled, proceeding through a monometallic, intramolecular Michael addition mechanism via eight-membered-ring cyclic ester enolate resting intermediates.[20] The coordination polymerization of acrylamides such as *N,N*-dimethyl acrylamide (DMAA) by this highly active catalyst system also proceeds in a living, isospecific, site-controlled manner, producing high MW poly(*N,N*-dimethyl acrylamide), P(DMAA), with a narrow MWD of M_w/M_n = 1.07, a quantitative isotacticity of *mm* > 99%, and a high melting transition temperature of T_m >307 ºC.[21] Most recently, we have built the fourth, *asymmetric* element into our polymerization system and successfully developed asymmetric coordination polymerization of *N,N*-diaryl acrylamides such as *N,N*-diphenyl acrylamide (DPAA) and *N*-phenyl-*N*-(4-tolyl)acrylamide (PTAA) using enantiomeric catalysts (*S,S*)-**1** and (*R,R*)-**1** to produce the corresponding optically active, one-handed helical poly(*N,N*-diaryl acrylamide)s, P(DPAA) and P(PTAA), as well as their rigid rod-like block copolymers with random-coil MMA blocks (Chart 1).[22]

Chart 1. Synthesis of right- and left-handed rigid helical poly(*N,N*-diaryl acrylamide)s and their rigid rod-random coil block copolymers with MMA.

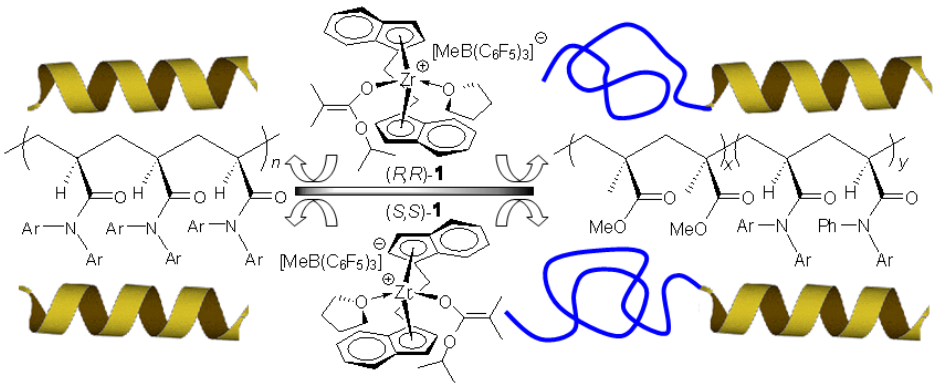

Among the three major strategies developed for the synthesis of chiral vinyl polymers overviewed above, the asymmetric anionic polymerization using chiral organolithium initiators, pioneered by Okamoto and co-workers,[13,14] also deals with functionalized vinyl monomers (which bear bulky side groups). However, such polymerization must be carried out at low temperatures (−78 °C or lower) to achieve an appreciable level of polymerization control as well as the polymer isotacticity and optical activity. Furthermore, in the chiral-initiator-controlled polymerization the enchaining monomer experiences varied degrees of asymmetric induction as a function of the growing chain length, giving rise to a large disparity in stereoregularity and optical activity of the polymer; even in the chiral-ligand-controlled anionic polymerization, such disparity still exists.[14a] In comparison, the recently developed asymmetric coordination polymerization system[22] exhibits the following three advanced features: (a) the living/controlled polymerization can be achieved at ambient temperature; (b) it exhibits a high degree of control in polymerization stereospecificity, which is much less sensitive to polymerization temperature because of its site-control nature; and (c) the reaction proceeds in a manner such that each enchaining monomer must coordinate to the chiral catalyst center before enchainment and is regulated by the same degree of chiral induction of the same asymmetric catalyst center, thereby producing chiral polymers of uniform asymmetric induction.

In our continuing studies of the asymmetric coordination polymerization of polar vinyl monomers such as acrylamides and methacrylates using enantiomeric chiral *ansa*-zirconocenium catalysts (*S,S*)-**1** and (*R,R*)-**1** and following our initial communication,[22] the current contribution focuses on the mechanism and scope (Chart 2) of this polymerization system and presents a full account of our investigation into: (a) characteristics and kinetics of the polymerization of diaryl acrylamides; (b) effects of the chain length of helical and nonhelical poly(acrylamide)s on optical activity; (c) the necessity of the *N,N*-diaryl side groups to render solution-stable helical conformations; (d) strategies to render solution solubility of rigid helical homopolymers by forming block copolymers with randomly coiled MMA blocks and by substitution in the aryl rings with a long-chain alkyl group; and (e) the ability of these enantiomeric catalysts to produce nonhelical, optically active block copolymers.

Chart 2. A list of acrylamide and methacrylate monomers (grouped into four classes) investigated in the current asymmetric coordination polymerization study.

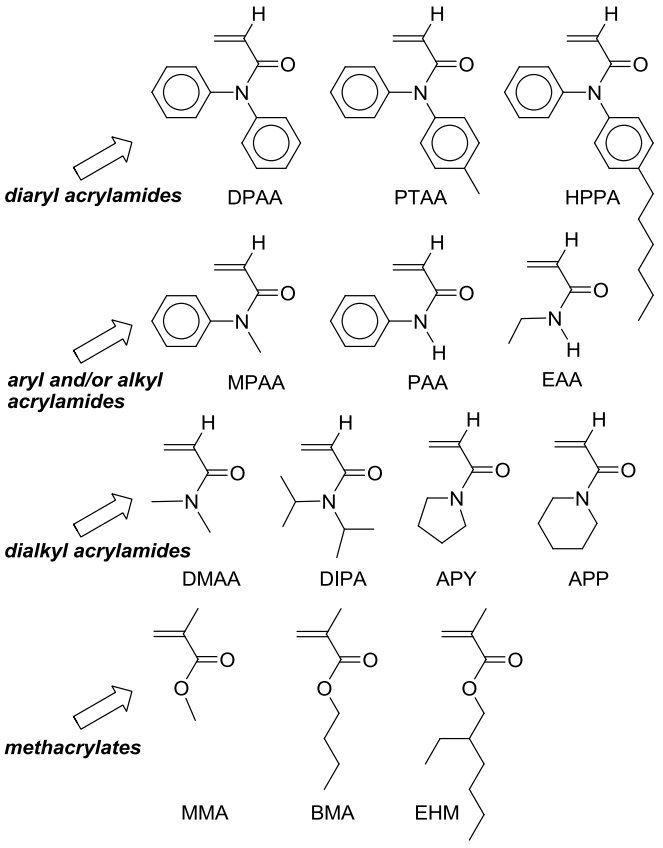

Experimental Section

Solvents and Methods. All syntheses and manipulations of air- and moisture-sensitive materials were carried out in flamed Schlenk-type glassware on a dual-manifold Schlenk line, a high-vacuum line, or in an argon or nitrogen-filled glovebox. HPLC grade organic solvents were sparged extensively with nitrogen during filling of the solvent reservoir and then dried by passage through activated alumina (for THF, Et_2O, and CH_2Cl_2) followed by passage through Q-5-supported copper catalyst (for toluene and hexanes) stainless steel columns. Toluene-d_8 and benzene-d_6 were degassed, dried over sodium/potassium alloy, and filtered before use, whereas $CDCl_3$, CD_2Cl_2, and 1,2-$C_6H_4Cl_2$ were degassed and dried over activated Davison 4 Å molecular sieves. NMR spectra were recorded on either a Varian Inova 300 (FT 300 MHz, ^{1}H; 282 MHz, ^{19}F) or a Varian Inova 400 spectrometer. Chemical shifts for ^{1}H were referenced to internal solvent resonances and are reported as parts per million relative to tetramethylsilane, whereas ^{19}F NMR spectra were referenced to external $CFCl_3$.

Commercial Reagents. Diethylene glycol dimethyl ether, *n*-BuLi (1.6 M in hexanes), butylated hydroxytoluene (BHT-H, 2,6-Di-*tert*-butyl-4-methylphenol), *p*-toluidine, indene, 1,2-dibromoethane, tetrachlorozirconium, triflic acid, lithium dimethylamide, diisopropylamine, piperidine, triethylamine, aniline, sodium azide, 1,1,3,3-tetramethyl guanidine, (2*S*,4*S*)-pentanediol (99% *ee*, $[\alpha]^{20}_D$ +39.8, *c* = 10, $CHCl_3$), (2*R*,4*R*)-pentanediol (97% *ee*, $[\alpha]^{21}_D$ –40.4, *c* = 10, $CHCl_3$), $(CF_3SO_2)_2O$, $PhBCl_2$, MeMgI (3.0 M in diethyl ether), 1,2-dibromobenzene, and CF_3COOH were purchased from Sigma-Aldrich. Diphenylamine, acryloyl chloride, copper (I) iodide, iodobenzene, *N,N*-dimethyl aniline, pyrrolidine, and 2,6-dimethyl pyridine were purchased from Alfa Aesar. Trimethylaluminum (neat) and tri(*n*-octyl)aluminum (neat) were purchased from Strem Chemical Co. whereas isopropyl isobutyrate and *N*-methyl aniline were purchased from TCI America. The above commercial reagents were used as received, except for the reagents described below. Diethylene glycol dimethyl ether, indene, 1,2-dibromoethane, *N,N*-dimethyl aniline, acryloyl chloride, and iodobenzene were degassed using three freeze-pump-

thaw cycles. *p*-Toluidine, $(CF_3SO_2)_2O$, and $PhBCl_2$ were vacuum-distilled. 2,6-Dimethyl pyridine, isopropyl isobutyrate, aniline, diisopropylamine, piperidine, triethylamine, and pyrrolidine were degassed and dried over CaH_2 overnight, followed by vacuum distillation. BHT-H was recrystallized from hexanes prior to use. 1,4-Dioxane (Fisher Scientific) was degassed, dried over sodium/potassium alloy, and vacuum-distilled. Tris(pentafluorophenyl)borane $B(C_6F_5)_3$ was obtained as a research gift from Boulder Scientific Co. and further purified by recrystallization from hexanes at −30 ºC.

Monomers (a total of 13). Methyl methacrylate (MMA) and *n*-butyl methacrylate (BMA) were purchased from Sigma-Aldrich, while 2-ethylhexyl methacrylate (EHM) and *N,N*-dimethyl acrylamide (DMAA) were purchased from TCI America; the above four monomers were first degassed, dried over CaH_2 overnight, and then vacuum transferred. Further purification of MMA involved titration with neat tri(*n*-octyl)aluminum to a yellow end point,[23] followed by distillation under reduced pressure. Literature procedures were used to prepare monomers *N,N*-diphenyl acrylamide (DPAA),[24] *N*-phenyl-*N*-(4-tolyl) acrylamide (PTAA),[14a] and *N*-(4-hexylphenyl)-*N*-phenyl acrylamide (HPPA).[14a] DPAA and PTAA were purified by three recrystalizations from a toluene/hexanes solvent mixture, whereas HPPA was purified by silica gel chromatography (eluent: hexane/diethyl ether = 3/1) and dried over CaH_2 overnight, followed by vacuum distillation. Other acrylamide monomers were prepared and purified in a similar manner. Specifically, *N,N*-diisopropyl acrylamide (DIPA), *N*-methyl-*N*-phenyl acrylamide (MPAA), *N*-phenyl acrylamide (PAA), acryloyl pyrrolidine (APY), and acryloyl piperidine (APP) were prepared by reacting two equiv of the appropriate amine with one equiv of acryloyl chloride in toluene at 0 °C and warming gradually the reaction mixtures to room temperature overnight with vigorous stirring. *N*-ethyl acrylamide (EAA) was prepared by purging a solution of acryloyl chloride in toluene with ethylamine at 0 °C and then warming the reaction mixture to room temperature overnight with vigorous stirring. MPAA was purified by three recrystallizations from a toluene/hexanes solvent mixture, while DIPA, APY, APP, and EAA were purified by

distillation and drying over CaH_2 overnight followed by additional vacuum distillation. PAA was purified by recrystallizations first from acetone and then from CH_2Cl_2. All purified monomers were stored in brown bottles kept inside a –30 °C glovebox freezer.

Noncommercial Reagents or Intermediates. The $(C_6F_5)_3B{\cdot}THF$ adduct was prepared by addition of THF to a toluene solution of the borane followed by removal of the volatiles and drying in vacuo. Literature procedures were employed for the preparation of the following compounds and metallocene complexes: $LiOC(O^iPr)=CMe_2$ [Li(IPIB)],[25] $(EBI)H_2$ [EBI = $C_2H_4(\eta^5\text{-Ind})_2$],[26] *rac*-(EBI)Zr$(NMe_2)_2$,[27] *rac*-(EBI)Zr$Me_2$,[27] *rac*-(EBI)ZrMe(OTf),[19] *rac*-(EBI)ZrMe[$OC(O^iPr)=CMe_2$],[19] *rac*-(EBI)Zr^+(THF)[$OC(O^iPr)=CMe_2$][$MeB(C_6F_5)_3$]$^-$(**1**),[19] (*S,S*)-(EBI)$ZrCl_2$,[28] and (*R,R*)-(EBI)$ZrCl_2$.[28]

Synthesis of Enantiomeric Catalysts 1. Scheme 1 outlines the entire 11-step synthesis of (*S,S*)-**1** starting from enantiopure 2,4-pentanediol to *S,S*-(EBI)$ZrCl_2$,[28] followed by subsequent conversions to (*S,S*)-(EBI)$ZrMe_2$ using Me_2Mg, to (*S,S*)-(EBI)ZrMe(OTf) using TMSOTf, to neutral methyl ester enolate precatalyst (*S,S*)-(EBI)ZrMe[$OC(O^iPr)=CMe_2$] {(*S,S*)-pre-**1**, $[\alpha]^{23}_D$ = +290°, *c* = 0.49 g/dL, CH_2Cl_2} using Li(IPIB), and finally to cationic ester enolate catalyst (*S,S*)-(EBI)Zr^+(THF)[$OC(O^iPr)=CMe_2$][$MeB(C_6F_5)_3$]$^-$ {(*S,S*)-**1**, $[\alpha]^{23}_D$ = −69.7°, *c* = 0.98 g/dL, CH_2Cl_2} using $(C_6F_5)_3B{\cdot}THF$. The procedures for the last four steps were identical to those already published for the racemic diastereomers, including the methylation step[29] and the final three steps.[19,30] The synthesis of the (*R,R*)-enantiomer follows the identical procedures for the (*S,S*)-enantiomer, leading to neutral methyl ester enolate precatalyst (*R,R*)-(EBI)ZrMe[$OC(O^iPr)=CMe_2$] (*R,R*-pre-**1**, $[\alpha]^{23}_D$ = –285°, *c* = 0.49 g/dL, CH_2Cl_2) and lastly cationic ester enolate catalyst (*R,R*)-(EBI)Zr^+(THF) [$OC(O^iPr)=CMe_2$][$MeB(C_6F_5)_3$]$^-$ {(*R,R*)-**1**, $[\alpha]^{23}_D$ = +69.8°, *c* = 0.98 g/dL, CH_2Cl_2 after methide abstraction by $(C_6F_5)_3B{\cdot}THF$. The spectroscopic data for enantiomeric **1** are identical to those already reported for *rac*-**1**.[19] It is worth noting that in the step of the preparation of dimethyl zirconocenes (*S,S*)-(EBI)$ZrMe_2$ and

(*R,R*)-(EBI)$ZrMe_2$, the ether-solvated magnesium salt co-products were inseparable from the desired dimethyl complexes by repeated recrystallization from various solvents or filtration over Celite; however, treatment of the crude product mixture under high vacuum (10^4 – 10^6 torr) at 80 °C for 6 h, followed by dissolution of the residue in toluene, filtration, and drying of the filtrate in vacuo afforded the clean dimethyl complexes.

Scheme 1. Outlined overall synthesis of enantiomeric catalysts (*S,S*)-**1** and (*R,R*)-**1**.

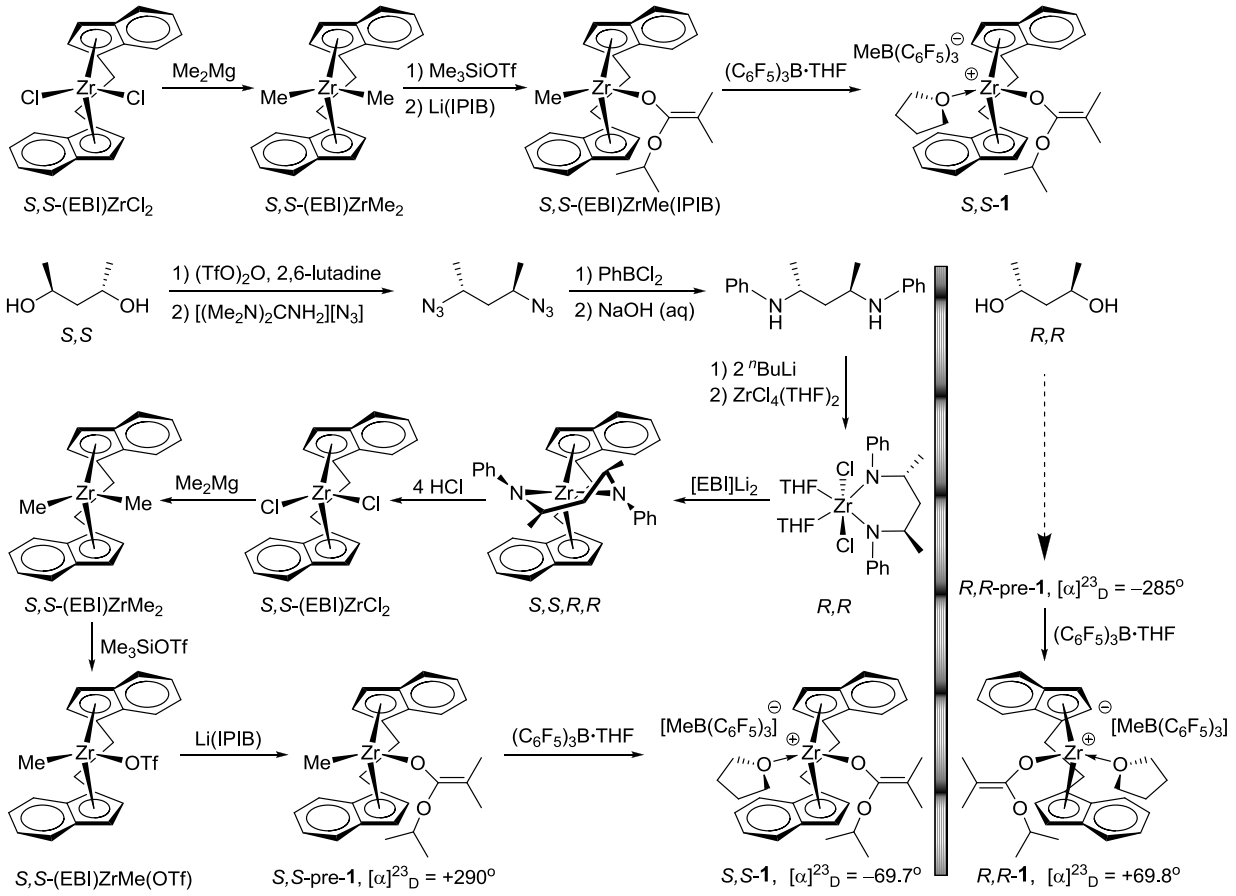

General Polymerization Procedures. Polymerizations were performed in 30-mL glass reactors inside the glovebox for the reactions carried out at ambient temperature (~23 °C). In a typical procedure for homopolymerization, predetermined amounts of $B(C_6F_5)_3$·THF and the appropriate pre-catalyst in a 1:1 molar ratio were premixed in 5 mL of CH_2Cl_2 and stirred for 10

min to cleanly generate the corresponding cationic catalyst.[20] A monomer was quickly added either as a solid or by pipette to the vigorously stirring solution, and the reaction was allowed to proceed for 3 h with continuous stirring. Polymerizations of DIPA and APY, which did not occur at ambient temperature, were carried out at 80 °C and performed in 25-mL Schlenk flasks equipped with stir bar and septum cap. Predetermined amounts of $B(C_6F_5)_3 \cdot THF$ and the appropriate pre-catalyst were dissolved in 5 mL 1,2-dichlorobenzene and stirred for 10 min at ambient before addition of monomer. Thereafter, the charged Schlenk flask was taken out of the glovebox and immersed in an oil bath that was pre-equilibrated at 80 °C, and the reaction proceed for 1 h with vigorous stirring. After the measured time interval, a 0.2 mL aliquot was taken from the reaction mixture via syringe and quickly quenched into a 4 mL vial containing 0.6 mL of undried "wet" $CDCl_3$ stabilized by 250 ppm of BHT-H; the quenched aliquots were later analyzed by ^1H NMR to obtain monomer conversion data. The polymerization was immediately quenched after the removal of the aliquot by addition of 5 mL 5% HCl-acidified methanol. The quenched mixture was precipitated into 100 mL of methanol, stirred for 1 h, filtered or centrifuged, washed with methanol, and dried in a vacuum oven at 50 °C overnight to a constant weight. P(DMAA) and P(APY) were precipitated into 100 mL diethyl ether and stirred for 1 h. The product was obtained as a sticky solid and dried in a vacuum oven at 50 °C overnight to a constant weight; the polymer was redissolved in minimum methylene chloride, precipitated into a 10-fold excess of diethyl ether, stirred for 1 h, filtered, washed with diethyl ether, and dried in a vacuum oven at 50 °C overnight to a constant weight.

The amounts of the monomers employed for the polymerizations are listed as follows: DPAA, 4.48 mmol; PTAA, 0.85 mmol; HPAA, 0.39 mmol; MPAA, 3.10 mmol; DIPA, 3.22 mmol; APY, 4.25 mmol; APP, 3.7 mmol; PAA, 1.36 mmol; EAA, 2.0 mmol; DMMA, 9.34 mmol; MMA, 9.34 mmol; BMA, 9.34 mmol; and EHM, 9.34 mmol. The amount of the precatalyst, in combination with 1 equiv of the activator $B(C_6F_5)_3 \cdot THF$, was adjusted according to

the [monomer]/[catalyst] ratio specified in the polymerization tables. For block copolymerizations of MMA with a second monomer, after in situ generation of the catalyst in the identical fashion as described above, 400 equiv of MMA was quickly added via pipette and vigorously stirred for 10 min (for a quantitative MMA conversion) before the addition of the second monomer. The polymerization of the second monomer proceeded for 3 h with continuous stirring.

Kinetics of DPAA Polymerization. Kinetic experiments for the polymerization of DPAA were carried out in 30 mL reactors inside of the glove box at ambient temperature (~23 °C) using the similar procedure as already described above, except that, at appropriate time intervals, 0.2 mL aliquots were withdrawn from the reaction mixture using a syringe and quickly quenched into 1 mL septum cap sealed vials containing 0.6 mL of undried "wet" $CDCl_3$ mixed with 250 ppm of BHT-H. The quenched aliquots were analyzed by ^{1}H NMR to determine monomer conversions. Specifically, predetermined amounts of $B(C_6F_5)_3 \cdot THF$ and *rac*-**1** in a 1:1 molar ratio were premixed in 5 mL of CH_2Cl_2 and stirred for 10 min before 2.24 mmol DPAA was added as a solid. Owing to the insolubility of P(DPAA), 0.746 mmol toluene was added to the reaction solution to act as an internal standard and the percent of the unreacted DPAA at a given time t, was determined by integration of the peaks for DPAA (6.5 ppm for one of the vinyl protons) and toluene (2.09 ppm for the methyl protons) according to the percent of unreacted DPAA = $(\mathbf{A}_{6.5}/\mathbf{A}_{2.09}) \times 100$, where $\mathbf{A}_{6.5}$ is the total integrals for the peaks centered at 6.5 ppm and $\mathbf{A}_{2.09}$ is the total integral for the peak centered at 2.09 ppm. Apparent rate constants (k_{app}) were extracted by linearly fitting a line to the plot of $\ln([DPAA]_0/[DPAA]_t)$ vs time t. The polymerization became heterogeneous at high monomer conversions (the conversion at which the heterogeneity becomes apparent depends on the initial [DPAA]/[Zr] ratio employed), which eliminated the ability to perform the NMR analysis of the aliquots taken at higher monomer conversions.

Polymer Characterizations. Gel permeation chromatography (GPC) and light scattering (LS) analyses of the polymers were carried out at 40 ºC and a flow rate of 1.0 mL/min, with $CHCl_3$ as the eluent, on a Waters University 1500 GPC instrument coupled with a Waters RI detector and a Wyatt miniDAWN Treos LS detector. The GPC instrument is equipped with one PLgel 5 μm guard and three PLgel 5 μm mixed-C columns (Polymer Laboratories; linear range of molecular weight = 200–2,000,000), and calibrated with 10 P(MMA) standards. Chromatograms were processed with Waters Empower software (version 2002); number-average molecular weight (M_n) and polydispersity (M_w/M_n) of polymers were given relative to P(MMA) standards. Weight-average molecular weight (M_w) was obtained from the analysis of the LS data which was processed with Wyatt Astra Software (version 5.3.2.15), and *dn/dc* values were determined assuming 100 % mass recovery of polymers with known concentrations. The insoluble P(DPAA) samples produced by *rac*-**1** were converted to the $CHCl_3$-soluble poly(methyl acrylate) derivative for their GPC analysis, using literature procedures.[14a]

Maximum rate decomposition temperatures (T_{max}) and decomposition onset temperatures (T_{onset}) of the polymers were measured by thermal gravimetric analysis (TGA) on a TGA 2950 Thermogravimetric Analyszer, TA Instrument. Polymer samples were heated from ambient temperatures to 600 °C at a rate of 20 °C/min. Values for T_{max} were obtained from derivative (wt%/°C) *vs*. temperature (°C) while T_{onset} values (initial and end temperatures) were obtained from wt% *vs*. temperature (°C) plots.

Optical rotations were measured on an Autopol III Automatic Polarimeter at 23°C. The measurements were conducted on 0.2 g/dL polymer solutions, 0.49 g/dL enantiomeric precatalyst solutions, and 0.98 g/dL enantiomeric cationic catalyst solutions. Polymer samples were dissolved in $CHCl_3$ except homopolymer P(DPAA), P(PTAA), P(MPAA), and P(APP) samples which were dissolved in $CHCl_3$ with addition of a small amount of CF_3COOH,[14a] and the enantiomeric catalysts in CH_2Cl_2. Circular dichroism (CD) spectra were obtained from an Aviv model 202 CD spectrometer. CD analysis was conducted on polymer solutions with

concentrations of 0.2g/dL. Block copolymers were dissolved in THF, while homopolymers were dissolved in $CHCl_3$, except P(DPAA), P(PTAA), P(MPAA), and P(APP) samples which were dissolved in $CHCl_3$ with addition of a small amount of CF_3COOH.

Results and Discussion

Kinetics of DPAA Polymerization. Our previous mechanistic studies have demonstrated that the coordination polymerization of *N,N*-dialkyl acrylamide DMAA by *rac*-**1** proceeds in a monometallic, site-control, coordination-conjugate addition mechanism through eight-membered-ring cyclic amide enolate intermediates (i.e., structure **A**, Scheme 2).[21] The resting state during a "catalytic" propagation cycle is the cyclic amide enolate **A** and associative displacement of the coordinated penultimate amide group by incoming acrylamide monomer to regenerate the active species is the rate-determining step, giving rise to the propagation kinetics that is first order in both concentrations of the monomer and the catalyst.

Scheme 2. Proposed initiation and propagation steps in the polymerization of acrylamides by *rac*-**1**.

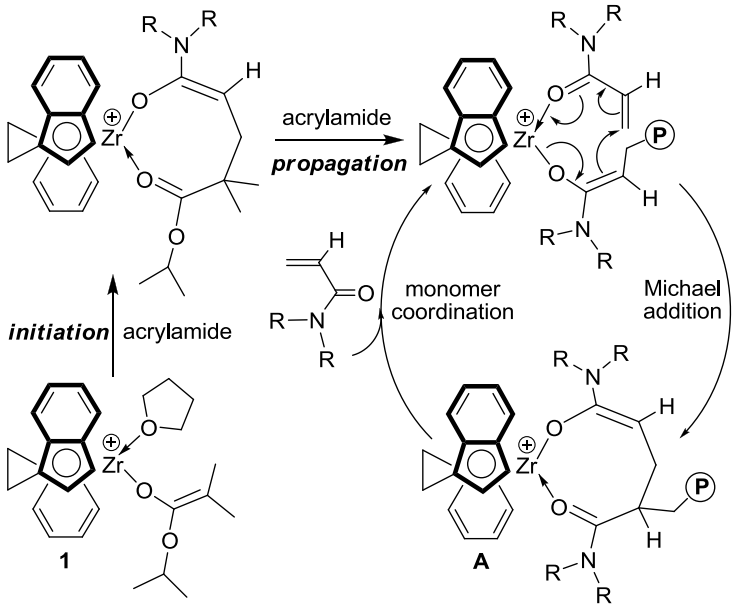

To examine if the polymerization of *N,N*-diaryl amides follows the same scheme established for *N,N*-dialkyl amides, kinetics of the DPAA polymerization by *rac*-**1** was investigated, the results of which were summarized in Figure 1. The kinetic experiments employed the $[DPAA]_0/[rac\text{-}\mathbf{1}]_0$ ratios ranging from 50 to 400; however, insolubility of the polymer hampered the efforts to perform accurately the NMR analysis of the aliquots taken at high conversions for the larger $[DPAA]_0/[rac\text{-}\mathbf{1}]_0$ ratio runs. Nevertheless, the available data collected clearly show that propagation is first order in [DPAA] for all the $[DPAA]_0/[rac\text{-}\mathbf{1}]_0$ ratios investigated in this study (Figure 1). Furthermore, a double logarithm plot (Figure 2) of the apparent rate constants (k_{app}), obtained from the slopes of the best-fit lines to the plots of $\ln([DPAA]_0/[rac\text{-}\mathbf{1}]_0)$ vs. time, as a function of $\ln[rac\text{-}\mathbf{1}]_0$ was fit to a straight line ($R^2 = 0.994$) of slope 0.987. Thus, the kinetic order with respect to [*rac*-**1**], given by the slope of ~1 (0.987), reveals that the propagation is also first order in catalyst concentration, indicating that the *N,N*-diaryl amide polymerization catalyst **1** follows the same mechanism as that of the *N,N*-dialkyl amide polymerization shown in Scheme 2.

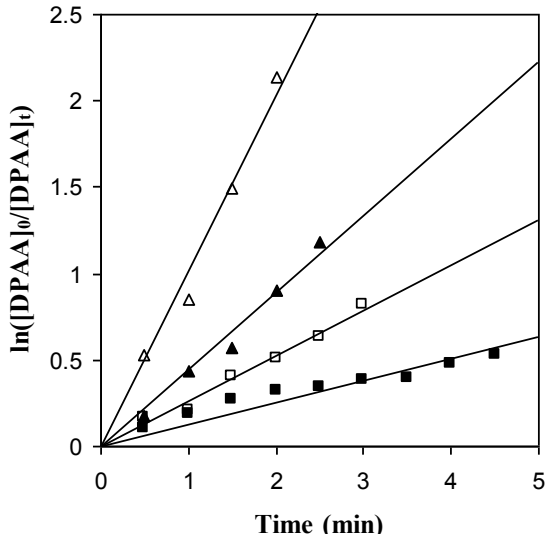

Figure 1. Semilogarithmic plots of $\ln([DPAA]_0/[DPAA]_t)$ vs. time for the polymerization of DPAA by *rac*-**1** in CH_2Cl_2 at ambient temperature (~23 ºC). Conditions: $[DPAA]_0 = 0.448$ M; $[rac\text{-}\mathbf{1}]_0 = 8.95$ mM (Δ), 4.47 mM (▲), 2.24 mM (□), 1.12 mM (■).

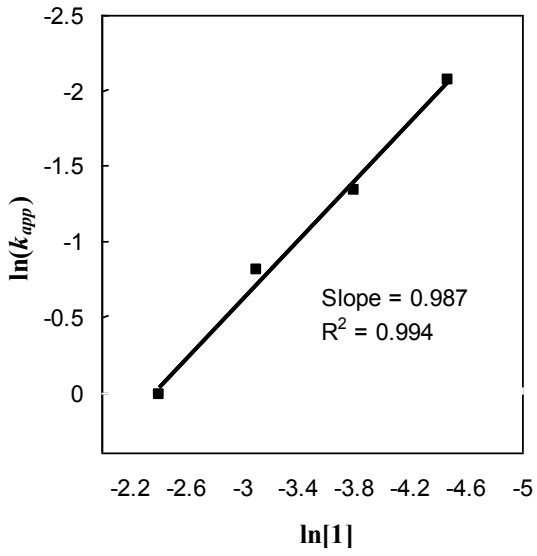

Figure 2. Plot of ln(k_{app}) vs. ln[**1**] for the DPAA polymerization by *rac*-**1** in CH_2Cl_2 at ambient temperature.

Polymerization of *N,N*-Diaryl Acrylamides. Racemic catalyst **1** was initially employed to examine the catalyst reactivity toward *N,N*-diaryl acrylamides for rendering solution-stable helical conformations of the corresponding highly isotactic polymers. Thus, polymerization of 50 and 200 equiv of DPAA in CH_2Cl_2 at ambient temperature using *rac*-**1** proceeds to quantitative monomer conversions (although the reaction started to become heterogeneous after ~5 min), affording P(DPAA) (runs 1 and 2, Table 1) with a high T_{max} (maximum-rate-decomposition temperature) of 484 °C in a narrow, one-step decomposition window (Figure 3). The rigid helical structure of highly isotactic P(DPAA)[14] can be viewed in the space-filing model of the most stable conformation as a 5_1 helix (Figure 4); the P(DPAA) produced by the highly isospecific coordination catalyst *rac*-**1** is also insoluble in common organic solvents, precluding its direct MW measurements by GPC. Accordingly, it was converted to the soluble poly(methyl acrylate) derivative by treatment with concentrated H_2SO_4 in MeOH at 90 °C for 24 h, followed by methylation with CH_2N_2.[14] The measured MW and MWD (M_w = 3.97 × 10^4, M_w/M_n = 1.03 and

M_w = 1.16 × 10^4, M_w/M_n = 1.13 for $[DPAA]_0/[rac\text{-}\mathbf{1}]_0$ = 200 and 50, respectively) of the poly(methyl acrylate) derivative (runs 1 and 2, Table 1) demonstrate the controlled/living nature of the DPAA polymerization.

Table 1. Selected Results of Polymerization of *N,N*-Diaryl Acrylamides by **1**.[a]

run no.	monomer	[monomer] /[**1**]	catalyst form	yield[b] (conv)	10^4 M_w[c] (g/mol)	MWD[c] (M_w/M_n)	$[\alpha]^{23}_D$[d] (deg)
1	DPAA	200	*rac*	97	3.97	1.03	
2	DPAA	50	*rac*	96	1.16	1.13	0.0
3	DPAA	50	*S,S*	96			−15.5
4	DPAA	50	*R,R*	96			+19.5
5	PTAA	50	*rac*	(100)			0.0
6	PTAA	50	*S,S*	(100)			−159
7	PTAA	50	*R,R*	(100)			+180
8	HPPA	50	*S,S*	(100)	19.8	1.25	+152
9	HPPA	50	*R,R*	(100)	18.1	1.38	−161

[a] Carried out in 5 mL of CH_2Cl_2 at ambient temperature for 3 h. [b] Isolated polymer yield or monomer conversion in parenthesis, (conv), measured by ^{1}H NMR. [c] Determined by GPC relative to P(MMA) standards for runs 1 and 2 which were based on the poly(methyl acrylate) derivatives, or by LS for runs 8 and 9. [d] Determined by polarimetry (c = 2 g/dL in $CHCl_3$; DPAA and PTAA polymer samples were dissolved in $CHCl_3$ with a small amount of CF_3COOH, while HPPA polymer samples were dissolved in $CHCl_3$ only.

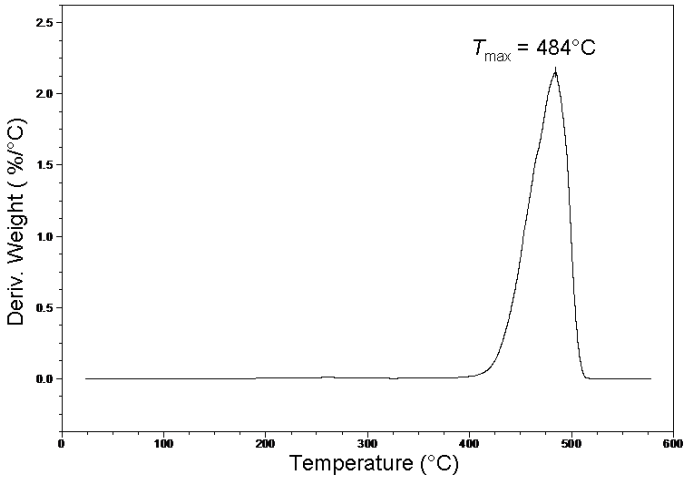

Figure 3. TGA derivative plot of P(DPAA) produced by *rac*-**1** (run 1, Table 1).

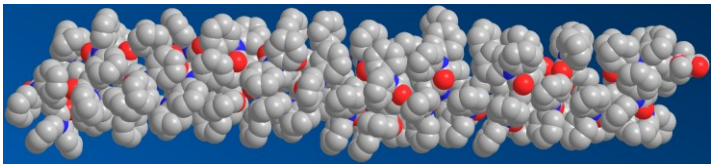

Figure 4. MM2-calculated 5_1 helical structure of a 50-mer of isotactic P(DPAA) viewed as a space filling model (carbon, nitrogen, and oxygen are grey, blue, and red, respectively; H atoms omitted).

Subsequently, we polymerized DPAA with enantiomeric catalysts (*R,R*)-**1** and (*S,S*)-**1**, successfully affording optically active P(DPAA)s with excess one-handed helicity (runs 3 and 4, Table 1). Thus, the enantiomeric catalysts produce polymers of opposite specific rotation to one another: $[\alpha]^{23}_{D}$ −15.5° by (*S,S*)-**1**, $[\alpha]^{23}_{D}$ +19.5° by (*R,R*)-**1**, showing the enantiomeric nature of the resulting polymers and determination of the handedness of the polymer helix by the configuration of the enantiomeric catalyst used. Furthermore, the P(DPAA) also exhibits opposite optical rotation to those of the respective neutral catalyst precursors used. Although the optically active P(DPAA) shows the same sign of optical rotation as that of each enantiomeric cationic zirconocenium catalyst, the possibility of the observed optical activity could arise from the catalyst residue in its cationic form is eliminated by the careful removal of the catalyst residue during post-polymerization workup procedures (see Experimental), by circular dichroism (CD) analysis that the catalyst did not exhibit any absorption peaks in the region observed for the polymer (vide infra), and also by control experiments that optically inactive, nonhelical, high MW polymers such as P(DMAA) and P(MMA) produced by either (*R,R*)-**1** or (*S,S*)-**1** always gave zero values by polarimetry, following the same post-polymerization workup procedures, which confirms the complete removal of the catalyst or ligand residue using our procedure.

We also examined the possible modulation on optical activity of the polymer by unsymmetrical substitution of the phenyl groups of poly(*N,N*-diary acrylamide)s. To this end, we extended this asymmetric coordination polymerization system to *N*-phenyl-*N*-(4-tolyl)acrylamide

(PTAA). Specifically, polymerizations of PTAA by *rac*-**1**, (*S,S*)-**1**, and (*R,R*)-**1** are as effective as the DPAA polymerization, producing rigid helical P(PTAA) whose optical activity and screw-sense helices are determined by the form of the catalyst employed: $[\alpha]^{23}_{D}$ = 0.0°, −159°, and +180° by *rac*-**1**, (*S,S*)-**1**, and (*R,R*)-**1**, respectively (runs 5–7, Table 1). These results were further confirmed by their CD spectra (Figure 5) which show no, positively signed, and negatively signed Cotton effects in the characteristic region of a $\pi \rightarrow \pi^*$ transition of the phenyl ring in the P(PTAA) produced by *rac*-**1**, (*S,S*)-**1**, and (*R,R*)-**1**, respectively, and that the latter two are near mirror images of each other. Of significance here are the observed approximately 10 times higher specific rotation values for P(PTAA) than P(DPAA).

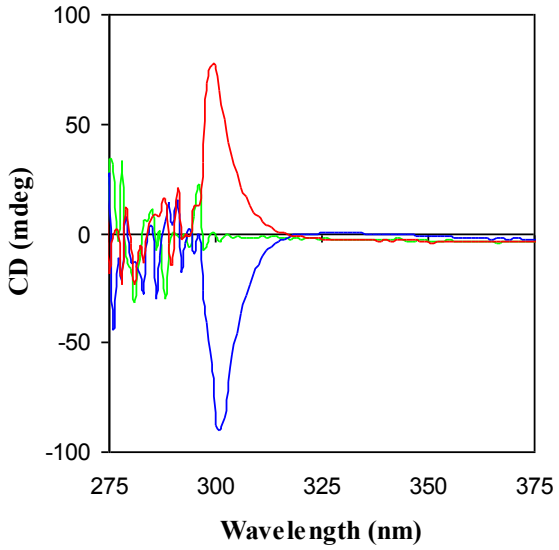

Figure 5. CD spectra ($CHCl_3$/CF_3COOH) of P(PTAA) produced by catalysts (*S,S*)-**1** (red), *rac*-**1** (green), and (*R,R*)-**1** (blue).

The stereoregular, rigid helical P(DPAA) and P(PTAA) produced are insoluble in common organic solvents, precluding their direct measurements of MW by GPC as well as optical activity by polarimetry and CD in common solvents such as $CHCl_3$ (without addition of CF_3COOH). We reasoned that a polymer based on *N*-(4-hexylphenyl)-*N*-phenyl acrylamide (HPPA)[14a] would be

possible to overcome this issue because the long-chain alkyl group on each repeat unit of the resulting polymer should enhance its solubility, and furthermore, the unsymmetrically substituted phenyl groups on *N* should give rise to the polymer with a large specific rotation [e.g., P(PTAA) vs. P(DPAA)]. Accordingly, polymerization of 50 equiv of HPPA was performed by catalysts (*S,S*)-**1** and (*R,R*)-**1**, satisfactorily leading to the optically active, one-handed helical P(HPPA) that is soluble directly in $CHCl_3$ (runs 8 and 9, Table 1); polymers of higher molecular weights were found to be insoluble in $CHCl_3$. The measured absolute MWs by light scattering are ~ 10 times higher than the calculated value strictly based on the monomer to catalyst feed ratio, likely due to association of the chains. Again, the enantiomeric catalysts produced P(HPPA)s of opposite specific rotation, but interestingly, the specific rotations of these polymers are opposite in sign to that of P(DPAA) or P(PTAA) produced by the same enantiomeric catalysts. It is currently unclear why there is alteration in sign of specific rotation, but it is important to note that these results do not give insight into the handedness of the helix, although it is assumed that the handedness of P(HPPA) is the same as that of P(DPAA) or P(PTAA) produced by the same enantiomeric catalysts due to the enantiomorphic site-control mechanism of the polymerization. Indeed, the CD analysis of the P(HPPA) produced by *rac*-**1**, (*S,S*)-**1**, and (*R,R*)-**1** showed no, positively, and negatively signed Cotton effects, respectively (Figure 6), which is the same as what was observed for P(PTAA) (*c.f.* Figure 5). As in P(PTAA), P(HPPA) with two nonequivalent aryl groups on amide *N* (i.e., unsymmetrical substitution) shows much larger specific rotations as compared to P(DPAA) with symmetrical substitution.

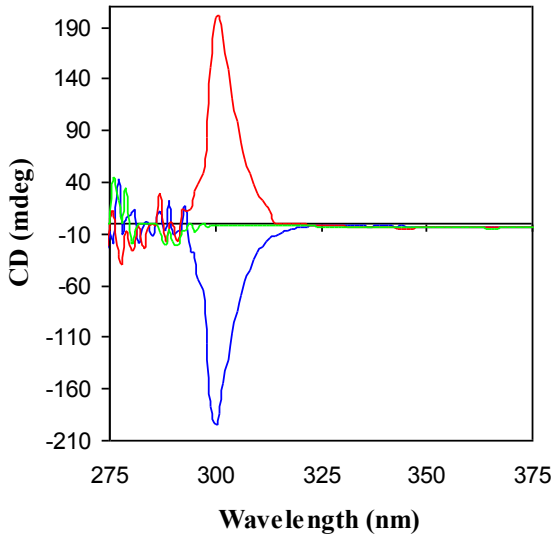

Figure 6. CD spectra ($CHCl_3$) of P(HPPA) produced by catalysts (*S*,*S*)-**1** (red), *rac*-**1** (green), and (*R*,*R*)-**1** (blue).

Block Copolymerization of *N*,*N*-Diaryl Acrylamides with MMA. The following three reasons prompted us to investigate the block copolymerizations of MMA with DPAA and PTAA: (a) use of a large MMA block to help solubilize the rigid helical acrylamide block; (b) further confirmation of the living/controlled nature of this polymerization system; and (c) production of the unique optically active, flexible random coil–rigid helical block copolymers. The block copolymerizations were carried out in a ratio of [MMA]/[acrylamide][**1**] = 400:50:1 at ambient temperature by starting the polymerization of MMA first, the results which were summarized in Table 2.

Table 2. Results of Block Copolymerization of MMA with *N*,*N*-Diaryl Acrylamides by **1**.[a]

run no.	comonomer	[M]/[co-M]/[**1**]	catalyst form	yield (%)	$10^4\ M_w$[b] (g/mol)	MWD[b] (M_w/M_n)	$[\alpha]^{23}_D$[c] (deg)
10	DPAA	400/50/1	*rac*	>99	376	1.19	0.0
11	DPAA	400/50/1	*S*,*S*	>99	358	1.15	−8.5
12	DPAA	400/50/1	*R*,*R*	>99	264	1.21	+11.0
13	PTAA	400/50/1	*rac*	>99	103	1.08	0.0
14	PTAA	400/50/1	*S*,*S*	>99	111	1.09	−27.0
15	PTAA	400/50/1	*R*,*R*	>99	123	1.07	+32.0

[a] Carried out in 5 mL of CH_2Cl_2 at ambient temperature for 10 min of MMA polymerization followed by 3 h of acrylamide polymerization. [b] Determined by LS. [c] Specific rotation measured in $CHCl_3$.

Indeed, block copolymers P(MMA)$_{400}$-*b*-P(DPAA)$_{50}$ and P(MMA)$_{400}$-*b*-P(PTAA)$_{50}$ are soluble in $CHCl_3$, but the measured absolute MWs by light scattering are substantially higher than the calculated value strictly based on the monomer-to-catalyst-feed ratio, likely due to the association of the polymer chains such as micelle formation. (The subscripted numbers shown in the block copolymer formula represent only the comonomer feed, and they do not necessarily or precisely reflect on copolymer composition.) Significantly, the block copolymers produced have narrow, unimodal MW distributions of M_w/M_n = 1.07–1.21), further confirming the living/controlled nature of the present polymerization system. The block copolymer composition is confirmed by TGA analysis (Figure 7) which showed 20 wt% for the P(DPAA) block in the block copolymer as compared to the calculated 18 wt% based on P(MMA)$_{400}$-*b*-P(DPAA)$_{50}$ or the monomer feed ratio. The optical activity of these block copolymers also hinges on the nature of the catalyst although, as expected, the specific rotation value of the block copolymer is much smaller than the respective homopolymer because of the weight fraction contribution of the large, optically inactive P(MMA) block; while *rac*-**1** afforded the optically inactive copolymer (runs 10 and 13, Table 2), (*S,S*)-**1** and (*R,R*)-**1** led to the copolymers of opposite optical rotation (runs 11 and 14 vs. runs 12 and 15, Table 2). These results were further confirmed by their CD spectra (Figures 8 and 9) which show no, positively signed, and negatively signed Cotton effects for the block copolymers produced by *rac*-**1**, (*S,S*)-**1**, and (*R,R*)-**1**, respectively.

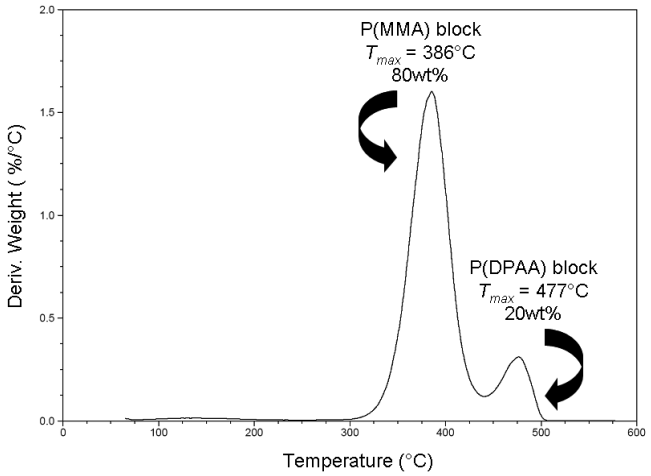

Figure 7. TGA derivative plot of P(MMA)$_{400}$-*b*-P(DPAA)$_{50}$ produced by (*S,S*)-**1** (run 11 in Table 2).

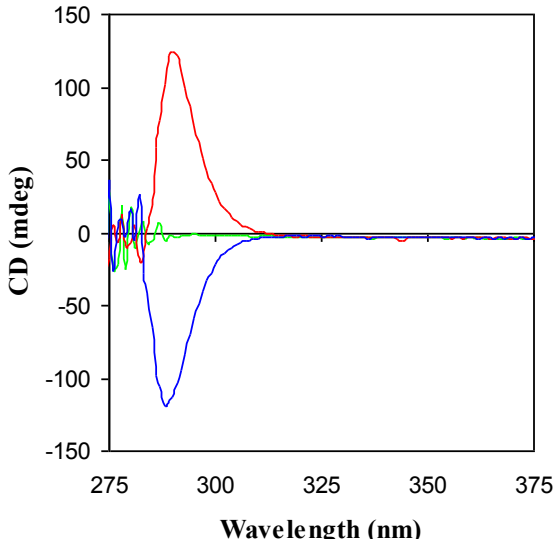

Figure 8. CD spectra (THF) of P(MMA)$_{400}$-*b*-P(DPAA)$_{50}$ produced by catalysts (*S,S*)-**1** (red), *rac*-**1** (green), and (*R,R*)-**1** (blue).

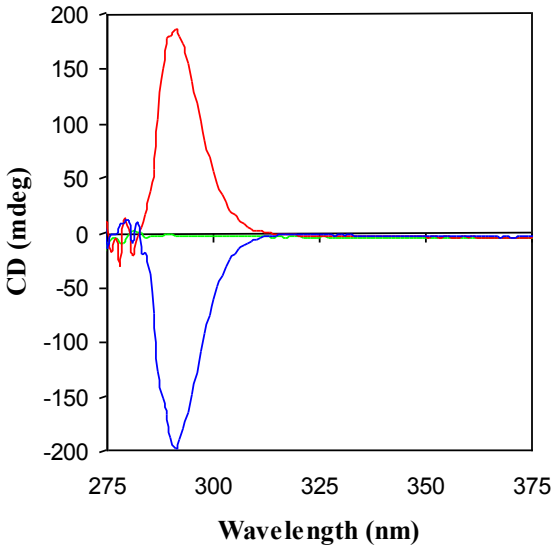

Figure 9. CD spectra (THF) of P(MMA)$_{400}$-*b*-P(PTAA)$_{50}$ produced by catalysts (*S*,*S*)-**1** (red), *rac*-**1** (green), and (*R*,*R*)-**1** (blue).

Effects of Chain Length on Optical Activity of Helical Poly(acrylamide)s. Because of the cryptochiral phenomenon of stereoregular vinyl polymers, only those low MW, enantiomeric oligomers exhibit measurable optical activity in solution, and the optical activity of such oligomers *increases* with a *decrease* in MW due to chain-end group effects (vide supra). However, the optical activity of the rigid helical poly(*N*,*N*-diaryl acrylamide)s of the current study does not rely on chain-end groups to eliminate reflection elements of symmetry, but rather by secondary structure of stable helical conformation. Intuitively, as the chain length of such polymers increases and the helical structure becomes more pronounced, the optical activity should rise. Thus, at shorter chain lengths the helix may not be fully developed, resulting in lower optical activity, and chain-end group effects on the chiroptical properties of the polymer become more significant. To test this hypothesis, we conducted the PTAA polymerization varying the [PTAA]/[(*R*,*R*)-**1**] ratio. The insolubility of the resulting P(PTAA) in common organic solvents prevented its direct MW analysis; thus, interpretation of the specific rotations of these polymers as a function of MW (chain length) was based on the [PTAA]/[(*R*,*R*)-**1**] ratio employed because

the controlled nature of this polymerization system was confirmed by other means (vide supra). As depicted in Figure 10, the specific rotation of the chiral polymer solution (in $CHCl_3$ with addition of a small amount of CF_3COOH) indeed increases with an increase in the monomer feed ratio (and thus the polymer chain length). Of significance, when the [PTAA]/[(*R,R*)-**1**] ratio is increased from 20 to 30 there is an enormous climb in the $[\alpha]^{23}_D$ value by 113.2 °! This large increase in specific rotation between these two ratios may correspond to the formation of a well-defined helix and multiple turns in the helix for the polymers synthesized with [PTAA]/[(*R,R*)-**1**] > 20. In comparison, when the [PTAA]/[(*R,R*)-**1**] ratio is increased from 30 to 50, there is a much smaller increase in specific rotation by 32.0°. We presently do not know, however, the maximum specific rotation of this polymer can achieve because higher MW P(PTAA)s become insoluble in $CHCl_3/CF_3COOH$, precluding their solution specific rotation measurements.

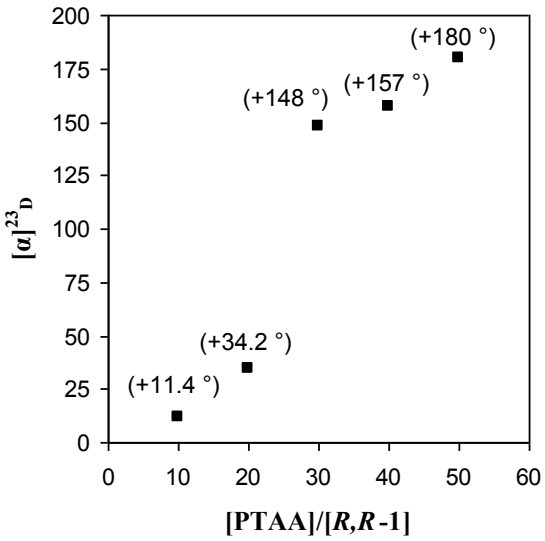

Figure 10. Plot of specific rotation $[\alpha]^{23}_D$ values of P(PTAA) vs. the [PTAA]/[(*R,R*)-**1**] ratio employed.

The use of soluble low MW P(HPPA) in $CHCl_3$ allowed establishing a direct plot between MW and optical activity. To this end, five P(HPPA) samples were prepared from the

polymerization using the [HPPA]/[(*R,R*)-**1**]) ratio = 10, 20, 30, 40, and 50 to produce the corresponding polymers with their absolute M_w and MWD measured by LS as well as specific rotations measured by polarimetry in $CHCl_3$ being summarized in Table 3. Again, the measured specific rotation (absolute value) of the chiral polymer increases with an increase in the polymer MW (chain length), Figure 11. However, surprisingly, the lowest MW polymer sample showed a small, but positive, specific rotation, whereas when the MW of P(HPPA) further increased the specific rotation became largely negative. This observation is most likely an effect of helix formation in that the small MW polymer does not fully develop the solution-stable helix and thus optical activity arises chiefly from the chirality in the main chain and nonequivalent chain-end groups; with further increasing MW the helix is more defined so that specific rotation is of the same sign for the polymers of the same screw sense and also becomes more largely negative with an increase in MW (Figure 11).

Table 3. Results of Polymerization of *N*-(4-Hexylphenyl)-*N*-phenyl Acrylamide (HPPA) by (*R,R*)-**1**.

run no.	[HPPA] /[**1**]	conv (%)	$10^4 M_w$[a] (g/mol)	MWD[a] (M_w/M_n)	$[\alpha]^{23}_D$[b] (deg)
16	10	>99	1.04	1.00	+1.5
17	20	>99	2.16	1.01	−7.8
18	30	>99	4.65	1.23	−11.0
19	40	>99	7.74	1.75	−67.6
20	50	>99	18.1	1.38	−161

[a] Determined by LS. [b] Specific rotation measured in $CHCl_3$.

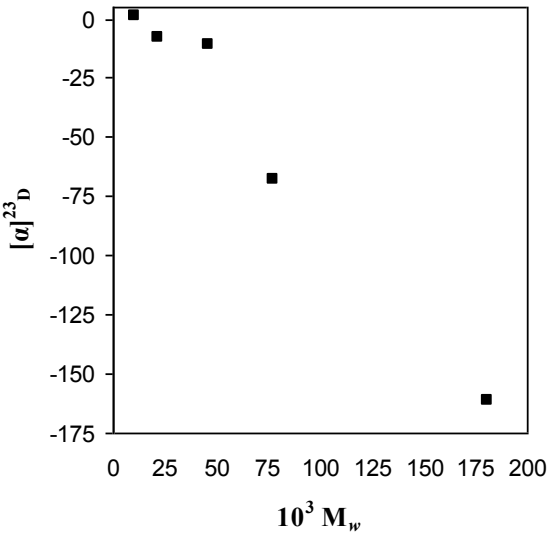

Figure 11. Plot of specific rotation $[\alpha]^{23}_{D}$ values of P(HPPA) produced by (*R,R*)-**1** vs. M_w.

Polymerization of Non-Diaryl Acrylamides. The above success in converting prochiral *N,N*-diaryl acrylamides to optically active, rigid helical polymers via asymmetric coordination polymerization brought forth a fundamental question of whether two aryl groups on amide *N* are of necessity in rendering solution-stable helical conformation. To answer this question, we investigated polymerizations of seven non-diaryl acrylamides by systematic replacement of one or both phenyl groups on *N* with H or alkyl groups of varying steric hindrance (see Chart II for structures), including *N*-aryl-*N*-alkyl acrylamide MPAA, *N*-aryl acrylamide PAA, *N*-alkyl acrylamide EAA, *N*,*N*-dialkyl acrylamides DMAA and DIPA, as well as *N*,*N*-cyclic $(CH_2)_n$ acrylamides APY (n = 4) and APP (n = 5). Selected polymerization results were summarized in Table 4.

Table 4. Selected Results of Polymerization of Non-Diaryl Acrylamides by (*R,R*)-**1**.[a]

run no.	M/co-M	[M]/[co-M /[**1**]	yield (conv)	$10^4 M_w$[b] (g/mol)	MWD[b] (M_w/M_n)	$[\alpha]^{23}_D$[c] (deg)
21	MPAA	50/1	97			+0.9
22	MPAA	30/1	(100)			+1.7
23	MPAA	10/1	(100)			+6.6
24	MPAA/MMA	50/400/1	(100)	21.2	1.01	+4.8
25	DMAA	50/1	>99			+6.0
26	DMAA	400/1	>99			0.0
27	DMAA/MMA	400/400/1	>99			+5.5
28	DMAA/MPAA	400/100/1	>99			+6.3
29	DIPA/MMA	50/400/1	(100)	18.8	1.01	+2.7
30	APP	50/1	(100)			+3.1
31	APP/MMA	50/400/1	(100)	10.0	1.29	+6.0

[a] Carried out in 5 mL of CH_2Cl_2 at ambient temperature for 10 min (for MMA and DMAA) or 3 h (for MPAA or APP), or in 5 mL of *o*-$C_6H_4Cl_2$ at 80 °C for 1 h (for DIPA and APY). [b] Determined by LS. [c] Specific rotation measured in $CHCl_3$ for block copolymers and DMAA homopolymers, or in $CHCl_3$ with addition of a small amount of CF_3COOH for MPAA and APP homopolymers.

Polymerizations of these non-diaryl acrylamides were first examined using *rac*-**1** to determine their reactivity toward the current catalyst system and also serve as comparative examples when analyzing the results by the enantiomeric catalysts. All homopolymers or block copolymers produced by *rac*-**1** gave zero readings in polarimetry as expected, and these results were not included in Table 4. P(MPAA) produced by (*R,R*)-**1** showed a small specific rotation of +0.9° (run 21, Table 4) in a [MPAA]/[(*R,R*)-**1**] ratio of 50; the polymer was almost cryptochiral based on the $[\alpha]^{23}_D$ values and also exhibited no Cotton effects from its CD analysis, implying that a helical structure was not formed. A further study of effects of the [MPAA]/[(*R,R*)-**1**] ratio on optical activity of the resulting polymer (runs 21–23, Table 4) confirmed the above conclusion. Thus, in sharp contrast to the optically active, rigid helical poly(*N,N*-diaryl acrylamide)s, a decrease in the MPAA monomer feed ratio (thus the polymer chain length) increases the specific rotation of the polymer (Figure 12), characteristic of the small optical activity due to configurational chirality relied on chain-end group effects rather than helically conformational chirality (vide supra). A block copolymer of 50 equiv of MPAA with 400 equiv of MMA (run 24, Table 4) was also prepared to enable MW analysis and examination of optical

activity of the copolymer. Interestingly, the enantiomeric copolymer $P(MMA)_{400}$-*b*-$P(MPAA)_{50}$ produced by (*R,R*)-**1** had a specific rotation of +4.8°, which is *much larger than* the specific rotation (+0.9°) of P(MPAA) synthesized using the same amount of MPAA. This observation is again in contrary to all prior observations made for helical *N,N*-diaryl acrylamide–random coil MMA block copolymers, further supporting the conclusion that MPAA with only one phenyl group on *N* cannot produce a polymer with solution-stable helicity. Impressively, MM2 modeling of P(MPAA) drew into the same conclusion (i.e., a random-coil structure, Figure 13).

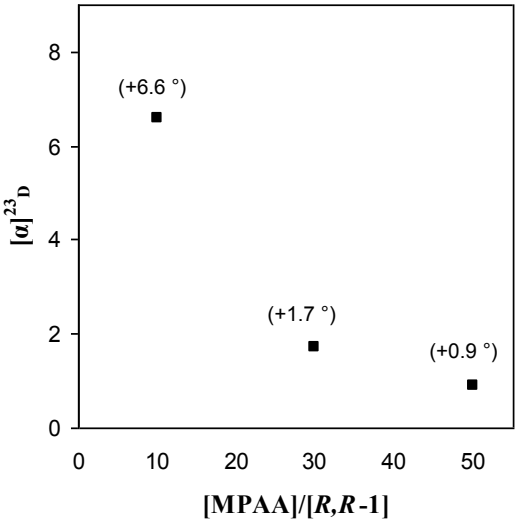

Figure 12. Plot of specific rotation $[\alpha]^{23}_{D}$ values of P(MPAA) vs. the [MPAA]/[(*R,R*-**1**)] ratio.

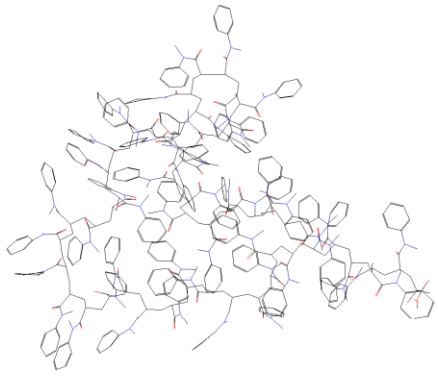

Figure 13. MM2-calculated random-coil structure of a 50-mer of isotactic P(MPAA) viewed as a wire frame model (carbon, nitrogen, and oxygen are grey, blue, and red, respectively; H atoms omitted).

Consistent with the inactivity of *rac*-**1** towards polymerization of *N*-isopropyl acrylamide (containing acidic *N*–H proton) but high activity towards polymerization of DMAA,[21] catalyst (*R,R*)-**1** is unable to polymerize either PAA or EAA but rapidly polymerizes DMAA to isotactic P(DMAA) that exhibited a specific rotation of +6.0° in a [DMAA]/[(*R,R*)-**1**] ratio of 50 (run 25, Table 4). The enantiomeric P(DMAA) produced at a higher ratio of [DMAA]/[(*R,R*)-**1**] = 400 became cryptochiral (zero optical rotation, run 26, Table 4) as expected; however, the block copolymer $P(DMAA)_{400}$-*b*-$P(MMA)_{400}$ *is* optically active with $[\alpha]^{23}_{D}$ = +5.5° (run 27, Table 4), whereas each respective homopolymer of the same composition is cryptochiral. Likewise, the block copolymer $P(DMAA)_{400}$-*b*-$P(MPAA)_{100}$ *is* optically active with $[\alpha]^{23}_{D}$ = +6.5° (run 28, Table 4), whereas each respective homopolymer of the same composition is cryptochiral. These findings, along with the previously observed much larger optical activity of the block copolymer $P(MMA)_{400}$-*b*-$P(MPAA)_{50}$ than $P(MPAA)_{50}$, point to *an exciting strategy for producing optically active, nonhelical polymers via block copolymer formation*. More discussion on this subject is described in next segment.

No polymerization occurred for DIPA or APY at ambient temperature; however, they were readily polymerized by catalyst **1** in *o*-dichlorobenzene at 80 °C (control runs without the catalyst showed no polymerization occurred at 80 °C up to 24 h). The resulting P(DIPA), with even a small [DIPA]/[(*R,R*)-**1**] ratio of 50 or 10, was insoluble in common solvents tested, inhibiting direct analysis of its optical activity. Subsequently, we synthesized the block copolymer $P(MMA)_{400}$-*b*-$P(DIPA)_{50}$ using (*R,R*)-**1** that showed a specific rotation of +2.7° (run 29, Table 4); the enantiomeric block copolymer was further analyzed by CD and showed no Cotton effects, implying that, like P(MPAA) and P(DMAA), it does not form a helical structure. P(APY) produced by (*R,R*)-**1** in a [APY]/[(*R,R*)-**1**] ratio of 200 is cryptochiral. However, according to MM2 modeling, the piperidine derivative APP would render a helical conformation (Figure 14). Accordingly, we polymerized APP using catalysts **1** achieving quantitative monomer

conversions. The enantiomeric homopolymer P(APP) and block copolymer $P(MMA)_{400}$-*b*-$P(APP)_{50}$ exhibited small, but significant specific rotations of +3.1° and +6.0°, respectively (runs 30 and 31, Table 4), initiating CD analysis for conformation of helical formation. Indeed, the CD spectra of P(APP) showed a large negative Cotton effect in the characteristic region of a $n \rightarrow n^*$ transition (Figure 15), thereby achieving the first chiral poly(*N,N-dialkyl* acrylamide) with solution-stable one-handed helicity.

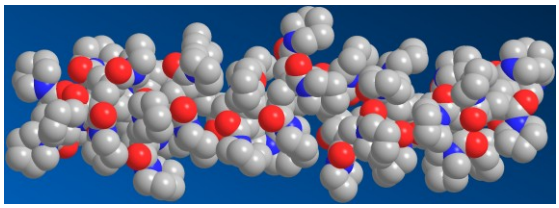

Figure 14. MM2-calculated approximately 6_1 helical structure of a 40-mer of chiral isotactic P(APP) viewed as a space filling model (carbon, nitrogen, and oxygen are grey, blue, and red, respectively; H atoms omitted).

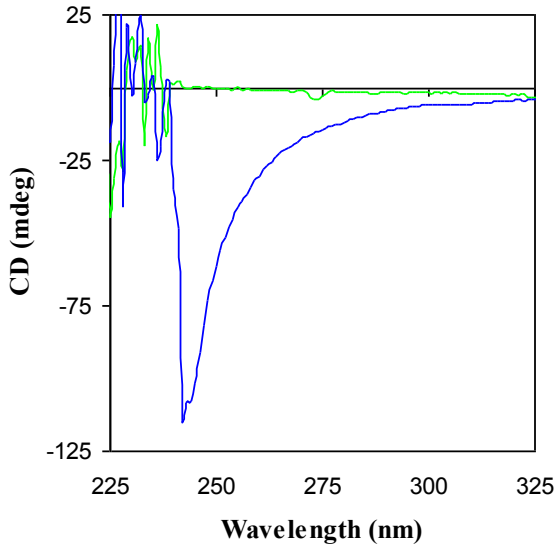

Figure 15. CD spectra ($CHCl_3/CF_3COOH$) of P(APP) by catalysts *rac*-**1** (green) and (*R,R*)-**1** (blue).

Polymerization of Methacrylates. Our above described findings that optical activity was observed with the P(MMA)-*b*-P(acrylamide) block copolymers, even when the acrylamide homopolymers do not form a helical structure, led to a hypothesis that in synthesizing block copolymers with methacrylates, the mirror plane that exists in homopolymers that renders them cryptochiral could be eliminated, giving rise to optically active, non-helical block copolymers. To ensure that the optical activity that could arise from the block copolymers was not influenced by chain-end groups, we systematically investigated the optical activity of enantiomeric P(MMA) to approximate the MW required to reach cryptochirality from polymers produced by our catalyst system (runs 32–35, Table 5). Similarly to the observations of Wulff,[7] the P(MMA) with M_n = 2.56×10^4 g/mol ($P_n \sim 250$) shows minimal optical activity. A further increase in MW gives the polymer without any optical activity. Ensuring that the second block was also long enough to reach cryptochirality, we polymerized *n*-butyl methacrylate (BMA) by (*S,S*)-**1** to find the M_n at which optical activity was not observed (run 36, Table 5).

Table 5. Results of Polymerization of Methacrylates by **1**.[a]

run no.	M/co-M	catalyst form	yield (%)	$10^4 M_n$[b] (g/mol)	MWD[b] (M_w/M_n)	$[\alpha]^{23}_D$[c] (deg)
32	MMA	*R,R*	>99	0.66	1.05	+5.4
33	MMA	*R,R*	>99	1.07	1.03	+4.5
34	MMA	*R,R*	>99	2.56	1.05	+0.9
35	MMA	*R,R*	>99	3.01	1.05	0.0
36	BMA	*S,S*	>99	1.99	1.04	0.0
37	400MMA/400BMA	*S,S*	>99	16.3	1.07	0.0
38	400MMA/100BMA	*S,S*	89	8.93	1.04	0.0
39	400MMA + 400BMA	*S,S*	88	14.2	1.05	0.0
40	400MMA/400BMA/400EHM	*S,S*	>99	22.5	1.04	0.0

[a] Carried out in 5 mL of CH_2Cl_2 at ambient temperature for 10 min (MMA), 30 min (BMA), and 1 h (EHM). [b] Determined by GPC relative to P(MMA) standards. [c] Determined by polarimetry (*c* = 2 g/dL in $CHCl_3$).

In contrast to the optically active P(MMA)-*b*-P(acrylamide) block copolymers, the $P(MMA)_{400}$-*b*-$P(BMA)_{400}$ synthesized by (*S,S*)-**1** was, surprisingly, optically inactive (run 37, Table 5). To perturb the symmetry of the block copolymer further, we polymerized

nonequivalent ratios of MMA and BMA by (*S,S*)-**1**, but still leading to an optically inactive copolymer (run 38, Table 5). Next, we produced random copolymer $P(MMA)_{400}$-*co*-$P(BMA)_{400}$, and it was found also optically inactive (run 39, Table 5). Lastly, we synthesized the ABC triblock methacrylate copolymer of MMA, BMA, and 2-ethylhexylmethacrylate (EHM) using (*S,S*)-**1**; again, the well-defined triblock copolymer (M_w/M_n = 1.04) showed no optical activity (run 40, Table 5). The sharp contrast between the optically active methacrylate-*b*-acrylamide block copolymers and methacrylate-*b*-methacrylate diblock or triblock copolymers may be explained by the following analysis: with the methacrylate-*b*-methacrylate block copolymers, the first nonequivalent atom from the asymmetric carbon on the main chain, in comparison of the two different monomer repeat units, is four atoms away, while the first nonequivalent atom between the two different monomers within the methacrylate-*b*-acrylamide block copolymers is attached directly to the asymmetric carbon.

Conclusions

We have investigated the kinetics and scope of the metallocene-mediated asymmetric coordination polymerization of acrylamide and methacrylate monomers using the enantiomeric catalysts (*S,S*)-**1** and (*R,R*)-**1** to produce optically active, stereoregular polymers of several different classes. Through kinetic studies it has been shown that the polymerization of *N,N*-diaryl acrylamides such as DPAA by **1** proceeds via a mechanism identical to the one already established for the polymerization of *N,N*-dialkyl acrylamides, namely a monometallic, coordination-conjugate addition process. In analyzing how chain length affects optical activity of polymers, we have shown that increasing MW will increase the optical activity of polymers which can form secondary structure of solution-stable helical conformations, whereas for random-coil polymers an increase in MW will gradually diminish the influence of chain-end groups on the overall chiroptical properties of the polymer, resulting in a decrease in optical activity to ultimately null when cryptochirality is reached.

The formation of optically active poly(acrylamide)s due to solution-stable helical conformations with an excess of one-handed helicity is dictated by the sterics and rigidity of the monomer repeat units. Diaryl acrylamides such as DPAA, PTAA, and HPPA are readily polymerized by the enantiomeric catalyst **1** to optically active helical polymers, with the unsymmetrically substituted monomers (PTAA and HPPA) giving the chiral polymers of much enhanced optical activity as compared to the one derived from symmetrically substituted DPPA. Introduction of the long-chain alkyl group to one the phenyl rings (i.e., HPPA) not only accomplishes the unsymmetrical substitution but also solves the solubility issue associated with rigid helical homopolymers, enabling direct MW analysis of such polymers by LS/GPC. All non-diaryl acrylamides investigated in this study led to nonhelical polymers, except for APP which was identified by MM2 modeling and successfully gave rise to the first optically active, helical poly(*N,N-dialkyl* acrylamide), P(APP).

We have also carried out extensive asymmetric block copolymerization studies of MMA with *N,N*-diaryl acrylamides to solve the solubility issue associated with helical homopolymers of acrylamides, to further confirm the living/controlled nature of the present polymerization system towards such polar monomers, and to produce the unique optically active, flexible random coil–rigid helical stereoblock copolymers. We further discovered that all the high MW methacrylate-*b*-acrylamide block copolymers produced by the enantiomeric catalysts **1** are optically active, even when the MW of both blocks far exceeds their cryptochiral MW and regardless of whether the acrylamide comonomer employed can render solution-stable helical conformation or not. On the other hand, all the methacrylate-*b*-methacrylate well-defined stereodiblock or triblock copolymers produced by the enantiomeric catalysts **1** are optically inactive, which is attributable to the similar structures of the methacrylate repeat units placing the first nonequivalent atom between the different methacrylate units too far away from the asymmetric carbon center.

Acknowledgment. This work was supported by the National Science Foundation (NSF-0718061). We thank Prof. Alan Kennan (CSU) for assistance in CD measurements and Boulder

Scientific Co. for the research gift of $B(C_6F_5)_3$. This dissertation chapter contains the manuscript of a communication [Miyake, G. M.; Mariott, W. R.; Chen. E. Y.-X. *J. Am. Chem. Soc.* **2007**, *129*, 6724-2725] and a full paper [Miyake, G. M.; Chen, E. Y.-X. *Macromolecules* **2008**, *41*, 3405-3416]. W.R.M. assisted in the synthetic work of the enantiomeric metallocene pre-catalysts.

References

(1) For selected reviews, see: (a) Yashima, E.; Maeda, K. *Macromolecules* **2008**, *41*, 3−12. (b) Yamamoto, C.; Okamoto, Y. *Bull. Chem. Soc. Jpn.* **2004**, *77*, 227−257. (c) Nakano, T.; Okamoto, Y. *Chem. Rev.* **2001**, *101*, 4013−4038. (d) Cornelissen, J. J. L. M.; Rowan, A. E.; Nolte, R. J. M.; Sommerdijk, N. A. J. M. *Chem. Rev.* **2001**, *101*, 4029−4070. (e) Okamoto, Y.; Nakano, T. *Chem. Rev.* **1994**, *94*, 349−372. (f) Okamoto, Y.; Yashima, E. *Prog. Polym. Sci.* **1990**, *15*, 263−298. (g) Wulff, G. *Angew. Chem. Int. Engl.* **1989**, *28*, 21−37. (h) Pino, P. *Adv. Polym. Sci.* **1965**, *4*, 393−456.

(2) Farina, M. *Top. Stereochem.* **1987**, *17*, 1−111.

(3) Pino, P.; Cioni, P.; Wei, J. *J. Am. Chem. Soc.* **1987**, *109*, 6189−6191.

(4) Kaminsky, W.; Ahlers, A.; Möller-Lindenhof, N. *Angew. Chem. Int. Ed*. **1989**, *28*, 1216−1218.

(5) Pino, P.; Galimberti, M.; Prada, P.; Consiglio, G. *Makromol. Chem.* **1990**, *191*, 1677−1688.

(6) Kaminsky, W. *Angew. Makromol. Chem.* **1986**, *145/146*, 149−160.

(7) Wulff, G.; Zweering, U. *Chem. Eur. J.* **1999**, *5*, 1898−1904.

(8) Beckerle, K.; Manivannan, R.; Lian, B.; Meppelder, G.-J. M.; Raabe, G.; Spaniol, T. P.; Ebeling, H.; Pelascini, F.; Mülhaupt, R.; Okuda, J. *Angew. Chem. Int. Ed*. **2007**, *46*, 4790−4793.

(9) Wulff, G.; Dhal, P. K. *Angew. Chem. Int. Engl.* **1989**, *28*, 196−198.

(10) Wulff, G. *Polym. News* **1991**, *16*, 167−173.

(11) (a) Coates, G. W.; Waymouth, R. M. *J. Am. Chem. Soc.* **1993**, *115*, 91−98. (b) Coates, G. W.; Waymouth, R. M. *J. Am. Chem. Soc.* **1991**, *113*, 6270−6271.

(12) Yeori, A.; Goldberg, I.; Kol, M. *Macromolecules* **2007**, *40*, 8521−8523.

(13) (a) Nakano, T.; Okamoto, Y. Hatada, K. *J. Am. Chem. Soc.* **1992**, *114*, 1318−1329. (b) Okamoto, Y.; Suzuki, K.; Ohta, K.; Hatada, K. Yuki, H. *J. Am. Chem. Soc.* **1979**, *101*, 4763−4765.

(14) (a) Shiohara, K.; Habaue, S.; Okamoto, Y. *Polym. J.* **1998**, *30*, 249−255. (b) Okamoto, Y.; Hayashida, H.; Hatada, K. *Polym. J.* **1989**, *21*, 543−549. (c) Okamoto, Y.; Adachi, M.; Shohi, H.; Yuki, H. *Polym. J.* **1981**, *13*, 175−177.

(15) For selected recent examples of helix-sense-selective polymerization, see: (a) Tang, H.-Z.; Garland, E. R.; Novak, B. M.; He, J.; Polavarapu, P. L.; Sun, F. C.; Sheiko, S. S. *Macromolecules* **2007**, *40*, 3575−3580. (b) Tsuji, M.; Azam, A. K. M. F.; Kamigaito, M.; Okamoto, Y. *Macromolecules* **2007**, *40*, 3518−3520. (c) Kajitani, T.; Okoshi, K.; Sakurai, S.-I.; Kumaki, J.; Yashima, E. *J. Am. Chem. Soc.* **2006**, *128*, 708−709. (d) Tang, H.-Z.; Boyle, P. D.; Novak, B. M. *J. Am. Chem. Soc.* **2005**, *127*, 2136−2142. (e) Tian, G.; Lu, Y.; Novak, B. M. *J. Am. Chem. Soc.* **2004**, *126*, 4082−4083. (f) Aoki, T.; Kaneko, T.; Maruyama, N.; Sumi, A.; Takahashi, M.; Sato, T.; Teraguchi, M. *J. Am. Chem. Soc.* **2003**, *125*, 6346−6347.

(16) (a) Azam, A. K. M. F.; Kamigaito, M.; Okamoto, Y. *J. Polym. Sci. Part A: Polym. Chem.* **2007**, *45*, 1304−1315. (b) Hoshikawa, N.; Hotta, Y.; Okamoto, Y. *J. Am. Chem. Soc.* **2003**, *125*, 12380−12381. (c) Nakano, T.; Okamoto, Y. *Macromolecules* **1999**, *32*, 2391−2393. (d) Nanano, T.; Shikisai, Y.; Okamoto, Y. *Polym. J.* **1996**, *28*, 51−60.

(17) (a) Serizawa, T.; Hamada, K.-I.; Akashi, M. *Nature* **2004**, *429*, 52−55. (b) Serizawa, T.; Hamada, K.; Kitayama, T.; Fujimoto, N.; Hatada, K.; Akashi, M. *J. Am. Chem. Soc.* **2000**, *122*, 1891−1899. (c) Hatada, K.; Kitayama, T.; Ute, K.; Nishiura, T. *Macromol. Symp.* **1998**, *132*, 221−230. (d) Spevacek, J.; Schneider, B. *Adv. Colloid Interface Sci.* **1987**, *27*, 81−150.

(18) Wulff, G.; Petzoldt, J. *Angew. Chem. Int. Ed. Engl.* **1991**, *30*, 849−850.

(19) Bolig, A. D.; Chen, E. Y.-X. *J. Am. Chem. Soc.* **2004**, *126*, 4897−4906.

(20) Rodriguez-Delgado, A.; Chen, E. Y.-X. *Macromolecules* **2005**, *38*, 2587−2594.

(21) (a) Mariott, W. R.; Chen, E. Y.-X. *Macromolecules* **2005**, *38*, 6822−6832. (b) Mariott, W. R.; Chen, E. Y.-X. *Macromolecule* **2004**, *37*, 4741−4743.

(22) Miyake, G. M.; Mariott, W. R; Chen, E. Y.-X. *J. Am. Chem. Soc.* **2007**, *129*, 6724−6725.

(23) Allen, R. D.; Long, T. E.; McGrath, J. E. *Polym. Bull.* **1986**, *15*, 127−134.

(24) Kim, Y. C.; Jeon, M.; Kim, S. Y. *Macromol. Rapid Commun*. **2005**, *26*, 1499−1503.

(25) Kim, Y.-J; Bernstein, M. P.; Galiano Roth, A. S.; Romesber, F. E.; Williard, P. G.; Fuller, D. J.; Harrison, A. T.; Collum, D. B. *J. Org. Chem.* **1991**, *56*, 4435−4439.

(26) (a) Grossman, R. B.; Doyle, R. A.; Buchwald, S. L. *Organometallics* **1991**, *10*, 1501−1505. (b) Collins, S.; Kuntz, B. A.; Taylor, N. J.; Ward, D. G. *J. Organomet. Chem.* **1988**, *342*, 21−29.

(27) Diamond, G. M.; Jordan, R. F.; Petersen, J. L. *J. Am. Chem. Soc.* **1996**, *118*, 8024−8033.

(28) LoCoco, M. D.; Jordan, R. F. *J. Am. Chem. Soc.* **2004**, *126*, 13918−13919.

(29) Rodewald, S.; Jordan, R. F. *J. Am. Chem. Soc.* **1994**, *116*, 4491−4492.

(30) Mariott, W. R.; Rodriguez-Delgado, A.; Chen, E. Y.-X. *Macromolecules* **2006**, *39*, 1318−1327.

Chapter 3

Coordination-Addition Polymerization and Kinetic Resolution of Methacrylamides by Chiral Metallocene Catalysts

Abstract

This contribution reports the first successful coordination-addition polymerization of *N,N*-dialkyl methacrylamides and the first example of kinetic resolution of a racemic methacrylamide by chiral metallocene catalysts. The polymerization of methacryloyl-2-methylaziridine (MMAz) by *rac*-(EBI)Zr^{+}(THF)[OC(O^{i}Pr)=CMe_2] [$MeB(C_6F_5)_3$]$^{-}$ (**1**) is stereospecific and also exhibits a high degree of control over polymerization. This polymerization follows first-order kinetics in both concentrations of monomer and catalyst, consistent with a monometallic propagation mechanism. Substituents on the highly strained aziridine ring stabilize the aziridine moiety against thermally induced cross-linking through its ring-opening reaction; thus, the polymer derived from methacryloyl tetramethyleneaziridine (MTMAz) exhibits greatly enhanced resistance towards thermal cross-linking over poly(MMAz), marking 57 °C and 42 °C higher onset cross-linking and maximum cross-linking temperatures, respectively. Enantiomeric catalyst (*S,S*)-**1** demonstrates experimentally and theoretically its ability to kinetically resolve the racemic MMAz monomer with a low stereoselectivity factor *s* of 1.8. Polymerizability of several methacrylamide monomers has been investigated via a combined experimental and theoretical (DFT) study that examines the degree of conjugation between the vinyl and carbonyl double bonds, relative polymerization reactivity, and relative energy for the formation of amide-enolate intermediates.

Introduction

There is increasing interest in the utilization of technologically important, single-site cationic group 4 metallocene catalysts,[1] which have been extensively investigated and successfully employed for the (co)polymerization of nonpolar vinyl monomers (α-olefins in particular),[2] for polymerizations of polar, functionalized vinyl monomers including methacrylates,[3–45] acrylates,[40,46–49] acrylamides,[50–53] and methyl vinyl ketone.[54] The polymerization of (meth)acrylates has also been studied computationally.[55–62] Certain catalyst structures exhibit a high degree of control over polymerization characteristics (activity and efficiency; polymer molecular weight, MW; MW distribution, MWD; livingness) and stereochemistry (polymer tacticity and stereocontrol mechanism), enabling the ambient-temperature synthesis of highly isotactic poly(methacrylate)s (≥ 95% *mm*)[8,12,35,43,44] and poly(acrylamide)s (>99% *mm*)[50–53] using chiral C_2-ligated zirconocenium complexes as well as highly syndiotactic poly(methacrylate)s (≥ 94% *rr*)[3] using chiral C_s-ligated zirconocenium complexes. An important *exception* here is the inability of such coordination metallocene catalysts to polymerize *N,N*-dialkyl *methacrylamides* such as *N,N*-dimethyl methacrylamide (DMMA),[52] although they can polymerize *acrylamides* such as *N,N*-dimethyl acrylamide (DMAA) rapidly in a stereospecific and living fashion.[50–53]

The non-polymerizability of DMMA has also been previously noted in anionic polymerizations by organolithium initiators,[63] which was attributed to a twisted, non-conjugated monomer conformation between the vinyl and carbonyl double bonds, caused by steric repulsions between the α-methyl group or the vinyl proton and the *N*-methyl group of DMMA. As compared to other polymerizable conjugated monomers such as DMAA, this twisted DMMA monomer conformation results in a less effective π overlap between these two functional groups and thus leads to unstable amide enolate intermediates upon nucleophilic attack by the initiator. This hypothesis was supported by MNDO calculations[63] and NMR studies;[64] the calculations reveal an energy minimum for the twisted confirmation that lies ~4.0 kcal/mol below either the *s-cis* or *s-*

trans conformation, while the ^{1}H and ^{13}C NMR studies show that the NMR features (chemical shifts and peak separations) for the vinyl protons and carbonyl carbons of the non-polymerizable *N,N*-dialkyl methacrylamides more closely resemble those of non-conjugated vinyl monomers than those of polymerizable, conjugated monomers. Introduction of the highly strained, three-membered aziridine ring into the monomer structure provided a clever solution to the non-polymerizability of *N,N*-dialkyl methacrylamides; Okamoto and Yuki[65] reported in 1981 successful anionic and radical polymerizations of *N*-methacryloylaziridine with BuLi or PhMgBr at –78 ºC and with AIBN, and most recently Ishizone and co-workers[66] reported living anionic polymerization of *N*-methacryloyl-2-methylaziridine (MMAz) with 1,1-diphenyl-3-methylpentyl lithium or diphenylmethyl potassium in the presence of LiCl or Et_2Zn at low temperatures (–40 ºC to –78 ºC).

Three unique features about MMAz and its analogous methacrylamide monomers can be appreciated. First, based on our DFT calculations (vide infra), linking the two *N*-alkyl groups into a small three-membered ring alleviates the non-bonding interaction incurred to DMMA, giving rise to the desired planar, C=C/C=O conjugated monomer conformation for MMAz and thereby solving the non-polymerizability issue with *N,N*-dialkyl methacrylamides. Second, the pendant strained aziridine ring provides needed reactivity towards further polymer functionalization or chain cross-linking, through its ring-opening reactions, for stable polymer network structures.[66] Third, MMAz is a racemic monomer, which can be tested for kinetic resolution polymerization, with appropriate enantiomeric catalysts, potentially leading to the enantiomeric monomer with appreciable % *ee* and the optically active polymer which predominately incorporates the other enantiomer from the racemic monomer poor. These three reasoned unique features about MMAz prompted our current research using chiral metallocene catalysts, including C_2-ligated ester enolate complex *rac*-(EBI)Zr^{+}(THF)[OC(O^{i}Pr)=CMe_2][$MeB(C_6F_5)_3$]$^{-}$ [**1**; EBI = $C_2H_4(\eta^5$-indenyl$)_2$][8,12,52] and C_s-ligated alkyl complex (CGC)Ti$Me^{+}MeB(C_6F_5)_3^{-}$ [**2**; CGC = $Me_2Si(\eta^5$-$C_5Me_4)$(^{t}BuN)],[17,55] as we have previously demonstrated their remarkable ability to precisely

control the polymerization of methacrylates and acrylamides and also to render asymmetric, living polymerization when enantiomeric catalysts **1** are employed.[50,51] Accordingly, this study was designed to address the following *four fundamental questions*: (1) Can such coordination metallocene catalysts, which have been shown not to polymerize non-conjugated methacrylamides such as DMMA,[52] polymerize conjugated methacrylamides such as MMAz? (2) If the answer to the polymerizability question is positive, then is the polymerization well-controlled and can the enantiomeric catalysts effect kinetic resolution of the racemic MMAz monomer? (3) Can we design other conjugated methacrylamide monomers with effective vinyl and carbonyl π overlap and thus good polymerizability, thereby allowing for a study of the polymer structure–property (e.g., thermal stability) relationship? (4) What determines polymerizability of methacrylamides? Chart 1 summarizes the catalysts employed and the scope of the methacrylamide monomers investigated in this study towards addressing the above four fundamental questions.

Chart 1. Chemical Structures of the Catalysts Employed and the Monomers Investigated in This Study.

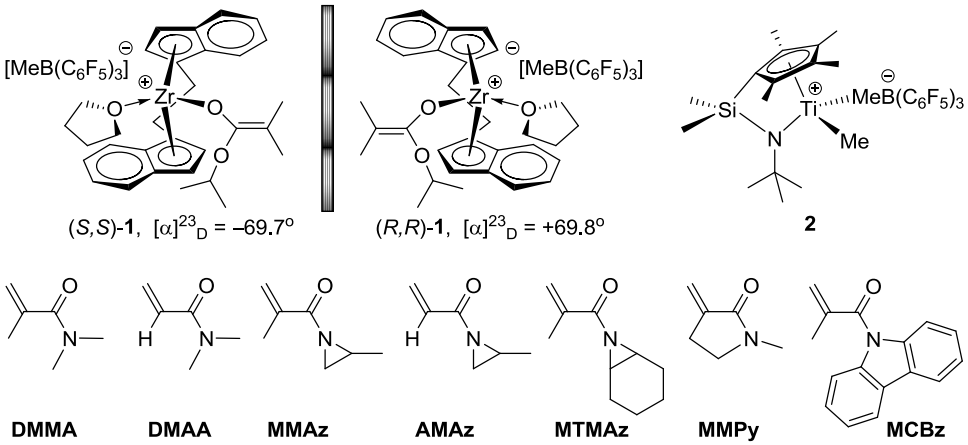

Experimental Section

Materials and Methods. All syntheses and manipulations of air- and moisture-sensitive materials were carried out in flamed Schlenk-type glassware on a dual-manifold Schlenk line, a high-vacuum line, or in an argon or nitrogen-filled glovebox. HPLC-grade organic solvents were sparged extensively with nitrogen during filling of the solvent reservoir and then dried by passage through activated alumina (for Et_2O, THF, and CH_2Cl_2) followed by passage through Q-5-supported copper catalyst (for toluene and hexanes) stainless steel columns. Benzene, Benzene-d_6 and toluene-d_8 were degassed, dried over sodium/potassium alloy and vacuum-distilled or filtered, whereas C_6D_5Br, $CDCl_3$, and CD_2Cl_2 were dried over activated Davison 4-Å molecular sieves. NMR spectra were recorded on either a Varian Inova 300 (FT 300 MHz, ^1H; 75 MHz, ^{13}C; 282 MHz, ^{19}F) or a Varian Inova 400 spectrometer. Chemical shifts for ^1H and ^{13}C spectra were referenced to internal solvent resonances and are reported as parts per million relative to tetramethylsilane, whereas ^{19}F NMR spectra were referenced to external $CFCl_3$. High resolution mass spectrometry (HRMS) data were collected using Agilent 6220 Accurate Time-of-flight LC/MS spectrometer.

Cyclohexene oxide, 2-methylaziridine, *n*-BuLi (1.6 M in hexanes), indene, 1,2-dibromoethane, tetrachlorozirconium, triflic acid, lithium dimethylamide, diisopropylamine, sodium azide, sodium hydride, 1,1,3,3-tetramethyl guanidine, (2*S*,4*S*)-pentanediol (99% *ee*, $[\alpha]^{20}_D$ +39.8 (c = 10, $CHCl_3$), (2*R*,4*R*)-pentanediol (97% *ee*, $[\alpha]^{21}_D$ –40.4 (c = 10, $CHCl_3$), $(CF_3SO_2)_2O$, $PhBCl_2$, MeMgI (3.0 M in diethyl ether), 1,2-dibromobenzene, and trifluoroacetic acid were purchased from Aldrich. Methacryloyl chloride, acryloyl chloride, triethylamine, *N,N*-dimethyl aniline, *N*-methylpyrrolidone, diethyl oxalate, carbazole, and 2,6-dimethyl pyridine were purchased from Alfa Aesar. Trimethylaluminum (neat) was purchased from Strem Chemical Co. and isopropyl isobutyrate was purchased from TCI America. All commercial reagents were used as received unless indicated as follows. Cyclohexene oxide, indene, 1,2-dibromoethane, 1,2-dibromobenzene, *N,N*-dimethyl aniline, methacryloyl chloride, and acryloyl chloride were

degassed using three freeze-pump-thaw cycles, while 2-methylaziridine, diisopropylamine, diethyl oxalate, $(CF_3SO_2)_2O$, and $PhBCl_2$ were vacuum-distilled. The following reagents, 2,6-dimethyl pyridine, triethylamine, and isopropyl isobutyrate were degassed and dried over CaH_2 overnight, followed by vacuum distillation. 1,4-Dioxane (Fisher) was degassed, dried over sodium/potassium alloy, and vacuum-distilled.

Tris(pentafluorophenyl)borane, $B(C_6F_5)_3$, was obtained as a research gift from Boulder Scientific Co. and further purified by recrystallization from hexanes at –35 ºC inside a glovebox. The $(C_6F_5)_3B$•THF adduct was prepared by addition of THF to a toluene solution of the borane followed by removal of the volatiles and drying in vacuo. Literature procedures were employed for the preparation of the following compounds and metallocene complexes: cyclohexenime,[67] $LiOC(O^iPr)=CMe_2$,[55] $(EBI)H_2$,[68] *rac*-$(EBI)Zr(NMe_2)_2$,[69] *rac*-$(EBI)ZrMe_2$,[69] *rac*-(EBI)ZrMe(OTf),[12] *rac*-(EBI)ZrMe[$OC(O^iPr)=CMe_2$],[12] *rac*-$(EBI)Zr^+(THF)[OC(O^iPr)=CMe_2][MeB(C_6F_5)_3]^-$ (**1**),[12] (*R,R*)- and (*S,S*)-$(EBI)ZrCl_2$,[70] (*R,R*)- and (*S,S*)-$(EBI)ZrMe_2$,[50,51] (*R,R*)- and (*S,S*)-(EBI)ZrMe(OTf),[50,51] (*R,R*)- and (*S,S*)-(EBI)ZrMe[$OC(O^iPr)=CMe_2$],[50,51] (*R,R*)- and (*S,S*)-**1**,[50,51] $(CGC)TiMe_2$,[71] and $CGCTiMe^+MeB(C_6F_5)_3^-$ (**2**).[72]

Monomer Preparations. Literature procedures were employed to prepare monomers methacryloyl-2-methylaziridine (MMAz),[66] acryloyl-2-methylaziridine (AMAz),[66] and α-methylene-*N*-methylpyrrolidone (MMPy).[73] Methacryloyl cyclohexenimine or methacryloyl tetramethyleneaziridine (MTMAz) was prepared by reacting cyclohexenimine with methacryloyl chloride in the presence of triethylamine. Specifically, a 200 mL Schlenk flask was loaded with cyclohexenimine (2.40 g, 24.7 mmol), triethylamine (2.49 g, 24.7 mmol), and CH_2Cl_2 (50 mL), and then capped with a septum. The solution of the mixture was cooled to 0 °C under positive N_2 flow before the dropwise addition of methacryloyl chloride (2.58 g, 24.7 mmol) via syringe. The reaction mixture was gradually warmed to room temperature, while being stirred for 15 h, after which the volatiles were removed in vacuo, affording a white solid. Et_2O (100 mL) was added to

the solid, and the resulting suspension was filtered through a medium porosity glass frit. The solvent of the filtrate was removed via roto-vap, and the residual monomer was purified by distillation, drying over CaH_2 overnight, and vacuum distillation (b.p. = 52–54 °C, 1 atm) affording 1.66 g (40.7%) of MTMAz as a colorless oil. ^{1}H NMR ($CDCl_3$, 23 °C): δ 5.99 and 5.55 (s, 2H, CH_2=), 2.61–2.59 (m, 2H, CH), 1.97–1.78 (m, 4H, CH_2), 1.90 (s, 3H, CH_3), 1.49–1.36 (m, 2H, CH_2), 1.19–1.17 (m, 2H, CH_2). ^{13}C NMR ($CDCl_3$, 23 °C): δ 180.9 (*C*=O), 139.5 (*C*=CH_2), 128.8 (C=*C*H_2), 36.39 (N*C*HCH_2), 23.65 (CH*C*$H_2$$CH_2$), 19.74 (CH$CH_2$*C*$H_2$), 18.38 (C*Me*). HRMS (APCI): *m*/*z* calcd for $C_{10}H_{16}NO$: $[M + H]^+$: 166.12264; found: 166.12296.

MCBz was prepared by reacting carbazole with methacryloyl chloride in THF in the presence of triethylamine. Specifically, a 500 mL Schlenk flask was loaded with carbazole (10.8 g, 64.6 mmol), triethylamine (6.54 g, 64.60 mmol), and 200 mL THF. The solution was cooled to 0 °C under positive N_2 flow before the dropwise addition of methacryloyl chloride (6.75 g, 64.59 mmol). The reaction mixture was gradually warmed to room temperature while being stirred for 24 h, after which the suspension was filtered through a medium porosity glass frit, the solvent of the filtrate was removed via roto-vap, and the resulting product was purified by three recrystallizations from a toluene/hexanes solution mixture affording a white solid (1.67 g, 10.9%) of MCBz. ^{1}H NMR ($CDCl_3$, 23 °C): δ 8.14 (d, *J* = 6.3 Hz, 2H, Ar), 8.01 (d, *J* = 5.7 Hz, 2H, Ar), 7.49–7.37 (m, 4H, Ar), 5.69 and 5.63 (s, 2H, CH_2=), 2.26 (s, 3H, CH_3). ^{13}C NMR ($CDCl_3$, 23 °C): δ 170.6 (*C*=O), 141.5 (*C*=CH_2), 138.4 (N*C*CH, Ar), 125.9 (C*C*CH, Ar), 122.4 (C=*C*H_2), 126.8, 123.4, 119.7 and 115.8 (Ar), 19.24 (C*Me*). HRMS (APCI): *m*/*z* calcd for $C_{16}H_{14}NO$: $[M + H]^+$: 236.10699; found: 236.10699.

General Polymerization Procedures. Polymerizations were performed in 30 mL oven-dried glass reactors inside the glovebox. In a typical polymerization procedure at ambient temperature, predetermined amounts of $B(C_6F_5)_3$•THF and the appropriate pre-catalyst were premixed in 10 mL of CH_2Cl_2 (for AMAz polymerizations) or 2 mL of CH_2Cl_2 (for MMAz and MTMAz polymerizations). For polymerizations with the (CGC)$TiMe_2$ precatalyst at 60 °C,

(CGC)$TiMe_2$ (7.80 mg, 23.8 μmol), $B(C_6F_5)_3$ (12.2 mg, 23.8 μmol), and 2 mL of 1,2-dichlorobenzene were added to a 25 mL Schlenk flask, which was capped with a septum. The flask was brought out of the box and connected to a Schlenk line and heated to 60 °C. After 10 min, the monomer (AMAz, 3.2 mmol; MMAz, 3.2 mmol; MTMAz, 1.5 mmol) was added via syringe and allowed to stir for a predetermined time interval. Polymerizations were stopped by pouring the solutions into a 10-fold excess of Et_2O and polymers were isolated by filtration or centrifugation, washed with Et_2O, and dried in vacuo at ambient temperature.

Kinetics of MMAz Polymerization. Kinetic experiments for the polymerization of MMAz were carried out in 30 mL reactors inside of the glovebox at room temperature using the similar procedure as already described above, except that, at appropriate time intervals, 0.1 mL aliquots were withdrawn from the reaction mixture using a syringe and quickly quenched into 1 mL septum-cap-sealed vials containing 0.6 mL of undried "wet" $CDCl_3$ mixed with 250 ppm of BHT-H. The quenched aliquots were analyzed by ^1H NMR for monomer conversion. The monomer conversion of MMAz at time *t* was determined by comparing the methyl singlet centered at 1.95 ppm of the unreacted monomer to the methyl peaks on the aziridine ring (monomer and polymer) and the methyl peak from the polymer main chain, which are centered at 1.30 ppm. Specifically, % monomer conversion was calculated by the formula $(A_{1.30} - A_{1.95})/(A_{1.30} + A_{1.95}) \times 100$, where $A_{1.30}$ is the total integral for the peaks centered at 1.30 ppm and $A_{1.95}$ is the total integral for the peak centered at 1.95 ppm.

Kinetic Resolution of (Meth)acryloyl-2-Methylaziridines: The kinetic resolution of (meth)acryloyl-2-methylaziridines was carried out in 30 mL reactors inside of the glovebox at ambient temperature using the similar procedure as already described above, except employing the enantiomeric catalyst (*S,S*)-**1**. At predetermined time intervals 0.1 mL (MMAz) or 0.2 mL (AMAz) aliquots were withdrawn from the polymerization reaction using a syringe and quickly quenched into 1 mL septum cap sealed vials containing 0.6 mL of undried "wet" $CDCl_3$ mixed

with 250 ppm of BHT-H. The quenched aliquots were analyzed by ^{1}H NMR for monomer conversion. The aliquots were then filtered through a silica column to completely remove polymer and catalyst residues, as confirmed by ^{1}H NMR and HPLC. The solvent was removed via roto-vap and the % *ee* of the monomer was measured using an Agilent 1100 Series HPLC with a flow rate of 1.0 mL/min. MMAz was analyzed with a Chiracel OB-H column at 25 °C (80:20 hexanes:^{i}PrOH, 1.0 mL/min, major enantiomer: 6.4 min, minor enantiomer: 7.8 min). AMAz was analyzed with a Chiracel AS-H column at 25 °C (97:3 hexanes:^{i}PrOH, 1.0 mL/min, major enantiomer: 11.2 min, minor enantiomer 10.4 min).

Polymer Characterizations. Gel permeation chromatography (GPC) and light scattering (LS) analyses of the polymers were carried out at 40 ºC and a flow rate of 1.0 mL/min, with DMF (for PMMAz samples produced by **1**) or $CHCl_3$ (for all other samples) as the eluent, on a Waters University 1500 GPC instrument and Wyatt miniDAWN Treos equipped with four 5 μm PL gel columns (Polymer Laboratories). LS data were processed with Wyatt Astra Software (version 5.3.2.15) and *dn/dc* values were determined assuming 100% mass recovery of polymers with known concentrations.

Maximum rate decomposition temperatures (T_{max}) and decomposition onset temperatures (T_{onset}) of the polymers were measured by thermal gravimetric analysis (TGA) on a TGA 2950 Thermogravimetric Analyszer, TA Instrument. Polymer samples were heated from ambient temperature to 600 °C at a rate of 20 °C/min. Values for T_{max} were obtained from derivative (wt%/°C) versus temperature (°C) plots while T_{onset} and T_{end} values (initial and end temperatures) were obtained from wt% *versus* temperature (°C) plots. Glass transition temperatures (T_g) and cross-linking temperatures (T_c) of the polymers were measured by differential scanning calorimetry (DSC) on a DSC 2920, TA Instrument.

Computational Details. The Amsterdam Density Functional (ADF) program[74] was used to obtain all the results concerning the mechanism of stereoselectivity. The electronic configuration

of the molecular systems was described by a triple-ζ STO basis set on Zr (ADF basis set TZV).[74a] Triple-ζ STO basis sets, augmented by one polarization function, were used for main group atoms (ADF basis sets TZVP).[74a] The inner shells on Zr (including 3d), C, N and O (1s), were treated within the frozen core approximation. Energies and geometries were evaluated using the local exchange-correlation potential by Vosko et al.,[75] augmented in a self-consistent manner with Becke's[76] exchange gradient correction and Perdew's[77] correlation gradient correction (BP86 functional). All geometries were localized in the gas phase. However, since methacrylamide polymerization is usually performed in a rather polar solvent, such as CH_2Cl_2, we performed single point energy calculations on the final geometries to take into account solvent effects. The ADF implementation of the conductor-like screening model (COSMO)[78] was used. A dielectric constant of 8.9, and a solvent radius of 2.94 Å were used to represent CH_2Cl_2 as the solvent. The following radii, in Å, were used for the atoms: H 1.16, C 2.00, N 1.40, O 1.50 and Zr 2.40. All the reported energies include solvent effects.

Results and Discussion

Polymerization of Methacrylamide MMAz. We have previously reported that the living/controlled polymerization of *N,N*-dialkyl and *N,N*-diaryl acrylamides by catalyst **1** proceeds via a monometallic, site-controlled, coordination-(conjugated) addition mechanism through eight-membered-ring amide enolate intermediates (Scheme 1).[50,52] The resting state during a propagation "catalysis" cycle is the cyclic amide enolate, and associative displacement of the coordinated penultimate amide group by incoming acrylamide monomer to regenerate the catalyst–monomer complex is the rate-determining step, giving rise to the propagation kinetics that is first order in both concentrations of the monomer and the catalyst. We also noted that the methacrylamide DMMA is not polymerized by such metallocene catalysts.[52]

Scheme 1. Initiation and Propagation Steps Involved in the Polymerization of Acrylamides by *rac*-1.

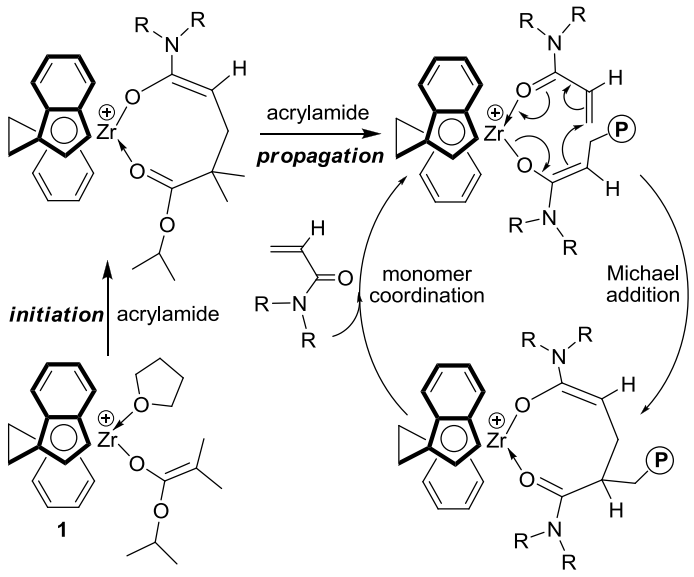

As a control to examine whether the reactive aziridine ring incorporated in the predictably polymerizable MMAz would remain intact under our metallocene polymerization conditions or not, we first investigated the polymerization of the acrylamide AMAz (which also adopts a stable conjugated *s-cis* conformation as predicted by DFT) with chiral, racemic catalyst **1** in CH_2Cl_2 at room temperature. The polymerization of 100 equiv AMAz by 1 equiv of **1** is rapid, achieving quantitative monomer conversion in < 1 min; it proceeds exclusively via C–C bond formation, as shown by the disappearance of the monomer vinyl protons, while leaving the aziridine ring intact, as confirmed by ^{1}H NMR of the resulting polymer. The polymer obtained has a M_w of 13.1 kg/mol (by LS detector) with a narrow MWD of 1.02 (run 1, Table 1), giving an initiator efficiency (I^*) of 87%. Hence, the polymerization of AMAz is fast, efficient and controlled, and it involves no ring-opening of the aziridine ring under the current conditions.

Table 1. Results of Polymerization of (Meth)acrylamides by 1 at Ambient Temperature [a]

run no.	monomer	[M]/[**1**]	time (min)	conv[b] (%)	M_w[c] (kg/mol)	PDI[c] (M_w/M_n)	I^*[d] (%)
1	AMAz	100	<1	100	13.1	1.02	87
2	MMAz	100	60	85.3	12.3	1.01	89
3	MMAz	200	60	81.3	22.3	<1.01	92
4	MMAz	400	60	83.9	80.9	<1.01	52
5	MTMAz	100	60	93.9	25.1	1.02	65

[a] Carried out in 10 mL (for AMAz) or in 2 mL (for MMAz and MTMAz) of CH_2Cl_2 at ambient temperature (~23 °C). [b] Monomer conversion measured by ^{1}H NMR. [c] Determined by light scattering. [d] Initiator efficiency (I^*) = M_n(calcd)/M_n(exptl), where M_n(calcd) = MW(M) × [M]/[**1**] × conversion% + MW of chain-end groups.

Having established the inertness of the aziridine ring toward the metallocene polymerization conditions, we subsequently investigated the polymerization of the methacrylamide MMAz by **1**. Gratifyingly, like the polymerization of AMAz, the polymerization of MMAz by **1** is effective and controlled (runs 2–4 vs. run 1, Table 1), although the latter polymerization is considerably slower even with a 5-fold increased concentration and did not achieve a high initiator efficiency at a higher [M]/[**1**] ratio of 400. Nonetheless, the MMAz polymerization by **1** exhibits a high degree of control in [M]/[**1**] ratios of ≤ 200, producing the well-defined polymer without ring-opening of the aziridine moiety within the MMAz repeat unit. As expected, this polymerization by the isospecific catalyst **1** yields the highly isotactic polymer, as shown by the ^{13}C NMR spectrum of the polymer (Figure 1).

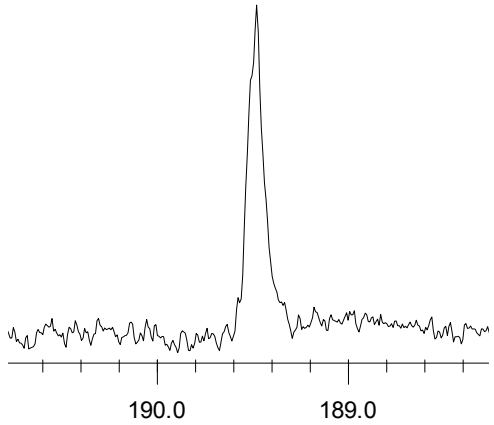

Figure 1. ^{13}C NMR showing the C=O region of poly(MMAz) (run 4, Table 1) in $CDCl_3$ at 60 °C.

Monitoring of the MMAz polymerization by **1** in a [M]/[**1**] ratio of 100 reveals a first-order dependence on [MMAz], a linear increase in MW with monomer conversion, and narrow MWDs ranging from 1.14–1.01 (Figure 2). Kinetic experiments employed the $[MMAz]_0/[\mathbf{1}]_0$ ratios ranging from 100–400, showing the first-order dependence on [MMAz] for the ratios (Figure 3). Furthermore, a double logarithm plot (Figure 4) of the apparent rate constants (k_{app}), obtained from the slopes of the best-fit lines to the plots of $\ln([MMAz]_0/[\mathbf{1}]_0)$ vs. time as a function of $\ln[\mathbf{1}]_0$, was fit to a straight line (R^2 = 0.99) with a slope of 1.12. Thus, the kinetic order with respect to [**1**], given by the slope of ~ 1, reveals that the propagation is also first order in catalyst concentration, indicating that the polymerization of MMAz by catalyst **1** follows the same coordination-addition mechanism as that of the acrylamide polymerization shown in Scheme 1.

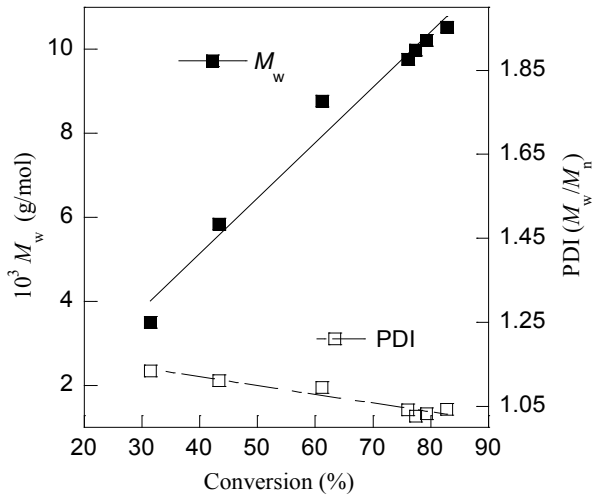

Figure 2. Plots of M_w and PDI of poly(MMAz) versus MMAz conversion in CH_2Cl_2 at ambient temperature (~23 °C): [MMAz] = 1.59 M, [*rac*-**1**] = 15.9 mM.

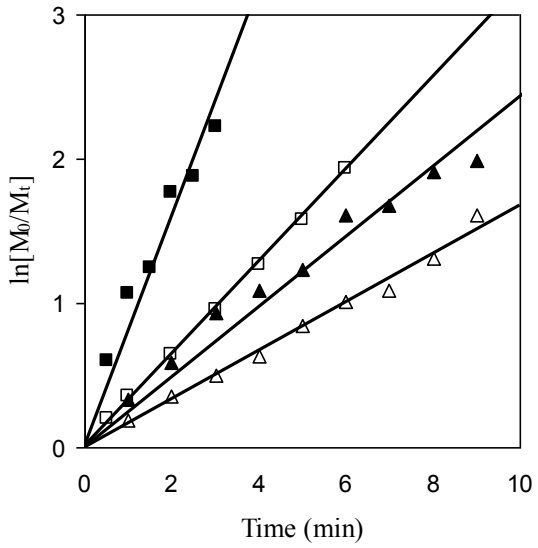

Figure 3. Semilogarithmic plots of $\ln([MMAz]_0/[MMAz]_t)$ vs time for the polymerization of MMAz by **1** in CH_2Cl_2 at ambient temperature (~23 ºC). Conditions: $[MMAz]_0$ = 1.59 M; $[\mathbf{1}]_0$ = 15.9 mM (■), 7.99 mM (□), 5.33 mM (▲), 3.99 mM (Δ).

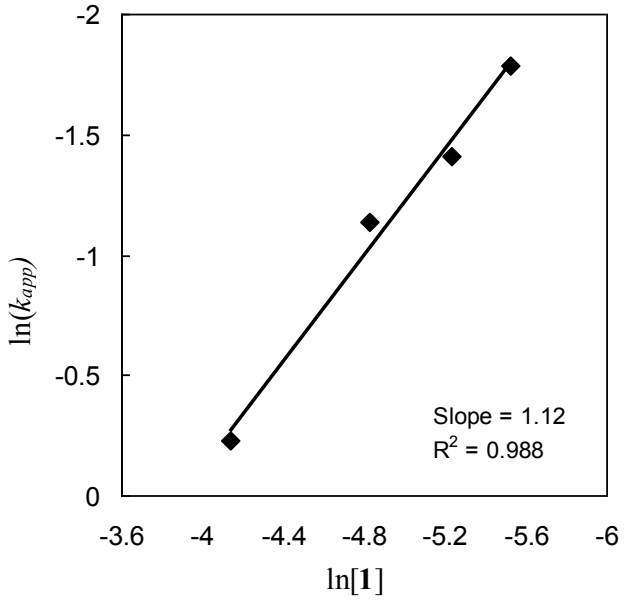

Figure 4. Plot of $\ln(k_{app})$ vs. ln[**1**] for the MMAz polymerization by **1** in CH_2Cl_2 at ambient temperature (~23 °C).

We also examined the MMAz polymerization using the C_s-ligated titanium alkyl complex **2**. The polymerization of 200 equiv of MMAz by 1 equiv of **2** in CH_2Cl_2 is sluggish at ambient temperature, achieving only 62.6 % monomer conversion in 27 h. The polymer produced exhibits a narrow MWD of 1.17 but its measured M_w of 108 kg/mol (by LS) is much larger than the calculated according to the monomer to catalyst feed ratio of 200. The rate of this polymerization is significantly enhanced when carried out at 60 °C in 1,2-dichlorobenzene, achieving similar conversion (64.7 %) in just 5 h. Again, the measured M_w of 104 kg/mol for the resulting polymer is considerably higher than the calculated, and the polymer produced at this elevated temperature also has a broader MWD of 1.38. The much higher MWs of these polymers afforded by **2** are presumably related to slow initiation by the titanium–alkyl ligand in **2**, as compared to propagation by the titanium–amide enolate ligand, while the broader MWD of the polymer produced at elevated temperature may be contributed to side reactions such as non-coordination pathways (i.e., radical polymerization) known for acrylamide polymerization by metallocene alkyl complexes[53] and partial ring-opening of the aziridine ring. The syndiotacticity of the poly(MMAz) cannot be accurately determined by ^{13}C NMR due to the overlapping of the *mr* and *rr* triad peaks in the C=O region.

Thermal Properties of Methacrylamide Polymers Incorporating the Aziridine Ring. We reasoned that substituents on the highly strained aziridine ring should sterically protect it against ring opening, thus making it less susceptible to thermally induced cross-linking. To this end, we synthesized an additional methacrylamide polymer, poly(MTMAz) with cyclic tetramethylene substitution, for a comparative study. The MTMAz monomer (Chart 1) was readily polymerized by **1** at ambient temperature in a [M]/[**1**] ratio of 100, achieving 94% monomer conversion in 1 h. The poly(MTMAz) obtained has a M_w of 25.1 kg/mol and a narrow MWD of 1.02 (run 5, Table 1). This polymer, together with poly(AMAz) and poly(MMAz)s produced by **1**, was analyzed by TGA and DSC.

TGA results showed that the methacrylamide polymers are more resistant to thermal degradation than the acrylamide derivative. Specifically, poly(MMAz) and poly(MTMAz) exhibit T_{onset} (initial) at 406 °C (T_{max} = 443 °C) and 391 °C (T_{max} = 435 °C), respectively, while poly(AMAz) has a T_{onset} at a much lower temperature of 337 °C (T_{max} = 419 °C). Interestingly, although all three polymers decomposed in a single decomposition process, the decomposition window for poly(AMAz) is much larger than either poly(MMAz) or poly(MTMAz). Thus, poly(AMAz) exhibits a T_{end} of 453 °C, while poly(MMAz) and poly(MTMAz) show T_{end} of 464 °C and 446 °C, respectively.

DSC analyses determined a higher T_g of 92.9 °C for poly(MMAz), as compared to a T_g of 57.7 °C for poly(AMAz); no noticeable glass transition was observable for poly(MTMAz). We also utilized DSC (Figure 5) to monitor the temperature (T_c, c for curing or cross-linking) required for inducing thermal cross-linking of the polymers through ring-opening of the aziridine ring.[66] The onset temperature for cross-linking of poly(AMAz) (118 °C) is lower than that of poly(MMAz (143 °C), but, interestingly, the temperature for maximum cross-linking of poly(AMAz) (206 °C) is higher than that of poly(MMAz) (189 °C), again reflecting a broad curing temperature window for poly(AMAz). Most significantly, poly(MTMAz) has a high onset T_c of 199 °C and maximum T_c of 231 °C, corresponding to the thermal enhancements of 57 and 42 °C in T_c indices as compared to poly(MMAz)!

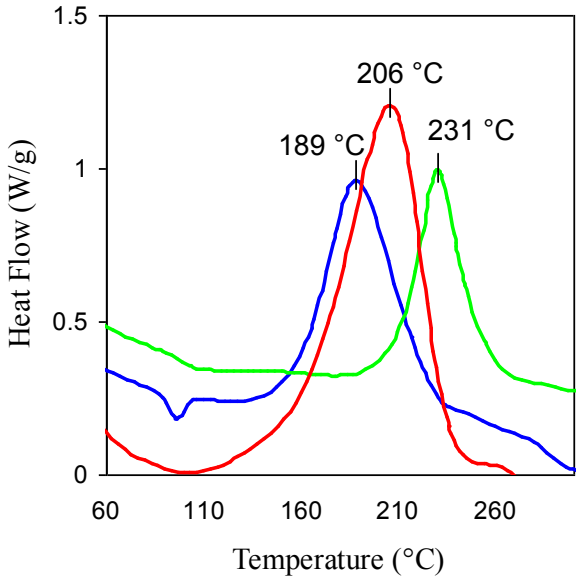

Figure 5. DSC plots of poly(MMAz) (blue), poly(AMAz) (red), and poly(MTMAz) (green) acquired at a scanning rate of 10 °C/min.

Kinetic Resolution of Methacrylamide MMAz. The above described success in the living/controlled polymerization of racemic AMAz and MMAz by the racemic catalyst **1** provided a strong basis for our investigation into the potential capability of the enantiomeric metallocene catalyst to discriminate between two enantiomers of the chiral methacrylamide monomer. Scheme 2 outlines the strategy of using enantiomeric catalyst (*S,S*)-**1** to preferentially polymerize one enantiomer from the racemic MMAz poor under ≤50% conversion, thus producing the chiral polymer enriched with this enantiomer while leaving the other enantiomer enriched in the unreacted monomer. To follow this reasoning, we first examined kinetic resolution of AMAz using enantiomeric (*S,S*)-**1** at ambient temperature by taking an aliquot of the polymerization at a monomer conversion of 53.5%. The unreacted monomer (after complete removal of the polymer and the catalyst residue) was then analyzed by chiral HPLC and found to have a low *ee* of 8.8%, giving a low stereoselectivity factor, or *s* value,[79] of 1.2. As this

polymerization is extremely rapid and complete in <1 min even in dilute conditions, a function of % *ee* vs. monomer conversion was not determined.

Scheme 2. Proposed Kinetic Resolution Polymerization of Racemic MMAz by Enantiomeric (*S*,*S*)-1

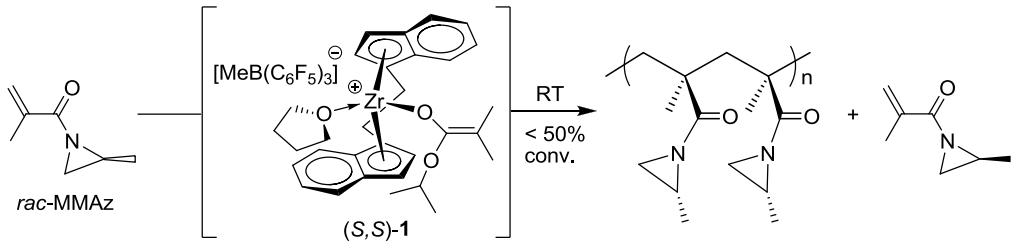

Next, we employed (*S,S*)-**1** to determine its ability to kinetically resolve MMAz. With the slower polymerization rate of MMAz, we were able to analyze several aliquots from a single polymerization reaction and compare the % *ee* values of the unreacted monomer vs. % monomer conversion (Figure 6). In the case of MMAz, enantiomeric (*S,S*)-**1** discriminates the enantiomers of the monomer to a greater extent than with MAz, although the kinetic resolution of MMAz is still inefficient (~ 1.8 *s* values for all aliquots analyzed). Given the stereo-differentiation rendered by a rather small methyl group at the remote γ position (in respect to the carbon-carbon double bond) of the monomer, the kinetic resolution of MMAz by the enantiomeric catalyst **1** can be appreciated. It is likely that a larger substituent, such as isopropyl or *tert*-butyl, or modified catalyst structures, could lead to a greatly enhanced kinetic resolution of such racemic monomers, which will be a subject of our continued investigation in this area.

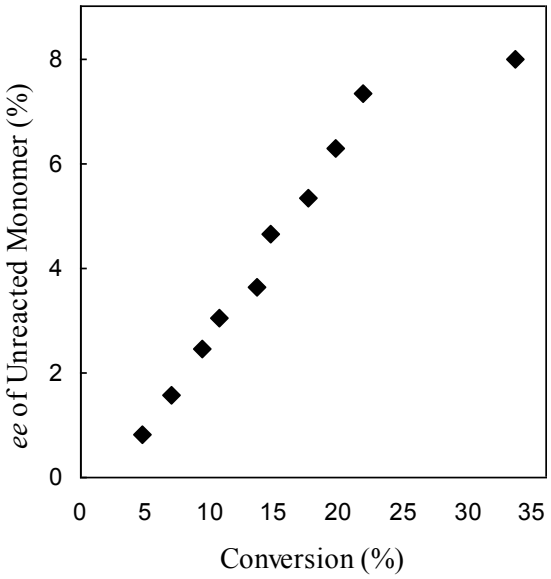

Figure 6. Plot of % *ee* of the unreacted MMAz vs. % monomer conversion for the kinetic resolution of MMAz by enantiomeric catalyst (*S,S*)-**1** at ambient temperature.

Enantioselectivity in the kinetic resolution of MMAz was examined by DFT calculations. We first investigated enantiofacial selectivity in the polymerization of the achiral *N*-methacryloylaziridine. As anticipated, DFT calculations analogous to those performed by some of us to rationalize the enantioselectivity in the polymerization of methyl methacrylate with C_2-symmetric metallocenes,[57] resulted in a $\Delta E^{\neq}_{\text{Stereo}}$ of ~3.5 kcal/mol, which is in qualitative agreement with the highly isotactic polymer obtained from the polymerization of MMAz. The most favored transition state was then used to investigate the kinetic resolution of the chiral racemic MMAz by adding a methyl group on the aziridine ring of both the monomer and the growing chain. Since two chiral C atoms are generated, we considered 4 possible transition states corresponding to different combinations of chirality on the growing chain and on the monomer. These four transition states are defined as *R*-chain/*R*-MMAz if *R* is the configuration of both chiral C atoms, *R*-chain/*S*-MMAz if *R* and *S* are the configuration of the chiral C atoms on the chain and on the monomer, respectively, and so on. The relative stability of these four transition states is reported in Table 2. In all cases we considered a (*S,S*) coordination of the EBI ligand.

Table 2. Relative Energies of Four Transition States for the Polymerization of MMAz by (*S*,*S*)-1.

Transition state	*E* (kcal/mol)
R-Chain/*R*-MMAz	0.0
R-Chain/*S*-MMAz	0.4
S-Chain/*R*-MMAz	1.1
S-Chain/*S*-MMAz	0.9

The numbers reported in Table 2 indicate that whatever is the configuration of the chiral C atom of the aziridine ring in the growing chain, there is no substantial selectivity in the selection between the two enantiomers of MMAz. In fact, in the case of an *R*-chain, addition of *R*-MMAz is favored by only 0.4 kcal/mol with respect to addition of *S*-MMAz, while in the case of an *S*-chain, addition of *S*-MMAz is favored by only 0.2 kcal/mol with respect to addition of *R*-MMAz. Although the most stable transition state corresponds to addition of an *R*-MMAz to an *R*-chain, it is clear that the small energy differences we calculated are in qualitative agreement with the low kinetic resolution obtained experimentally. The structures of the four transition states, depicted in Figure 7, clearly show that in all cases the methyl group on the aziridine ring can be placed quite away from the EBI ligand as well as from other atoms of the chain and of the monomer, which explains the low efficiency of the kinetic resolution.

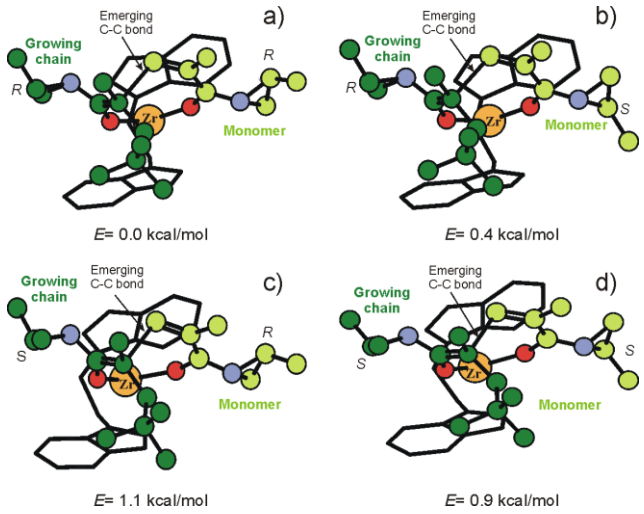

Figure 7. Transition states for the kinetic resolution of MMAz by (*S*,*S*)-**1**. Hydrogen atoms were omitted for clarity.

Polymerizability of Methacrylamides. Within two polymerizable methacrylamides (MMAz and MTMAz) investigated so far, the highly strained three-membered aziridine ring built into the methacrylamide monomer structure is believed to render their stable planar conjugated monomer conformations. Natural questions are how the aziridine ring works in this function and can one identify other moieties function the same way. Successfully addressing these questions will promote rational design of polymerizable methacrylamides and thus substantially expand the polymerizable methacrylamide monomer family.

An apparent design of a planar methacrylamide monomer is to covalently link the α-methyl to one of the methyl groups on N as in the monomer structure of MMPy (Chart 1) which was shown to be radically polymerizable.[73] Another approach is to place sterically bulky, rigid aromatic groups on N for its conjugation with the aromatic ring rather than with the carbonyl group, which could prevent twisting of the C=C bond relative to the C=O bond. To this end, we resided the monomer MCBz (Chart 1). However, neither MMPy nor MCBz was polymerized by **1**, even with extended reaction times (24 h) or elevated temperatures (80 °C). In radical polymerization using AIBN as initiator, MMPy[73] is less reactive than MMAz,[66] which can be explained by the effectiveness of conjugation between the vinyl and carbonyl double bonds, derived from analysis of NMR spectra of monomers as shown by Kodaira et al.[64] Specifically, as effective conjugation in such *α,β*-unsaturated amide monomers downfield-shifts the vinyl protons rendering the more reactive C=C double bond, comparing the vinyl proton ^{1}H NMR ($CDCl_3$) chemical shifts in MMPy (δ 5.81 and 5.19 ppm) vs. those in MMAz (δ 6.09 and 5.63 ppm) suggests poor π overlap between the vinyl and carbonyl double bonds in MMPy; this also explains the inactivity of catalyst **1** toward MMPy in that the C=C double has low reactivity reflected by the upfield-shifted vinyl protons.

Likewise, inspection of the NMR spectra of MCBz provides insight into its non-polymerizability by catalyst **1**. First, in its ^{1}H NMR, the vinyl protons have resonances at 5.69 and 5.63 ppm in $CDCl_3$, as in the case of the non-polymerizable DMMA (δ 5.19 and 5.03 ppm),

corresponding to the much higher magnetic field than the vinyl protons in the polymerizable MMAz. Second, if there is effective conjugation between the vinyl and carbonyl double bonds, then in the ^{13}C NMR there shows a small $\Delta\delta$ between the α- and β-carbon chemical shifts. Accordingly, the non-polymerizable MCBz and DMMA have $\Delta\delta$ of 19.1 ppm and 25.4, respectively, while the polymerizable MTMAz, MMA and MMAz have smaller Δδ of 10.7 ppm, 10.8 ppm and 15.3 ppm, respectively.

To systematically rationalize the reactivity of the different acrylamides listed in Chart 1, we performed DFT calculations on these monomer molecules. To characterize the assumed geometry, we use the torsional angle θ, defined as the C=C–C=O torsional angle (Chart 2), and the torsional angle ω, defined as the O=C–N–X_C torsional angle, where X_C is the middle point between the two C atoms bonded to the N atom (Chart 2). According to this definition, if the C=C bond and the N atom are conjugated to the C=O bond, then the θ and ω dihedral angles should be close to 0° and 90°, respectively.

Chart 2. Definition of the Torsional Angles θ and ω in *N,N*-Dialkyl Methacrylamides.

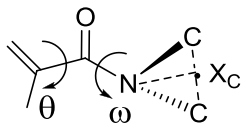

According to our DFT calculations, DMAA, MMAz, AMAz, MTMAz and MMPy assume a substantially planar geometry based on their small θ values (3.4–12.9°, Table 3), whereas DMMA and MCBz assume a strongly non-planar geometry, as indicated by their θ value of 131.0° and 137.7°, respectively. As described in the Introduction, DMMA is forced to assume a non-planar conformation at both the θ and ω angles because of steric repulsion between the methacrylic methyl and one of the N-bonded methyl groups.

Table 3. DFT Calculated Torsional Angles and Energies of Amide Enolate Formation.

Monomer	θ (deg)	ω (deg)	*E* (kcal/mol)
DMAA	6.3	59.7	19.2
MMAz	9.7°	66.5	18.4
AMAz	3.4°	73.7	14.3
MTMAz	12.9°	72.4	16.9
MMPy	6.0°	112.9	26.8
DMMA	131.0°	46.5	22.5
MCBz	137.7°	2.6	10.4

Moving to the ω angle we found that with the exception of MCBz, which presents an ω angle close to 0°, all the monomers present ω angles deviating considerably from 90° (see Table 3), which indicates somewhat limited conjugation of the N lone pair to the C=O bond. Moreover, in AMAz, MMAz and MTMAz the geometric constraint of the three-membered aziridine ring forces an almost sp^3 hybridization at the N atom, which results in remarkably reduced ring strain[80] but imposes a pyramidal geometry at the N atom. Consequently, the lone pair of the N atom is in a sp^3 atomic orbital that geometrically cannot overlap properly with π orbitals of the C=O bond in AMAz, MMAz and MTMAz, suppressing conjugation between the N atom and the C=O bond. However, in terms of monomer geometry the presence of the aziridine ring, as previously noted, pulls the N substituents away from the methacryclic methyl group, allowing for the monomers to assume a planar geometry around the θ angle. The ω close to 0° of MCBz, which indicates complete absence of conjugation between the N atom and the C=O bond, can be rationalized considering that the N atom participates to the extended aromatic systems of the N-substituent.

Focusing on the θ angle, our findings qualitatively correlate with the proposal that non-planar acrylamides, such as DMMA and MCBz, are non-polymerizable because of poor overlap between the π orbitals of the vinyl C=C and carbonyl C=O bonds. The only exception here is represented by MMPy, which is planar but non-polymerizable by the current catalyst system. In order to provide further insights into this issue, we also investigated the enolate formation

energies that can formally be derived from the hypothetic reaction depicted in Scheme 3 in the case of DMMA. This reaction allows us to investigate the acrylamide to enolate conversion without the steric bulkiness of the (EBI)Zr ligand. The basic idea here is that the amide-enolate is a good model of the amide-enolate chain formed during the polymerization.

Scheme 3. Hypothetic Reaction Designed to Investigate the Stability of the Amide-Enolate Chain

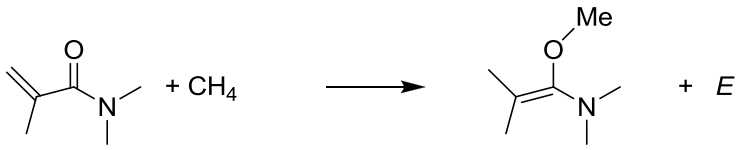

The energetic values *E* of the reaction shown in Chart 3 are reported also in Table 3. First, all the *E* values are positive, which means that the amide-enolates are less stable than separated acrylamide and methane. Within this scheme, the smaller is *E* the easiest is enolate formation and, consequently, polymerization. Indeed, our calculations indicate that the polymerizable DMAA, MMAz, AMAz and MTMAz monomers exhibit rather smaller *E* values compared to the non polymerizable DMMA and MMPy monomers. The only exception here is represented by MCBz.

The relative stability of the enolate intermediates can be easily rationalized considering that a formal C=C double bond is localized on the internal C–C bond of the monomers. The amide-enolate from DMMA, *E* = 22.5 kcal/mol, is destabilized by the same steric interactions that impose a non-planar geometry in the monomer. The amide-enolate from MMPy, *E* = 26.8 kcal/mol, is destabilized by having the C=C bond moved into the six-membered ring, which introduces higher ring stain. In the DMAA, AMAz, MMAz and MTMAz derived amide-enolates, *E* = 14.3–19.2 kcal/mol, the geometric constraint of the three-membered-aziridine ring, as discussed above, prevents the N atom to assume a sp^2 planar geometry, so that the N atom is not conjugated to the C=C bond, and no steric interaction between the N substituents and other groups are introduced. MCBz, with a *E* = 10.4 kcal/mol, presents the only exception. This low *E*

value is associated with the participation of the N atom to the extended aromatic systems of the N-substituent. As noted above, this interaction effectively removes participation of N atom of MCBz to the amide bond, which reduces the energy loss in the monomer to enolate transformation. According to this chemical framework, MCBz should be a highly polymerizable monomer. However, MCBz is by far the monomer with the bulkier N group, which suggests that the experimental non-polymerizability of MCBz could be connected to severe steric repulsion between the bulky aromatic N-substituent and the metallocene skeleton. To investigate better this point, we investigated the transition state of the Michael addition step in the case of MCBz, see Figure 8.

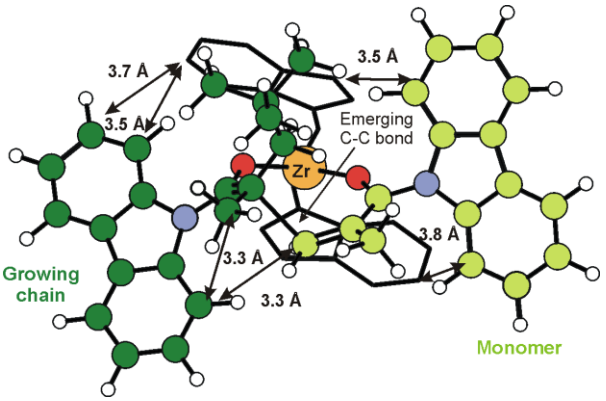

Figure 8. Transition state for the Michael addition in MCBz polymerization by **1**.

Visual inspection reveals several short distances between atoms of the bulky *N*-substituent of both the growing chain and the monomer with other atoms. The remarkable steric pressure in the transition state revealed in Figure 8 is also evident by comparison with the stable transition states of MMAz, (see Figure 7). Energetically, to reach the transition state for Michael addition from separated (EBI)Zr-(amide-enolate) and monomer, (see Scheme 4) is approximately 20 kcal/mol more expensive for MCBz than for MMAz, which is another indication of the highly destabilizing steric interactions in the case of MCBz polymerization.

Scheme 4. Reaction Used to Estimate Steric Effects in MCBz Polymerization by **1**

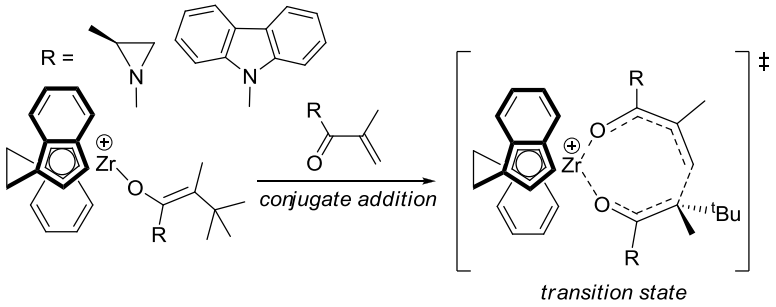

Concluding this part, our DFT results suggest that DMAA, AMAz, MMAz and MTMAz are polymerizable monomers toward conjugate addition polymerization due to stability of the resulting amide enolate chain. As for the non-polymerizable DMMA, MMPy and MCBz monomers, DMMA is non-polymerizable because of steric repulsion between the *N*-substituents and the methyl group in the methacrylic position, MMPy is non-polymerizable because of ring strain in the amide-enolate growing chain, and MCBz is non-polymerizable because of steric repulsion between the large *N* substituent and the EBI skeleton during the Michael addition step.

Conclusions

We reported in this contribution the first successful coordination-addition polymerization of *N,N*-dialkyl *methacrylamides* by metallocene catalysts. The polymerizable methacrylamides investigated in this study are MMAz and MTMAz, both of which incorporate the highly strained three-membered aziridine ring. The geometric constraint of the aziridine ring forces an almost sp^3 hybridization at the N atom that adopts a pyramidal geometry and suppresses conjugation between the N atom and the C=O bond, thereby effectively pulling the N substituents away from the methacryclic methyl group and allowing for the monomers to assume a planar geometry with substantial conjugation between the vinyl and carbonyl double bonds.

The polymerization by chiral zirconocenium catalyst **1** is highly stereospecific and exhibits a high degree of control over polymerization. Kinetic studies showed that the methacrylamide polymerization proceeds in the same manner as the acrylamide polymerization by **1**, with

intramolecular conjugate addition within the catalyst–monomer complex being the fast step and associative displacement of the coordinated penultimate amide group within the eight-membered-ring amide enolate resting intermediate by incoming monomer to regenerate the catalyst–monomer complex being the rate-determining step.

Excitingly, we demonstrated experimentally and theoretically the capability of enantiomeric catalyst **1** for kinetic resolution of the racemic MMAz monomer. The stereoselectivity factor ($s \sim 1.8$) is currently low but still appreciative, given the small methyl group on the aziridine ring. It is anticipated that larger substituents with more pronounced stereo-differentiation will greatly enhance kinetic resolution of such racemic methacrylamide monomers by this catalyst. The research directed to this effort is underway.

We also investigated the scope of the polymerizable methacrylamide monomers for two purposes. First, the substituent on the highly strained aziridine ring was explored to module thermally induce cross-linking process occurring through ring-opening of the aziridine ring. To this end, we found that poly(MTMAz) with the cyclic tetramethylene substitution greatly enhance resistance towards thermal cross-linking as marked by an enhancement of 57 °C in onset T_c and 42 °C in maximum T_c over poly(MMAz) with the methyl substitution. Second, pendant moieties other than aziridines were explored to overcome the propensity for *N,N*-disubstituted methacrylamides to assume the twisted confirmation. Although neither of the monomers tested (MMPy and MCBz) derived from two different designs are polymerizable using metallocene catalyst **1**, analysis of their ^{1}H and ^{13}C NMR features and comparing them with the known conjugated polymerizable *α,β*-unsaturated ester and amide monomers provided insight into their non-polymerizability or relative reactivity. These studies, combined with DFT calculations on the monomer geometry and relative energy for the formation of amide-enolate intermediates, show that non-polymerizable methacrylamides either do not exhibit conjugation between the C=C and C=O bonds (e.g., DMMA, MCBz) or have high energy for the amide enolate formation (e.g., MMPy).

Acknowledgment. This work was supported by the National Science Foundation (NSF-0718061) for the work carried out at Colorado State University and INSTM (Cineca Grant Key-Project 2008) for the work carried out at the University of Salerno. We thank Prof. Tom Rovis (CSU) for assistance in % *ee* measurements and Boulder Scientific Co. for the research gift of $B(C_6F_5)_3$. This dissertation chapter contains the manuscript of a full paper published in *Macromolecules* [Miyake, G. M.; Caporaso, L.; Cavallo, L.; Chen, E. Y.-X. *Macromolecules* **2009**, *42*, 1462-1471]. Caporaso and Cavallo performed the computational portion of this work.

References

(1) Selected recent reference works and reviews: (a) Chen, E. Y.-X.; Rodriguez-Delgado, A. "Complexes of Zirconium and Hafnium in Oxidation State IV" in *Comprehensive Organometallic Chemistry III;* Bochmann, M. Vol. Ed.; Mingos, M. P.; Crabtree, R. H. Chief Eds.; Elsevier: Oxford, **2007**; Vol. 4, pp 759−1004. (b) Cuenca, T. "Complexes of Titanium in Oxidation State IV" in *Comprehensive Organometallic Chemistry III;* Bochmann, M. Vol. Ed.; Mingos, M. P.; Crabtree, R. H. Chief Eds.; Elsevier: Oxford, **2007**; Vol. 4, pp 323−696. (d) Bochmann, M. Cationic Group 4 Metallocene Complexes and Their Role in Polymerisation Catalysis: the Chemistry of Well Defined Ziegler Catlaysts. *J. Chem. Soc. Dalton Trans.* **1996**, 255−270. (e) Jordan, R. F. Chemistry of Cationic Dicyclopentadienyl Group 4 Metal–Alkyl Complexes. *Adv. Organomet. Chem.* **1991**, *32*, 325−387.

(2) Selected books, reference works, or journal reviews: (a) *Stereoselective Polymerization with Single-Site Catalysts*, Baugh, L. S.; Canich, J. A. M., Eds.; CRC Press: Boca Raton, FL, **2007**. (b) Resconi, L.; Chadwick, J. C.; Cavallo, L. "Olefin Polymerizations with Group IV Metal Catalysts" in *Comprehensive Organometallic Chemistry III;* Bochmann, M. Vol. Ed.; Mingos, M. P.; Crabtree, R. H. Chief Eds.; Elsevier: Oxford, **2007**; Vol. 4, pp 1005−1166. (c) Domski, G. J.; Rose, J. M.; Coates, G. W.; Bolig, A. D.; Brookhart, M. Living Alkene Polymerization: New Methods for the Precision Synthesis of Polyolefins. *Prog. Polym. Sci.* **2007**, *32*, 30−92. (d) Marks, T. J. Ed. *Proc. Natl. Acad. Sci. U.S.A.* **2006**, *103*, 15288−15354 and contributions therein (issue on "*Polymerization Special Feature*"). (e) Gibson, V. C.; Spitzmesser, S. K. Advances in Non-Metallocene Olefin Polymerization Catalysis. *Chem. Rev.* **2003**, *103*, 283−315. (f) Gladysz, J. A., Ed. *Chem. Rev.* **2000**, *100*, 1167−1681 and contributions therein (issue on *Frontiers in Metal-Catalyzed Polymerization*). (g) Brintzinger, H. H.; Fischer, D.; Mülhaupt, R.;

Rieger, B.; Waymouth, R. M. Stereospecific Olefin Polymerization. *Angew. Chem., Int. Ed.* **1995**, *34*, 1143−1170.

(3) Ning, Y.; Chen, E. Y.-X. *J. Am. Chem. Soc.* **2008**, *130*, 2463−2465.

(4) Mariott, W. R.; Escudé, N. C.; Chen, E. Y.-X. *J. Polym. Sci. Part A: Polym. Chem.* **2007**, *45*, 2581−2592.

(5) Lian, B.; Thomas, C. M.; Navarro, C.; Carpentier, J.-F. *Organometallics* **2007**, *26*, 187−195.

(6) Ning, Y.; Chen, E. Y.-X. *Macromolecules* **2006**, *39*, 7204−7215.

(7) Rodriguez-Delgado, A.; Mariott, W. R.; Chen, E. Y.-X. *J. Organomet. Chem.* **2006**, *691*, 3490–3497.

(8) Rodriguez-Delgado, A.; Chen, E. Y.-X. *Macromolecules* **2005**, *38*, 2587−2594.

(9) Kostakis, K.; Mourmouris, S.; Kotakis, K.; Nikogeorgos, N.; Pitsikalis, M.; Hadjichristidis, N. *J. Polym. Sci. Part A: Polym. Chem.* **2005**, *43*, 3305−3314.

(10) Ning, Y.; Cooney, M. J.; Chen, E. Y.-X. *J. Organomet. Chem.* **2005**, *690,* 6263–6270.

(11) Lian, B.; Lehmann, C. W.; Navarro, C.; Carpentier, J.-F. *Organometallics* **2005**, *24*, 2466–2472.

(12) Bolig, A. D.; Chen, E. Y.-X. *J. Am. Chem. Soc.* **2004**, *126*, 4897–4906.

(13) Stojcevic, G.; Kim, H.; Taylor, N. J.; Marder, T. B.; Collins, S. *Angew. Chem. Int. Ed.* **2004**, *43*, 5523−5526.

(14) Strauch, J. W.; Fauré, J.-L.; Bredeau, S.; Wang, C.; Kehr, G.; Fröhlich, R.; Luftmann, H.; Erker, G. *J. Am. Chem. Soc.* **2004**, *126*, 2089−2104.

(15) Karanikolopoulos, G.; Batis, C.; Pitsikalis, M.; Hadjichristidis, N. *J. Polym. Sci. Part A: Polym. Chem.* **2004**, *42*, 3761−3774.

(16) Ferenz, M.; Bandermann, F.; Sustmann, R.; Sicking, W. *Macromol. Chem. Phys.* **2004**, *205*, 1196–1205.

(17) Rodriguez-Delgado, A.; Mariott, W. R.; Chen, E. Y.-X. *Macromolecules* **2004**, *37*, 3092–3100.

(18) Lian, B.; Toupet, L.; Carpentier, J.-F. *Chem. Eur. J.* **2004**, *10*, 4301–4307.

(19) Jensen, T. R.; Yoon, S. C.; Dash, A. K.; Luo, L.; Marks, T. J. *J. Am. Chem. Soc.* **2003**, *125*, 14482–14494.

(20) Chen, E. Y.-X.; Cooney, M. J. *J. Am. Chem. Soc.* **2003**, *125*, 7150−7151.

(21) Mariott, W. R. Chen, E. Y.-X. *J. Am. Chem. Soc.* **2003**, *125*, 15726–15727.

(22) Jin, J.; Mariott, W. R.; Chen, E. Y.-X. *J. Polym. Chem. Part A: Polym. Chem.* **2003**, *41*, 3132–3142.

(23) Batis, C.; Karanikolopoulos, G.; Pitsikalis, M.; Hadjichristidis, N. *Macromolecules* **2003**, *36*, 9763–9774.

(24) Karanikolopoulos, G.; Batis, C.; Pitsikalis, M.; Hadjichristidis, N. *Macromol. Chem. Phys.* **2003**, *204*, 831−840.

(25) Bolig, A. D.; Chen, E. Y.-X. *J. Am. Chem. Soc.* **2002**, *124*, 5612−5613.

(26) Jin, J.; Chen, E. Y.-X. *Organometallics* **2002**, *21*, 13–15.

(27) Jin, J.; Wilson, D. R.; Chen, E. Y.-X. *Chem. Commun.* **2002**, 708−709.

(28) Jin, J.; Chen, E. Y.-X. *Macromol. Chem. Phys.* **2002**, *203*, 2329–2333.

(29) Bandermann, F.; Ferenz, M.; Sustmann, R.; Sicking, W. *Macromol. Symp.* **2001**, *174*, 247−253.

(30) Karanikolopoulos, G.; Batis, C.; Pitsikalis, M.; Hadjichristidis, N. *Macromolecules* **2001**, *34*, 4697–4705.

(31) Bolig, A. D.; Chen, E. Y.-X. *J. Am. Chem. Soc.* **2001**, *123*, 7943–7944.

(32) Frauenrath, H.; Keul, H.; Höcker, H. *Macromolecules* **2001**, *34*, 14–19.

(33) Nguyen, H.; Jarvis, A. P.; Lesley, M. J. G.; Kelly, W. M.; Reddy, S. S.; Taylor, N. J.; Collins, S. *Macromolecules* **2000**, *33*, 1508−1510.

(34) Bandermann, F.; Ferenz, M.; Sustmann, R.; Sicking, W. *Macromol. Symp.* **2000**, *161*, 127−134.

(35) Cameron, P. A.; Gibson, V.; Graham, A. J. *Macromolecules* **2000**, *33*, 4329−4335.

(36) Stuhldreier, T.; Keul, H.; Höcker, H. *Macromol. Rapid Commun.* **2000**, *21*, 1093−1098.

(37) Chen, E. Y.-X.; Metz, M. V.; Li, L.; Stern, C. L.; Marks, T. J. *J. Am. Chem. Soc.* **1998**, *120*, 6287−6305.

(38) Shiono, T.; Saito, T.; Saegusa, N.; Hagihara, H.; Ikeda, T.; Deng, H.; Soga, K. *Macromol. Chem. Phys.* **1998**, *199*, 1573−1579.

(39) Hong, E.; Kim, Y.; Do, Y. *Organometallics* **1998**, *17*, 2933−2935.

(40) Li, Y.; Ward, D. G.; Reddy, S. S.; Collins, S. *Macromolecules* **1997**, *30*, 1875−1883.

(41) Deng, H.; Shiono, T.; Soga, K. *Macromol. Chem. Phys.* **1995**, *196*, 1971−1980.

(42) Deng, H.; Shiono, T.; Soga, K. *Macromolecules* **1995**, *28*, 3067−3073.

(43) Soga, K.; Deng, H.; Yano, T.; Shiono, T. *Macromolecules* **1994**, *27*, 7938−7940.

(44) Collins, S.; Ward, D. G.; Suddaby, K. H. *Macromolecules* **1994**, *27*, 7222−7224.

(45) Collins, S.; Ward, S. G. *J. Am. Chem. Soc.* **1992**, *114*, 5460−5462.

(46) Lian, B.; Thomas, C. M.; Navarro, C.; Carpentier, J.-F. *Macromolecules* **2007**, *40*, 2293−2294.

(47) Mariott, W. R.; Rodriguez-Delgado, A.; Chen, E. Y.-X. *Macromolecules* **2006**, *39*, 1318–1327.

(48) Kostakis, K.; Mourmouris, S.; Pitsikalis, M.; Hadjichristidis, N. *J. Polym. Sci. Part A: Polym. Chem.* **2005**, *43*, 3337−3348.

(49) Deng, H.; Soga, K. *Macromolecules* **1996**, *29*, 1847−1848.

(50) Miyake, G. M.; Chen, E. Y.-X. *Macromolecules* **2008**, *41*, 3405–3416.

(51) Miyake, G. M.; Mariott, W. R.; Chen, E. Y.-X. *J. Am. Chem. Soc.* **2007**, *129*, 6724−6725.

(52) Mariott, W. R.; Chen, E. Y.-X. *Macromolecules* **2005**, *38*, 6822−6832.

(53) Mariott, W. R.; Chen, E. Y.-X. *Macromolecules* **2004**, *37*, 4741–4743.

(54) Spaether, W.; Klaß, K.; Erker, G.; Zippel, F.; Fröhlich, R. *Chem. Eur. J.* **1998**, *4*, 1411–1417.

(55) Ning, Y.; Caporaso, L.; Correa, A.; Gustafson, L. O.; Cavallo, L.; Chen, E. Y.-X. *Macromolecules* **2008**, *41*, 6910–6919.

(56) Caporaso, L.; Cavallo, L. *Macromolecules* **2008**, *41*, 3439–3445.

(57) Caporaso, L.; Gracia-Budrìa, J.; Cavallo, L. *J. Am. Chem. Soc.* **2006**, *128*, 16649−16654.

(58) Tomasi, S.; Weiss, H.; Ziegler, T. *Organometallics* **2007**, *26*, 2157−2166.

(59) Tomasi, S.; Weiss, H.; Ziegler, T. *Organometallics* **2006**, *25*, 3619−3630.

(60) Hölscher, M.; Keul, H.; Höcker, H. *Macromolecules* **2002**, *35*, 8194–8202.

(61) Hölscher, M.; Keul, H.; Höcker, H. *Chem. Eur. J.* **2001**, *7*, 5419–5426.

(62) Sustmann, R.; Sicking, W.; Bandermann, F.; Ferenz, M. *Macromolecules* **1999**, *32*, 4204–4213.

(63) Xie, X.; Hogen-Esch, T. E. *Macromolecules* **1996**, *29*, 1746–1752.

(64) Kodaira, T.; Tanahashi, H.; Hara, K. *Polym. J.* **1990**, *22*, 649–659.

(65) Okamoto, Y.; Yuki, H. *J. Polym. Sci. Polym. Chem. Ed.* **1981**, *19*, 2647–2650.

(66) (a) Suzuki, T.; Kusakabe, J.; Ishizone, T. *Macromolecules* **2008**, *41*, 1929–1936. (b) Suzuki, T.; Kusakabe, J.; Ishizone, T. *Macromol. Symp.***2007**, *249-250*, 412–416.

(67) Christoffers, J.; Schulze, Y.; Pickardt, J. *Tetrahedron* **2001**, *57*, 1765–1769.

(68) (a) Grossman, R. B.; Doyle, R. A.; Buchwald, S. L. *Organometallics* **1991**, *10*, 1501−1505. (b) Collins, S.; Kuntz, B. A.; Taylor, N. J.; Ward, D. G. *J. Organomet. Chem.* **1988**, *342*, 21–29.

(69) Diamond, G. M.; Jordan, R. F.; Petersen, J. L. *J. Am. Chem. Soc.* **1996**, *118*, 8024–8033.

(70) LoCoco, M.D.; Jordan, R. F. *J. Am. Chem. Soc.* **2004**, *126*, 13918–13919.

(71) (a) Carpentier, J.-F.; Maryin, V. P.; Luci, J.; Jordan, R. F. *J. Am. Chem. Soc.* **2001**, *123*, 898–909. (c) Stevens, J. C.; Timmers, F. J.; Wilson, D. R.; Schmidt, G. F.; Nickias, P. N.; Rosen, R. K.; Knight, G. W.; Lai, S. Eur. Pat. Appl. EP 0 416815 A2, **1991**.

(72) Chen, Y.-X.; Marks, T. J. *Organometallics* **1997**, *16*, 3649–3657.

(73) Ueda, M.; Takahashi, M.; Suzuki, T. *J. Polym Sci. Polym. Phys. Ed.,* **1983**, *20*, 1139–1149.

(74) (a) ADF2007, *Theoretical Chemistry, Vrije Universiteit, Amsterdam*, 2007, Users's Manual. (b) Baerends, E. J.; Ellis, D. E.; Ros, P. *Chem. Phys.* **1973,** *2,* 41–51.

(75) Vosko, S. H.; Wilk, L.; Nusair, M. *Can. J. Phys.* **1980,** *58,* 1200–1211.

(76) Becke, A. D. *Phys. Rev. A* **1988,** *38,* 3098–3100.

(77) (a) Perdew, J. P. *Phys. Rev. B* **1986,** *33,* 8822–8824. (b) Perdew, J. P. *Phys. Rev. B* **1986,** *34,* 7406–7406.

(78) (a) Klamt, A.; Schüürmann, G. *J. Chem. Soc., Perkin Trans.* **1993**, 799–805. (b) Pye, C. C.; Ziegler, T. *Theor. Chem. Acc.* **1999,** *101,* 396–408.

(79) Eliel, A. L.; Wilen, S. H.; Mander, L. N. *Stereochemistry of Organic Compounds*; John Wiley & Sons, Inc.: New York, 1994; pp 266–268.

(80) The ideal sp^3 valence angle of 109.47° is closer to the 60° valence angle of a three-membered ring than the ideal sp^2 value of 120°.

Chapter 4

Stereospecific Polymerization of Chiral Oxazolidinone-Functionalized Alkenes

Abstract

Acryloyl and vinyl monomers functionalized with the chiral oxazolidinone auxiliary have been successfully polymerized in a stereospecific fashion to highly isotactic, optically active polymers, through either the previously established isospecific coordination polymerization (for acryloyl monomers) or a novel isospecific cationic polymerization (for vinyl monomers). Specifically, conjugated chiral acryloyl oxazolidinones, *N*-acryloyl-(*R* or *S*)-4-phenyl-2-oxazolidinone [(*R* or *S*)-AOZ], are readily polymerized by chiral *ansa*-zirconocenium coordination catalysts, (*R,R*-, *S,S*-, or *R,R*/*S,S*)-$[C_2H_4(\eta^5\text{-Ind})_2]Zr^+(THF)[OC(O^iPr)=CMe_2][MeB(C_6F_5)_3]^-$ (**1**), in an isospecific manner through a catalyst-site controlled mechanism, producing the corresponding optically active chiral polymers, (*R* or *S*)-PAOZ. Owing to the nature of stereocontrol dictated by the chiral catalyst site, even the coordination polymerization of the parent AOZ, without the chiral side group, also affords PAOZ with nearly quantitative isotacticity. A series of experiments have shown that the chiral polymers (*R* or *S*)-PAOZ exhibit no chiral amplifications, despite having stereoregularly placed stereogenic centers in the main-chain, and the optical activity of the polymers arises solely from their chiral auxiliary, a consequence of adopting a random-coil secondary structure and thus having a cryptochiral chain. In sharp contrast, the chiral isotactic polymers derived from non-conjugated chiral vinyl oxazolidinones, *N*-vinyl-(*R*)-4-phenyl-2-oxazolidinone [(*R*)-VOZ] and its *para*-hexyloxy-phenyl derivative (*R*)-HVOZ (designed to solve the solubility issue of the resulting polymer), exhibit substantial chiral amplifications by virtue of adopting a solution-stable, one-handed helical

conformation. The synthesis of such helical vinyl polymers has been accomplished by the development of a novel isospecific cationic polymerization using Lewis and Brønsted acids, such as $[Ph_3C][B(C_6F_5)_4]$, $BF_3{\cdot}Et_2O$, and $[H(Et_2O)_2][B(C_6F_5)_4]$, through a chiral auxiliary-controlled mechanism. Noteworthy is the combination of the near quantitative isotactic placement of the stereogenic centers of the polymer main-chain with the chiral side-groups located near those stereocenters that renders one-handed helicity of (*R*)-PVOZ and (*R*)-PHVOZ. Significantly, this novel cationic polymerization process, operating at ambient temperature, effectively assembles two elements of polymer local chirality—side-chain chirality and main-chain chirality—into global chirality in the form of excess one-handed helicity. Furthermore, the resulting chiral helical vinyl polymers exhibit considerably higher thermal decomposition temperatures and polymer crystallinity, in comparison to the random-coil chiral acryloyl polymers, having a similarly high degree of main-chain stereoregularity.

Introduction

Optically active synthetic polymers are of considerable current interest.[1] Such polymers are not only fundamentally intriguing (due to their rich and complex architectures derived from macromolecular chirality that diverges from that of small molecule chirality) but are also technologically important (due to their unique chiral arrays that give rise to a number of potential, and in some cases commercially implemented, applications such as chiral separation).[1] We are particularly interested in the utilization of chiral *N,O*-functionalized polar vinyl polymers[2] as potential chiral polymeric ligands/stabilizers for transition metal nanocluster catalysts[3] en route to asymmetric catalysis.[4] This interest stems from the observation that *N,O*-functionalized polar vinyl polymers, such as poly(vinylpyrrolidone) (PVP), are among the most common, effective stabilizers for transition-metal nanoclusters,[5] and the reasoning that chiral polymers have the suitable length scale and binding rigidity as well as "high chirality"[6] that can match the extended surface of the nanoclusters. However, optically active PVP is not accessible; even if enantiomerically pure or enriched stereoregular PVP is synthesized, such a vinyl polymer with configurational main-chain chirality without chiral side-groups *cannot* be optically active since the entire polymer chain (by the infinite chain model) contains a mirror plane (for isotactic polymers) or a glide mirror plane and translational mirror planes perpendicular to the chain axis (for syndiotactic polymers).[1j,l] On the other hand, a polymer assuming a one-handed helical conformation is inherently chiral. [1] Many polymers are known to form a helical structure in the solid state; however, they typically adopt optically inactive, on-average random-coil conformations in solution due to fast solution dynamics of the polymer chain with low helix-inversion barriers. Our MM2 modeling indicated that isotactic PVP would adopt a random-coil conformation, suggesting that enantiomeric chiral PVP with appreciable molecular weight (MW), if synthesized, would be optically inactive. In short, there exists a need for the synthesis of optically active, chiral PVP variants.

A solution to this fundamental problem is to install a chiral auxiliary into conjugated or non-conjugated vinyl monomers which, upon polymerization, will lead to optically active polymers. If such polymerization proceeds in a stereospecific manner, then the resulting stereoregular polymers could attain additionally helical chirality due to control of the polymer secondary structure. Pino and Lorenzi first demonstrated that isotactic vinyl polymers bearing chiral side-groups, such as poly-(*S*)-3-methyl-1-pentene, can exist in solution with excess one-handed helicity and that the optical activity of such polymers increased with increasing isotacticity.[7] With this concept and the goal of this work in mind, three reasons led us to enantiomeric (*R* or *S*)-4-phenyl-2-oxazolidinone-functionalized conjugated and non-conjugated vinyl monomers *N*-acryloyl-(*R* or *S*)-4-phenyl-2-oxazolidinone [(*R* or *S*)-AOZ] and *N*-vinyl-(*R*)-4-phenyl-2-oxazolidinone [(*R*)-VOZ] (Chart 1). *First*, the chiral oxazolidinone group has been used as a chiral auxiliary in organic synthesis for over 30 years.[8] *Second*, the resulting *N,O*-functionalized chiral polymers, (*R* or *S*)-PAOZ and (*R*)-PVOZ, structurally resemble that of PVP, in addition to being optically active. *Third*, introduction of the phenyl group at 4-position of the oxazolidinone ring could sterically induce a solution-stable helical conformation of the isotactic polymer, thereby effectively assembling two elements of local chirality—side-chain chirality (stereocenters at 4-positions of the side chain) and main-chain chirality (stereocenters generated at 2-vinyl carbon positions during stereoselective polymerization)—into global chirality (formation of excess one-handed helicity). Indeed, MM2 modeling of the isotactic $[(R)\text{-VOZ}]_{30}$ predicts a chiral 4_1 helical structure (Chart 2).

Chart 1. Structures of Chiral 2-Oxazolidinone-funcationzalized Conjugated Acrylamide and Non-Conjugated Vinyl Monomers Employed in This Study.

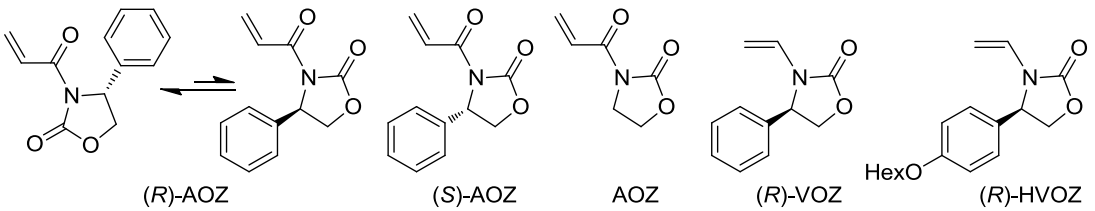

Chart 2. Primary Structure of (*R*)-PVOZ (**A**) as well as MM2-Calculated 4_1 Helical Structure of [(*R*)-VOZ]$_{30}$, Shown from Top (**B**), Side (**C**), and Ribbon (**D**) Views (carbon, nitrogen, and oxygen are shown in grey, blue, and red, respectively; hydrogen atoms omitted for clarity).

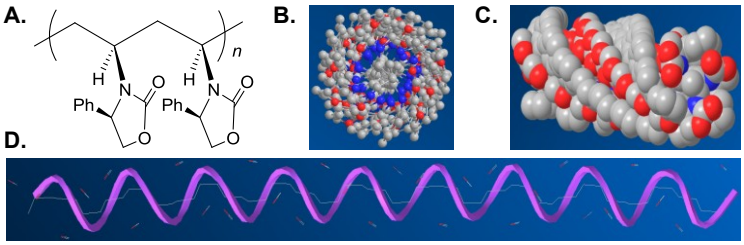

Free-radical polymerization has been previously employed to polymerize conjugated vinyl monomers bearing chiral auxiliary groups stereoselectively.[9] However, due to unfavorable dipole interactions between the oxazolidinone and acryloyl carbonyls, conjugated AOZ with a chiral auxiliary at the 4-position favors a rotamer which shields the auxiliary away from the reactive center (*c.f.,* left rotamer of (*R*)-AOZ, Chart 1), providing little stereochemical control in additions to the C=C bond.[10] Using a suitable Lewis acid (LA), such as Sc(OTf)$_3$, should lock the auxiliary in the preferred conformation for control of stereochemistry (*c.f.,* right rotamer of (*R*)-AOZ, Chart 1), through bidentate chelation of the LA to both carbonyls of the monomer; however, such complexation renders the radical and monomer too electron-deficient to react efficiently for homopolymerizations. Nevertheless, (4*S*)-AOZ can be radically copolymerized with electron-rich isobutylene in the presence of a LA, yielding isotactic alternating copolymer with a *m*/*r* dyad ratio of >95:5.[10] In the case of chiral oxazolidine acrylamides, stereocontrolled (through chiral auxiliary control[11]) free-radical polymerization has been achieved without LA additives, producing isotactic polymers with a *m*/*r* dyad ratio reaching 92:8.[12] Interestingly, the non-conjugated, unsubstituted VOZ undergoes rapid decomposition (*devinylation*) to 2-oxazolidione and acetaldehyde in acidic aqueous solution with pH < 4.0 so that the radical polymerization in

the presence of polymethacrylic acid was successful only at pH ≥4.0.[13] This monomer, upon free-radical polymerization by AIBN, was reported to form water-soluble polymers with MW ranging from 450 to 100,000 (by microisopiestic measurements),[14] or a water-insoluble polymer which decomposes at ~300 °C without melting. An attempt to polymerize this monomer by a Ziegler-Natta coordination catalyst ($TiCl_3/HONH_3^+Cl^-$) led to no polymer formation, but instead the acid-catalyzed devinylation product.[15] Acid-catalyzed devinylation of *N*-vinyl heterocyclic monomers has also been noted elsewhere.[16] VOZ monomers having alkyl or phenyl substituents at 5-postions can be polymerized by AIBN in dioxane or in bulk.[17] The polymers derived from radical polymerization of VOZ monomers are essentially atactic.[18]

As can be seen from the above overview, AOZ and VOZ monomers have previously been successfully polymerized only by radical polymerization methods, while the polymerization of (4*R* or 4*S*)-VOZ monomers of our current interest has not been reported. Furthermore, chiral auxiliary-controlled radical polymerization has led to formation of an isotactic copolymer of (4*S*)-AOZ with isobutylene, but the isotactic homopolymer of (4*R* or 4*S*)-AOZ of interest herein was previously unknown. Lastly, no stereoregular polymers derived from VOZ monomers have been reported.

We hypothesized that the synthetic challenges identified above could be met by employing isospecific, enantiomeric (*R,R* or *S,S*)-*ansa*-metallocenium coordination catalysts that were recently developed for the asymmetric coordination polymerization of functionalized vinyl monomers such as prochiral acrylmides leading to optically active, helical vinyl polymers.[19] Our reasoning is threefold: *First*, we have already shown that catalyst **1** polymerizes prochiral conjugated acrylamides with bulky substituents, such as *N,N*-diarylacrylamides, to highly isotactic, chiral polymers adopting a solution-stable, one-handed-helical conformation, where the handedness of the helix is dictated by the chirality of the catalyst (Chart 3).[19] In contrast, if the monomer is not sufficiently sterically bulky [*i.e.* methyl methacrylate (MMA)], the resulting polymer does not form a solution-stable helix, but instead a random coil conformation; such low-

MW enantiomeric oligomers can exhibit some optical activity arising from the devoid of mirror planes due to non-equivalent chain-end groups, but as the MW increases, the effects of the chain-end groups on the chiroptical properties of the polymers diminishes so that the optical activity decreases to null as the polymer becomes cryptochiral.[20,21] *Second*, we reasoned that the zirconocene ester enolate cation **1** can serve as both initiator (the enolate ligand as nucleophile) *and* LA catalyst as chelator for the two carbonyls in the AOZ monomer,[22] thus rendering both high activity *and* high stereochemical control in AOZ polymerization (*vide supra*). Studies in the polymerization of chiral AOZ monomers by the enantiomeric catalysts **1** will determine if they can produce isolatable, right- and left-handed, solution-stable helical polymers bearing the same chiral auxiliary, trapped in a kinetically-stable state—a case of catalyst-site control. Comparative studies using the racemic catalyst and other catalysts with different stereochemical control will also reveal whether the chiral auxiliary will dictate the handedness of the helix, either through an initial formation of a preferred single-handed helix or through a thermodynamic mutarotation to the preferred helical conformation—the case of chiral auxiliary control. *Third*, being a class of electron-rich monomers, chiral VOZ could be cationically polymerized by metallocenium or other related cations and isospecificity rendered by the chiral auxiliary, if devinylation is overcome by appropriate strategies such as spontaneous polymer precipitation. As indicated in Chart 2, highly isotactic (*R*)-PVOZ will most likely adopt a solution-stable helical structure, thereby accomplishing our goal of synthesizing those needed optically active polymers. Herein we report our findings in testing each of these three hypotheses.

Chart 3. Asymmetric Polymerization by Enantiomeric Catalysts **1** for the Synthesis of Right- and Left-Handed Helical Poly[*N*-phenyl-*N*-(4-tolyl)acrylamide)s and Their Block Copolymers with MMA. Shown on the Bottom are the CD Spectra of Homopolymers and Block Copolymers by (*S,S*)-**1** (red), *rac*-**1** (green), and (*R,R*)-**1** (blue).[19,20]

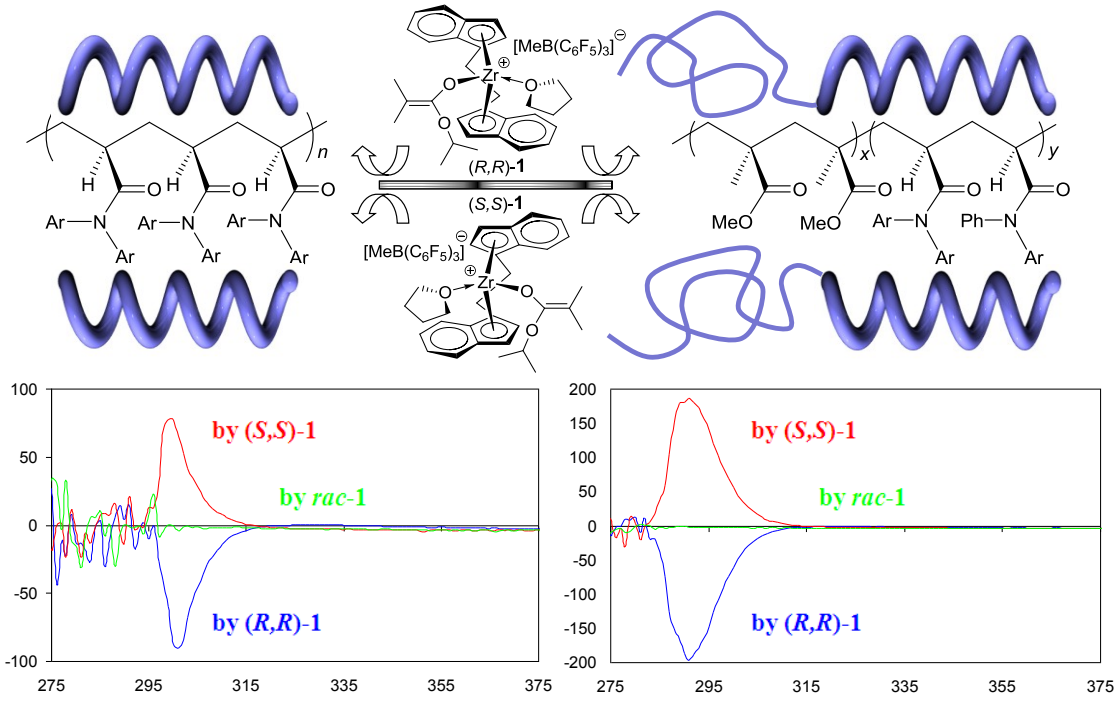

Experimental

Materials, Reagents, and Methods. All syntheses and manipulations of air- and moisture-sensitive materials were carried out in flame-dried Schlenk-type glassware on a dual-manifold Schlenk line, a high-vacuum line, or in an argon or nitrogen-filled glovebox. HPLC-grade, non-stabilized organic solvents were sparged extensively with nitrogen during filling of the solvent reservoir and then dried by passage through activated alumina (for THF, Et_2O, and CH_2Cl_2) followed by passage through Q-5-supported copper catalyst (for toluene and hexanes) stainless steel columns. HPLC-grade DMF was degassed, dried over CaH_2 overnight, followed by vacuum transfer. Toluene-d_8 and benzene-d_6 were degassed, dried over sodium/potassium alloy, and filtered before use, whereas $CDCl_3$, CD_2Cl_2, DMSO-d_6 were degassed and dried over activated Davison 4 Å molecular sieves. NMR spectra were recorded on a Varian Inova 300 MHz, 400

MHz, or 500 MHz (for polymer tacticity analysis) spectrometer. Chemical shifts for ^{1}H and ^{13}C spectra were referenced to internal solvent resonances and are reported as parts per million relative to tetramethylsilane, whereas ^{19}F NMR spectra were referenced to external $CFCl_3$.

Acetaldehyde diethyl acetal, aniline, ^{n}BuLi (1.6 M in hexanes), butylated hydroxytoluene (BHT-H, 2,6-Di-*tert*-butyl-4-methylphenol), camphor sulfonic acid, 1,2-dibromobenzene, 1,2-dibromoethane, diisopropylamine, indene, lithium dimethylamide, (2*S*,4*S*)-pentanediol (99% *ee*, $[\alpha]^{20}_{D}$ +39.8, c = 10, $CHCl_3$), (2*R*,4*R*)-pentanediol (97% *ee*, $[\alpha]^{21}_{D}$ –40.4, c = 10, $CHCl_3$), sodium azide, tetrachlorozirconium, 1,1,3,3-tetramethyl guanidine, and triethylamine, triflic acid, as well as $(CF_3SO_2)_2O$, $PhBCl_2$, MeMgI (3.0 M in diethyl ether), $BF_3{\cdot}Et_2O$, $^{i}Bu_3Al$ (neat), AIBN, and CF_3COOH, were purchased from Aldrich. MMAO (2.2 wt % Al in heptane) was purchased from Akzo Nobel. Acryloyl chloride and 2,6-dimethyl pyridine were purchased from Alfa Aesar. Trimethylaluminum (neat) was purchased from Strem Chemical Co. whereas (*S*)- and (*R*)-4-phenyl-2- oxazolidinone, isopropyl isobutyrate, and *N*-methyl aniline were purchased from TCI America. Indene, 1,2-dibromoethane, *N,N*-dimethyl aniline, and acryloyl chloride were degassed using three freeze-pump-thaw cycles. Diisopropylamine, triethylamine, $(CF_3SO_2)_2O$, and $PhBCl_2$ were vacuum-distilled. 2,6-Dimethyl pyridine, isopropyl isobutyrate, and aniline were degassed and dried over CaH_2 overnight, followed by vacuum distillation. BHT-H was recrystallized from hexanes prior to use. 1,4-Dioxane (Fisher Scientific) was degassed, dried over sodium/potassium alloy, and vacuum-distilled. All other commercial reagents were used as received.

Borate salts $[Ph_3C][B(C_6F_5)_4]$ and $[HN(Me_2)Ph][B(C_6F_5)_4]$ as well as borane $B(C_6F_5)_3$ were obtained as a research gift from Boulder Scientific Co.; the borane was further purified by recrystallization from hexanes at –35 ºC. The $(C_6F_5)_3B{\cdot}THF$ adduct was prepared by addition of THF to a toluene solution of the borane followed by removal of the volatiles and drying in vacuo. Literature procedures were employed for the preparation of the following compounds and metallocene complexes: (*S*)-AOZ,[23] (*R*)-AOZ,[23] AOZ,[24] (*R*)-VOZ,[25] $[H(Et_2O)_2]^{+}[B(C_6F_5)_4]^{-}$,[26] $LiOC(O^{i}Pr)=CMe_2$,[27] $(EBI)H_2$ [EBI = $C_2H_4(\eta^5\text{-Ind})_2$],[28] *rac*-$(EBI)Zr(NMe_2)_2$,[29] *rac*-

(EBI)$ZrMe_2$,[29] *rac*-(EBI)ZrMe(OTf),[30] *rac*-(EBI)ZrMe[OC(O^{i}Pr)=CMe_2],[30] *rac*-(EBI)Zr^+(THF)[OC(O^{i}Pr)=CMe_2][$MeB(C_6F_5)_3$]$^-$ (*rac*-**1**),[30] (*S,S*)-(EBI)$ZrCl_2$,[31] (*R,R*)-(EBI)$ZrCl_2$,[31] (*S,S*)-(EBI)ZrMe[OC(O^{i}Pr)=CMe_2],[19,20] (*R,R*)-(EBI)ZrMe[OC(O^{i}Pr)=CMe_2],[19,20] (*S,S*)-(**1**),[19,20] and (*R,R*)-(**1**).[19,20]

(*R*)-Methyl 2-((*tert*-butoxycarbonyl)amino)-2-(4-(hexyloxy)phenyl)acetate. To a flame-dried flask with a magnetic stir bar was added (*R*)-methyl 2-((*tert*-butoxycarbonyl)amino)-2-(4-hydroxyphenyl)acetate (19.4 g, 68.8 mmol, 1.0 equiv), anhydrous K_2CO_3 (23.8 g, 172 mmol, 2.5 equiv), and anhydrous DMF (250 mL). The mixture solution was cooled to 0 ºC, after which 1-iodohexane (25.4 mL, 172 mmol, 2.5 equiv) was added and the reaction was allowed to stir overnight at room temperature. Diethyl ether (1000 mL) was added and the mixture washed with water (2 × 500 mL), saturated $KHSO_4$ (500 mL), and brine (500 mL). The solution was dried with $MgSO_4$ and concentrated to give a yellow oil which was purified by silica gel chromatography (9:1 hexanes: EtOAc) to yield the desired product as a clear oil (14.1 g, 56%). R_f = 0.18 (9:1 hexanes:EtOAc). $[\alpha]_D^{21}$ = –45.5 (*c* = 0.013 g/mL, MeOH). ^{1}H NMR (400 MHz, $CDCl_3$): δ 7.22 (d, *J* = 8.5 Hz, 2H), 6.82 (m, 2H), 5.44 (bd, *J* = 6.4 Hz, 1H), 5.21 (bd, *J* = 7.2 Hz, 2H), 3.90 (t, *J* = 6.6 Hz, 2H), 3.67 (s, 3H), 1.73 (m, 2H), 1.39 (s, 9H), 1.29 (m, 5H) 0.87 (m, 3H). ^{13}C NMR (100 MHz, $CDCl_3$): δ 172.1, 159.4, 155.0, 128.9, 128.5, 115.0, 80.2, 68.2, 57.2, 52.8, 31.7, 29.4, 28.5, 25.9, 22.8, 14.2. IR (NaCl, neat): 3440, 3380, 2955, 2933, 2872, 1747, 1717, 1612, 1511, 1247, 1169 cm^{-1}. HRMS (ESI+) calcd for $C_{20}H_{31}NNaO_5$: 365.2202; found: 365.2217.

(*R*)-4-(4-(Hexyloxy)phenyl)oxazolidin-2-one. To a solution of $LiAlH_4$ (1.61 g, 42.5 mmol, 1.1 equiv) in THF (200 mL) was added dropwise a solution of (*R*)-methyl 2-((*tert*-butoxycarbonyl)amino)-2-(4-(hexyloxy)phenyl)acetate (14.1 g, 38.7 mmol, 1.0 equiv) in THF (150 mL). The reaction was stirred at room temperature until the starting material was consumed by TLC analysis, after which 10 % KOH was added and the reaction mixture filtered and concentrated to yield an off-white solid. The solid was dissolved in THF (400 mL) and cooled to

0 ºC, after which thionyl chloride (22.4 mL, 309 mmol, 8.0 equiv) was added dropwise and the solution stirred for an additional 3 h at 0 ºC then warmed to room temperature and stirred overnight. The reaction was concentrated to give a viscous oil that was crystallized with hexanes and filtered, yielding the desired product as a white amorphous solid (7.01 g, 68%). R_f = 0.22 (1:1 hexanes:EtOAc). $[\alpha]_D^{21}$ = –12.5 (*c* = 0.8 g/dL, MeOH). ^{1}H NMR (400 MHz, $CDCl_3$): δ 7.20 (m, 2H), 6.85 (m, 2H), 5.87 (bs, 1H), 4.86 (m, 1H), 4.64 (m, 1H), 4.12 (m, 1H), 3.91 (m, 2H), 1.74 (m, 2H), 1.42 (m, 2H), 1.29 (m, 4 H), 0.87 (m, 3H). ^{13}C NMR (100 MHz, $CDCl_3$): δ 159.8, 159.7, 131.3, 127.5, 115.3, 72.9, 68.3, 56.2, 31.7, 29.3, 25.9, 22.8, 14.2. IR (NaCl, neat): 3284, 2932, 2860, 1756, 1613, 1514, 1246, 1032 cm^{-1}. HRMS (ESI+) calcd for $C_{15}H_{22}NO_3$: 263.1521; found: 263.1526.

(*R*)-4-(4-(Hexyloxy)phenyl)-3-vinyloxazolidin-2-one (HVOZ). To a flame-dried flask was added palladium(II) trifluoroacetate (63 mg, 0.19 mmol, 0.05 equiv), 1,10-phenanthroline (34 mg, 0.19 mmol, 0.05 equiv), and *n*-butyl vinyl ether (4.9 mL, 37.9 mmol, 10.0 equiv). This mixture was stirred for 5 min, followed by the addition of (*R*)-4-(4-(hexyloxy)phenyl)oxazolidin-2-one (1.0 g, 3.79 mmol, 1.0 equiv). The reaction was heated to 75 ºC for 12 h, filtered through celite, and concentrated. Purification of the crude product by silica gel chromatography gave a viscous oil which was crystallized with pentanes and filtered to yield the desired product as a white solid (1.07 g, 98%). R_f = 0.15 (9:1 hexanes:EtOAc). $[\alpha]_D^{21}$ = –44.8 ° (*c* = 1.70 g/dL, CH_2Cl_2); m.p. (ºC): 52–53. ^{1}H NMR (400 MHz, $CDCl_3$): δ 7.14 (d, *J* = 8.5 Hz, 2H), 6.87 (d, *J* = 8.4 Hz, 2H), 6.77 (dd, *J* = 16.0, 9.3 Hz, 1H), 4.95 (dd, *J* = 9.0, 5.4 Hz, 1H), 4.66 (m, 1H), 4.28 (d, *J* = 9.3 Hz, 1H), 4.08 (m, 2H), 3.91 (t, *J* = 6.5 Hz, 2H), 1.74 (m, 2H), 1.42 (m, 2H), 1.30 (m, 4H), 0.87 (m, 3H). ^{13}C NMR (100 MHz, $CDCl_3$): δ 159.7, 155.9, 129.8, 129.0, 127.3, 115.4, 96.0, 71.0, 68.3, 58.0, 31.7, 29.4, 25.9, 22.8, 14.2. IR (NaCl, neat): 2932, 2871, 1765, 1639, 1613, 1514, 1394, 1246 cm^{-1}. HRMS (ESI+) calcd for $C_{17}H_{24}NO_3$: 289.1678; found 289.1679.

General Polymerization Procedures. Polymerizations were performed in 30-mL glass reactors inside the glovebox for ambient temperature (~25 ºC) runs or in 25-mL Schlenk flasks interfaced to a dual-manifold Schlenk line with an external temperature bath for runs at other temperatures. In a typical procedure for polymerizations of conjugated acryloyl oxazolidinones (AOZ), predetermined amounts of $B(C_6F_5)_3 \cdot THF$ and the appropriate metallocene ester enolate pre-catalyst in a 1:1 molar ratio were premixed in 5 mL of CH_2Cl_2 and stirred for 10 min to cleanly generate the corresponding cationic ester enolate catalyst.[19,20,32] The amount of catalyst employed was determined by the [monomer] to [catalyst] ratio specified in the polymerization tables. Monomer (0.737 mmol) was quickly added as a solid to the vigorously stirring solution, and the polymerization was allowed to proceed for 3 h with continuous stirring. For polymerization of vinyl oxazolidines (VOZ), monomer (1.06 mmol) was dissolved in the solvent described in the polymerization tables, before addition of initiator as a solid or solution via syringe, and the polymerization was allowed to stir for the time specified in the polymerization tables. After the measured time interval, a 0.2 mL aliquot was taken from the reaction mixture via syringe and quickly quenched into a 4 mL vial containing 0.6 mL of undried "wet" $CDCl_3$ stabilized by 250 ppm of BHT-H; the quenched aliquots were analyzed by ^1H NMR to obtain monomer conversion data. The polymerization was immediately quenched after the removal of the aliquot by the addition of 5 mL 5% HCl-acidified methanol. The quenched mixture was precipitated into 50 mL of methanol, stirred for 1 h, filtered or centrifuged, washed with methanol, and dried in a vacuum oven at 50 °C overnight to a constant weight.

For polymerizations carried out at other temperatures, the catalyst (or monomer solution) was loaded in a 25-mL Schlenk flask equipped with a stir bar and a septum cap inside the glovebox. The charged Schlenk flask was taken out of the glovebox, interfaced to a dual-manifold Schlenk line, and immersed in a pre-equilibrated bath at desired temperature. The polymerization was started by adding rapidly the monomer (or catalyst solution) via gas-tight syringe under positive N_2 pressure. The remaining procedures were the same as those ambient-temperature

polymerization runs. Polymerizations using C_s-ligated metallocenium catalysts for the synthesis of syndiotactic polymers followed the literature procedure.[33]

Polymer Characterizations. Gel permeation chromatography (GPC) analyses of the polymers were carried out at 40 °C and a flow rate of 1.0 mL/min, with DMF as the eluent, on a Waters University 1500 GPC instrument equipped with four 5 μm PL gel columns (Polymer Laboratories) and calibrated using 10 PMMA standards. Chromatograms were processed with Waters Empower software (version 2002); number-average molecular weight (M_n) and molecular weight distribution (MWD = M_w/M_n) of polymers were given relative to PMMA standards. Glass transition temperatures (T_g) of the polymers were measured by differential scanning calorimetry (DSC) on a DSC 2920, TA Instrument. Polymer samples were first heated to 150 °C at 20 °C/min, equilibrated at this temperature for 4 min, then cooled to 30 °C at 20 °C/ min, held at this temperature for 4 min, and reheated to 230 °C (for AOZ polymers) or 390 °C (for VOZ polymers) at 10 °C/min. All T_g values were obtained from the second scan, after removing the thermal history from the first heating cycle. Maximum rate decomposition temperatures (T_{max}) and decomposition onset temperatures (T_{onset}) of the polymers were measured by thermal gravimetric analysis (TGA) on a TGA 2950 thermogravimetric analyzer, TA Instrument. Polymer samples were heated from ambient temperatures to 600 °C at a rate of 20 °C/min. Values for T_{max} were obtained from derivative (wt%/°C) *vs* temperature (°C), while T_{onset} values (initial and end temperatures) were obtained from wt% *vs* temperature (°C) plots.

Optical rotations were measured on an Autopol III Automatic Polarimeter at 23°C. The measurements were conducted on 0.2 g/dL polymer solutions in $CHCl_3$. Circular dichroism (CD) spectra were obtained from an Aviv model 202 CD spectrometer. CD analysis was conducted on polymer solutions with concentrations of 0.2 g/dL in $CHCl_3$. Powder X-ray diffraction (XRD) analyses were performed on powder samples with a Scintag X2 Advanced Diffraction System using Cu Kα (λ = 1.540562 Å) radiation and a Peltier detector on the diffracted-beam side. In all cases measurements were performed with a step size of 0.02° with 1.2 second per step. The

tacticity of (*R*)-PAOZ and (*R*)-PVOZ was analyzed by ^{13}C NMR in DMSO-d_6 at 100 °C according to the procedures established for polyacrylamides[34] and for the parent PVOZ,[18] respectively. NMR data of the polymers representing each of three classes of the polymers described in this study were listed below.

Poly(*N*-acryloyl-2-oxazolidinone) (PAOZ). ^{1}H NMR (DMSO-d_6, 500 MHz, 100 °C) for PAOZ: δ 4.37 (m, CH_2O, 2H), 3.87 (m, CH_2N, 2H), 3.73, 3.68, 3.60 (m, C*H*, unresolved triads, 1H), 1.86, 1.71, 1.67, 1.55, 1.48 (m, CH_2, unresolved diads and tetrads, 2H). ^{13}C NMR (DMSO-d_6, 125 MHz, 100 °C) δ 174.4 (*C*=O, *rr* + *mr*), 174.3 (*C*=O, *mm*), 152.7 (*C*=O, ring), 61.50 (*C*H$_2$O), 42.09 (*C*H$_2$N), 37.24 (*C*H), 34.75 (*C*H$_2$).

Poly[*N*-acryloyl-(*R*)-4-phenyl-2-oxazolidinone] [(*R*)-PAOZ]. ^{1}H NMR (DMSO-d_6, 500 MHz, 100 °C): δ 7.28 (m, Ar, 5H), 5.38 (m, C*H*, 1H), 4.64–4.14 (m, CH_2O, 2H), 3.84, 3.76, 3.67 (m, C*H*, unresolved triads, 1H), 1.88, 1.74, 1.46 (m, CH_2, 2H). ^{13}C NMR (DMSO-d_6, 125 MHz, 100 °C): δ 174.3 (*C*=O, *rr* + *mr*), 173.9 (*C*=O, *mm*), 153.0, (*C*=O, ring), 139.7, 129.1, 128.3, 125.9 (Ar), 70.18 (*C*H$_2$O), 57.98 (*C*HN), 39.04 (*C*H), 36.01 (*C*H$_2$).

Poly[*N*-vinyl-(*R*)-4-(4-(hexyloxy)phenyl)-2-oxazolidinone] [(*R*)-PHVOZ]. ^{1}H NMR (500 MHz, $CDCl_3$, 50 °C): δ 7.62 (bs, Ar, 2H), 6.99 (bs, Ar, 2H), 4.53 (m, 1H), 4.25 (m, 1H), 4.03 (m, 2H), 3.77 (m, 1H), 1.82 (bs, 2H), 1.49 (bs, 2H), 1.35 (bs, 5H), 0.89 (bs, 4H), 0.77 (bs, 1 H). ^{13}C NMR ($CDCl_3$, 125 MHz, 50 °C): δ 159.6 (*C*-O), 158.0 (*C*=O, *mmmm*), 132.4, 129.6, 115.2 (Ar), 70.26 (*C*H$_2$O), 68.24 (*C*H$_2$O), 56.23 (*C*HN), 48.54 (*C*H), 35.64 (*C*H$_2$), 31.60 (*C*H$_2$), 29.36 (*C*H$_2$), 25.84 (*C*H$_2$), 22.56 (*C*H$_2$), 13.90 (*C*H$_3$).

Results and Discussion

Stereospecific Coordination Polymerization of Chiral Acryloyl Oxazolidinones. As a control and test to examine the compatibility of the oxazolidinone functionality attached to the acryloyl monomer with the cationic metallocenium coordination catalyst, we first polymerized

the parent unsubstituted, prochiral acryloyl-2-oxazolidinone (AOZ) with *rac*-**1** at ambient temperature. In accordance with the stereospecific coordination polymerization of *N,N*-diarylacrylamides[19,20] and *N,N*-dialkylacrylamides[34a,b,c] by such metallocene catalysts, the polymerization of AOZ by *rac*-**1** is rapid and produces highly stereoregular, but optically inactive, PAOZ with a near quantitative isotacticity (*mm*%) of ~ 99% as determined by ^{13}C NMR (see Experimental). Since AOZ contains no chiral auxiliary, the observed stereochemistry must be attributed to the catalyst-site controlled polymerization rendered by the C_2-ligated chiral catalyst.[2] Next, we polymerized both (*R*)- and (*S*)-AOZ monomers using *rac*-**1** (2 mol%) for 3 h at ambient temperature, achieving quantitative monomer conversions and affording the corresponding isotactic, *optically active* polymers, (*R*)-PAOZ and (*S*)-PAOZ, with MW's = 11.1 and 9.98 kg/mol, respectively (runs 1 and 4, Table 1). The observed MW's are close to the calculated MW of 10.9 kg/mol, and therefore the polymerization shows its control over the resulting polymer MW. The polymers exhibit unimodal MWD's, but they are relatively broad (>2.0), as compared to the typically narrow MWD's (<1.2) observed for poly(alkyl methacrylate)s and poly(alkyl acrylamide)s produced by *rac*-**1**.[30,32,34b] The formation of polymers with relatively broad, unimodal MWD's are normally attributed to the slower rate of chain initiation than the rate of chain propagation for polymerization systems with single-site catalysts.[2] However, in the case of the current system, it could also be attributable to the possibility that the enantiomeric monomer was preferentially polymerized by one enantiomer of the racemic catalyst. To test this hypothesis, we investigated the ability of the (*R,R*)-**1** enantiomer to effect the kinetic resolution polymerization of *rac*-(*R/S*)-AOZ, ideally polymerizing one enantiomer preferentially via a large stereoselectivity factor while resolving the other enantiomerically pure. The actual experiment showed that (*R,R*)-**1** was unable to kinetically resolve (*R/S*)-AOZ, as several aliquots taken during the course of polymerization, when analyzed by chiral HPLC, revealed no enantiomeric excess of the unreacted monomer, demonstrating that each enantiomer of the catalyst polymerizes the enantiomeric monomers with equal efficacy. Furthermore, the specific

rotations of the isolated polymers are strikingly similar to their respective monomers. More specifically, $[\alpha]^{23}_{D}$ of (*R*)-AOZ is –159 °, while the isolated polymer has the same value (within experimental error) of $[\alpha]^{23}_{D}$ = –158 °. Likewise, the specific rotation of (*S*)-AOZ is +159 °, and it is +182 ° for its derived polymer. *Significantly*, the minimal to no change in both magnitude and sign of specific rotations of these polymers, in comparison to their respective monomers, is *drastically different than* the chiral helical polymer examples discussed above, where helix formation resulted in polymers with largely different optical rotations (and sometime in signs as well) than their corresponding monomers.

Table 1. Selected Results of Polymerization of (*R* and *S*)-AOZ by Chiral Catalysts **1**. [a]

run no.	monomer form	catalyst form	conv. [b] (%)	10^3 M_n [c] (g/mol)	MWD [c] (M_w/M_n)	$[\alpha]^{23}_{D}$ [d] (°)
1	(*R*)-AOZ	*rac*-**1**	100	11.1	2.41	–158
2	(*R*)-AOZ	(*R,R*)-**1**	100	6.77	1.77	–160
3	(*R*)-AOZ	(*S,S*)-**1**	100	7.88	1.42	–154
4	(*S*)-AOZ	*rac*-**1**	100	9.98	2.07	+182
5	(*S*)-AOZ	(*R,R*)-**1**	100	7.23	1.77	+170
6	(*S*)-AOZ	(*S,S*)-**1**	100	8.27	1.74	+185

[a] Carried out in 5 mL CH_2Cl_2 at ambient temperature (~25 °C); 2 mol% catalyst. [b] Conversion measured by ^{1}H NMR. [c] Determined by GPC relative to PMMA standards. [d] 0.2 g/dL, $CHCl_3$.

Efforts in explaining the above results obtained in the polymerization of (*R* and *S*)-AOZ monomers have led to the formulation of the following three hypotheses (possible scenarios): (1) the polymers produced by *rac*-**1** form an equal mixture of right- and left-handed helical structures, where the helicity is determined by the chirality of the catalyst, and therefore the optical activity arising from the secondary structures cancel each other out; (2) one-handed chiral helical polymers are produced, but the helicity is dictated by the chiral side-groups of the isotactic polymers; or (3) the polymers produced adopt random-coil conformations, where the stereoregular main chain becomes cryptochiral, and therefore the optical activity is controlled by the chiral auxiliary. Several lines of key evidence detailed below unequivocally disproof hypotheses 1 and 2 and thus show that the third scenario is strongly suggested for the present chiral AOZ polymers.

First, we employed enantiomeric catalysts **1** for the polymerization of (*R* and *S*)-AOZ since the results will reveal if excess one-handed helicity could be formed or not. (*R*)-AOZ was polymerized efficiently by (*R,R*)- and (*S,S*)-**1**, affording the corresponding polymers with MW's = 6.77 and 7.88 kg/mol and MWD's = 1.77 and 1.42, respectively (runs 2 and 3, Table 1). Intriguingly, the specific rotations of all the polymers derived from (*R*)-AOZ are rather similar (i.e., $[\alpha]^{23}_{D}$ varied from a narrow range from –154 ° to –160 °), regardless of the form of the catalyst utilized (runs 1–3). Furthermore, all the polymers show nearly identical Cotton effects, as revealed by their CD spectra (Figure 1), which is in sharp contrast to the chiral helical polymers with one-handed helicity being dictated by the chirality of the catalyst (*vide supra*). Hence, since the polymers derived from (*R*)-AOZ are optically indistinguishable, these results clearly ruled out hypothesis (1) which assumes that each enantiomeric catalyst produces AOZ polymer kinetically trapped in the right- or left-handed, solution-stable helix.

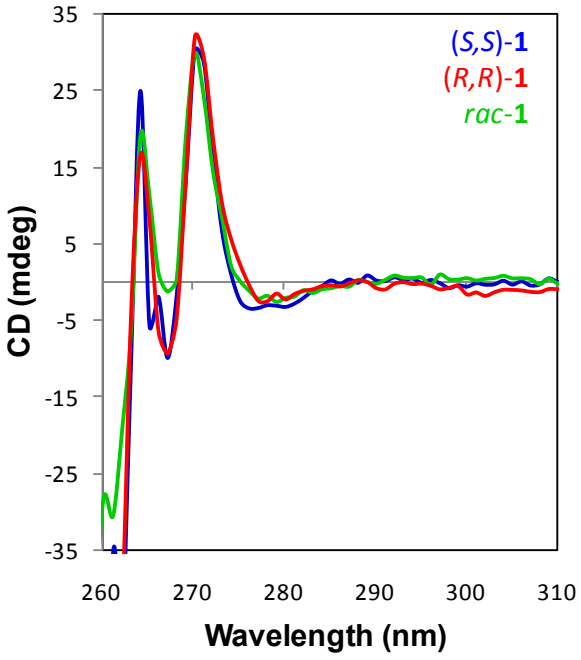

Figure 1. CD Spectra of (*R*)-AOZ polymers produced by catalysts (*S,S*)-**1** (blue), (*R,R*)-**1** (red), and *rac*-**1** (green).

Second, the study of the chiroptical properties of the polymers derived from (*S*)-AOZ using three different forms of catalyst **1** provides additional evidence for disproof of hypothesis 1. As in the case of the (*R*)-AOZ monomer, (*S*)-AOZ was quantitatively polymerized by the enanantiomeric catalysts to isotactic, optically active polymers with MW's = 7.23 and 8.27 kg/mol and MWD's = 1.77 and 1.74, by (*R,R*)- and (*S,S*)-**1**, respectively (runs 5 and 6, Table 1). Also identical to the observations with the polymers composed of (*R*)-AOZ, the (*S*)-AOZ based polymers exhibited rather similar optical rotations, regardless of catalyst form employed (i.e., $[\alpha]^{23}_{D}$ = +182, +170, and +185 ° for polymers produced by *rac*-, (*R,R*)-, and (*S,S*)-**1**, respectively), and again nearly identical CD spectra (Figure 2). Hence, these results strongly back the above conclusion (point 1), based on the findings in the polymerization of (*R*)-AOZ, that the enantiomeric catalysts do not convert the enantiomeric AOZ to a kinetically trapped right- or left-handed solution-stable helical polymer.

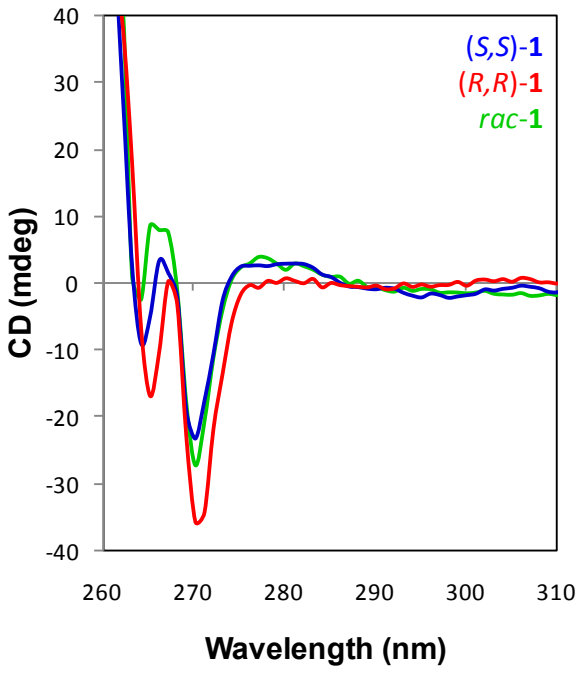

Figure 2. CD Spectra of (*S*)-AOZ polymers produced by catalysts (*S,S*)-**1** (blue), (*R,R*)-**1** (red), and *rac*-**1** (green).

Third, we ascertained the possibility of the chiral side-groups of the polymer dictating helicity (hypothesis 2), due to the observed large change in CD spectra for the isolated polymers, as compared to their respective monomers (Figure 3). Again, this possibility is inconsistent with the observation that there was no chiral amplification and exhibited only minimal differences in specific rotations of the polymers than their respective monomers, as shown by the examples described above. A hypothetical helix-helix stereo-mutation was also not observed for these polymers, as the specific rotation of the solution did not change, immediately after dissolution, nor after 4 days.

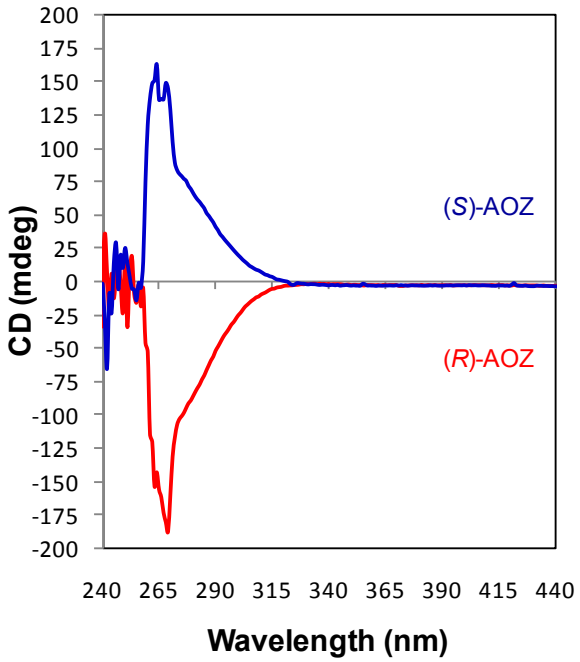

Figure 3. CD Spectra of chiral AOZ monomers: (*S*)-AOZ (blue) and (*R*)-AOZ (red).

Fourth, the results of our copolymerization studies provide additional evidence for disproof of hypothesis 2. We reasoned that if the chiral auxiliary of the AOZ monomers dictates the formation of a single-handed helical polymer during the course of polymerization, then we can reveal this phenomenon through copolymerizations, specifically, through investigating chiral

amplifications manifestable by the majority rules[35] or "sergeants and soldiers" effects.[36] In both effects, a small chiral bias results in a chiral amplification in the entire polymer chain, leading to highly optically active polymers. To this end, we copolymerized *nonequivalents* of (*R*)- and (*S*)-AOZ by *rac*-**1** (since no kinetic resolution polymerization proceeded, we can employ the *racemic* catalyst directly) (runs 7–9, Table 2). The copolymers with 10, 20, and 40 % *ee* of (*R*)-AOZ exhibited very similar MW and MWD, but no chiral amplification was observed in their CD spectra. Furthermore, in examining specific rotations of these polymers, there was just an additive effect in optical rotation, not a chiral amplification. Specifically, the polymers with 10, 20, and 40 % *ee* of (*R*)-AOZ had $[\alpha]^{23}_{D}$ = –15.9, –33.8, and –70.7 ° (from run 7 to 9), increasingly linearly with % *ee*, as was observed in vinyl polymers not forming excess one-handed helicity.[37]

Table 2. Selected Results of Copolymerization of (*R*)- with (*S*)-AOZ by *rac*-**1**.[a]

run no.	(*R*)-AOZ (mol %)	(*S*)-AOZ (mol %)	conv. (%)	10^3 M_n (g/mol)	MWD (M_w/M_n)	$[\alpha]^{23}_{D}$ (°)
7	55	45	100	8.34	1.37	–15.9
8	60	40	100	8.79	1.39	–33.8
9	70	30	100	8.89	1.42	–70.7

[a] See footnotes in Table 1 for explanations.

To examine the ability of these chiral monomers to influence helicity through the "sergeants and soldiers" effect, we copolymerized (*S*)-AOZ with the structurally similar, prochiral acryloyl-2-oxazolidinone (AOZ). As a control, we polymerized AOZ alone with *rac*-**1**. The optically inactive polymer produced by *rac*-**1** exhibited a MW of 6.03 kg/mol and a MWD of 1.69 (run 10, Table 3). Next, we incorporated 4, 10, and 20 mol % of chiral (*S*)-AOZ into the monomer feed, quantitatively producing the corresponding optically active copolymers (runs 11–13, Table 3). However, the specific rotation increased only linearly with incorporation of the chiral monomer and also no large Cotton effects were observed in the CD spectra, again indicating the lack of chiral amplification. *Overall*, the combination of the results obtained in the homopolymerization of the enantiomeric monomers with the chiral amplification studies, through copolymerization of the mixed chiral-chiral and chiral-achiral monomer feeds, led to the

conclusion that the side-groups of the repeat units are not bulky enough and too far (3 atoms) away from the isotactically placed stereogenic centers of the polymer backbone to sterically induce helicity into the polymer. Instead, random-coil secondary structures form.

Table 3. Selected Results of Copolymerization of Achiral AOZ with Chiral (*S*)-AOZ by *rac*-**1**.[a]

run no.	(*S*)-AOZ (%)	AOZ (%)	conv. (%)	10^3 M_n (g/mol)	MWD (M_w/M_n)	$[\alpha]^{23}_D$ (°)
10	0	100	100	6.03	1.69	0.0
11	4	96	100	7.40	1.41	+18.3
12	10	90	100	7.87	1.43	+28.1
13	20	80	100	8.67	1.43	+35.8

[a] See footnotes in Table 1 for explanations.

Fifth, disproof of hypotheses 1 and 2 by the above four sets of experiments led to the key, third hypothesis that remains consistent with, and thus supported by, all the data: the chiral isotactic AOZ polymers adopt a random-coil conformation and the optical activity is dictated by the chiral auxiliary. This scenario was further supported by the observation that *all* (*R*)-AOZ polymers with different main-chain stereoconfigurations, specifically, the isotactic polymer by C_2-ligated metallocenium catalyst **1**, the syndiotactic polymer by the C_s-ligated metallocenium catalysts,[33] and the atactic polymer by the free radical initiator (AIBN), showed nearly identical Cotton effects in their CD spectra (Figure 4).

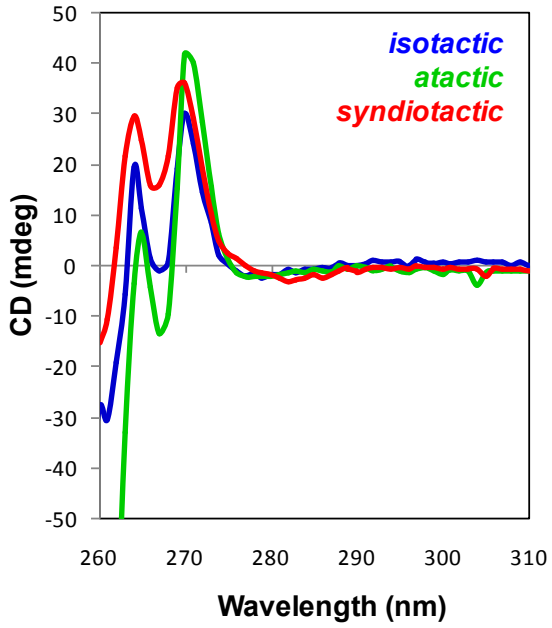

Figure 4. CD Spectra of (*R*)-AOZ derived polymers with different main-chain stereoconfigurations: isotactic polymer (blue), syndiotactic polymer (red), and atactic polymer (green).

Sixth, modeling of isotactic $[(R)\text{-AOZ}]_{30}$ by MM2 calculations also led to a random-coil chain secondary structure (Figure 5), thus providing additional support to hypothesis 3. This modeling result is in sharp contrast to the calculated helical structure for isotactic $[(R)\text{-VOZ}]_{30}$ (*c.f.,* Chart 2), the discussion of which immediately follows.

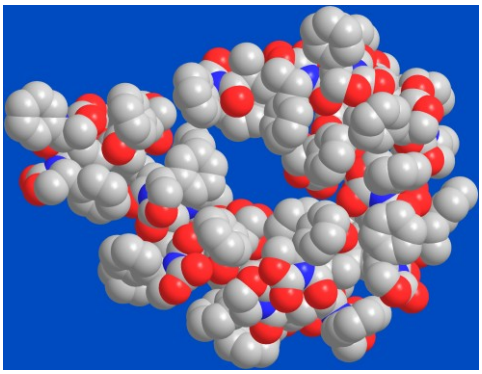

Figure 5. Modeled random-coil structure of $[(R)\text{-AOZ}]_{30}$ shown in the space filling mode (carbon, nitrogen, and oxygen are shown in grey, blue, and red, respectively; hydrogen atoms omitted for clarity).

Stereospecific Cationic Polymerization of Chiral Vinyl Oxazolidinones. As the above studies have shown, the chiral auxiliary of the repeat units in the chiral AOZ polymers are not bulky enough, being three atoms away from the polymer backbone stereocenters, to sterically induce helicity into the polymer. Accordingly, we reasoned that if we brought the chiral side-groups *closer* to the stereocenters of the polymer main-chain in polymers derived from non-conjugated *N*-vinyl-4-(*R*)-phenyl-2-oxazolidinone [(*R*)-VOZ)], where the chiral auxiliary is only two atoms away from the main-chain stereocenters, then the side-groups could be effective in rendering solution-stable helical polymers.

However, there presents two *challenges* in coordination polymerization of (*R*)-VOZ. First, it is a non-conjugated vinyl monomer, so it cannot be polymerized via a coordination conjugate-addition mechanism by zirconocenium ester enolate catalysts such as **1**.[2] Second, it is a heteroatom (*N,O*)-functionalized vinyl monomer, so it cannot be polymerized (at least directly) via a coordination insertion mechanism by metallocenium alkyl catalysts such as *rac*-(EBI)ZrMe$^+$MeB$(C_6F_5)_3^-$.[2] A potential strategy here is to use protected (coordinated) hetereoatom-functionalized vinyl monomers with aluminum Lewis acids, which can be readily removed post-polymerization.[38] Initial attempts to polymerize (*R*)-VOZ with *rac*-(EBI)ZrMe$_2$ activated with 500 equiv of MAO—which we reasoned could not only abstract the methyl group to form the active zirconcenium catalyst species,[39] but also protect the heteroatoms of (*R*)-VOZ from interfering with the migratory insertion polymerization process—failed to form any isolable polymer after 24 h of reaction. Next, we pre-complexed (*R*)-VOZ with 0 to 3 equiv of ^{i}Bu$_3$Al and subjected the complexed monomer to polymerization by *rac*-(EBI)ZrMe$_2$ activated with equimolar B$(C_6F_5)_3$ [which generates *in situ* the active species, *rac*-(EBI)ZrMe$^+$MeB$(C_6F_5)_3^-$][39] at ambient temperature or 80 °C for up to 24 h. However, this also yielded no polymer products. We also repeated these polymerization procedures, but using [Ph$_3$C][B$(C_6F_5)_4$] as the activator. For the runs using ^{i}Bu$_3$Al as the complexing agent, no polymerization was observed at various reaction temperature and time. *Surprisingly*, in the absence of ^{i}Bu$_3$Al, the polymerization at

ambient temperature by *in situ* activation of *rac*-(EBI)$ZrMe_2$ with equimolar $[Ph_3C][B(C_6F_5)_4]$ proceeded rapidly, with the polymer immediately crashing out of solution.

This intriguing, exciting result raised the question of what is the actual catalyst species responsible for the successful polymerization of (*R*)-VOZ? Note that zirconocenium species such as *rac*-(EBI)$ZrMe^+MeB(C_6F_5)_3^-$ are inactive for this polymerization. However, it is known that activation of the metallocene dimethyl pre-catalyst with $[Ph_3C][B(C_6F_5)_4]$ proceeds in a step-wise fashion: the first step is the rapid methide abstraction to form the transient μ-Me dimer, a result of stabilization of the initially formed metallocene cation by the other half of the neutral dimethyl species, instead of the anion $[B(C_6F_5)_4]^-$, due to its extremely weakly coordination nature.[40] The slower proceeding step is the gradual conversion of the stable dimer to the highly unstable, reactive mononuclear zirconocenium species by the other half of $[Ph_3C][B(C_6F_5)_4]$ (Scheme 1). Thus, the complexity of this activation process presented 4 possible species being responsible for the observed polymerization activity: the mononuclear zirconocenium cation, the dinuclear cation, the dimethyl precatalyst, and the activator $[Ph_3C][B(C_6F_5)_4]$.

Scheme 1. Step-wise activation of *rac*-(EBI)$ZrMe_2$ by $[Ph_3C][B(C_6F_5)_4]$.

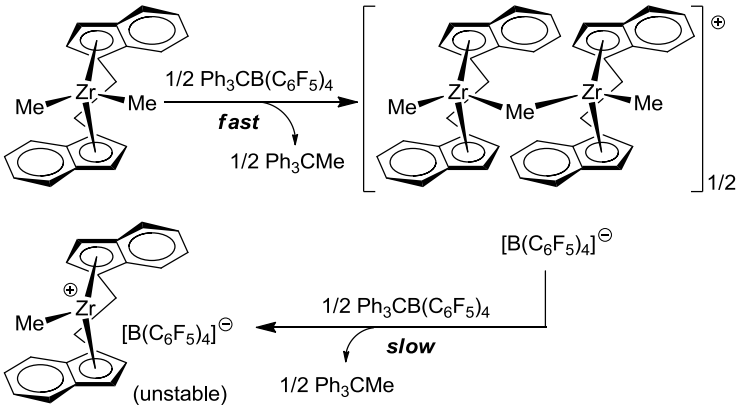

Control experiments subsequently ruled out the neutral precatalyst *rac*-(EBI)$ZrMe_2$ and the mononuclear zirconocenium cation *rac*-(EBI)$ZrMe^+$ as the active species for this polymerization. The independently prepared dinuclear complex[40] from the reaction of 2 equiv of *rac*-(EBI)$ZrMe_2$

with 1 equiv of $[Ph_3C][B(C_6F_5)_4]$ also exhibited no polymerization activity. Lastly, we found that addition of a catalytic amount of $[Ph_3C][B(C_6F_5)_4]$ to a toluene solution of (*R*)-VOZ resulted in rapid polymerization with the polymer crashing out of solution, the same phenomenon as seen in the polymerization by *in situ* activation of *rac*-(EBI)$ZrMe_2$ with equimolar $[Ph_3C][B(C_6F_5)_4]$ (*vide supra*). These results conclusively pointed to $[Ph_3C][B(C_6F_5)_4]$—intended as the activator for the metallocene precatalyst—as the actual active species responsible for the observed polymerization activity. Unfortunately, all isolated polymers using different {(*R*)-VOZ}:{$[Ph_3C][B(C_6F_5)_4]$} ratios (5–50), solvents (toluene and CH_2Cl_2), and temperature (0 °C and 25 °C), are insoluble in all common organic solvents and concentrated acids tested, even at elevated temperatures (up to the boiling points of the solvents). The polymer yield was held nearly constant of ~60% for runs at {(*R*)-VOZ}:{[Ph3C][$B(C_6F_5)_4$]} = 50 at 25 °C for 2 h in toluene or CH_2Cl_2, but the polymerization in THF was almost completely shut down (0.65 % yield). The $[Ph_3C][B(C_6F_5)_4]$ initiator can be substituted by other cationic initiators such as $BF_3{\cdot}Et_2O$. From a view point of devinylation that plaques the polymerization of the unsubstituted VOZ[13,15] and other *N*-vinyl heterocyclic monomers[16] using acids, it is *intriguing* and actually *fortunate* that instantaneous precipitation of the resulting polymer prevented such devinylation to a large extent, enabling us to achieve the first successful cationic polymerization of VOZ monomers with good polymer yields up to 80% (at 0 °C) and also the first successful synthesis of highly isotactic PVOZ (*vide infra*).

The insolubility of the resulting non-crosslinking (*R*)-PVOZ in all common organic solvents suggests a rigid-rod-like chiral polymer adopting a one-handed helical conformation—as predicted by modeling (*c.f.,* Chart 2)—a result of having a highly isotactic backbone stereoconfiguration generated through a novel chiral auxiliary-controlled, isospecific cationic polymerization mechanism. However, to provide concrete evidence for such a polymer structure, the insolubility associated with (*R*)-PVOZ must be solved to allow characterization of the polymer. To this end, we synthesized the *para*-hexyloxy substituted derivative, (*R*)-4-(4-

(hexyloxy)phenyl)-3-vinyloxazolidin-2-one [(*R*)-HVOZ)], according to Scheme 2, and subsequently investigated its cationic polymerization behavior.

Scheme 2. Outlined synthesis of (*R*)-HVOZ.

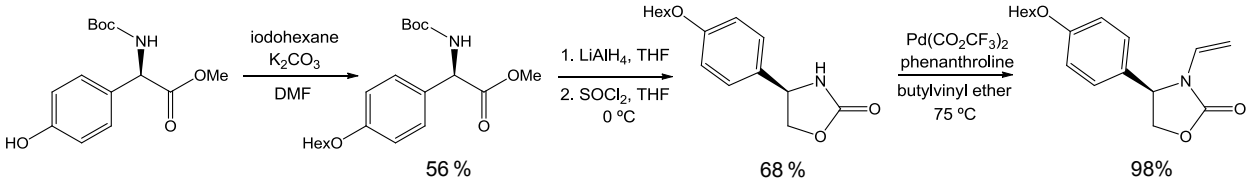

Gratifyingly, (*R*)-HVOZ was also polymerized by $[Ph_3C][B(C_6F_5)_4]$, and the polymerization remained homogeneous during the course of polymerization. The resulting polymers are soluble in common organic solvents, thus enabling characterizations of the polymers by GPC for MW and MWD, NMR for tacticity, as well as by optical rotation and CD for optical activity. However, the isolated polymer yield was very low (6.0%, run 14, Table 4), even after extended reaction time (24 h) at ambient temperature. Nonetheless, the polymer had a relatively narrow MWD of 1.65 and a MW of 7.63 kg/mol. Considering side reactions at ambient temperature often observed for cationic polymerization, we lowered the polymerization temperature to 0 °C (run 15) and –20 °C (run 16), but doing so did not improve the polymer yield. The use of $BF_3{\cdot}Et_2O$ as initiator enhanced the polymer yield somewhat (to ~10%, run 17) at 25 °C, but variations in polymerization temperature (runs 18 and 19) lowered the yield. Brønsted acids were also examined, including $[H(Et_2O)_2]^+[B(C_6F_5)_4]^-$ (run 20) and $[HN(Me_2)Ph]^+[B(C_6F_5)_4]^-$, but the polymer yield was never higher than 10%.

Table 4. Selected Results of Cationic Polymerization of (*R*)-HVOZ.[a]

run no.	initiator	temp (°C)	yield (%)	10^3 M_n (g/mol)	MWD (M_w/M_n)
14	$[Ph_3C][B(C_6F_5)_4]$	25	6.0	7.63	1.65
15	$[Ph_3C][B(C_6F_5)_4]$	0	2.0	7.11	1.69
16	$[Ph_3C][B(C_6F_5)_4]$	–20	5.8	5.20	1.81
17	$BF_3{\cdot}Et_2O$	25	9.5	6.53	1.60
18	$BF_3{\cdot}Et_2O$	0	6.9	6.68	1.79
19	$BF_3{\cdot}Et_2O$	–20	6.3	5.26	1.78
20	$[H(Et_2O)_2][B(C_6F_5)_4]$	25	9.5	7.31	1.64

[a] See footnotes in Table 1 for explanations.

Hypothesizing that devinylation may be the cause for the low polymer yield seen in the cationic polymerization of (*R*)-HVOZ, we investigated the stoichiometric reaction of (*R*)-HVOZ with $[Ph_3C][B(C_6F_5)_4]$. Indeed, the isolated product from the reaction was (*R*)-4-(4-(hexyloxy)phenyl)oxazolidin-2-one, the devinylation product. Likewise, the polymerization reaction of (*R*)-HVOZ with a catalytic amount of $[Ph_3C][B(C_6F_5)_4]$ led to (after quenching the reaction, separating the MeOH insoluble polymer fraction, and removing the solvent) isolation of almost exclusively the oxazolidinone. Although acid-catalyzed decomposition of *N*-vinyl heterocyclic monomers via devinylation,[13,15] even in the solid state,[16] is known, it was surprising to see the sharp contrast in the extent of the monomer decomposition between the heterogeneous polymerization of (*R*)-VOZ and the homogenous polymerization of (*R*)-HVOZ. A further study through monitoring the reaction of $[Ph_3C][B(C_6F_5)_4]$ with 5 equiv of (*R*)-HVOZ revealed a valuable insight: isotactic polymer was formed initially, but over time the backbone methylene proton signals corresponding to an isotactic configuration disappeared and the proton signal for the oxazolidinone appeared. Hence, this experiment showed that some polymerization initially occurs, followed by decomposition to give oxazolidinone, thus competing with the direct devinylation of the monomer. This valuable insight also explains the drastic difference in polymer yields between the polymerizations of (*R*)-VOZ and (*R*)-HVOZ: the hexyloxy substitution in (*R*)-HVOZ should have none to minimal effects on the rate of monomer devinylation, but instead it is the insolubility of (*R*)-PVOZ, upon forming and crashing out of solution, that prevents it from decomposition. Obviously, this mechanism of devinylation prevention does not apply to the soluble (*R*)-PHVOZ.

On the other hand, the solubility of (*R*)-PHVOZ allowed us to investigate its tacticity and optical properties, despite the observed low polymer yield. As anticipated, analysis of the ^{13}C NMR spectrum of (*R*)-PHVOZ produced by $[Ph_3C][B(C_6F_5)_4]$ at ambient temperature clearly reveals its high isotacticity, as evidenced by the single *mmmm* pentad peak in the C=O region which is collaborated by the single methine and methylene backbone carbon peaks (Figure 6).

Outlined in Scheme 3 is the proposed chiral auxiliary-controlled isospecific cationic polymerization for the production of isotactic, chiral vinyl oxazolidinone-functionalized vinyl polymers, where the concept of stereocontrol in repeated vinyl additions is analogous to the stereocontrol observed in the free radical polymerization of chiral acrylamides.[10,11,12] *More importantly*, combination of this near quantitatively isotactic placement of the stereogenic centers of the polymer main-chain with the chiral side-groups located near those stereocenters of the backbone rendered one-handed helicity for (*R*)-PVOZ and (*R*)-PHVOZ. Owing to the insolubility of (*R*)-PVOZ, its helical structure was only inferred by modeling (*c.f.,* Chart 2). Thanks to the solubility of (*R*)-PHVOZ, the helical structure is now directly supported by the experimental results, including the greatly changed specific rotation, in both magnitude and sign, in going from the monomer (*R*)-HVOZ to the polymer (*R*)-PHVOZ (–44.8 °C to +156; run 14, Table 4), as well as the drastically different CD spectra between the monomer and the polymer (Figure 7). Each of these observables represents chiral amplifications characteristic of helical-structure formation.

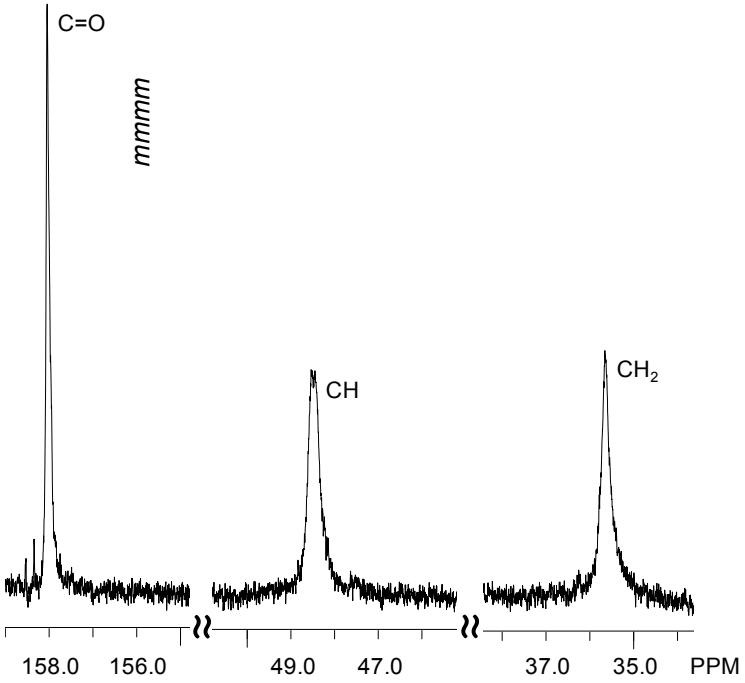

Figure 6. Carbonyl as well as main-chain CH and CH_2 regions in the ^{13}C NMR (125 MHz, $CDCl_3$, 50 °C) of (*R*)-PHVOZ produced by $[Ph_3C][B(C_6F_5)_4]$ at ambient temperature.

Scheme 3. Proposed chiral auxiliary-controlled isospecific cationic polymerization of (*R*)-(H)VOZ.

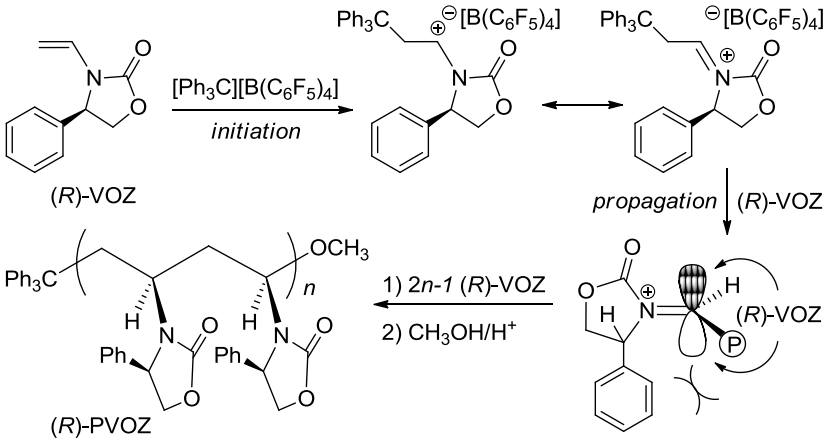

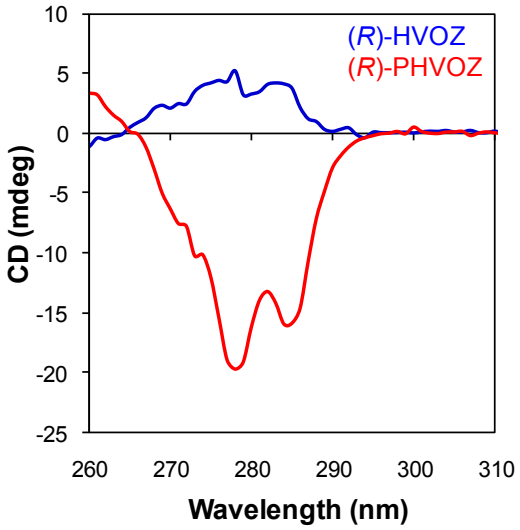

Figure 7. CD Spectra of monomer (*R*)-HVOZ (blue) and polymer (*R*)-PHVOZ (red).

Physical Properties of Stereoregular (*R*)-PAOZ and (*R*)-PVOZ. Polymer thermal transition, decomposition, and crystallinity were analyzed by DSC, TGA, and XRD, respectively, and comparisons were made between the rigid-rod-like helical polymer (*R*)-PVOZ, produced via isospecific cationic polymerization by $[Ph_3C][B(C_6F_5)_4]$, and the random-coil polymer (*R*)-PAOZ, produced via isospecific coordination polymerization by catalyst **1**. In the DSC trace, no T_g was observed for (*R*)-PVOZ in the conditions employed, which is not surprising for such a highly

isotactic and crystalline polymer.[34b,c] On the other hand, (*R*)-PAOZ exhibited a high T_g of 196 °C. In the TGA trace, (*R*)-PVOZ showed a very narrow, one-step decomposition window with high decomposition temperatures of $T_{initial}$ = 435 °C, T_{end} = 481 °C (Figure 8), and T_{max} = 460 °C. In comparison, (*R*)-PAOZ showed in its TGA trace a relatively broader, one-step decomposition window, with much lower decomposition temperatures of $T_{initial}$ = 351 °C, T_{end} = 412 °C, and T_{max} = 390 °C (Figure 9).

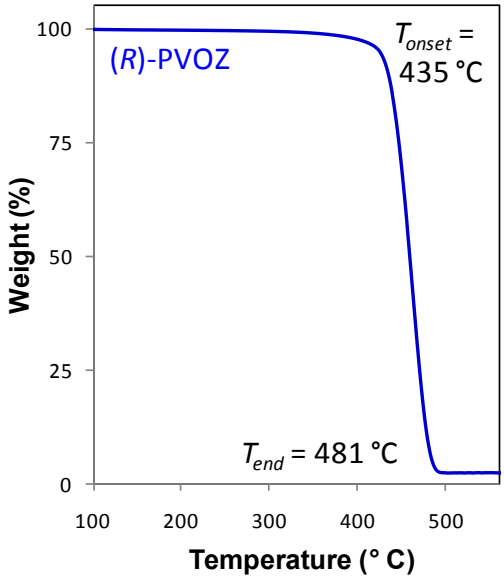

Figure 8. TGA plot of (*R*)-PVOZ produced by $[Ph_3C][B(C_6F_5)_4]$ in CH_2Cl_2.

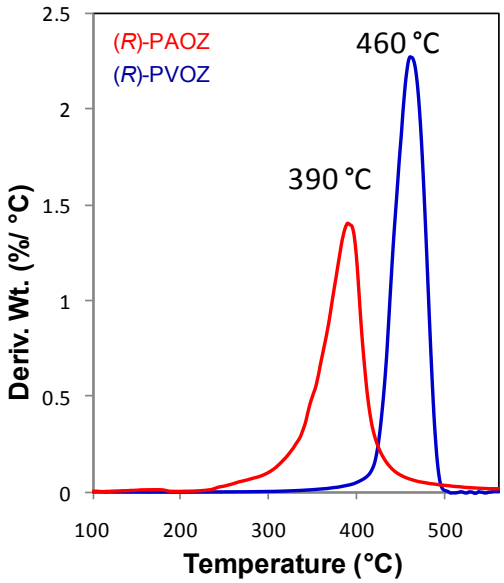

Figure 9. TGA derivative plots of (*R*)-PAOZ (red, run 3, Table 1) and (*R*)-PVOZ produced by $[Ph_3C][B(C_6F_5)_4]$ in CH_2Cl_2.

The XRD plots show significant differences in the crystallinity in the as-quenched polymers, (*R*)-PVOZ and (*R*)-PAOZ (Figure 10). Although both isotactic polymers exhibit three distinct scattering peaks [*d* spacing: 1.03 nm, 0.58 nm, and 0.38 nm for (*R*)-PVOZ], the sharpness and intensity of the scattering peaks of (*R*)-PVOZ is significantly greater, indicating a higher degree of crystallinity, as compared to (*R*)-PAOZ. Overall, these characterizations demonstrated that the chiral isotactic vinyl polymer (*R*)-PVOZ is considerably more thermally stable and more crystalline than the chiral isotactic acrylamide polymer (*R*)-PAOZ, characteristics attributable to the rigid-rod-like, helical structure of the chiral vinyl polymer.

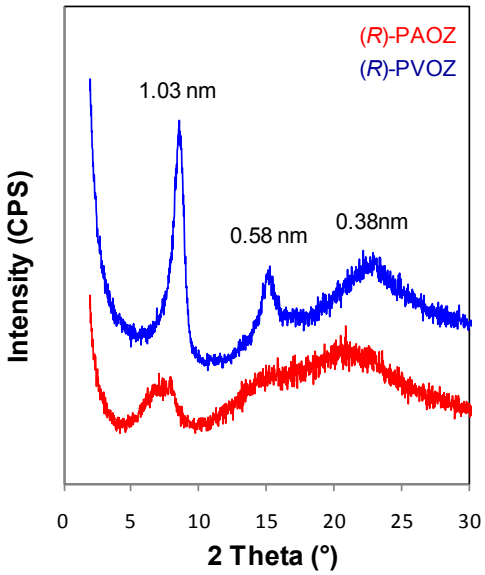

Figure 10. Overlay XRD plots of (*R*)-PAOZ (red, run 3, Table 1) and (*R*)-PVOZ produced by $[Ph_3C][B(C_6F_5)_4]$ in CH_2Cl_2.

Conclusions

Chiral oxazolidinone-functionalized alkenes have been successfully polymerized at ambient temperature in a stereospecific fashion, leading to the corresponding highly isotactic, optically active polymers. Depending on whether the monomer is conjugated or not, the polymerization proceeds through one of two mechanisms. For conjugated chiral acryloyl oxazolidinones, (*R* or *S*)-AOZ, *isospecific coordination* polymerization is brought about by chiral catalysts **1**. in both racemic and enantiomeric forms. This polymerization is catalyst-site controlled, producing highly isotactic, optically active polymers (*R* or *S*)-PAOZ. Owing to the nature of chiral catalyst-site control, the coordination polymerization of the parent AOZ without the chiral side group also affords PAOZ with nearly quantitative isotacticity. Our extensive studies have demonstrated that these oxazolidinone-functionalized, chiral isotactic poly(acrylamide)s adopt a random-coil structure, thus having a cryptochiral chain and exhibiting no chiral amplifications; their optical activity arises solely from the chiral auxiliary. These results

are rationalized by the chiral side-groups in these chiral poly(acrylamide)s not being sufficiently bulky and located too far away from the isotactically placed stereocenters of the main chain to induce sterically a solution-stable helical conformation.

In order to polymerize non-conjugated chiral vinyl oxazolidinones, we successfully developed a novel ambient-temperature *isospecific cationic* polymerization using Lewis and Brønsted acids. This polymerization is chiral auxiliary-controlled and also produces highly isotactic, optically active polymers, (*R*)-PVOZ and (*R*)-PHVOZ. However, in sharp contrast to the chiral acrylamide polymers, these vinyl polymers adopt a solution-stable helical conformation, thereby manifesting substantial chiral amplifications. Both modeling of the insoluble (*R*)-PVOZ and experimental results obtained from the soluble (*R*)-PHVOZ polymer have yielded the same result: a chiral helical structure. Synthetically, the facile acid-catalyzed devinylation presented a major challenge to the homogenous, stereospecific cationic polymerization of (*R*)-HVOZ, thus severally limiting its polymer yield. Efforts are underway to search for more effective strategies to eliminate or largely suppress such side reactions.

The chiral helical vinyl polymers synthesized herein are of particular interest for two key reasons. First, they effectively assemble two elements of polymer local chirality—side-chain chirality and main-chain chirality—into global chirality in the form of excess one-handed helicity. Second, these *N,O*-functionalized chiral vinyl polymers represent chiral variants of structurally similar PVP, the currently most widely employed effective ligand/stabilizer in transition-metal nanocluster chemistry. Such globally assembled helical chiral polymers already showed their superior physical properties such as having considerably higher thermal decomposition temperatures and polymer crystallinity, as compared to the random coil chiral acryloyl polymers having similarly high main-chain stereoregularity. Our research in utilizing both classes of chiral polymers synthesized herein as chiral ligands/stabilizers for transition-metal nanoclusters and their subsequent asymmetric catalysis is currently underway, the results of which will appear elsewhere in due course.

Acknowledgment. This work was supported by the National Science Foundation (NSF-0756633). We thank Prof. Alan Kennan of CSU for access to his CD spectrometer and Boulder Scientific Co. for the research gifts of $B(C_6F_5)_3$, $[Ph_3C]^+[B(C_6F_5)_4]^-$, and $[HN(Me_2)Ph]^+[B(C_6F_5)_4]^-$. This dissertation chapter contains the manuscript of a full paper published in *Macromolecules* [Miyake, G. M.; DiRocco, D.; Liu, Q.; Oberg, K. M.; Bayram, E.; Finke, R. G.; Rovis, T.; Chen, E. Y.-X. *Macromolecules* **2010**, *43*, 7504-7514]. D.D., Q. L., K. M. O., and E.B. prepared the chiral monomers.

References

(1) Selected reviews: (a) Yashima, E. *Polym. J.* **2010**, *42*, 3–16. (b) Ikai, T.; Okamoto, Y. *Chem. Rev.* **2009**, *109*, 6077–6101. (c) Yashima, E.; Maeda, K.; Iida, H.; Furusho, Y.; Nagai, K. *Chem. Rev.* **2009**, *109*, 6102–6211. (d) Okamoto, Y. *J. Polym. Sci. Part A: Polym. Chem.* **2009**, *47*, 1731–1739. (e) Yashima, E.; Maeda, K.; Furusho, Y. *Acc. Chem. Res.* **2008,** *41*, 1166–1180. (f) Yashima, E.; Maeda, K. *Macromolecules* **2008**, *41*, 3−12. (g) Okamoto, Y.; Ikai, T. *Chem. Soc. Rev.* **2008**, *37*, 2593−2608. (h) Hembury, G. A.; Borovkov, V. V.; Inoue, Y. *Chem. Rev.* **2008**, *108*, 1–73. (i) Yamamoto, C.; Okamoto, Y. *Bull. Chem. Soc. Jpn.* **2004**, *77*, 227−257. (j) Nakano, T.; Okamoto, Y. *Chem. Rev.* **2001**, *101*, 4013−4038. (k) Cornelissen, J. J. L. M.; Rowan, A. E.; Nolte, R. J. M.; Sommerdijk, N. A. J. M. *Chem. Rev.* **2001**, *101*, 4029−4070. (l) Okamoto, Y.; Nakano, T. *Chem. Rev.* **1994**, *94*, 349−372. (m) Wulff, G. *Polym News* **1991**, *16*, 167−173. (n) Okamoto, Y.; Yashima, E. *Prog. Polym. Sci.* **1990**, *15*, 263−298. (o) Wulff, G. *Angew. Chem. Int. Engl.* **1989**, *28*, 21−37. (p) Farina, M. *Top. Stereochem.* **1987**, *17*, 1–111. (q) Pino, P. *Adv. Polym. Sci.* **1965**, *4*, 393−456.

(2) Recent reviews: (a) Chen, E. Y.-X. *Chem. Rev.* **2009**, *109*, 5157–5214. (b) Chen, E. Y.-X. *Dalton Trans*. **2009**, 8784–8793.

(3) Selected reviews: (a) Finney, E. E.; Finke, R. G. *J. Colloid Interface Sci.* **2008**, *317*, 351–374. (b) Starkey-Ott, L.; Finke, R. G. *Coord. Chem. Rev.,* **2007**, *251*, 1075–1100. (c) Astruc, D.; Lu, F.; Aranzaes, J. R. *Angew. Chem. Int. Ed.* **2005**, *44*, 7852–7872. (d) Aiken, J. D. III; Finke, R. G. *J. Mol. Catalysis A: Chemical*, **1999**, *145*, 1–44.

(4) Selected recent examples: (a) Yamamoto, T.; Suginome, M. *Angew. Chem. Int. Ed.* **2009**, *48*, 539–542. (b) Reggelin, M.; Doerr, S.; Klussmann, M.; Schultz, M.; Holbach, M. *Proc. Natl. Acad. Sci.* **2004**, *101*, 5461–5466. (c) Reggelin, M.; Schultz, M.; Holbach, M. *Angew. Chem. Int. Ed.* **2002**, *41*, 1614–1617.

(5) Selected recent examples: (a) Starkey-Ott; L.;Hornstein, B. J.; Finke, R. G. *Langmuir* **2006**, *22*, 9357–9367. (b) Seo, D.; Park, J. C.; Song, H. *J. Am. Chem. Soc.* **2006**, *128*, 14863–14870. (c) Wiley, B.; Sun, Y.; Mayers, B.; Xia, Y. *Chem. Eur. J.* **2005**, *11*, 454–463.

(6) Gao, D.; Schefzick, S.; Lipowitz, K. B. *J. Am. Chem. Soc.* **1999**, *121*, 9481–9482.

(7) Pino, P.; Lorenzi, G. P. *J. Am. Chem. Soc.* **1960**, *82*, 4745–4747.

(8) Ager, D. J.; Prakash, I.; Schaad, D. R. *Aldrichim. Acta* **1997**, *30*, 3–12.

(9) Recent reviews: (a) Satoh, K.; Kamigaito, M. *Chem. Rev.* **2009**, *109*, 5120–5156. (b) Kamigaito, M.; Satoh, K. *Macromolecules* **2008**, *41*, 269–276.

(10) Mero, C. L.; Porter, N. A. *J. Org. Chem.* **2000**, *65*, 775–781.

(11) Porter, N. A.; Breyer, R.; Swann, E.; Nally, J.; Pradhan, J.; Allen, T.; McPhil, A. T. *J. Am. Chem. Soc.* **1991**, *113*, 7002–7010.

(12) Porter, N. A.; Allen, T. R.; Breyer, R. A. *J. Am. Chem. Soc.* **1992**, *114*, 7676–7683.

(13) Endo, T.; Numazawa, R.; Okawara, M. *Makromol. Chem.* **1971**, *146*, 247–256.

(14) Drechsel, E. K. *J. Org. Chem.* **1957**, *22*, 849–851.

(15) Kutner, A. *J. Org. Chem.* **1961**, *26*, 3495–3498.

(16) For examples: (a) Meyers, R. A.; Christman, E. M. *J. Polym. Sci. Part A-1.* **1968**, *6*, 945–950. (b) Lashua, S. C.; Hibbard, B. B. *US Pat.* **1966**, 3,284,414.

(17) (a) Walles, W. E.; Tousignant, W. F.; Houtman, T. Jr. *US Pat.* **1970**, 3,539,540. (b) Bakke, W. W. *US Pat.* **1962**, 3,033,829.

(18) Trumbo, D. L. *Polym. Bull.* **1993**, *31*, 569–575.

(19) Miyake, G. M.; Mariott, W. R.; Chen, E. Y.-X. *J. Am. Chem. Soc.* **2007**, *129*, 6724–6725.

(20) Miyake, G. M.; Chen, E. Y.-X. *Macromolecules* **2008**, *41*, 3405–3416.

(21) Wulff, G.; Zweering, U. *Chem. Eur. J.* **1999**, *5*, 1898−1904.

(22) Chelation of a cationic zirconocene center to both carbonyls of *N*-acryloyl-2-oxazolidinone has been demonstrated in: (a) Bondar, G. V.; Aldea, R.; Levy, C. J.; Jaquith, J. B.; Collins,

S. *Organometallics* **2000**, *19*, 947–949. (b) Jaquith, J. B.; Levy, C. J.; Bondar, G. V.; Wang, S.; Collins, S. *Organometallics* **1998**, *17*, 914–925. (c) Lin, S.; Bondar, G. V.; Levy, C. J.; Collins, S. *J. Org. Chem.* **1998**, *63*, 1885–1892.

(23) (a) Gao, Y.; Wei, C.-Q.; Burke, T. R.; *Org. Lett.* **2001**, *3*, 1617–1620. (b) Nicolas, E.; Russell, K. C.; Knollenberg, J.; Hruby, V. J. *J. Org. Chem.* **1993**, *58*, 7565–7571.

(24) Evans, D. A.; Miller, S. J.; Lectka, T.; von Matt, P. *J. Am. Chem. Soc.* **1999**, *121*, 7559–7573.

(25) Gaulon, C.; Dhal, R.; Dujardin, G. *Synthesis* **2003**, *14*, 2269–2272.

(26) Jutzi, P.; Müller, C.; Stammler, A.; Stammler, H. *Organometallics* **2000**, *19*, 1442–1444.

(27) (a) Ning, Y.; Caporaso, L.; Correa, A.; Gustafson, L. O.; Cavallo, L.; Chen, E. Y.-X. *Macromolecules* **2008**, *41*, 6910–6919. (b) Kim, Y.-J; Bernstein, M. P.; Galiano Roth, A. S.; Romesber, F. E.; Williard, P. G.; Fuller, D. J.; Harrison, A. T.; Collum, D. B. *J. Org. Chem.* **1991**, *56*, 4435–4439.

(28) (a) Grossman, R. B.; Doyle, R. A.; Buchwald, S. L. *Organometallics* **1991**, *10*, 1501−1505. (b) Collins, S.; Kuntz, B. A.; Taylor, N. J.; Ward, D. G. *J. Organomet. Chem.* **1988**, *342*, 21−29.

(29) Diamond, G. M.; Jordan, R. F.; Petersen, J. L. *J. Am. Chem. Soc.* **1996**, *118*, 8024−8033.

(30) Bolig, A. D.; Chen, E. Y.-X. *J. Am. Chem. Soc.* **2004**, *126*, 4897–4906.

(31) LoCoco, M. D.; Jordan, R. F. *J. Am. Chem. Soc.* **2004**, *126*, 13918–13919.

(32) Rodriguez-Delgado, A.; Chen, E. Y.-X. *Macromolecules* **2005**, *38*, 2587–2594.

(33) Zhang, Y.; Ning, Y.; Caporaso, L.; Cavallo, L.; Chen, E. Y.-X. *J. Am. Chem. Soc.* **2010**, *132*, 2695–2709.

(34) (a) Miyake, G. M.; Caporaso, L.; Cavallo, L.; Chen, E. Y.-X. *Macromolecules* **2009**, *42*, 1462–1471. (b) Mariott, W. R.; Chen, E. Y.-X. *Macromolecules* **2005**, *38*, 6822−6832. (c) Mariott, W. R.; Chen, E. Y.-X. *Macromolecules* **2004**, *37*, 4741–4743. (d) Kobayashi, M.;

Okuyama, S.; Ishizone, T.; Nakahama, S. *Macromolecules* **1999**, *32*, 6466−6477. (e) Xie, X.; Hogen-Esch, T. E.; *Macromolecules* **1996**, *29*, 1746−1752. (f) Bulai, A.; Jimeno, M. L.; de Queiroz, A.-A. A.; Gallardo, A.; Roman, J. S. *Macromolecules* **1996**, *29*, 3240–3246.

(35) Jha, S. K.; Cheon, K.; Green, M. M.; Selinger, J. V. *J. Am. Chem. Soc.* **1999**, *121*, 1665–1673.

(36) Green, M. M.; Reidy, M. P.; Johnson, R. J.; Darling, G.; Oleary, D. J.; Willson, G. *J. Am. Chem. Soc.* **1989**, *111*, 6452–6454.

(37) (a) Green, M. M.; Jha, S. K. *Chirality* **1997**, *9*, 424–427. (b) Pino, P.; Ciardelli, F.; Motagnoli, G.; Pieroni, O. *J. Polym. Sci., Part B: Polym. Lett.* **1967**, *5*, 307–311.

(38) Boffa, L. S.; Novak, B. M. *Chem. Rev*. **2000**, *100*, 1479–1493.

(39) Chen, E. Y.-X. Marks, T. J. *Chem. Rev.* **2000**, *100*, 1391–1434.

(40) (a) Chen, Y.-X., Metz, M. V.; Li, L.; Stern, C. L.; Marks, T. J. *J. Am. Chem. Soc.* **1997**, *120*, 6287–6305. (b) Bochmann, M.; Lancaster, S. J. *Angew. Chem. Int. Ed. Engl.* **1994**, *33*, 1634-1637.

Chapter 5

Helix-Sense Control and Effects on Enantioselectivity of Poly(Cinchona Phenyl Acetylene) Organocatalysts

Abstract

Two pseudo-enantiomeric monomers, (4-benzoyl cinchonidine) acetylene [BCdA] and (4-benzoyl cinchonine) acetylene [BCnA], have been synthesized and subsequently polymerized by $[Rh(nbd)Cl]_2$ (nbd = norbornadiene) to synthesize stereoregular (*cis*-transoidal) P(BCdA) and P(BCnA). These polymers exhibit excess one-handed helicity in solution, and in identical solvents, assume helical conformations that are of opposite-handedness as evidenced by nearly mirror image CD spectra. By altering the solvent in which these polymers are dissolved in, from chloroform to tetrahydrofuran, the handedness of these helical polymers can be switched. Bearing cinchonidine and cinchonine organocatalyst functionalities, an investigation on the effects of the helicity and helix-sense on the enantioselectivity was then conducted for the enantioselective addition of 2-napthalenethiol to 2-cyclohexenone.

Communication

Anchoring chiral organocatalyst functionalities onto a polymer support is an effective means of enabling a catalyst to be easily separated from the reaction medium and recycled.[1] However, there are few reports that exploit the ability of the polymer to form a helical secondary structure to increase the enantioselectivity of these organocatalysts, and in most cases, the helical polymer supported catalysts usually exhibits a decrease in enantioselectivity, as compared to the monomeric catalyst.[2] Thus, when poly[*N*-(4-ethynylbenzyl)ephedrine] was used to catalyze the enantioselective addition of diethylzinc to benzaldehyde, the *ee* was 30-49%, while the *ee* of the reaction catalyzed by the monomeric *N*-(4-benzyl)ephedrine was 80 %.[2c] An exception is the asymmetric epoxidation of chalcone derivatives by poly(phenylacetylene)s bearing oligopeptide pendents, where the *ee* of the reaction catalyzed by these helical polymeric organocatalysts was as high as 38 %, but the same reaction catalyzed by the mononomeric catalysts exhibited minimal enantioselectvity (<2%).[3] Despite these interesting reports, in all cases, the polymers could only assume one specific handedness, leaving to curiosity, the enantioselectivity of the same catalyst system, but supported on the opposite-handed, helical polymer. It would therefore be ideal to have the identical polymer supported organocatalyst in both right- and left-handed helical conformations, allowing for direct comparison of the effects of the helix-sense on enantioselectivity, a prior unaccomplished feat.

Cinchona alkaloids are well-established, highly enantioselective organocatalysts.[4] Furthermore, it has been shown that when chiral cinchona alkaloids, such as quinidine, are interacted with the dynamic helical polymer, poly((4-carboxyphenyl)acetylene), excess one-handed helicity is induced in the polymer.[5] Inspired by these two observations, we hypothesized that in synthesizing a poly(cinchona phenyl acetylene), we would not only produce a polymer that possesses an efficient organocatalyst functionality, but also exhibits excess one-handed helicity, allowing for investigation into the effects of helix-sense on the enantioselectivity of this polymer supported catalyst.

Communicated herein is the synthesis of two novel pseudo-enantiomeric helical poly(cinchona phenyl acetylene)s and the employment of these polymers as asymmetric organocatalysts. Excitingly, we discovered the ability to readily control the helix-sense of these polymers, providing an unprecedented opportunity for the investigation on the effects of the helix-sense of the polymer on the enantioselectivity of these catalysts (Chart 1).

Chart 1. Helix-sense inversion of P(BCdA) and its Effects of Enantioselectivity.

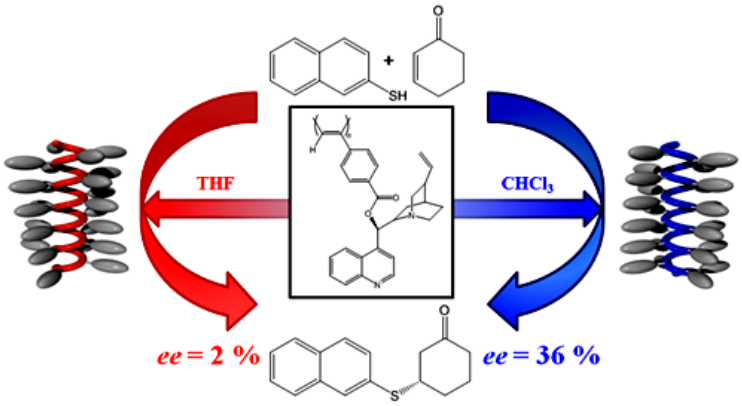

Specifically, two diastereomeric monomers, (4-benzoyl cinchonidine) acetylene [BCdA] and (4-benzoylcinchonine) acetylene [BCnA], have been prepared and subsequently polymerized by $[Rh(nbd)Cl]_2$ (nbd = norbornadiene) to synthesize stereoregular (*cis*-transoidal) P(BCdA) and P(BCnA) (Scheme 1).[6] These polymers exhibit intense circular dichroism (CD) in the absorption region of the conjugated polyene backbone, providing evidence that they are assuming helical conformations with excess one-handed helicity.[7] In identical solvents, the CD of P(BCdA) and P(BCnA) are nearly mirror images of one another, showing that the polymers are assuming helical conformations of opposite handedness. Interestingly, there is a large change in the absorption spectra and CD pattern when changing the solvent from $CHCl_3$ to THF (Figure 1). Specifically, when switching from $CHCl_3$ to THF, there is a slight blue shift in the absorbance max (λ_{max}) of the two

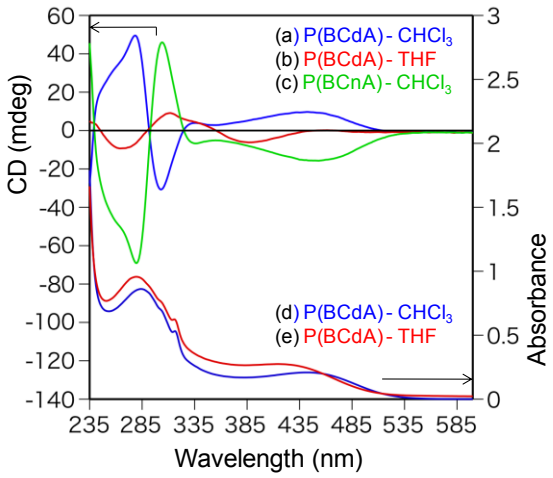

Figure 1. (a) CD of P(BCdA) in $CHCl_3$ (blue); (b) CD of P(BCdA) in THF (red); (c) CD of P(BCnA) in $CHCl_3$ (green); (d) absorption spectra of P(BCdA) in $CHCl_3$ (red); and, (e) absorption spectra of P(BCdA) in THF. Measured at room temperature (c = 0.1 mg/mL).

chromophores, accompanied with a visible color change, from orange to yellow, of the polymer solutions. Furthermore, in the CD pattern of P(BCdA) in $CHCl_3$ and THF, there is an inversion in sign of the Cotton effects as well as a change in absolute intensities of these Cotton effects. These results strongly suggest that that helix-sense of P(BCdA) is inverted in $CHCl_3$ and THF and that the pitch is altered.[8] These phenomena are also observed for P(BCnA). Although the helix-sense can be inverted in selected solvents, the polymers are very stable in solution, up to 6 days, and when exposed to heat or small chiral guest molecules.[6]

Table 1. Results of the Enantioselective Conjugate Addition of 2-Napthalenethiol to 2-Cyclohexen-1-one.[a]

run no.	Catalyst	solvent	time (hrs)	conv (%)	*ee*[b] (%)
1	BCdA	$CHCl_3$	40	88.8	8
2	BCdA	THF	40	>99	2
3	P(BCdA)	$CHCl_3$	96	92.4	36
4	P(BCdA)	THF	96	97.1	2
5	P(BCnA)	$CHCl_3$	90	>99	-30
6	P(BCnA)	THF	90	>99	-14
7[d]	BCdA	$CHCl_3$	15	98.9	10
8[d]	P(BCdA)	$CHCl_3$	36	100	22
9[d,e]	P(BCdA)	$CHCl_3$	36	100	16

[a]Carried out with 1 mol% catalyst in 1 mL of the specified solvent at 0 °C. [b]Determined by ^{1}H NMR analysis. [c]Determined by HPLC analysis. [d]Run at room temperature. [e]Catalyst compressed for 1 hr at 400 kg/cm^2.

With the ability to readily control the helix-sense of these polymers, we were provided an exciting opportunity to explore the effects of the helix-sense on the enantioselectivity of these catalysts. To this end, we have investigated the ability of these polymers to catalyze the enantioselective conjugate addition of 2-napthalenethiol to 2-cyclohexen-1-one[9] at 0 °C and the effects of the helix-sense on enantioselectivity, the results of which are summarized in Table 1. As a control, and to reveal possible solvent effects, we utilized the monomer, BCdA, as the catalyst for this reaction. BCdA proved to be a poor asymmetric catalyst for this reaction, however, there was a small solvent effect observed, so that in $CHCl_3$ and THF the product is synthesized in 8 and 2 % *ee*, respectively (runs 1 and 2, Table 1). We next employed P(BCdA) as the catalyst for this reaction. Gratifyingly, in $CHCl_3$ the helix-sense increases the enantioselectivity and the (*S*)-enantiomer was synthesized in 36 % *ee*, while in THF the helix-sense is non-influential and the product is formed with 2 % *ee*, thus clearly showing a large influence on the enantioselectivity by the helix-sense (runs 3 and 4, Table 1). Similarly, when using the pseudo-enantiomeric polymer, P(BCnA), in $CHCl_3$, the (*R*)-enantiomer is produced in 30 % ee, and in THF, 14 % *ee* (runs 5 and 6, Table 1).

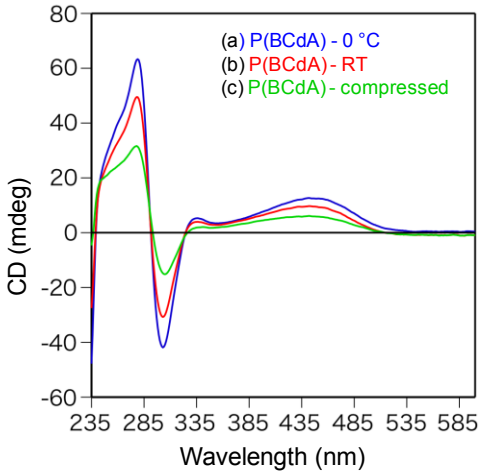

Figure 2. CD of P(BCdA) at (a) 0 °C (blue); (b) room temperature; and, (c) after compression for 1 hr, at room temperature (green) (c = 0.1 mg/mL; $CHCl_3$).

We next investigated the ability to perturb the helicity of P(BCdA) and its effects on the enantioselectivity of the catalyst. Thus, we performed the reaction at room temperature and using a polymer catalyst after it had been compressed, both of which decrease the intensities observed in the Cotton effects, as compared to the CD acquired at 0 °C (Figure 2). As a control, we first ran the reaction with the monomer BCdA, to eliminate possible temperature effects on the enantioselectivity. At room temperature, BCdA catalyzes the reaction to 10 % *ee*, while at 0 °C, 8 % *ee*, showing that the reaction catalyzed by this catalyst functionality is not very sensitive to temperature, from 0 °C to room temperature (runs 7 and 1, Table 1). However, when comparing the reaction catalyzed by P(BCdA) at 0 °C and room temperature, there is a decrease in *ee* from 36 to 22 % (runs 8 and 3, Table 1). Furthermore, when utilizing the compressed polymer as the catalyst (which shows an even further decrease in the intensities in the CD) the *ee* is reduced even further to 16 % (run 9, Table 1). Thus, in comparing the reaction catalyzed by a polymer with the same helix-sense, there is a clear correlation in decreasing *ee* with decreasing magnitudes in the CD.

In summary, we have reported the synthesis of two novel, pseudo-enantiomeric, poly(cinchona phenyl acetylene)s that exhibit excess one-handed helicity, and have the unique capability for helix-sense inversion, allowing for an unprecedented investigation into the effects of the helix-sense of the polymer backbone on the enantioselectivity of an organocatalyzed reaction. Modifications and derivatives of these polymers should further increase the enantioselectivity of these catalysts, and will be the focus of our future work.

Experimental Section

Materials and Methods

The NMR spectra were measured using a Varian AS500 spectrometer (Varian, Palo Alto, CA) operating at 500 MHz for ^{1}H and 125 MHz for ^{13}C using TMS as the internal standard. The absorption and CD spectra were obtained in a 0.1 cm quartz cell using a JASCO V570 spectrophotometer and a JASCO J820 spectropolarimeter, respectively. The optical rotations were measured in a 5 cm quartz cell on a JASCO P-1030 polarimeter. SEC measurements were performed with a JASCO PU-980 liquid chromatograph equipped with a UV-vis detector (JASCO UV-1570, 280 nm) using Tosoh TSKgel α-3000 (30 cm) and α—5000 (30 cm) SEC columns in series. DMF containing 10 mmol LiCl was used as the eluent at a flow rate of 0.5 mL/min. The molecular weight calibration curve was obtained with polystyrene standards (Tosoh). HPLC analysis was conducted on a JASCO PU-2080 Plus liquid chromatograph with Multi UV-vis (JASCO MD-2010 Plus) and polarimetric (JASCO OR-2090 Plus, Hg-Xe without filter) detectors at room temperature, using a Chirolpak AS-H column. A 50:50 hexanes:isopropanol solvent mixture was used as the eluent at a flow rate of 1.0 mL/min. The electron spray ionization mass spectra (ESI-MS) were recorded on a JEOL JMS-T100CS spectrometer (Akishima, Japan). Lasar Raman spectra were taken on a JASCO RMP-200 spectrophotometer. Melting points were measured on a Yanakao melting point apparatus and are uncorrected.

All starting materials and dehydrated solvents were purchased from Aldrich, Wako Pure Chemical Industries (Osaka, Japan), and Tokyo Kasei Kogyo (TCI) (Tokyo, Japan) and were used as recieved, except for Et_3N, which was dried over CaH_2 overnight, followed by vacuum distillation. (4-carboxyphenyl)acetylene was prepared by a literature procedure.[5]

Polymer Synthesis

1. Synthesis of poly((4-benzoyl cinchonidine)acetylene).

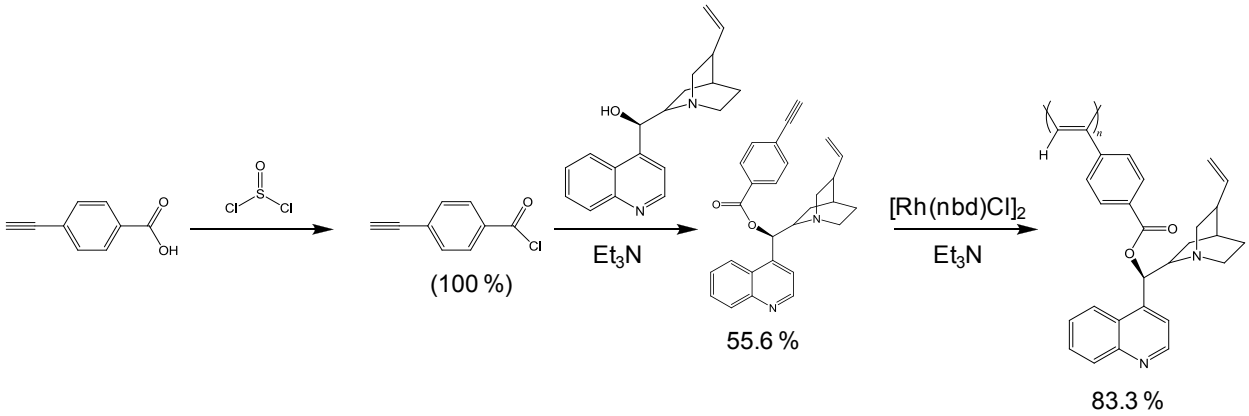

Scheme 1. Synthesis of poly((4-benzoyl cinchonidine)acetylene).

Poly((4-benzoyl cinchonidine)acetylene) [P(BCdA)] was synthesized in a three-step procedure, as outlined in Scheme 1. A 50 mL flask was charged with (4-carboxyphenyl)acetylene (1.50 g, 10.26 mmol) and a stir bar and equipped with a 3-way stop-cock. The flask was pulled under dynamic vacuum for 1 hr. Thionyl chloride was sparged with N_2 and 30.0 mL (41.13 mmol, 40eq) was added to the flask under positive N_2 flow via syringe. The flask was heated to 40 °C and stirred for 4 hrs. The flask was allowed to cool to room temperature and the excess thionyl chloride was removed via vacuum and dried extensively. It was assumed that this reaction afforded 100 % (4-benzoylchloride)acetylene, and this crude product was used as is in the next step.

Cinchonidine (1.00 g, 3.39 mmol, 1 eq) and a stir bar were loaded into a 200 mL flask that was equipped with a 3-way stop-cock. The flask was pulled under dynamic vacuum for 1 hr before 50 mL of dry THF and Et_3N (2.37 mL, 17.00 mmol, 5 eq) were added under positive N_2 flow via syringe. The solution was cooled to 0 °C. (4-benzoylchloride)acetylene (0.838 g, 5.9 mmol, 1.5 eq) was dissolved in 20 mL of dry THF and added dropwise to the cinchonidine solution with vigorous stirring. The solution was allowed to warm to room temperature and stirred overnight. The suspension was filtered and the volatiles were removed from the filtrate affording a pale yellow solid that was purified by silica-gel chromatograpy ($CHCl_3$, acetone). Final purification of the product was performed by recrystallization form a CH_2Cl_2/hexanes solvent mixture, affording 798 mg (55.6 %) of (4-benzoylcinchonidine)acetylene as a white crystalline solid. ^{1}H NMR ($CDCl_3$, 23 °C): δ 8.81 (d, *J* = 4.5 Hz, 1H, Ar), 8.24 (d, *J* = 8.5 Hz, 1H, Ar), 8.07 (d, *J* = 8.5 Hz, 1H, Ar), 7.97 (d, *J* = 8, 2H, Ar), 7.67-7.64 (m, 1H, Ar), 7.57-7.54 (m, 1H, Ar), 7.51 (d, *J* = 8.5, 2H, Ar), 7.38 (d, *J* = 4.5, 1H, Ar), 6.73 (d, *J* = 6.5, 1H, CHO), 5.58-5.74 (m, 1H, CH=), 4.97-4.93 (m, 2H, CH_2=), 3.46-3.41 (m, 1H), 3.18 (s, 1H, CH≡), 3.16-3.10 (m, 1H), 3.04-2.99 (m, 1H), 2.65-2.56 (m, 2H), 2.24 (bs, 1H), 1.91-1.83 (m, 2H), 1.73-1.67 (m, 1H), 1.65-1.61 (m, 1H), 1.54-1.49 (m, 1H). ^{13}C NMR ($CDCl_3$, 23 °C): δ 164.8, 149.9, 148.6, 145.1, 141.5, 132.3, 130.5, 129.6, 129.5, 129.3, 127.4, 127.0, 125.9, 123.2, 114.7, 82.6, 80.5, 74.8, 59.8, 56.6, 42.5, 39.6, 37.8, 27.8, 27.6, 24.3. $[\alpha]^{25}_D$= 92.8 ° (c = 2 mg/mL, DMF). *m*/*z* calcd for $C_{28}H_{26}N_2O_2$: [M + H]+: 423.2073; found: 423.2062.

400 mg (0.947 mmol) of (4-benzoylcinchonidine)acetylene was added to a 30 mL reactor equipped with stir bar and 3-way stop-cock. The flask was pulled under dynamic vacuum for 1hr before 4.0 mL of dry DMF and 132 µL (0.947 mmol) of dry Et_3N were added via syringe under positive N_2 flow. 4.4 mg of [Rh(nbd)Cl]2 (9.47 µmol) was dissolved in 1.0 mL of dry DMF and added to the acetylene solution via syringe with vigorous shaking. The solution immediately turned a dark yellow color and was placed in a 30 °C oil bath for 18 hrs. After 18 hrs the solution was poured into 50 mL of Et_2O affording a bright yellow precipitate that was isolated by

centrifugation. The yellow solid was was 3 times with Et_2O and dried extensively under vacuum to afford 333 mg (83.3 %) of poly(benzoylcinchonidine)acetylene. The molecular weight (M_n) and molecular weight distribution (M_w/M_n) were estimated to be 92.0 x 10^3 and 2.40, respectively, as determined by SEC analysis, as described above. ($[\alpha]^{25}_D$= +1189 °; 2 mg/mL, $CHCl_3$; $[\alpha]^{25}_D$= -193 °; 2 mg/mL, DMF). The stereoregularity of P(BCdA) was investigated by ^{1}H NMR and Raman spectroscopies. However, the ^{1}H NMR spectrum was inconclusive due to broadening of the main chain protons. The Raman spectrum of P(BCdA) gave useful information and showed intense peaks at 1557, 1345, and 897 cm^{-1}, which can be assigned to the C=C, C-C, and C-H bond vibration in *cis* polyacetylenes (Figure 1). After compressing this polymer sample for 1 hr at 400 kg/cm2, the Raman spectrum was reacquired, showing a disappearance in the peaks, and confirming a lack of a *cis-transoidal* conformation (Figure 2).

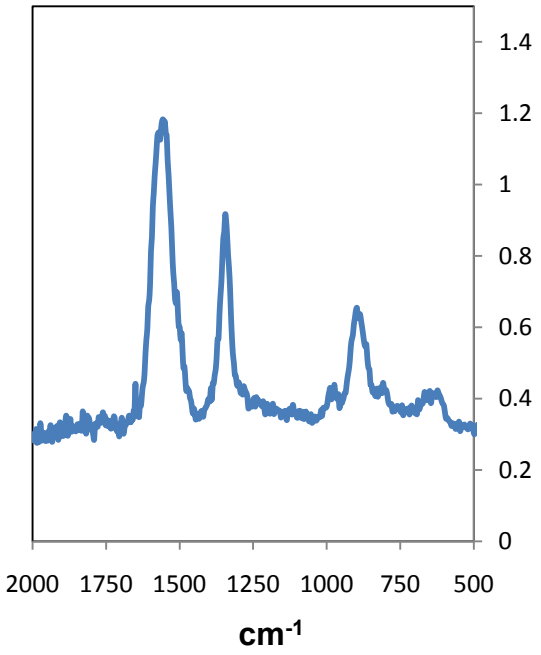

Figure 3. Raman spectrum of P(BCdA) showing a highly *cis-transoidal* conformation.

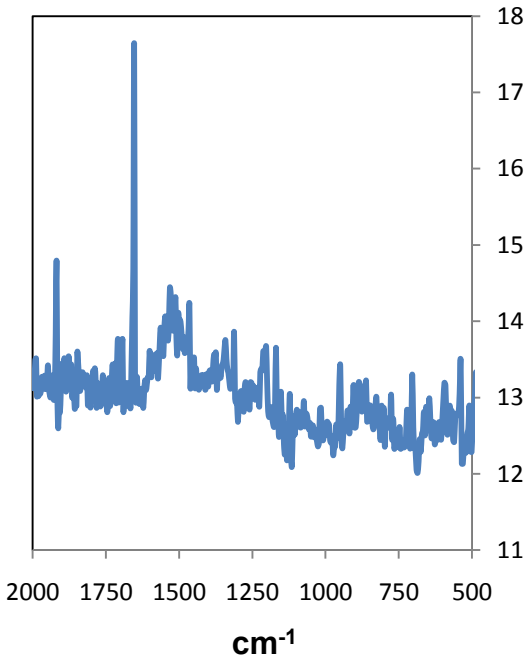

Figure 4. Raman spectrum of P(BCdA) after being compressed for 1 hr at 400 kg/cm^2 confirming a lack of a *cis-transoidal conformation*.

2. Synthesis of poly((4-benzoyl cinchonine)acetylene).

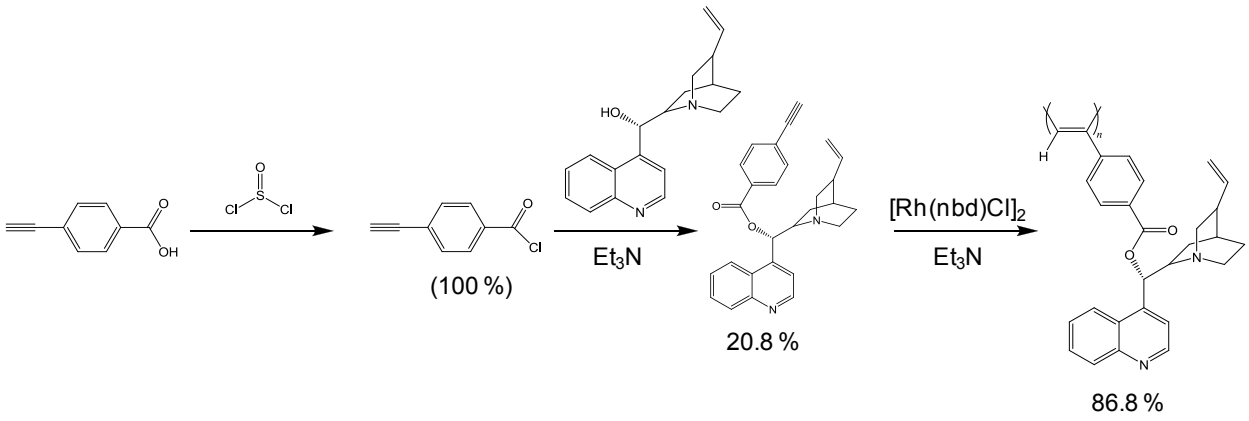

Scheme 2. Synthesis of poly((4-benzoyl cinchoninine)acetylene).

Poly((4-benzoyl cinchonidine)acetylene) [P(BCnA)] was synthesized in a three-step procedure, as outlined in Scheme 2. Cinchoninine (1.00 g, 3.39 mmol, 1 eq) and a stir bar were loaded into a 200 mL flask that was equipped with a 3-way stop-cock. The flask was pulled under

dynamic vacuum for 1 hr before 50 mL of dry THF and Et_3N (2.37 mL, 17.00 mmol, 5 eq) were added under positive N_2 flow via syringe. The solution was cooled to 0 °C. (4-benzoylchloride)acetylene (0.838 g, 5.9 mmol, 1.5 eq) was dissolved in 20 mL of Dry THF and added dropwise to the cinchoninine solution with vigorous stirring. The solution was allowed to warm to room temperature and stirred overnight. The suspension was filtered and the volatiles were removed from the filtrate affording a pale yellow solid that was purified by silica-gel chromatograpy ($CHCl_3$, acetone). Final purification of the product was performed by recrystallization form a CH_2Cl_2/hexanes solvent mixture, affording 298 mg (20.8 %) of (4-benzoylcinchoninine)acetylene as a white crystalline solid. ^{1}H NMR ($CDCl_3$, 23 °C): δ 8.79 (d, *J* = 4.5, 1H, Ar), 8.23 (d, *J* = 8.5, 1H, Ar), 8.06 (d, *J* = 8, 1H, Ar), 7.97 (d, *J* = 8.5, 2H, Ar), 7.67-7.64 (m, 1H, Ar), 7.57-7.54 (m, 1H, Ar), 7.49 (d, *J* = 8, 2H, Ar), 7.38 (d, *J* = 4.5, 1H, Ar), 6.73 (d, *J* = 7.5, 1H, CHO), 5.98-5.01 (m, 1H, CH=), 5.06-4.99 (m, 2H, CH_2=), 3.40-3.35 (m, 1H), 3.18 (s, 1H, CH≡), 2.93-2.84 (m, 2H), 2.77-2.73 (m, 1H), 2.68-2.62 (m, 1H), 2.24-2.19 (m, 1H), 1.91-1.87 (m, 1H), 1.79 (bs, 1H), 1.59-1.54 (m, 1H), 1.52-1.49 (m, 2H). ^{13}C NMR ($CDCl_3$, 23 °C): δ 164.8, 149.9, 148.5, 145.3, 139.9, 132.1, 130.4, 129.6, 129.2, 127.3, 126.9, 125.9, 123.2, 118.4, 114.9, 82.6, 80.5, 74.4, 59.8, 49.7, 49.0, 39.4, 27.6, 27.5, 26.2, 23.8. $[\alpha]^{25}_D$= -92.8 ° (c =2 mg/mL, DMF). *m/z* calcd for $C_{28}H_{26}N_2O_2$: [M + H]+: 423.2073; found: 423.2064.

200 mg (0.475 mmol) of (4-benzoylcinchoninine)acetylene was added to a 30 mL reactor equipped with stir bar and 3-way stop-cock. The flask was pulled under dynamic vacuum for 1hr before 4.0 mL of dry DMF and 65.9 μL (0.475 mmol) of dry Et_3N were added via syringe under positive N_2 flow. 2.2 mg of [Rh(nbd)Cl]2 (9.47 μmol) was dissolved in 1.0 mL of dry DMF and added to the acetylene solution via syringe with vigorous shaking. The solution immediately turned a dark yellow color and was placed in a 30 °C oil bath for 18 hrs. After 18 hrs the solution was poured into 50 mL of Et_2O affording a bright yellow precipitate that was isolated by centrifugation. The yellow solid was was 3 times with Et_2O and dried extensively under vacuum to afford 174 mg (86.8 %) of poly(benzoylcinchoninine)acetylene. The molecular weight (M_n)

and molecular weight distribution (M_w/M_n) were estimated to be 141 x 10^3 and 2.71, respectively, as determined by SEC analysis, as described above. ($[\alpha]^{25}_D$= -1147 °; 1 mg/mL, $CHCl_3$; $[\alpha]^{25}_D$= +50.8 °; 0.5 mg/mL, DMF). The stereoregularity of P(BCnA) was investigated by ^{1}H NMR and Raman spectroscopies. However, the ^{1}H NMR spectrum was inconclusive due to broadening of the main chain protons. The Raman spectrum of P(BCdA) gave useful information and showed intense peaks at 1563, 1345, and 897 cm^{-1}, which can be assigned to the C=C, C-C, and C-H bond vibration in *cis* polyacetylenes (Figure 3).

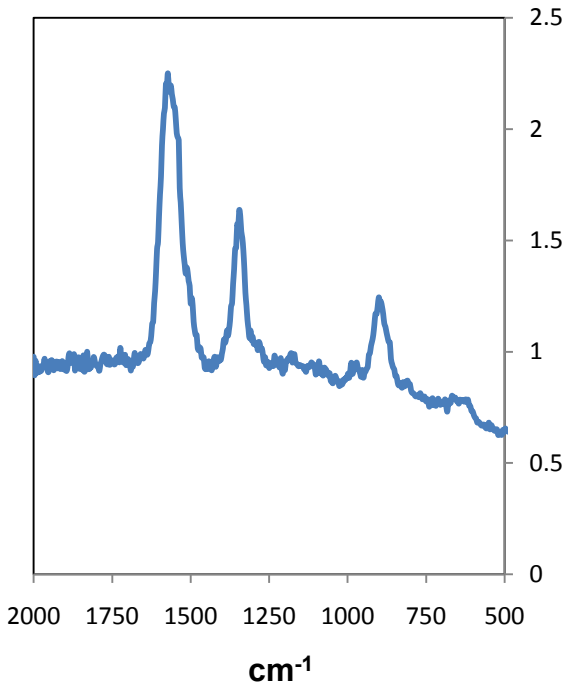

Figure 5. Raman spectrum of P(BCnA) showing a highly *cis-transoidal* conformation.

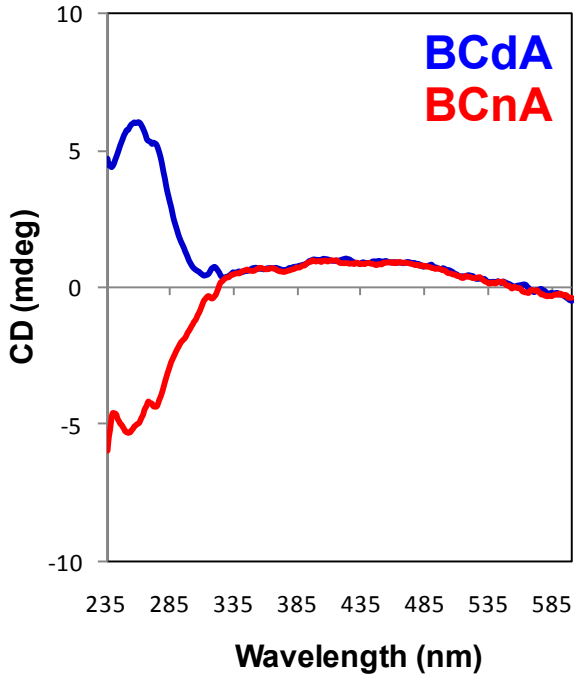

Figure 6. CD of BCdA (blue) and BCnA (red) measured at room temperature (c = 0.1 mg/mL; $CHCl_3$).

Table 2: Optical Rotations of Benzyl Cinchona Acetylene Monomers and Polymers

Sample	$[\alpha]^{25}_D$ in $CHCl_3$ (°)	$[\alpha]^{25}_D$ in DMF (°)
BCdA	N.D.	92.8
P(BCdA)	+1189	-193
BCnA	N.D.	-92.8
P(BCnA)	-1147	+50.8

Stabilitiy of the Helical Conformation of P(BCdA)

To investigate the thermal stability of the helical secondary structure of P(BCdA), solutions in $CHCl_3$ (Figure 1) and THF (Figure 2) were heated from 0 °C to 45 °C, and the CD was monitored every 15 °C. The solution was equilibrated at each temperature for 5 min before the CD was acquired. As expected, in both solvents there is a decrease in intensity in the CD with increasing temperature, but importantly, there is not a switch in sign of the Cotton effects. More so, when the polymer solutions are cooled back to room temperature, the intensities in the CD return to their original values, showing the thermal stability of the helical structure of P(BCdA) in

both $CHCl_3$ and THF. Additionally, after 6 days in solution at room temperature, the CD remained unchanged. The effect on the CD of P(BCdA) after the addition of (+)- or (-)-camphor sulfonic acid was investigated (Figure 7). To a 1 mL solution with concentration of 1 mg/mL of P(BCdA) in $CHCl_3$ was added 10 µL of 0.059 **M** (+)- or (-)-camphor sulfonic acid. This solution was then immediately analyzed by CD. After 1 day, the solution containing 1 eq of (+)-camphor sulfonic acid was re-examined, and the CD remained unchanged.

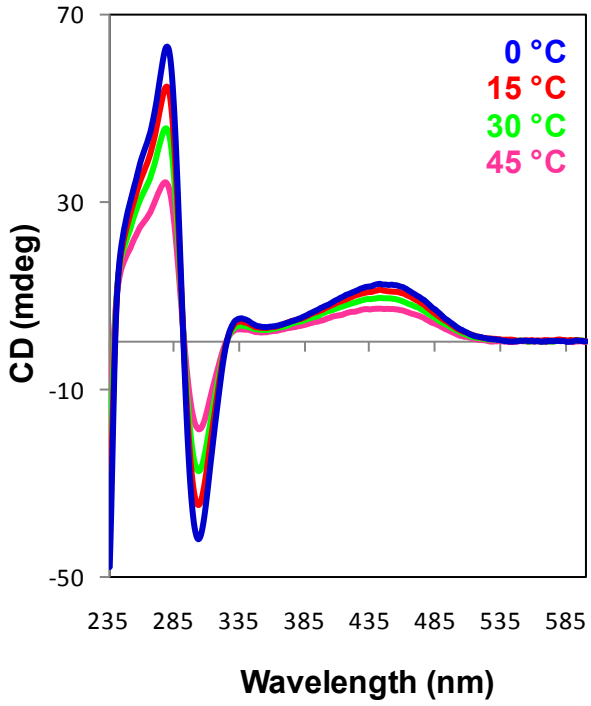

Figure 7. Variable temperature CD of P(BCdA) (c = 0.25 mg/mL; $CHCl_3$).

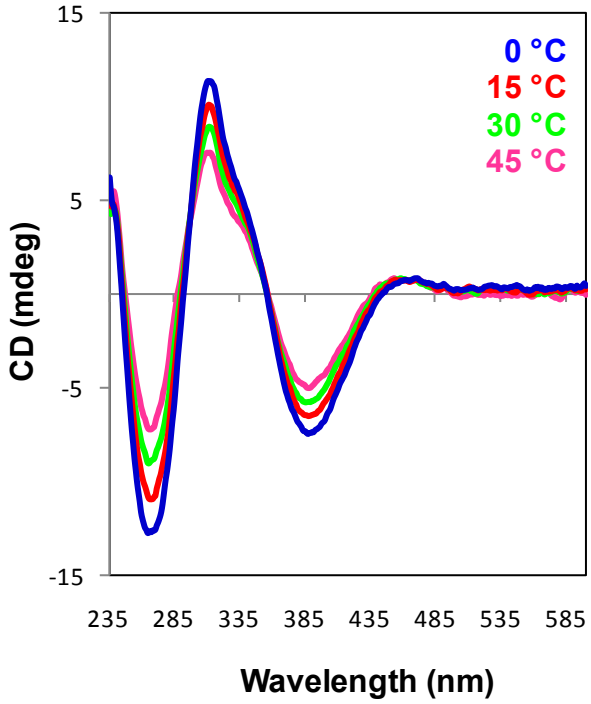

Figure 8. Variable temperature CD of P(BCdA) (c = 0.25 mg/mL; THF).

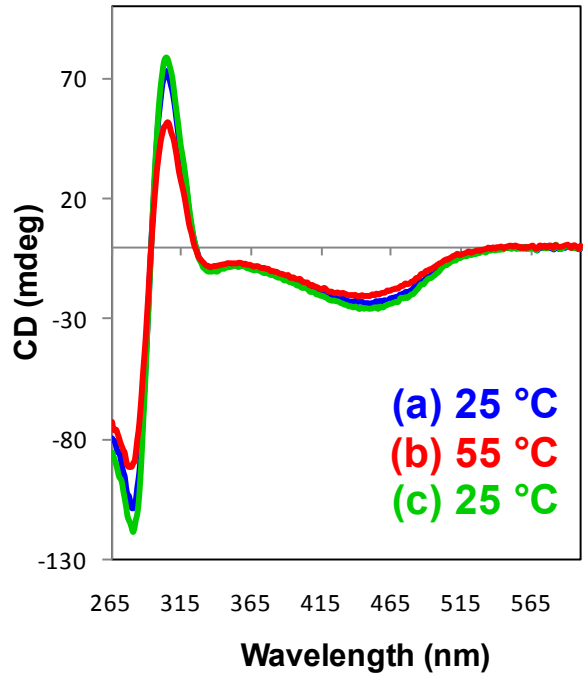

Figure 9. Variable temperature CD of P(BCnA); (a) initial CD at 25 °C; (b) CD at 55 °C; (c) CD after heat treatment, at 25 °C (c = 0.50 mg/mL; CHCl3).

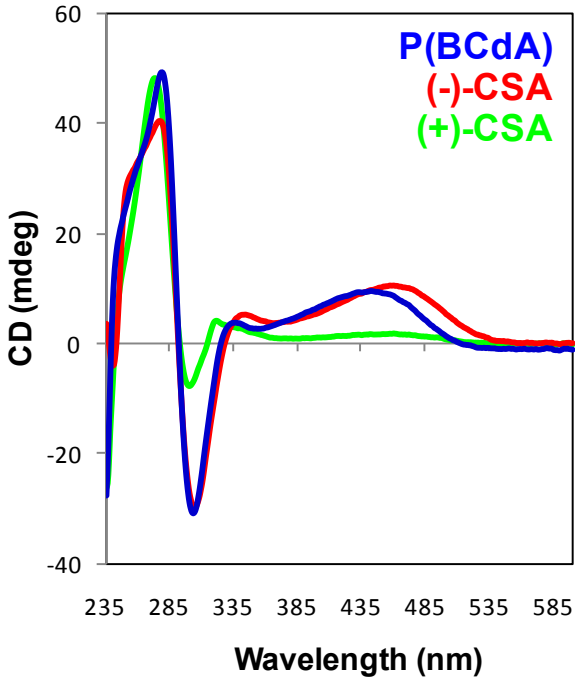

Figure 10. CD of P(BCdA) after addition of (+)- and (-)-camphor sulfonic acid (c ~ 0.25 mg/mL; $CHCl_3$).

Enantioselective Conjugate Addition of 2-Napthalenethiol to 2-Cyclohexen-1-one

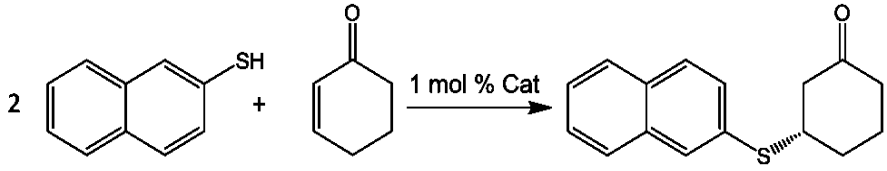

Scheme 3. Enantioselective Conjugate Addition of 2-Napthalenethiol to 2-Cyclohexen-1-one.

A modified literature procedure was implemented for the synthesis of 3-(β-Napthylthio)cyclohexanone.[9] In a glass-reactor, 2-napthalenethiol (74.9 mg, 0.468 mmol, 2 eq) and specific catalyst (1 mol %) were dissolved in 1 mL of either THF or $CHCl_3$. To this solution was added 2-cyclohexen-1-one (22.7 µL, 0.234 mmol, 1 eq) via syringe. This reactor was sealed, and placed in a temperature-controlled bath, at the temperatures specified in the tables. After the pre-determined time reaction time was completed, the solution was directly passed through a short plug of silica, which was washed with ~3 mL of Et_2O. The volatiles were removed via

vacuum and the % conversion was determined by ^{1}H NMR analysis and % *ee* was determined by HPLC analysis.

Acknowledgement. This work was supported by a NSF/JSPS EAPSI Fellowship (NSF-0913269). This dissertation chapter contains the manuscript for a communication, to be submitted. The work described was performed in the laboratory of Professor Eiji Yashima at Nagoya University in Nagoya, Japan. G.M.M. would like to thank the Yashima Laboratory for their generous hospitality and invaluable assistance during his research stay.

References

(1) Dickerson, T.; Reed, N. N.; Janda, J. D.; *Chem. Rev.* **2002**, *102*, 3325-3344.

(2) (a) Terada, K.; Masuda, T.; Sanda, F. *J. Poly. Sci., Part A: Polym. Chem.* **2009,** *47*, 4971-4981. (b) Miyabe, T.; Hase, Y.; Iida, H.; Maeda, K.; Yashima, E. *Chirality* **2009**, *21*, 44-50. (c) Yashima, E.; Maeda, Y.; Okamoto, Y. *Polym. J.*, **1999**, *31*, 1033-1036.

(3) Maeda, K.; Tanaka, K.; Morino, K.; Yashima, E. *Macromolecules* **2007**, *40*, 6783-6785.

(4) (a) Gaunt, M. J.; Johansson, C. C. C. *Chem. Rev*. **2007**, *107*, 5596-5605. (b) Tian, S.; Chen, Y.; Hang, J.; Tang, L.; McDaid, P.; Deng, L. *Acc. Chem. Res*. **2004**, *37*, 621-631.

(5) Yashima, E.; Masushima, T.; Okamoto, Y. *J. Am. Chem. Soc.* **1997**, *119*, 6345-6359.

(6) See Experimental Section.

(7) Yashima, E.; Maeda, K.; Furusho, Y. *Acc. Chem. Res.* **2008,** *41*, 1166-1180.

(8) Yashima, E.; Maeda, K.; Sato, O. *J. Am. Chem. Soc.* **2001**, *123*, 8159-8160.

(9) (a) McDaid, P.; Chen, Y.; Deng, L. *Angew. Chem. Int. Ed.* **2002**, *41*, 338-340. (b) Hiemstra, H.; Wynberg, H. *J. Am. Chem. Soc.* **1981***, 103*, 417-430.

Chapter 6

Coordination Polymerization of Renewable Butyrolactone-Based Vinyl Monomers by Lanthanide and Early Metal Catalysts

Abstract

This contribution reports the first study of coordination-addition polymerization of renewable butyrolactone-based vinyl monomers, MBL (α-methylene-*γ*-butyrolactone) and MMBL (*γ*-methyl-α-methylene-*γ*-butyrolactone), using neutral lanthanocene(II), non-lanthanocene(III), and cationic group 4 metallocene catalysts. The samarocene(II) catalyst, $Cp^*_2Sm(THF)_2$, promotes a rapid, efficient, and controlled polymerization of MBL and MMBL in DMF at ambient temperature, exhibiting a high TOF of 3000 h^{-1}, typically near quantitative initiator efficiency, and the ability to control the polymer MW. The resulting atactic PMBL and PMMBL have high T_g's of 194 ºC and 227 ºC. Owing to the living/controlled characteristics of this polymerization, well-defined random and block copolymers of MBL with MMA and MMBL can be readily synthesized. Results of the kinetic and polymerization studies indicate that the true active species is the trivalent samarocene centers attached to the single growing polymer chain, derived presumably from a redox-then-radical-coupling process. In comparison, the polymerizations by non-lanthanocene(III) silylamides, $Ln[N(SiMe_3)_2]_3$ (Ln = La, Nd, Sm, Er), and by cationic group 4 metallocene and half-metallocene catalysts incorporating C_2 and C_s symmetric ligands are much slower and less effective. Catalytic polymerization of MBL by $Cp^*_2Sm(THF)_2$ has also been realized in the presence of an enolizable organo acid as a suitable chain transfer agent.

Introduction

Coordination polymerization of polar vinyl monomers such as (meth)acrylates and (meth)acrylamides by single-site metal catalysts has attracted increasing interest due to its precision in the catalyst-based stereochemical and architectural control as well as its ability to produce new classes of polymeric materials unattainable by other means of polymerization.[1] In this context, remarkable successes have been achieved in metal-catalyzed coordination-addition polymerizations of polar vinyl monomers by early metal and main-group[2] as well as lanthanide[3] catalysts, which show a dazzling display of a variety of stereomicrostructures they can generate, in addition to their high activity and high degree of control over polymerization characteristics. Especially, methyl methacrylate (MMA) has been most widely investigated; mechanistic studies of the MMA polymerization catalyzed by various types of group 4 cationic metallocene complexes, including those supported by C_2,[4,5] C_{2v},[6,7,8,9,10] C_1,[11,12,13] CGC (constrained geometry catalyst),[14, 15,16,17] and C_s[18] ligated catalysts, as well as isoelectronic neutral lanthanide complexes, including lanthanocene(III) [19,20] and lanthanocene(II)[21,22] catalysts, have revealed important insights into polymerization kinetics, fundamental steps (initiation, propagation, and termination/side reactions), and stereocontrol events. Theoretical/computational investigations[23,24,25,26,27,28] provide a synergistic understanding of such polymerization reactions, especially aspects of stereocontrol mechanisms[14,18,23,25] in the MMA polymerization by chiral *ansa*-zirconocenium complexes. Certain catalyst structures exhibit a high degree of control over polymerization characteristics (activity and efficiency; polymer molecular weight, MW; MW distribution, MWD; livingness) and stereochemistry (polymer tacticity and stereocontrol mechanism), enabling the ambient-temperature synthesis of highly isotactic poly(methacrylate)s (≥95% *mm*)[4,29,30,31] and poly[(meth)acrylamide]s (>99% *mm*)[32,33,34,35,36] using chiral C_2-ligated zirconocenium complexes as well as highly syndiotactic poly(methacrylate)s (≥ 94% *rr*)[18,37] using chiral C_s-ligated zirconocenium complexes.

Sustainability-related research in polymer synthesis has gained increasing attention and recently been directed at examining the possibility of replacing petroleum-based raw materials by naturally occurring, renewable feedstocks for the production of polymeric materials in large commodity and specialty chemicals markets.[38,39,40] In this context, renewable butyrolactone-based vinyl monomers MBL (α-methylene-*γ*-butyrolactone) and MMBL (*γ*-methyl-α-methylene-*γ*-butyrolactone) are of particular interest. MBL, or tulipalin A, is a natural material found in tulips and the MBL ring is an integral building block of many (~10% known) natural products,[41] while its methyl derivative MMBL can be prepared via a 2-step process from the biomass-derived levulinic acid.[42,43] From a structural point of view, MBL can be described as the cyclic analog of MMA (Chart 1); however, MBL exhibits greater reactivity in free radical polymerization[44] than typical methacrylate monomers, such as MMA, due to the presence of the nearly planar five-membered lactone ring which provides maximum resonance stabilization for the active radical species, as well as the presence of the higher energy exocyclic carbon-carbon double bond (relative to the vinyl group of MMA), as a result of the ring strain and the fixed *s-cis* conformation[45] (Chart 1). From a materials property point of view, PMBL, the polymer resulting from radical polymerization, has a considerably higher T_g (glass-transition temperature) of 195 ºC than a typical T_g of 105 ºC of atactic PMMA and exhibits excellent solvent resistance (as evidenced by its insolubility in common organic solvents such as $CHCl_3$ and THF),[46] attributable to the conformational rigidity of the chain incorporating the butyrolactone ring. Added benefits to the materials properties (e.g., optical properties and resistance to solvent, heat, and scratch) of the copolymers and blends have also been manifested by incorporating MBL units.[47,48,49] The sustainability and the advantageous structural features of MBL as well as the superior materials properties of PMBL prompted DuPont scientists to explore the prospects of using MBL to displace the petroleum-based methacrylate monomers for specialty chemicals production.[50] MBL has already been successfully polymerized by various radical polymerization mechanisms,[44,45,46,51,52,53,54] by group-transfer polymerization,[55] and by anionic polymerization;[46] it

has been copolymerized with various co-monomers[44] such as MMA,[56] styrene,[53,57] methoxystyrene,[58] and vinyl thiophenes.[59] MMBL has also been polymerized by free-radical emulsion polymerization[60,61] as well as by radical, anionic, and group-transfer polymerization methods.[62]

Chart 1. Renewable butyrolactone-based vinyl monomers vs MMA.

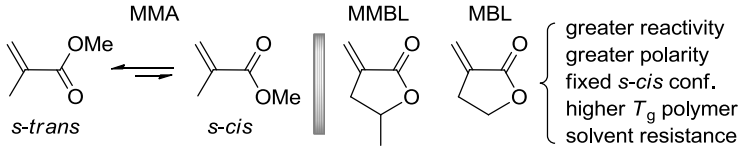

In view of the above outlined benefits of MBL and MMBL and their derived polymers as well as the remarkable successes already achieved by single-site lanthanide and early metal catalysts in coordination polymerization of acrylic monomers, it was surprising that, to the best of our knowledge, there were no reports on the utilization of such catalysts for *coordination* polymerization of the renewable butyrolactone-based vinyl monomers MBL and MMBL. Accordingly, this contribution reports the *first* such study using neutral lanthanocene(II), non-lanthanocene(III), and cationic group 4 metallocene catalysts (Chart 2): $Cp^*_2Sm(THF)_2$ (**1**, Cp^* = η^5-C_5Me_5),[63] $[Cp^*_2Sm(THF)_2]^+[BPh_4]^-$,[64] $Ln[N(SiMe_3)_2]_3$ (Ln = La, Nd, Sm, Er),[65] $Cp_2ZrMe[OC(OR)=CMe_2]$[10,66]/$Cp_2ZrMe^+MeB(C_6F_5)_3^-$,[67] $\{(CGC)Ti(THF)[OC(O^iPr)=CMe_2]\}^+$ $MeB(C_6F_5)_3^-$ [**2**, CGC = $Me_2Si(\eta^5$-$(Me_4C_5)(^tBuN)]$,[16] and $\{[(p$-$Et_3SiPh)_2C(Cp)(2,7$-$^tBu_2$-Flu)]Zr[OC(O^{i}Pr)=CMeCH$_2$C(Me$_2$)C(O^{i}Pr)=O]$\}^+[B(C_6F_5)_4]^-$ (**3**).[18] Most notably, our results show that: (a) samarocene **1** promotes the highly active, effective and controlled polymerization of (M)MBL in DMF at room temperature (RT) as well as the catalytic polymerization in the presence of an enolizable organo acid; (b) the resulting atactic PMBL and PMMBL have high T_g's of 194 ºC and 227 ºC, respectively, and the T_g and onset decomposition temperatures of the

atactic PMMBL are ~120 °C and 40 °C higher than those of atactic PMMA having comparable MW; (c) results of the kinetic and polymerization studies indicate that the true active species is the trivalent samarocene centers attached to the single growing polymer chain; and (d) the non-lanthanocene silylamides and cationic group 4 catalysts are less active and effective in such polymerizations.

Chart 2. Neutral lanthanide and cationic group 4 catalysts employed in this study.

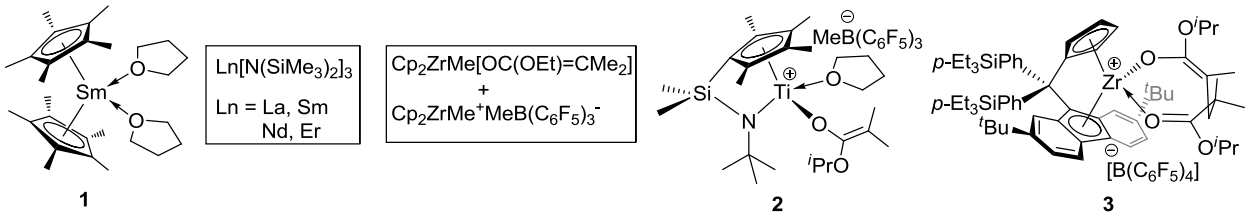

Experimental

Materials and methods

All syntheses and manipulations of air- and moisture-sensitive materials were carried out in flamed Schlenk-type glassware on a dual-manifold Schlenk line, a high-vacuum line, or in an argon or nitrogen-filled glovebox. HPLC-grade organic solvents were sparged extensively with nitrogen during filling of the solvent reservoir and then dried by passage through activated alumina (for Et_2O, THF, and CH_2Cl_2) followed by passage through Q-5-supported copper catalyst (for toluene and hexanes) stainless steel columns. HPLC-grade DMF was degassed, dried over CaH_2 overnight, followed by vacuum transfer (not by distillation). Benzene, Benzene-d_6 and toluene-d_8 were degassed, dried over sodium/potassium alloy and vacuum-distilled or filtered, whereas C_6D_5Br, $CDCl_3$, and CD_2Cl_2 were dried over activated Davison 4-Å molecular sieves. NMR spectra were recorded on either a Varian Inova 300 (FT 300 MHz, ^1H; 75 MHz, ^{13}C; 282 MHz, ^{19}F) or a Varian Inova 400 spectrometer. Chemical shifts for ^1H and ^{13}C spectra were

referenced to internal solvent resonances and are reported as parts per million relative to tetramethylsilane, whereas ^{19}F NMR spectra were referenced to external $CFCl_3$.

Isopropyl isobutyrate, 1,2,3,4,5-pentamethylcyclopentadiene, α-methylene-γ-butyrolactone (MBL) and γ-methyl- α-methylene-γ-butyrolactone (MMBL) were purchased from TCI America. Indene, methyl methacrylate (MMA), methyl isobutyrate (MIB), 3-methyl-2-butanone (MBO), dimethyl malonate (DMM), butylated hydroxytoluene (BHT-H, 2,6-di-*tert*-butyl-4-methylphenol), potassium bis(trimethlsilyl)amide (0.5 M in toluene), *n*-BuLi (1.6 M in hexanes), 1,2-dibromoethane, tetrachlorozirconium, triflic acid, samarium iodide (0.1 M in THF), and lithium dimethylamide were purchased from Aldrich. Trimethylaluminum (neat) was purchased from Strem Chemical Company. Trimethylsilyl trifluoromethanesulfonate (TMSOTf) was purchased from Alfa Aesar and redistilled under nitrogen atmosphere prior to use. Indene, and 1,2-dibromoethane were degassed using three freeze-pump-thaw cycles. Isopropyl isobutyrate, 1,2,3,4,5-pentamethylcyclopentadiene, MIB, MBO, DMM, MBL, MMBL, and MMA were degassed and dried over CaH_2 overnight, followed by vacuum distillation. MMA was further purified by titration with neat tri(*n*-octyl)aluminum (Strem Chemical) to a yellow end point,[68] and vacuum distillation. BHT-H was recrystallized from hexanes prior to use. All other reagents were used as received.

Tris(pentafluorophenyl)borane, $B(C_6F_5)_3$, was obtained as a research gift from Boulder Scientific Co. and further purified by recrystallization from hexanes at –35 ºC inside a glovebox. The $(C_6F_5)_3B$•THF adduct was prepared by addition of THF to a toluene solution of the borane followed by removal of the volatiles and drying in vacuo. Literature procedures were employed for the preparation of the following compounds and metallocene complexes: $K(C_5Me_5)$,[69] $LiOC(O^iPr)=CMe_2$,[14] $Cp_2ZrMe[OC(OR)=CMe_2]$,[10,66] $Cp_2ZrMe^+MeB(C_6F_5)_3^-$,[67] $\{[(p\text{-}Et_3SiPh)_2C(Cp)(2,7\text{-}^tBu_2\text{-}Flu)]Zr[OC(O^iPr)=CMeCH_2C(Me_2)C(O^iPr)=O]\}^+[B(C_6F_5)_4]^-$ (**3**),[18] $CGCTiMe^+MeB(C_6F_5)_3^-$,[70] $\{(CGC)Ti(THF)[OC(O^iPr)=CMe_2]\}^+MeB(C_6F_5)_3^-$ (**2**),[16] $Cp^*_2Sm(THF)_2$ (**1**),[63] $[Cp^*_2Sm(THF)_2]^+[BPh_4]^-$,[64] and $Ln[N(SiMe_3)_2]_3$ (Ln = La, Nd, Sm, Er).[65]

General polymerization procedures

Polymerizations were performed in 30 mL oven-dried glass reactors inside the glovebox. In a typical polymerization procedure at ambient temperature (~25 ºC), predetermined amounts of the appropriate catalyst or pre-catalyst combinations were premixed in 5 mL of CH_2Cl_2 for group 4 catalysts[4,5,18] or in 3 mL DMF for lanthanide catalysts before addition of MBL (400 mg; 4.07 mmol) or MMBL (457 mg; 4.07 mmol). Polymerizations were quenched at the time specified in the tables with 5 mL of 5 % HCl in methanol, and the polymer was precipitated into 50 mL of methanol and collected by filtration and centrifugation, before being washed extensively with methanol to remove any catalyst residue or unreacted monomer. Polymers were then dried at 50 °C overnight in a vacuum oven. Conversion data was performed by adding toluene (289 μL; 2.72 mmol), as an external standard, to the reaction solution. At specified times 0.2 mL aliquots were withdrawn from the solution and quenched into septum sealed vials containing 0.7 mL of undried "wet" $CHCl_3$.[4,18] Percent conversion was then calculated by comparing the integration of the vinyl protons of the unreacted monomer to the methyl protons of toluene.

Polymer characterizations

Gel permeation chromatography (GPC) analyses of the polymers were carried out at 40 ºC and a flow rate of 1.0 mL/min, with DMF as the eluent, on a Waters University 1500 GPC instrument equipped with four 5 μm PL gel columns (Polymer Laboratories). Tacticities of PMBL[44,55] and PMMBL[62] were measured by ^{13}C NMR. Decomposition onset temperatures (T_{onset}) of the polymers were measured by thermal gravimetric analysis (TGA) on a TGA 2950 Thermogravimetric Analyszer, TA Instrument. Polymer samples were heated from ambient temperature to 600 °C at a rate of 20 °C/min. Values for $T_{10\%}$ and T_{onset} (initial and end temperatures) were obtained from wt% *versus* temperature (°C) plots. Glass transition temperatures (T_g) of the polymers were measured by differential scanning calorimetry (DSC) on a DSC 2920, TA Instrument. Polymer samples were first heated to 250 °C at 20 °C/min,

equilibrated at this temperature for 4 min, then cooled to 25 °C at 20 °C/ min, held at this temperature for 4 min, and reheated to 300 °C at 10 °C/min. All T_g values were obtained from the second scan.

Results and Discussion

Polymerization of (M)MBL by cationic group 4 metallocenes

Coordination-addition polymerization of acrylic monomers by cationic group 4 metallocenium catalysts is typically carried out in hydrocarbons such as toluene and polar non-coordinating solvents such as CH_2Cl_2, whereas polar coordinating solvents such as THF and DMF usually shut down the polymerization.[1] Owing to the insolubility of PMBL in toluene or CH_2Cl_2, polymerization of MBL by group 4 catalysts in such solvents proceeds in a *heterogeneous* fashion, thereby negatively impacting the catalyst activity and control over the polymerization. For instance, polymerization of 400 equiv of MBL in CH_2Cl_2 at RT by the two-component catalyst system, $Cp_2ZrMe[OC(OEt)=CMe_2]$ as initiator and $Cp_2ZrMe^+MeB(C_6F_5)_3^-$ as catalyst, following the MMA polymerization protocol,[10] afforded PMBL (which crashed out of the solution) in only 20% yield after 3 h; as anticipated, the same polymerization carried out in DMF yielded no isolable polymer products.

As in the polymerization of MBL by the C_{2v}-ligated catalyst, the insolubility of PMBL in CH_2Cl_2 produced by the C_s-ligated zirconocene catalyst **3**, which has been shown to be a highly active and syndiospecific polymerization catalyst for MMA polymerization,[18] resulted in only a modest isolated polymer yield of 40 %. Nevertheless, this polymerization is free of any ring-opening of the butyrolactone ring, as confirmed by NMR of the polymer, and the resulting PMBL also exhibits a unimodal, relatively narrow MWD of 1.37 (run 1, Table 1). The polymerization is efficient with a high initiator efficiency of $I^* = 90\%$, but it is not stereospecific, producing only a syndio-biased polymer with *rr* = 50.8 % (23.1% *mr*), presumably due to the significantly reduced

sterics of the monomer by bonding the methoxy methyl and the α-methyl group in MMA to form the five-membered butyrolactone ring in MBL. On the other hand, the polymerization of MMBL proceeds in a homogenous fashion due to the solubility of PMMBL in CH_2Cl_2, thereby rendering a quantitative monomer conversion in 5 h at RT. The resulting PMMBL exhibits a M_n of 2.98 $\times 10^4$ with a [MMBL]/[Zr] ratio of 200, giving an I^* of 76%; it also exhibits a unimodal, relatively narrow MWD of 1.33 (run 2) and a low syndiotacticity of 51.1% *rr* (39.7% *mr*).

Table1. Selected results of (M)MBL polymerization by group 4 metallocenes [a]

run no.	monomer	catalyst	time (h)	[monomer] /[catalyst]	conv. [b] (yield)	10^4 M_n [c] (g/mol)	MWD [c] (M_w/M_n)	I^* [d] (%)
1	MBL	**3**	5	200	(40)	0.89	1.37	90
2	MMBL	**3**	5	200	100	2.98	1.33	76
3	MBL	**2**	24	200	100	60.2, 4.52	1.03, 1.32	3.3, 44
4	MMBL	**2**	24	200	100	23.2, 0.53	1.64, 1.14	9.7, 425

[a] Carried out in 5 mL CH_2Cl_2 at RT (~ 25 °C). [b] Conversion, measured by ^{1}H NMR, or in parenthesis, isolated yield. [c]Determined by GPC relative to PMMA standards. [d]Initiator efficiency (I^*) = M_n(calcd)/M_n(exptl), where M_n(calcd) = MW(monomer) × [monomer]/[catalyst] × conversion% + MW of chain-end groups.

The (CGC)Ti ester enolate catalyst **2** and the related alkyl derivative CGCTiMe$^+$MeB$(C_6F_5)_3^-$ have been shown to be efficient, living,[16] and robust (up to 100 °C)[15] catalyst for MMA polymerization. Both polymerizations of MBL and MMBL by **2** afforded quantitative monomer conversions, but the resulting polymers exhibit bimodal MWDs (runs 3 and 4), with the higher MW fraction being 15% for PMBL and 18% for PMMBL. The polymerization by the alkyl catalyst behaves similarly, and it is currently unclear why the (CGC)Ti catalyst gives bimodal PMBL and PMMBL; the polymerization in the presence of 5 equiv of the potent radical trap, galvinoxyl, still afforded a similarly bimodal MWD, thus eliminating the possibility of a secondary radical mechanism contributing to the bimodal MWD.

Polymerization of (M)MBL by lanthanocene(II) $Cp^*_2Sm(THF)_2$ (1)

In coordination polymerization of polar vinyl monomers, lanthanocene catalysts *differ* from group 4 metallocene catalysts in two most notable aspects:[1] first, group 4 catalysts are active for polymerization as cationic species, whereas group 3 catalysts are active in their neutral form (isoelectronic to cationic group 4 metals). To illustrate this point, we tested MBL polymerization by the cationic Sm(III) species $[Cp^*_2Sm(THF)_2]^+[BPh_4]^-$ and found no activity, which also confirms that such cations do not ring-open the butyrolactone ring. On the other hand, the same polymerization by the neutral Sm(II) $Cp^*_2Sm(THF)_2$ is highly active (Table 2). Second, unlike the polymerization by cationic group 4 catalysts, which is inactive in polar coordinating solvents, such as THF and DMF, such polar solvents can, however, be used for the MMA polymerization by lanthanocene catalysts without noticeably altering the polymerization results including PMMA syndiotacticity, M_n, and MWD.[19] Uniquely, the coordination polymerization system by neutral lanthanocenes involves *no counteranions*, and as such the influence of solvent is limited to the effect on the polymerization rates as donor solvent molecules may compete with polar monomer molecules for coordination to the highly electrophilic metal center. Hence, the ability of lanthanocene catalysts to perform the MBL polymerization in DMF is significant because the solubility of the resulting high-MW PMBL renders a homogeneous process, allowing for the polymerization to achieve high conversions and to better control polymer characteristics. To demonstrate this point, we tested MBL polymerization by **1** in toluene; although 90% of the 50 equiv of MBL was quickly (10 min) converted to PMBL, the polymerization immediately becomes heterogeneous, due to the insolubility of the resulting polymer in toluene, and the isolated polymer exhibits a bimodal MWD with the higher MW fraction being ~40% (run 5, Table 2). On the other hand, the polymerization of 100 equiv of MBL in DMF remained homogeneous throughout the course of polymerization, achieving a quantitative monomer conversion in 10 min; no ring-opening of the butyrolactone ring was observed, and the resulting polymer exhibits a unimodal, relatively narrow MWD of 1.39 (run 6, Table 2).

Table 2. Selected results of polymerization of MBL by samarocene(II) **1** [a]

run no.	monomer (solvent)	[monomer] /[**1**]	conv (yield)	$10^4 M_n$ (g/mol)	MWD (M_w/M_n)	I^* (%) (unimetallic)	I^* (%) (bimetallic)
5	MBL (toluene)	50	(89.7)	15.6	1.53		
				0.95	1.19	46	92
6	MBL (DMF)	100	100	1.71	1.39	57	114
7	MBL (DMF)	200	100	4.09	1.59	48	96
8	MBL (DMF)	300	100	5.98	1.29	49	98
9	MBL (DMF)	400	100	8.59	1.37	46	92

[a] Carried out at RT (~ 25 °C) for 10 min. See the footnotes under Table 1 for other explanations.

Another interesting aspect of the MBL polymerization by samarocene(II) catalyst **1** is the calculated initiator efficiency I^* values. For example, the polymerization of 200 equiv of MBL achieved the quantitative monomer conversion in 10 min, but the measured M_n (4.09×10^4) of the atactic PMBL (49.3% *mr* and 29.5% *rr*) was approximately twice what was calculated based on the monomer to metal center ratio and a unimetallic mechanism, giving rise to a low I^* of 48% (run 7, Table 2). On the other hand, the calculated I^* was 96% with a bimetallic model (i.e., two Sm centers producing a single polymer chain). The polymerizations in other monomer-to-**1** ratios (100–400, runs 6–9, Table 2) showed the same characteristics. Similar observations were previously made in the polymerization of MMA by the divalent lanthanocenes $Cp^*_2Ln(THF)_2$ (Ln = Yb, Sm), as first reported by Yasuda and co-workers: despite the polymerization being living, the calculated I^* based on a unimetallic mechanism was less than 40 %.[19] It was later shown by Boffa and Novak[22] that the MMA polymerization by the divalent samarocene proceeds through a redox-then-radical-coupling process, with the true active species being a trivalent samarocene center. This process was proposed to involve a one-electron transfer from samarium(II) to MMA, affording samarium(III) cation and an MMA radical anion, which combine to form a samarium enolate radical; two radicals then combine in head-to-tail fashion, affording a bimetallic diinitiator that is the active species in the living polymerization of MMA.[22] Hence, two samarium metal centers produce one polymer chain, and the MW is double what is expected based off of the monomer to metal center ratio. On the basis of this analysis and the literature precedence for the

MMA polymerization, a chain initiation and propagation mechanism for the MBL polymerization can be similarly outlined in Scheme 1.

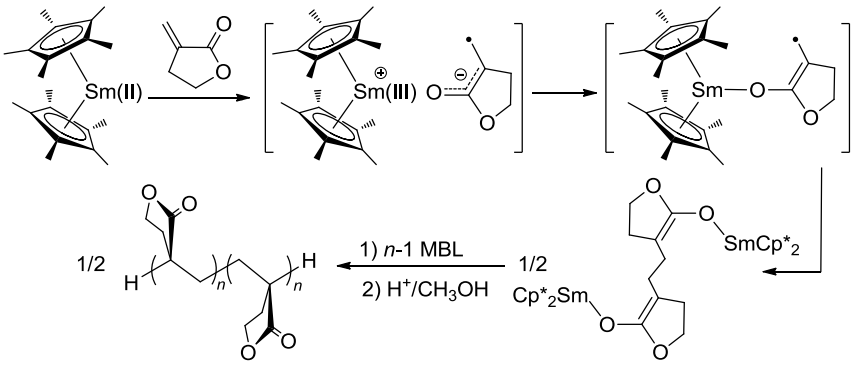

Scheme 1. Proposed chain initiation and propagation in the MBL polymerization by $Cp^*_2Sm(THF)_2$

The control of the polymerization over polymer MW was demonstrated by a linear increase in M_n with increasing the [MBL]/[**1**] feed ratio from 100 to 400 (Fig. 1). The polymerization of MMBL by **1** was as successful as that of MBL (runs 10–13, Table 3). Kinetic profiling of the MMBL polymerization at a given [monomer]:[**1**] ratio yielded essentially the same apparent rate to that of the MBL polymerization, with TOF = 3000 h^{-1} (run 13). Likewise, the control over MW of the resulting PMMBL was shown by a linear increase in MW with increasing the [MMBL]:[**1**] ratio. However, the glass transition temperature (T_g) of the atactic PMMBL produced (49.2% *mr*, 33.1% *rr*, M_n = 5.48 $\times 10^4$, run 11, Table 3) is 227 °C, which is considerably higher than the T_g of PMBL (194 °C) having a similar M_n of 5.98 $\times 10^4$ (Fig. 2). Furthermore, PMMBL exhibits greatly enhanced thermal properties. Specifically, the temperature of 10 % weight loss ($T_{10\%}$) of PMBL is 350 °C, while for PMMBL $T_{10\%}$ was 15 °C higher at 365 °C (Fig. 3). Accordingly, the initial (T_{ini}) and end (T_{end}) onset temperatures of PMMBL (T_{ini} = 356 °C, T_{end} = 441 °C) are 12 °C and 25 °C higher than those of PMBL (T_{ini} = 344 °C, T_{end} = 406 °C). Even more dramatically, the T_g and onset decomposition temperatures of the PMMBL are ~120 °C and 40 °C higher than the T_g (105

°C) and onset decomposition temperatures (T_{ini} = 340 °C, T_{end} = 399 °C) of the atactic PMMA with comparable MW.

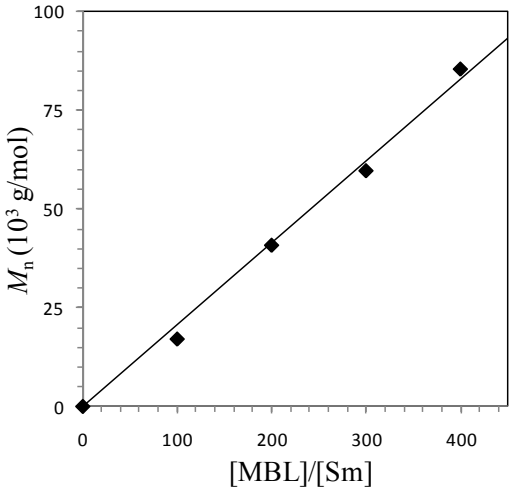

Fig. 1 Plot of M_n of PMBL as a function of the [MBL] to [**1**] ratio (all achieving 100% conversion).

Table 3. Selected results of MMBL polymerization and (M)MBL copolymerization by **1** [a]

run no.	monomer	[monomer] /[**1**]	conv (yield)	10^4 M_n (g/mol)	MWD (M_w/M_n)
10	MMBL	100	100	1.73	1.19
11	MMBL	300	100	5.48	1.86
12	MMBL	400	100	6.06	1.59
13	MMBL	500	100	6.95	1.69
14	MMA: MBL	200:200	100	5.91	1.41
15	MMA + MBL	200 +200	100	5.75	1.61
16	MBL: MMBL	100:100	100	3.29	1.60
17	MBL + MMBL	100 +100	100	3.31	1.36

[a] Carried out in DMF at RT (~ 25 °C) for 10 min. See the footnotes under Table 1 for other explanations.

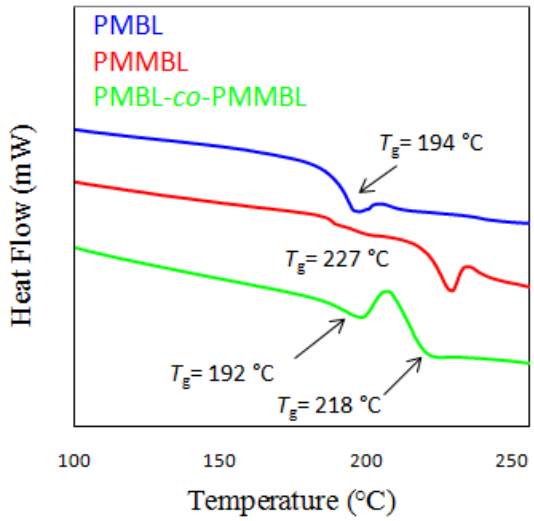

Fig. 2 DSC plots of PMBL (blue, M_n = 5.98 ×10^4, run 8, Table 2), PMMBL (red, M_n = 5.48 ×10^4, run 11, Table 3), and PMBL-*b*-PMMBL (green, M_n = 3.31 ×10^4, run 17, Table 3).

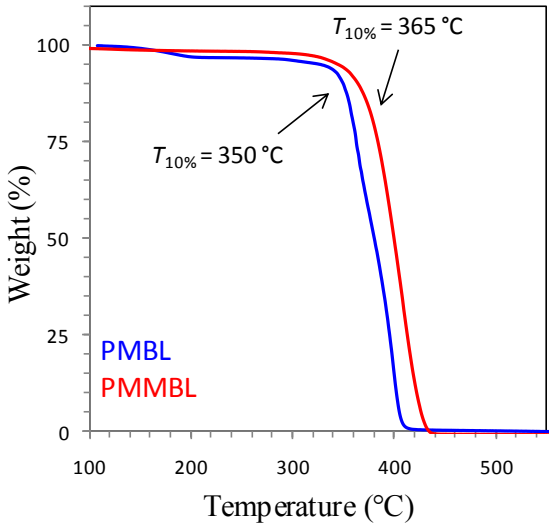

Fig. 3 TGA plots of PMBL (blue, M_n = 5.98 ×10^4, run 8, Table 2) and PMMBL (red, M_n = 5.48 ×10^4, run 11, Table 3).

Studies of the polymerization kinetics revealed that this polymerization follows zero-order kinetics in [MMBL] for all the [MMBL]/[**1**] ratios investigated (Fig. 4). The double logarithmic plot of the apparent rate constants (k_{app}), obtained from the slopes of the best-fit lines to the plots of $[M]_t/[M]_0$ vs time, as a function of ln[**1**] was fit to a straight line (R^2 = 0.954) with slope = 2.02

(Fig. 5). Thus, the kinetic order with respect to [**1**], given by the slope of ~2, shows that the polymerization is second-order in catalyst concentration, as a result of two samarium species working in tandem to produce one polymer chain, consistent with the mechanism depicted in Scheme 1. A zero-order dependence on monomer concentration in this polymerization suggests that the rate determining step is the intramolecular conjugate Michael addition of the coordinated monomer into the polymer chain (i.e., the C–C bond forming step), whereas the monomer coordination through the displacement of the coordinated penultimate polymer chain end by the incoming monomer is relatively fast, resembling the MMA polymerization by the (CGC)Ti catalyst.[14]

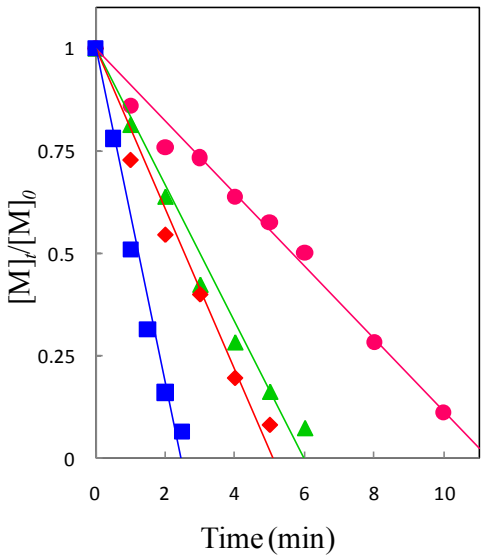

Fig. 4 Zero-order kinetic plots of the polymerization of MMBL by **1** in DMF at RT (~ 25 °C). Conditions: [MMBL] = 1.36 M; [**1**] = 4.54 (■), 3.42 (♦), 2.71 (▲), and 2.27 (●) mM.

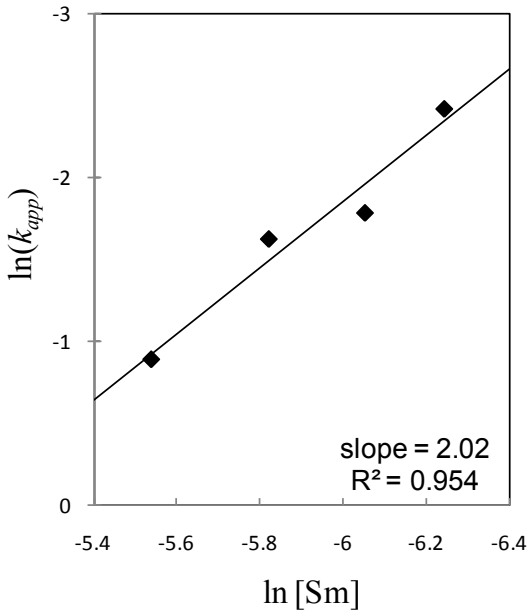

Fig. 5 Plot of ln(k_{app}) vs ln[**1**] for the polymerization of MMBL by **1** in DMF at ambient temperature.

Samarocene catalyst **1** has also been employed for successful copolymerization of MBL with MMA and with MMBL. Thus, both statistical (run 14, Table 3) and block (run 15, Table 3) copolymerizations of MBL (200 equiv) with MMA (200 equiv) in 10 min afforded quantitative yields of the isolated, defined random copolymer, PMMA-*ran*-PMBL, and block copolymer, PMMA-*b*-PMBL, showing a unimodal MWD of 1.41 and 1.61, respectively. Similarly, defined random copolymer PMBL-*ran*-PMMBL and block copolymer PMBL-*b*-PMMBL, with a unimodal MWD of 1.60 and 1.36, respectively, can be readily produced by statistical (run 16, Table 3) and block (run 17, Table 3) copolymerizations of MBL and MMBL. The block copolymer PMBL-*b*-PMMBL shows two T_g's at 192 and 218 °C on DSC traces (Fig. 2), corresponding to the T_g of the microphase separated PMBL and PMMBL domains, respectively.

Polymerization of MBL by non-lanthanocene(III) Ln[N(SiMe$_3$)$_2$]$_3$ (Ln = Sm, La, Nd, Er)

There has been growing interest in developing non-metallocene lanthanide catalysts for the polymerization of functionalized vinyl monomers.[1] Most non-lanthanocene catalysts utilize bulky ligands to simulate the electronics, sterics, and symmetry of Cp-based ligands, but they generally exhibit lower polymerization activity and degree of polymerization control. Thus, homoleptic lanthanum silylamide La[N(SiMe$_3$)$_2$]$_3$ affords atactic PMMA at ambient temperatures in toluene, with a broad MWD of 3.01.[71] Since it has been shown that the activity of MBL is greater than that of MMA, we investigated the polymerization of MBL by such trivalent non-metallocene lanthanide catalysts. Utilizing a series of lanthanide silylamides, Ln[N(SiMe$_3$)$_2$]$_3$ (Ln = La, Nd, Sm, Er) having different ionic radii, we sought to compare effects on the polymerization of MBL of not only ligand substitution [as compared to Cp*$_2$Sm(THF)$_2$], but also the metal center in these complexes, the results of which are summarized in Table 4.

Table 4. Results of MBL polymerization by Ln[N(SiMe$_3$)$_2$]$_3$ [a]

run no.	Ln	[MBL] /[Ln]	Time (h)	conv[b] (yield)	10^4 M_n (g/mol)	MWD (M_w/M_n)	I^* (%)
18	La	400	21	(82.5)	1.77	2.16	183
19	Nd	400	21	(62.5)	2.39	1.98	103
20	Sm	400	21	(82.5)	2.23	1.90	145
21	Er	400	21	(87.1)	1.87	1.51	183
22	Er	500	48	87.1	1.96	1.28	200
23	Er	600	48	49.9	1.64	1.44	179

[a] Carried out in DMF at RT (~ 25 °C) for 10 min. See the footnotes under Table 1 for other explanations.

The activity of these non-metallocene lanthanide complexes for the polymerization of MBL was much lower than that of the metallocene catalyst Cp*$_2$Sm(THF)$_2$, requiring a long reaction time of 21 h to achieve >80% (La, Sm, Er) or only > 60 % (Nd) monomer conversions (runs 18–21, Table 4); this is compared to the 10-min reaction time for quantitative MBL conversion by Cp*$_2$Sm(THF)$_2$ (TOF = 2,400 h^{-1}), which is >130 times faster. There was no clear activity trend relative to the ionic radius of the Ln(III) center, although the smallest Er ion in this series gave

the highest isolated polymer yield, and it also afforded PMBL with the narrowest MWD of 1.51 (run 21); the PMBL produced is atactic with 45.3% *mr* (34.1% *rr*). Intriguingly, the least active Nd catalyst gave an *I** ~ 100% (run 19), suggesting that only one silylamide ligand per metal participated in chain initiation, whereas the most active Er catalyst gave an *I** ~ 183% (run 21), indicating that approximately two silylamide ligands per Er are involved in chain initiation. This near 200% *I** trend is held when the MBL feed is increased to 500 equiv (200%, run 22) and 600 equiv (179%, run 23) per metal. In this context, the La catalyst (183%, run 18) behaves similarly to the Er catalyst, while the Sm catalyst (145%, run 20) is somewhere between the Er and Nd catalysts.

Catalytic polymerization of MBL by $Cp^*_2Sm(THF)_2$ in the presence of organo acids

To render catalytic production of polymer chains in the coordination-addition polymerization catalyzed by metal complexes, a suitable chain-transfer agent (CTA) added externally must effectively cleave the growing polymer chain from the active center, and the resulting new species containing part of the CTA moiety (typically in its deprotonated form) must efficiently reinitiate the polymerization.[1] It has been shown that organic acids such as alkyl thiols and enolizable ketones are effective CTA's to transform the living MMA polymerization by $Cp^*_2SmMe(THF)$ into a chain transfer polymerization for the catalytic production of PMMA, although the effectiveness for the catalytic polymer production by this system is limited (TON = 5) even with a [CTA]/[Sm] ratio as high as 29.[72] As our current work studies a different monomer (MBL) and uses a different catalyst (divalent samarocene **1**), we first screened three different organo acids, 3-methyl-2-butanone (MBO), methyl isobutyrate (MIB), and dimethyl malonate (DMM), for their relative effectiveness as a CTA in promoting the catalytic polymerization of MBL by $Cp^*_2Sm(THF)_2$, the results of which are summarized in Table 5.

Table 5. Results of chain transfer polymerizations of MBL catalyzed by **1** [a]

run no.	CTA	[MBL]/[CTA]/[**1**]	conv (yield)	10^3 M_n (g/mol)	MWD (M_w/M_n)	I* % (bimetallic)
24	MBO	500/20/1	100	9.34	1.57	1060
25	MIB	500/20/1	100	28.6	1.81	350
26	DMM	500/20/1	0			
27	none	400/0/1	100	85.9	1.37	92
28	MBO	400/10/1	(97.5)	9.22	1.54	845
29	MBO	400/30/1	(92.5)	7.27	1.41	1020
30	MBO	400/50/1	(87.5)	6.58	1.40	1020

[a] Carried out in DMF at RT for 15 h. MBO = 3-methyl-2-butanone, MIB = methyl isobutyrate (MIB), DMM = dimethyl malonate (DMM). See the footnotes under Table 1 for other explanations.

It can be seen from the table, under identical conditions ([MBL]/[CTA]/[**1**] = 500/20/1), the ketone MBO is most effective as judged by its I* of 1060% (run 24), equating to approximately 10 polymer chains produced per bimetallic catalyst (i.e., TON ~ 10). The ester MIB is much less effective, giving an I* of 350% (run 25), while the α-diester DMM completely halts the polymerization (run 26), similar to the zirconocenium-catalyzed MMA polymerization in the presence of DMM.[73] Concentrating on MBO and fixing the [MBL]/[catalyst] ratio as 400, we gradually increased the [CTA]/[catalyst] ratio from 0 to 10 to 30 and to 50, in efforts to examine to what extent MBO can be effective as a CTA. In the absence of MBO, the I* based on the bimetallic mechanism (vide supra) was calculated to be 92% (run 27, Table 5, see also run 9 in Table 2). Addition of 10 equiv of MBO brought I* up to 845% (run 28), effectively promoting catalytic polymerization of MBL with a TON of ~8.5. Increasing the MBO amount by threefold (30 equiv) only moderately enhanced the I* to 1020% (TON ~10, run 29), and in fact, a further increase of MBO to 50 equiv resulted in no additional enhancement over I* (run 30); in the latter case, although the MW was lowered as it should, the polymer yield also dropped, giving rise to no net change in the I* value. Overall, the catalytic MBL polymerization by **1** can be effected by addition of MBO as a suitable CTA. Scheme 2 outlines the reaction sequence, based on what has been proposed for the chain transfer polymerization of MMA by the samarocene(III) catalyst,[1,72]

except that in this case two Sm centers carry a single polymer chain as a result of the redox-then-radical-coupling chain-initiation process (vide supra).

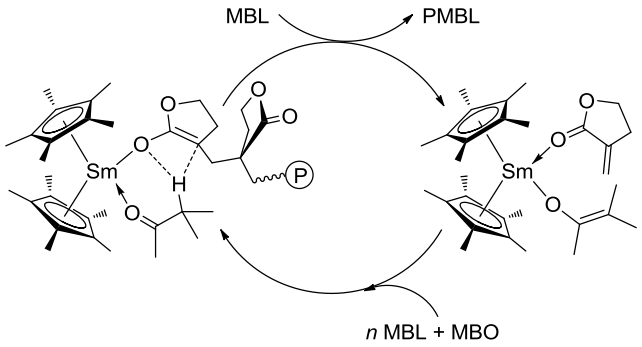

Scheme 2. Chain transfer polymerization of MBL catalyzed by $Cp^*_2Sm(THF)_2$ (the same events at the other Sm center omitted for clarity).

Conclusions

The samarocene(II) complex, $Cp^*_2Sm(THF)_2$, catalyzes rapid, efficient, and controlled coordination polymerization of renewable butyrolactone-based vinyl monomers MBL and MMBL in DMF at RT, as demonstrated by its high TOF of up to 3000 h^{-1}, typically near quantitative initiator efficiency, and ability to control the polymer MW with the monomer-to-catalyst ratio or monomer conversion. The resulting atactic PMBL (M_n = 5.98 $\times 10^4$, M_w/M_n = 1.29) and PMMBL (M_n = 5.48 $\times 10^4$, M_w/M_n = 1.86) exhibit high T_g's of 194 ºC and 227 ºC, respectively, and PMMBL also shows greatly enhanced thermal properties. More remarkably, the T_g and onset decomposition temperatures of the PMMBL are ~120 °C and 40 °C higher than the T_g and onset decomposition temperatures of the atactic PMMA with comparable MW. Thanks to the living/controlled characteristics of this polymerization, defined random and block copolymers of MBL with MMA and MMBL can be readily synthesized through statistical and sequential block copolymerization procedures.

Kinetic studies revealed that the polymerization by $Cp^*_2Sm(THF)_2$ is zero-order in [MMBL] and second-order in [catalyst], as a result of two samarium centers working in tandem to produce one polymer chain. This result, coupled with the polymerization initiator efficiency result which also pointed to the bimetallic nature of the propagation, conforms to the proposed MMA polymerization mechanism by the same divalent catalyst involving a redox-then-radical-coupling initiation process, with the true active species being the two trivalent samarocene centers attached to the single growing polymer chain.

The MBL polymerization by non-lanthanocene(III) silylamides, $Ln[N(SiMe_3)_2]_3$ (Ln = La, Nd, Sm, Er), are much slower (>130 times) than the polymerization by $Cp^*_2Sm(THF)_2$. The polymerization by these lanthanide silylamides is also ill-controlled and can involve more than one silyamide ligand in chain initiation. The polymerization of MBL and MMBL by cationic group 4 metallocene and half-metallocene catalysts incorporating C_2 and C_s symmetric ligands investigated in this study is also slower and less effective than the divalent samarocene catalyst; as such catalysts are limited to the polymerization in hydrocarbon or non-coordinating polar media, polymerization of MBL is a heterogeneous process.

Importantly, catalytic polymerization of MBL by $Cp^*_2Sm(THF)_2$ has been realized in the presence of a suitable chain transfer agent. Thus, addition of 20 equiv of the enolizable organo acid, 3-methyl-2-butanone, to the MBL (500 equiv) polymerization catalyzed by $Cp^*_2Sm(THF)_2$ brought about the production of approximately10 polymer chains per dimeric propagating species.

Acknowledgments

This work was supported by the National Science Foundation (NSF-0718061). We thank Boulder Scientific Co. for the research gifts of $B(C_6F_5)_3$ and $[Ph_3C][B(C_6F_5)_4]$, and Dr. John Belot for some samples of $Ln[N(SiMe_3)_2]_3$. This dissertation chapter contains the manuscript of a full paper

that was published in *Dalton Transactions* [Miyake, G. M.; Newton, S. E.; Mariott, W. R.; Chen, E. Y.-X. *Dalton Trans.* **2010**, *39*, 6710-6718]. S.E.N. performed solvent screening conditions for the polymerizations and W.R.M. initiated the investigation of zirconocene catalyst systems.

References

(1) Chen, E. Y.-X. *Chem. Rev.* **2009**, *109*, 5157–5214.

(2) Chen, E. Y.-X. *Dalton Trans,* **2009**, 8784–8793.

(3) Yasuda, H. *Prog. Polym. Sci*. **2000**, *25*, 573−626.

(4) Rodriguez-Delgado, A.; Chen, E. Y.-X. *Macromolecules* **2005**, *38*, 2587−2594.

(5) Bolig, A. D.; Chen, E. Y.-X. *J. Am. Chem. Soc.* **2004**, *126*, 4897−4906.

(6) Ning, Y.; Cooney, M. J.; Chen, E. Y.-X. *Organomet. Chem,* **2005**, *690,* 6263–6270.

(7) Stojcevic, G.; Kim, H.; Taylor, N. J.; Marder, T. B.; Collins, S. *Angew. Chem. Int. Ed.* **2004**, *43*, 5523−5526.

(8) Lian, B.; Toupet, L.; Carpentier, J.-F. *Chem. Eur. J,* **2004**, *10*, 4301–4307.

(9) Bandermann, F.; Ferenz, M.; Sustmann, R.; Sicking, W. *Macromol. Symp,* **2001**, *174*, 247–253.

(10) Li, Y.; Ward, E. G.; Reddy, S. S.; Collins, S. *Macromolecule,* **1997**, *30*, 1875−1883.

(11) Strauch, J. W.; Fauré, J.-L. Bredeau, S.; Wang, C.; Kehr, G.; Fröhlich, R.; LuftmannH.; Erker, G. *J. Am. Chem. Soc.* **2004**, *126*, 2089–2104.

(12) Jin, J.; Mariott, W. R.; Chen, E. Y.-X. *J. Polym. Chem. Part A: Polym. Chem.* **2003**, *41*, 3132–3142.

(13) Frauenrath, H.; Keul, H.; Höcker, H. *Macromolecules* **2001**, *34*, 14–19.

(14) Ning, Y.; Caporaso, L.; Correa, A.; Gustafson, L. O.; Cavallo, L.; Chen, E. Y.-X. *Macromolecules* **2008**, *41*, 6910–6919.

(15) Lian, B.; Thomas, C. M.; Navarro, C.; Carpentier, J.-F. *Organometallic,* **2007**, *26*, 187−195.

(16) Rodriguez-Delgado, A.; Mariott, W. R.; Chen, E. Y.-X. *Macromolecules* **2004**, *37*, 3092–3100.

(17) Nguyen, H.; Jarvis, A. P.; Lesley, M. J. G.; Kelly, W. M.; Reddy, S. S.; Taylor, N. J.; Collins, S. *Macromolecules* **2000**, *33*, 1508−1510.

(18) Zhang, Y.; Ning, Y.; Caporaso, L.; Cavallo, L.; Chen, E. Y.-X. *J. Am. Chem. Soc.* **2010**, *132*, in press (DOI: 10.2021/ja908818y).

(19) Yasuda, H.; Yamamoto, H.; Yamashita, M.; Yokota, K.; Nakamura, A.; Miyake, S.; Kai, Y.; Kanehisa, N. *Macromolecules* **1993**, *26*, 7134−7143.

(20) Yasuda, H.; Yamamoto, H.; Yokota, K.; Miyake, S.; Nakamura, A. *J. Am. Chem. Soc.* **1992**, *114*, 4908−4909.

(21) Boffa. L. S.; Novak, B. M. *Macromolecules* **1997**, *30*, 3494−3506.

(22) Boffa, L. S.; Novak, B. M. *Macromolecules* **1994**, *27*, 6993−6995.

(23) Caporaso, L.; Cavallo, L. *Macromolecules* **2008**, *41*, 3439−3445.

(24) Tomasi, S.; Weiss, H.; Ziegler, T. *Organometallics* **2007**, *26*, 2157−2166.

(25) Caporaso, L.; Gracia-Budrìa, J.; Cavallo, L. *J. Am. Chem. Soc.* **2006**, *128*, 16649−16654.

(26) Tomasi, S.; H. Weiss, H.; Ziegler, T. *Organometallics* **2006**, *25*, 3619−3630.

(27) Hölscher, M.; Keul, H.; Höcker, H. *Macromolecules* **2002**, *35*, 8194−8202.

(28) Sustmann, R.; Sicking, W.; Bandermann, F.; Ferenz, M. *Macromolecules* **1999**, *32*, 4204−4213.

(29) Cameron, P. A.; Gibson, V.; Graham, A. J. *Macromolecules* **2000**, *33*, 4329−4335.

(30) Deng, H.; Shiono, T.; Soga, K. *Macromolecules* **1995**, *28*, 3067−3073.

(31) Collins, S.; Ward, D. G.; Suddaby, K. H. *Macromolecules* **1994**, *27*, 7222−7224.

(32) Miyake, G. M.; Caporaso, L.; Cavallo, L.; Chen, E. Y.-X. *Macromolecules* **2009**, *42*, 1462−1471.

(33) Miyake, G. M.; Chen, E. Y.-X. *Macromolecules* **2008**, *41*, 3405−3416.

(34) Miyake G. M.; Mariott, W. R.; Chen, E. Y.-X. *J. Am. Chem. Soc.* **2007**, *129*, 6724−6725.

(35) Mariott, W. R.; Chen, E. Y.-X. *Macromolecules* **2005**, *38*, 6822−6832.

(36) Mariott, W. R.; Chen, E. Y.-X. *Macromolecules* **2004**, *37*, 4741–4743.

(37) Ning, Y.; Chen, E. Y.-X. *J. Am. Chem. Soc.* **2008**, *130*, 2463−2465.

(38) Tullo, A. H. *C&E News* 2008, *86,* 21–25.

(39) Williams, C. K.; Hillmyer, M. A., *Polym. Rev.* **2008**, *48*, 1−10.

(40) Meier, M. A. R.; Metzger, M. J. O.; Schubert, S. *Chem. Soc. Rev.* **2007**, *36*, 1788−1802.

(41) Hoffman, H. M. R.; Rabe, J. *Angew. Chem. Int. Ed. Engl.* **1985**, *24*, 94–110.

(42) Manzer, L. E. *ACS Symp. Ser.* **2006**, *921*, 40–51.

(43) Manzer, L. E. *Appl. Catal. A: Gen.* **2004**, *272*, 249–256.

(44) Akkapeddi, M. K. *Polymer* **1979**, *20*, 1215–1216.

(45) Stansbury, J. W.; Antonucci, J. M. *Dent. Mater.* **1992**, *8*, 270–273.

(46) Akkapeddi, M. K. *Macromolecules* **1979**, *12*, 546–551.

(47) Kimura, Y.; Nakamura, S. *JP* 2009046560 A, **2009**.

(48) Pickett, J. E.; Ye, W. *US Pat.,* 2007/0122625, **2007**.

(49) Bandenburg, C. J. *WO* 2004069926, **2004**.

(50) Mullin, R. *C&E News* **2004**, *82,* 29–37.

(51) Mosnáček, J.; Yoon, J. A.; Juhari, A.; Koynov, K.; Matyjaszewski, K. *Polymer* **2009**, *50*, 2087–2094.

(52) Mosnáček, J.; Matyjaszewski, K. *Macromolecules* **2008**, *41*, 5509–5511.

(53) Ueda, M.; Takahashi, M.; Imai, Y.; Pittman, C. U. Jr. *J. Polym. Sci.: Polym. Chem.* **1982**, *20*, 2819–2828.

(54) Gridnev, A. A.; Ittel, S. D. *WO* 2000035960 A2, **2000**.

(55) Sogah, D. Y.; Hertler, W.R.; Webster, O. W.; Cohen, G. M. *Macromolecules* **1987**, *20*, 1473–1488.

(56) van den Brink, M.; Smulders, W.; van Herk, A. M.; German, A. L. *J. Polym. Sci.: Polym. Chem.* **1999**, *37*, 3804–3816.

(57) Koinuma, H.; Sato, K.; Hirai, H. *Makromol. Chem., Rapid Commun.* **1982**, *3*, 311–315.

(58) Lee, C.; Hall, H. K. Jr. *Macromolecules* **1989**, *22*, 21–25.

(59) Trumbo, D. L. *Polym. Bull.* **1991**, *26*, 271–275.

(60) Qi, G.; Nolan, M.; Schork, F. J.; Jones, C. W. *J. Polym. Sci.: Polym. Chem.* **2008**, *46*, 5929–5944.

(61) Bandenburg, C. J. *US Pat.,* 6 841 627 B2, **2005**.

(62) Suenaga, J.; Sutherlin, D. M.; Stille, J. K. *Macromolecules* **1984**, *17*, 2913–2916.

(63) Evans, W. J.; Grate, J. W.; Choi, H. W.; Bloom, I.; Hunter, W. E.; Atwood, J. L. *J. Am. Chem. Soc.* **1985**, *107*, 941–946.

(64) Evans, W. J.; Ulibarri, T. A.; Chamberlain, L. R.; Ziller, J. W.; Alvarez, D. Jr. *Organometallics* **1990**, *9*, 2124–2130.

(65) Schuetz, S. A.; Day, V. W.; Sommer, R. D.; Rheingold, A. L.; Belot, J. A. *Inorg. Chem.* **2001**, *40*, 5292–5295.

(66) Ning, Y.; Zhu, H.; Chen, E. Y.-X. *J. Organomet. Chem.* **2007**, *692*, 4535−4544.

(67) Yang, X.; Stern, C. L.; Marks, T. J. *J. Am. Chem. Soc.* **1994**, *116*, 10015−10031.

(68) Allen, R. D.; Long, T. E.; McGrath, J. E.; *Polym. Bull.* **1986**, *15*, 127−134.

(69) Evans, W. J.; Kozimor, S. A.; Ziller, J. W.; Kaltsoyannis, N. J. *J. Am. Chem. Soc.* **2004**, *126*, 14533–14547.

(70) Chen, Y.-X.; Marks, T. J. *Organometallics* **1997**, *16*, 3649–3657.

(71) Gauvin, R.; Mortreux, A. *Chem. Commun.* **2005**, 1146–1148.

(72) Nodono, M.; Tokimitsu, T.; Tone, S.; Makino, T.; Yanangase, A. *Macromol. Chem. Phys.* **2000**, *201*, 2282–2288.

(73) Mariott, W. R.; Rodriguez-Delgado, A.; Chen, E. Y.-X. *Macromolecules* **2006**, *39*, 1318–1327.

Chapter 7

Living Polymerization of Naturally Renewable Butyrolactone-Based Vinylidene Monomers by Ambiphilic Silicon Propagators

Abstract

Naturally renewable butyrolactone-based vinylidene monomers, α-methylene-γ-butyrolactone (MBL) and γ-methyl-α-methylene-γ-butyrolactone (MMBL), have been successfully polymerized in a rapid and living fashion, using ambiphilic silicon propagating species consisting of both the nucleophilic silyl ketene acetal (SKA) initiating moiety and the electrophilic silylium catalyst. Uniquely, the R_3Si^+ catalyst is derived directly from the SKA initiator upon *in situ* oxidative activation with a catalytic amount of the trityl borate activator. Investigations into effects of SKA (thus the resulting R_3Si^+ catalyst) and activator (thus the resulting counteranion) structures have revealed that the $Me_2C{=}C(OMe)OSi^iBu_3/Ph_3CB(C_6F_5)_4$ combination is the most active *and* controlled system for (M)MBL polymerizations. Thus, under ambient conditions and with a low catalyst loading (0.05 mol% relative to monomer), this polymerization system rapidly (within 10 minutes) and completely converts MMBL to PMMBL with controlled low to high (M_n = 5.43 × 10^5 g/mol) MW's and narrow MW distributions (1.01–1.06). Well-defined block copolymers of MBL and MMBL with MMA as well as block and statistical copolymers of MBL with MMBL have also been readily synthesized. Atactic homopolymers, PMBL and PMMBL, produced herein exhibit high glass transition temperatures (T_g's) of 194°C and 225 °C, respectively, representing T_g enhancements of ~90 °C (for PMBL) and ~120 °C (for PMMBL) over the T_g of the typical atactic PMMA. The critical MW of PMMBL has been estimated to be ~47 kg/mol.

Introduction

As petroleum resources continue to be depleted, polymer chemists face the challenge of gradually replacing existing petroleum-based polymeric materials with those derived from naturally occurring, renewable resources in a technologically and economically competitive fashion.[1,2,3,4,5] In this context, renewable butyrolactone-based vinylidene monomers, such as MBL (α-methylene-γ-butyrolactone) and MMBL (γ-methyl-α-methylene-γ-butyrolactone), are of particular interest in exploring the prospects of substituting the petroleum-based methacrylate monomers for specialty chemicals production.[6] MBL, or tulipalin A, is a natural substance found in tulips and the MBL ring is an integral building block of many (~10% known) natural products,[7] while its γ-methyl derivative MMBL can be readily prepared via a 2-step process from the biomass-derived levulinic acid.[8,9] Structurally, MBL can be described as the cyclic analog of MMA (methyl methacrylate), Chart 1; however, it exhibits greater reactivity in free radical polymerization[10] than typical methacrylate monomers such as MMA, due to the presence of both the nearly planar five-membered lactone ring, which provides a high degree of resonance stabilization for the active radical species, *and* the higher energy exocyclic C=C double bond, as a result of the ring strain and the fixed *s-cis* conformation.[11] The cyclic ring in MBL also imparts significant enhancements in the materials properties of the resulting PMBL (Chart 1), as compared to PMMA, thanks to the conformational rigidity of the polymer chain through incorporation of the butyrolactone moiety. Thus, the T_g (glass-transition temperature) of PMBL produced by the radical polymerization is 195 °C,[12] which is about 90 °C higher than that of atactic PMMA. Additionally, PMBL has increased optical properties as well as resistance to solvent (as evidenced by its insolubility in common organic solvents such as $CHCl_3$ and THF), heat, and scratch.[13,14,15] Some of these materials property enhancements have also been observed for PMMBL.[16]

Chart 1. Renewable butyrolactone-based vinylidene monomers (M)MBL and polymers P(M)MBL vs MMA and PMMA.

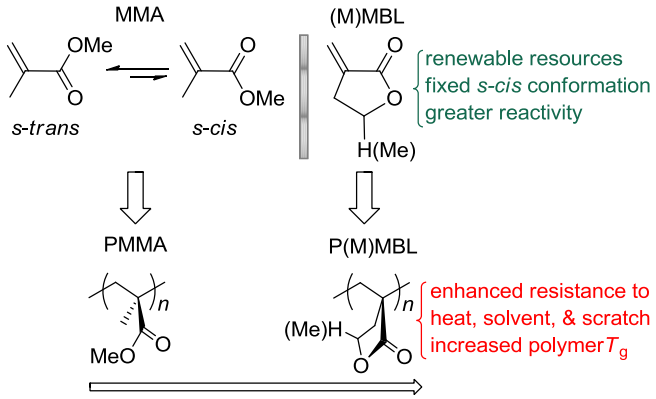

Several types of polymerization processes have been employed to polymerize MBL to low to high MW (molecular weight) polymers, including various radical polymerization mechanisms,[10,11,12,17,18,19,20] group-transfer polymerization,[21] anionic polymerization,[12] and coordination polymerization by metallocene complexes.[16] MBL has been copolymerized with various co-monomers[10] such as MMA,[22] styrene,[19,23] methoxystyrene,[24] and vinyl thiophenes.[25] While the polymerization of MMBL has been studied to a much lesser extent, it has also been polymerized by free-radical emulsion polymerization[26,27] as well as by radical, anionic, and group-transfer polymerization methods which required long reaction times (2 to 44 h), often at low temperatures, achieving low to high, but never complete conversions, with unknown polymerization and polymer MW characteristics.[28] Most recently, we found that the coordination polymerization of MBL and MMBL in DMF by the divalent decamethylsamarocene catalyst is fast (with TOF, turn over frequency, > 3,000 h^{-1}), efficient (with I^*, initiator efficiency, approaching 100 %), and controlled, leading to PMBL and PMMBL with relatively narrow MWD's (molecular weight distributions) as well as their well-defined block copolymers with MMA or with each other.[16] The resulting atactic PMBL and PMMBL have high T_g's of 194 ºC and 227 ºC, respectively.

Metal catalysts/initiators have been extensively utilized to effect stereochemically or architecturally controlled coordination polymerization of polar vinyl and vinylidene monomers such as (meth)acrylates and (meth)acrylamides under ambient conditions.[29] We recently developed a highly active, efficient, and living/controlled (meth)acrylate polymerization system catalyzed by *metalloid* silylium ions, R_3Si^+, at room temperature.[30] The highly active, *ambiphilic* propagating species contains both the nucleophilic SKA (silyl ketene acetal) moiety and the electrophilic silylium ion (or silyl cation) sites, Scheme 1. This propagator is generated by a unique *"monomer-less"* initiation involving oxidative activation of ^{R}SKA (trialkylsilyl methyl dimethylketene acetal) by a catalytic amount of TTPB [trityl tetrakis(pentafluorophenyl)borate, $Ph_3CB(C_6F_5)_4$], leading to the R_3Si^+-activated MMA derived from vinylogous *hydride abstraction* of ^{R}SKA with Ph_3C^+ (i.e., the monomer is generated from the initiator), followed by subsequent Michael addition of ^{R}SKA to the activated MMA (or silylated MMA), Scheme 1. A propagation "catalysis" cycle consists of a fast step of recapturing the silylium catalyst from the ester group of the growing polymer chain by the incoming MMA, followed by a *r.d.s.* of the C–C bond coupling via intermolecular Michael addition of the polymeric SKA to the silylated MMA (see the propagation manifold, Scheme 1). This novel polymerization system can produce high molecular weight ($M_n > 10^5$ g/mol) and well-defined (M_w/M_n = 1.04–1.12) homo and copolymers with a high silylium catalyst TOF (up to 1,500 h^{-1} for methacrylates) to an exceptionally high TOF (up to 120,000 h^{-1} for acrylates) 25 °C.[31] Recently, strong Brønsted acid trifluoromethanesulfonimide ($HNTf_2$) was also utilized to activate SKA leading to living polymerization of MMA, through the same silylium-catalyzed propagation process.[32] Intriguingly, earlier fast "group transfer polymerization" systems using SKA as initiator and additionally employing different combinations of a Lewis acid and a Me_3Si-containg reagent, such as $Me_3SiOTf/B(C_6F_5)_3$,[33] Me_3SiI/HgI_2,[34] or $Me_3SiI/RAl(OAr)_2$,[35] may also involve the silylium-catalyzed process as demonstrated in the SKA/TTPB system.[30,31] Considering the high activity and living nature, as well as potentially a broad implication of the silylium-catalyzed polymerization process for

(meth)acrylates, we reasoned that the SKA/TTPB system could be an excellent system for the polymerization of renewable monomers (M)MBL because the reactivity of (M)MBL lies somewhere between methacrylates and acrylates. Accordingly, the central objective of this study was to examine the characteristics of (M)MBL polymerizations using the unique ambiphilic silicon propagator derived from the activation of SKA with TTPB.

Scheme 1. Living/Controlled (meth)acrylate Polymerization Catalyzed by R_3Si^+ [30,31]

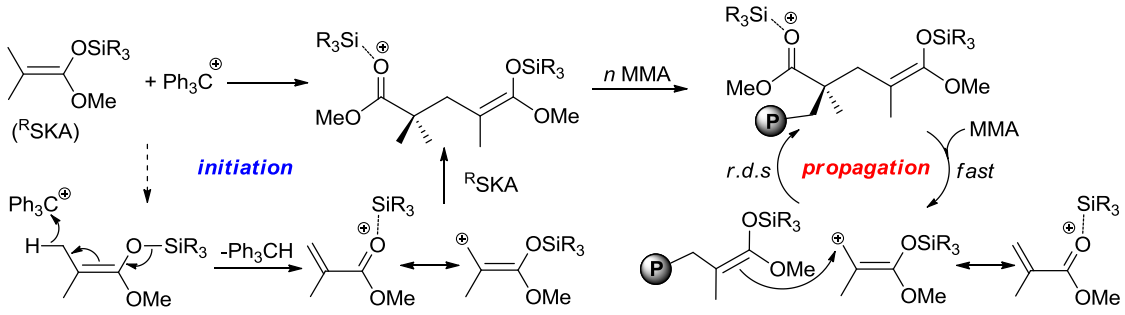

Experimental Section

Materials and methods. All syntheses and manipulations of air- and moisture-sensitive materials were carried out in flamed Schlenk-type glassware on a dual-manifold Schlenk line, a high-vacuum line, or in an argon or nitrogen-filled glovebox. HPLC-grade organic solvents were sparged extensively with nitrogen during filling of the solvent reservoir and then dried by passage through activated alumina (for Et_2O, THF, and CH_2Cl_2) followed by passage through Q-5-supported copper catalyst (for toluene and hexanes) stainless steel columns. HPLC-grade DMF was degassed, dried over CaH_2 overnight, followed by vacuum transfer (not by distillation). NMR solvents $CDCl_3$ and DMSO-d_6 were dried over activated Davison 4-Å molecular sieves, and NMR spectra were recorded on a Varian Inova 300 (FT 300 MHz, ^1H; 75 MHz, ^{13}C), a Varian Inova 400 MHz, or an Inova 500 MHz spectrometer. Chemical shifts for ^1H and ^{13}C spectra were referenced to internal solvent resonances and are reported as parts per million relative to tetramethylsilane.

Monomers α-methylene-γ-butyrolactone (MBL) and γ-methyl-α-methylene-γ-butyrolactone (MMBL) were purchased from TCI America, while methyl methacrylate (MMA), dimethylketene methyl trimethylsilyl acetal (^{Me}SKA), chlorotriisobutylsilane, diisopropylamine, and methyl isobutyrate were purchased from Aldrich. These chemicals were degassed, dried over CaH_2 overnight, followed by vacuum distillation, while MMA was further purified by titration with neat tri(*n*-octyl)aluminum (Strem Chemical) to a yellow end point,[36] followed by vacuum distillation. Butylated hydroxytoluene (BHT-H, 2,6-di-*tert*-butyl-4-methylphenol) was purchased from Aldrich and was recrystallized from hexanes prior to use. Activator $Ph_3CB(C_6F_5)_4$ (TTPB)[37] was obtained as a research gift from Boulder Scientific Co. and used as received. Modified literature procedures were employed to prepare the following compounds: dimethylketene methyl triisobutylsilyl acetal $Me_2C{=}C(OMe)OSi(^{i}Bu)_3$ (^{iBu}SKA),[31] $H(Et_2O)_2B(C_6F_5)_4$,[38] and trityl [tris(tetrachlorobenzenediolato) phosphate(V)] [Ph_3C][*rac*-TRISPHAT].[39]

General polymerization procedures. Polymerizations were performed in 30 mL oven-dried glass reactors inside the glovebox at ambient temperature (~25 ºC). In a typical polymerization procedure (which is the same as established for MMA polymerization[30,31]), predetermined amounts of the appropriate SKA initiator and MBL (0.500 mL; 6.07 mmol) or MMBL (0.648 mL; 6.07 mmol) were premixed in a flask with 4 mL of CH_2Cl_2, and with vigorous stirring, TTPB (1.00 mL, 3.03 mM in CH_2Cl_2, 3.03 μmol) was added to start the polymerization. Polymerizations were quenched at the time specified in the tables with 5 mL of 5 % HCl in methanol, and the polymer was precipitated into 50 mL of methanol and collected by filtration and centrifugation, before being washed extensively with methanol to remove any catalyst residue or unreacted monomer. Polymers were then dried at 50 °C overnight in a vacuum oven to a constant weight. ^{1}H NMR (DMSO-d_6, 300 MHz, 100 °C) for PMBL: δ 4.34 (b.s, 2H, OC*H*$_2$), 2.24-1.99 (m, 4H, C*H*$_2$, C*H*$_2$). ^{13}C NMR (DMSO-d_6, 125 MHz, 100 °C) for PMBL: δ 179 (*C*=O), 64.36 (O*C*H$_2$), 44.22, 43.90, 43.74 (quaternary carbon, *rr*, *mr*, *mm*), 41.89–40.58 (main-chain *C*H$_2$, unresolved tetrads), 30.47 (β-*C*H$_2$). ^{1}H NMR (DMSO-d_6, 300 MHz, 100 °C) for

PMMBL: δ 4.64 (b.s, 1H, C*H*), 2.31 (b.s, 2H, CH_2), 1.99 (b.s, 2H, CH_2), 1.39 (b.s, 3H, CH_3). ^{13}C NMR (DMSO-d_6, 125 MHz, 100 °C) for PMMBL: δ 178 (*C*=O), 72.65 (O*C*H), 46.48, 46.15, 45.80 (quaternary carbon, *rr*, *mr*, *mm*), 43.05 (β-*C*H_2), 40.53, 39.19, 37.69 (main-chain *C*H_2, *rr*, *mr*, *mm*), 19.46 (*C*H_3). DEPT experiments were used to remove the DMSO signals in the ^{13}C NMR experiments.

Conversion data was performed by adding toluene (289 μL; 2.72 mmol), as an external standard, to the reaction mixture. At specified times 0.2 mL aliquots were withdrawn from the solution and quenched into septum sealed vials containing 0.7 mL of undried "wet" $CHCl_3$. Percent conversion was then calculated by comparing the integration of the vinyl protons of the unreacted monomer to the methyl protons of toluene.

Polymer characterizations. Gel permeation chromatography (GPC) and Light Scattering (LS) analyses of the polymers were carried out at 40 ºC and a flow rate of 1.0 mL/min, with DMF as the eluent, on a Waters University 1500 GPC instrument coupled with a Waters RI detector and a Wyatt miniDAWN Treos LS detector equipped with four 5 μm PL gel columns (Polymer Laboratories). Chromatograms were processed with Waters Empower software (version 2002); number-average molecular weight (M_n) and polydispersity (M_w/M_n) of polymers were given relative to PMMA standards. Weight-average molecular weight (M_w) was obtained from the analysis of the LS data which was processed with Wyatt Astra Software (version 5.3.2.15), and *dn/dc* values were determined assuming 100 % mass recovery of polymers with known concentrations. Tacticities of PMBL[10,21] and PMMBL[28] were measured by ^{13}C NMR in DMSO-d_6 at 100 °C. Decomposition onset temperatures (T_{onset}) of the polymers were measured by thermal gravimetric analysis (TGA) on a TGA 2950 Thermogravimetric Analyszer, TA Instrument. Polymer samples were heated from ambient temperature to 600 °C at a rate of 20 °C/min. Values for $T_{10\%}$ and T_{onset} (initial and end temperatures) were obtained from wt% *versus* temperature (°C) plots. Glass transition temperatures (T_g) of the polymers were measured by differential scanning

calorimetry (DSC) on a DSC 2920, TA Instrument. Polymer samples were first heated to 150 °C at 20 °C/min, equilibrated at this temperature for 4 min, then cooled to 30 °C at 20 °C/ min, held at this temperature for 4 min, and reheated to 300 °C at 10 °C/min. All T_g values were obtained from the second scan, after removing the thermal history.

Results and Discussion

Homopolymerization Characteristics. Table 1 summarizes the selected results of polymerizations of MBL and MMBL by the SKA/TTPB (0.05 mol% relative to monomer) system (where M = monomer, MBL or MMBL, and I = initiator ^{Me}SKA or $^{i\text{Bu}}$SKA). Given the unique initiation mechanism by which the SKA/TTPB system operates (*c.f.* Scheme 1), a polymerization with an $x[M]_0/y[SKA]_0/z[TTPB]_0$ ratio will have the *total* equivalency of the propagating SKA = $y - 2z + z = y - z$, thereby giving a [M]/[I] ratio of $x/(y - z)$.[30] Thus, a MBL polymerization with ^{Me}SKA being the initiator and [MBL] = 1.10 M, [^{Me}SKA] = 11.6 mM and [TTPB] = 0.551 mM (i.e., 400:4.2:0.2) gives the calculated [M]/[I] ratio of 100. This polymerization in CH_2Cl_2 became heterogeneous instantaneously upon addition of the TTPB activator (due to the insolubility of PMBL in CH_2Cl_2) and afforded a low isolated polymer yield of only 31.6% in 10 min of reaction (run 1, Table 1). Under the same conditions, but utilizing $^{i\text{Bu}}$SKA, a quantitative polymer yield was achieved (run 2), despite the heterogeneous polymerization. However, increasing the MBL to $^{i\text{Bu}}$SKA feed ratios to 200 and 400 significantly reduced the polymer yields to modest 57.1% (run 3) and low 12.5% (run 4). Furthermore, the heterogeneity of the MBL polymerization in CH_2Cl_2 resulted in bimodal MWD's of the polymers (runs 1–4), with the high MW fraction comprising of approximately 10–15% of the polymer sample. Nevertheless, the polymerization by the SKA + TTPB system is free of any ring-opening of the butyrolactone ring, and the PMBL produced by $^{i\text{Bu}}$SKA is essentially atactic, with a triad distribution of 39.3% *rr*, 37.3% *mr*, 23.4% *mm* (run 3). Polar, donor solvents such as DMF (in

which PMBL is soluble) deactivate the silylium catalyst through adduct formation, thus shutting down the polymerization.

Table 1. Selected Results of Polymerization of (M)MBL by SKA + TTPB [a]

run no.	M	I	[M]/[I]	time (min)	conv[b] (yield)	M_W[c] (kg/mol)	MWD[c] (M_w/M_n)
1	MBL	^{Me}SKA	100	10	(31.6)	129, 25.6	1.13, 1.31
2	MBL	$^{i\text{Bu}}$SKA	100	10	(>99)	427, 12.2	1.46, 1.21
3	MBL	$^{i\text{Bu}}$SKA	200	10	(57.1)	169, 18.9	1.57, 1.08
4	MBL	$^{i\text{Bu}}$SKA	400	10	(12.5)	374, 19.9	1.24, 1.04
5	MMBL	^{Me}SKA	200	10	64.2	50.3	1.22
6	MMBL	$^{i\text{Bu}}$SKA	100	10	100	18.8	1.06
7	MMBL	$^{i\text{Bu}}$SKA	200	10	100	31.0	1.02
8	MMBL	$^{i\text{Bu}}$SKA	400	15	100	93.2	1.03
9	MMBL	$^{i\text{Bu}}$SKA	600	30	100	176	1.01
10	MMBL	$^{i\text{Bu}}$SKA	800	120	100	548	1.01

[a] Carried out in 5 mL CH_2Cl_2 at ambient temperature (~25 °C). [b] Conversion, measured by ^{1}H NMR, or in parenthesis, isolated yield. [c] Determined by Light Scattering.

Similarly to MBL, the polymerization of MMBL is more rapid when utilizing $^{i\text{Bu}}$SKA as the initiator (thus the $^{i}Bu_3Si^+$ catalyst), as compared to ^{Me}SKA (thus the Me_3Si^+ catalyst). Specifically, when MMBL in a [M]/[I] ratio of 200 was polymerized by ^{Me}SKA + TTPB and $^{i\text{Bu}}$SKA + TTPB, after 10 min, 64.2% and 100% monomer conversion was observed, respectively (runs 5 and 7). Not only is the polymerization of MMBL by $^{i\text{Bu}}$SKA more rapid (TOF up to 12,000 h^{-1}) than that by ^{Me}SKA (TOF = 7,680 h^{-1}), it is also more *efficient and controlled* as shown by the following two levels of evidence. First, the M_W (determined by LS) of the polymer produced by ^{Me}SKA was 50.3 kg/mol (M_n = 41.2 kg/mol), while the polymer produced by $^{i\text{Bu}}$SKA had a M_W of 31.0 kg/mol (M_n = 30.4 kg/mol), giving initiator efficiencies (I^*) of 34.9% and 73.8 %, respectively. Second, the MWD of the polymer produced by ^{Me}SKA was relatively broad (1.22), but the polymer by $^{i\text{Bu}}$SKA has an extremely narrow MWD of 1.02. Also noteworthy is the high activity of the MMBL polymerization of this system that achieves a complete monomer conversion in 10 min at ambient temperature, as compared to the MMBL polymerization by conventional mechanisms, including radical, anionic, and group-transfer polymerization methods, which required 2 h to 44 h, often at low temperatures, achieving low to high, but never complete

conversions.[28] The PMMBL produced by $^{i\text{Bu}}$SKA and TTPB is syndio-biased atactic, with a triad distribution of 45.8% *rr*, 39.9% *mr*, 14.3% *mm* (run 8).

Monitoring the polymerization in a [MMBL]/[I] of 600 (run 9) reveals living characteristics of the polymerization by $^{i\text{Bu}}$SKA + TTPB, in that there is a linear increase in MW with increasing monomer conversion, while MWD remains nearly constant during the course of polymerization (Figures 1 and 2). This polymerization was further examined over the [MMBL]/[I] ratios from 200 to 800 (runs 7–10, Table 1). In all cases, the polymerization follows zero-order dependence on monomer concentration (Figure 3), thus proceeding through the same mechanism that has been established previously for the polymerization of MMA (*c.f.* Scheme 1).[30,31] Specifically, the *r.d.s.* of a propagation "catalysis" cycle is the C–C bond coupling via Michael addition of the polymeric SKA to the silylated monomer, while recapturing the silylium catalyst coordinated to the growing polymer chain by the incoming monomer is relatively fast, thereby giving rise to the zero-order dependence on monomer concentration. Quantitative monomer conversions can be achieved for all runs, and the resulting polymers exhibit narrow MWD's (≤ 1.03) but the MW's for the high [M]/[I] ratio runs are much higher than the calculated, typically a consequence of sacrificial consumption of the highly active catalysts like silylium ions as a scavenger (the effect of which is especially magnified at low catalyst loadings under high [M]/[I] ratios). Remarkable, a high MW PMMBL with a M_w of 548 kg/mol and an extremely narrow MWD of 1.01 (M_n = 543 kg/mol) was produced with a [M]:[I] ratio of only 800:1.

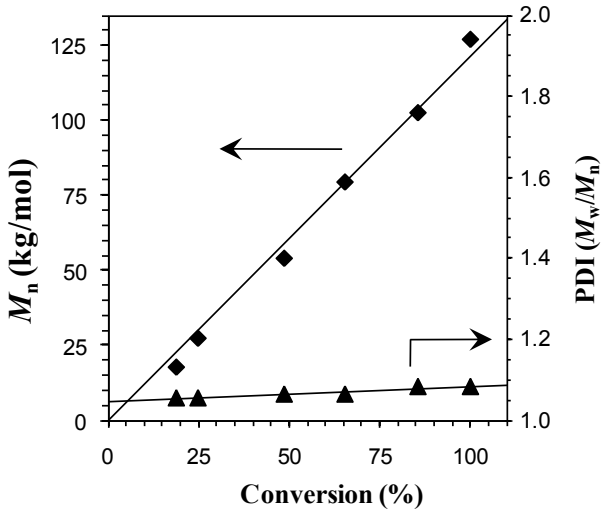

Figure 1. Plot of M_n (obtained by GPC against PMMA standard) and PDI of PMMBL vs monomer conversion for the polymerization of MMBL by $^{i\text{Bu}}$SKA + TTPB (run 9, Table 1).

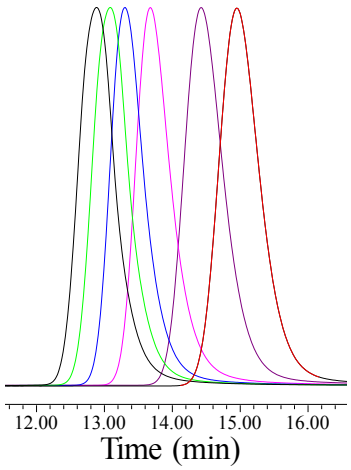

Figure 2. Overlay of GPC traces of aliquots taken during the polymerization plotted in Figure 1. M_n (kg/mol) and PDI (M_w/M_n) for traces from right (low MW) to left (high MW) are: 17.6, 1.06; 27.2, 1.06; 53.9, 1.07; 79.4, 1.07; 103, 1.09; and 127, 1.09.

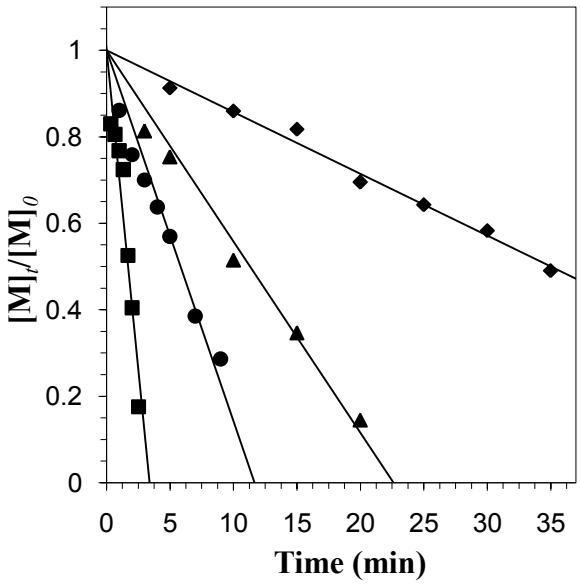

Figure 3. Zero-order kinetic plots of $[M]_t/[M]_0$ vs time for the polymerization of MMBL by $^{i\text{Bu}}$SKA + TTPB in CH_2Cl_2 at ambient temperature (~25 °C). Conditions: [MMBL] = 1.074 *M*; [TTPB] = 0.537 m*M*; [$^{i\text{Bu}}$SKA] = 5.91 mM (■), 3.22 mM (●), 2.33 mM (▲), 1.88 mM (♦).

Effects of Initiator and Activator. Focusing on the homogeneous polymerization of MMBL in CH_2Cl_2, we further investigated the effects of the SKA initiator ($Me_2C{=}C(OMe)OSiR_3$, thus the effect of the structure of the resulting R_3Si^+ catalyst) and the activator (thus the effects of the initiation process and the structure of the resulting counteranions). We have previously shown that there is a remarkable selectivity of SKA on monomer structure for the polymerization of (meth)acrylates by SKA + TTPB.[31] Specifically, the Me_3Si^+ catalyst derived from $^{\text{Me}}$SKA bearing a small silyl group is highly active and efficient for the polymerization of MMA, but inefficient for the polymerization of the sterically less demanding *n*-butyl acrylate (^{n}BA). In contrast, the $^iBu_3Si^+$ catalyst derived from $^{i\text{Bu}}$SKA bearing the bulky silyl group exhibits low activity in the polymerization of MMA, but exceptional activity, efficiency, and control for the polymerization of ^{n}BA.[31] In the context of (M)MBL, in forming the cyclic butyrolactone ring, they can be considered to be sterically smaller than MMA.

Indeed, our initial results discussed above demonstrated that the polymerization of MMBL by $^{i}Bu_3Si^+$ is more rapid, efficient, and controlled than that by Me_3Si^+.

Table 2 compiles more complete data to illustrate the effects of initiator and activator structures. Using TTPB (0.05 mol% relative to monomer) as activator in a fixed [MMBL]:[SKA] ratio of 200:1, the polymerizations using ^{Me}SKA and $^{i\text{Bu}}$SKA gave apparent rate constants (derived from the zero-order plot of $[M]_t/[M]_0$ vs time) of 0.114 mol/L·min^{-1} (run 11, Table 2) and 0.295 mol/L·min^{-1} (run 14, Table 2), respectively, thus indicating a 2.6-fold activity enhancement by $^{i}Bu_3Si^+$ over Me_3Si^+. When replacing TTPB with the Brønsted acid activator $H(Et_2O)_2B(C_6F_5)_4$, coupled with either ^{Me}SKA or $^{i\text{Bu}}$SKA, the apparent rate constant was reduced by either 22% (run 12) or 38% (run 15), accordingly. Lastly, when substituting TTPB with $[Ph_3C]$[*rac*-TRISPHAT] containing the racemic, hexacoordinate bulky chiral phosphate anion, the rate of the polymerization was increased by 63% (run 13 vs run 11) when coupled with ^{Me}SKA, but decreased by 25% (run 16 vs run 14) when coupled with $^{i\text{Bu}}$SKA. These results suggest the importance of the cation–anion steric interplay (ion-pairing) on polymerization activity, where the bulky TRISPHAT anion enhances the activity of the small Me_3Si^+ cation while decreasing the activity of the large $^{i}Bu_3Si^+$ cation, as compared with the pairing $[B(C_6F_5)_4]^-$ counteranion. On the other hand, the racemic chiral phosphate anion did not noticeably impact the tacticity (45.7% *rr*, 43.0% *mr*, 11.3% *mm*) of the resulting polymer (run 16, Table 2). Regardless of the activators (thus counteranions) utilized, polymerizations employing ^{Me}SKA never achieved quantitative monomer conversion, even with extended reaction times (up to 24 h), while all runs with $^{i\text{Bu}}$SKA achieved quantitative monomer conversion within 10 min. Overall, these results show that the reactivity of MMBL lies between MMA and ^{n}BA, but the selectivity of MMBL for the silylium R_3Si^+ catalyst structure is much like that of ^{n}BA examined previously.[31]

Table 2. Results of Polymerization of MMBL with Varied Initiator and Activators. [a]

run no.	M	I	activator	time (min)	conv[b] (%)	M_W[c] (kg/mol)	MWD[c] (M_w/M_n)	k_{app}[d] (mol/L·min^{-1})
11	MMBL	^{Me}SKA	TTPB	10	64.2	50.3	1.22	0.114
12	MMBL	^{Me}SKA	$HB(C_6F_5)_4$	10	71.2	40.2	1.27	0.089
13	MMBL	^{Me}SKA	TRISPHAT	10	81.2	48.7	1.32	0.186
14	MMBL	$^{i\text{Bu}}$SKA	TTPB	10	100	31.0	1.02	0.295
15	MMBL	$^{i\text{Bu}}$SKA	$HB(C_6F_5)_4$	10	100	40.0	1.07	0.182
16	MMBL	$^{i\text{Bu}}$SKA	TRISPHAT	10	100	36.2	1.01	0.222

[a] Carried out in 5 mL CH_2Cl_2 at ambient temperature in a fixed [MMBL]:[SKA] ratio of 200:1. [b] Conversion, measured by ^{1}H NMR. [c] Determined by Light Scattering. [d] Determined from the slope of the best-fit line from the zero-order kinetic plots.

Copolymerization Characteristics. The copolymerization studies outlined in Scheme 2 were aimed at further testing the living nature of the MMBL polymerization by the $^{i\text{Bu}}$SKA + TTPB system and also exploring the synthesis of unimodal polymers comprised of MBL. While the synthesis of the well-defined PMBL was not achieved by the current system through the homopolymerization approach (due to the insolubility of PMBL in the polymerization medium, vide supra), we found that copolymerization of MMA (300 equiv, which was polymerized first) with equimolar MBL successfully afforded the CH_2Cl_2-soluble, well-defined block copolymer with a very narrow MWD of 1.01 (run 17, Table 3). The measured M_n of 67.7 kg/mol is compared with the calculated M_n of 48.2 kg/mol, thus giving a good *I** of 72 %. The block copolymerization of MMA with MMBL proceeded in a similar manner, also affording the well-defined diblock copolymer with a narrow MWD of 1.03 and a good *I**of 78% (run 18, Table 3). Not surprisingly, switching the order in which the monomers were added for both cases (i.e., polymerizing (M)MBL prior to MMA) resulted in the formation of only homopolymers P(M)MBL; this observation mirrors what has been observed in the block copolymerization of MMA (which must be polymerized first) and ^{n}BA (the more reactive monomer).[30]

Scheme 2. Copolymerization of (M)MBL with MMA and with each other

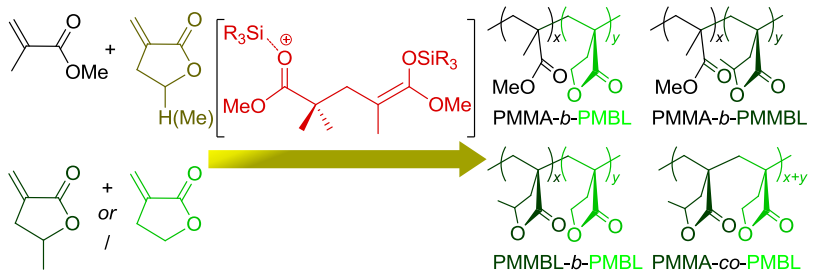

Table 3. Results of Copolymerizations of MBL, MMBL, and MMA by $^{i}Bu_3Si^+$ [a]

run no.	M1+M2 (block) M1/M2 (random)	[M1]:[M2]: [I]	time (h)	Yield (%)	M_W [b] (kg/mol)	MWD [b] (M_w/M_n)
17	MMA+MBL	300:300:1	1:3	80.8	68.4	1.01
18	MMA+MMBL	300:300:1	1:3	80.7	68.1	1.03
19	MMBL+MBL	300:300:1	0.17:1	93.6	117	1.02
20	MMBL/MBL	300:300:1	1.17	91.3	123	1.01

[a] Carried out in 5 mL CH_2Cl_2 at ambient temperature. [b] Determined by Light Scattering.

We also examined block and statistical copolymerizations of MBL and MMBL by $^{i\text{Bu}}$SKA + TTPB in CH_2Cl_2 at ambient temperature. By polymerizing MMBL first in the block copolymerization or polymerizing MMBL and MBL simultaneously in the statistical copolymerization, well-defined diblock copolymer PMMBL-*b*-PMBL (M_w = 117 kg/mol, MWD = 1.02, run 19, Table 3) and statistical copolymer PMMBL-*co*-PMBL (M_w = 123 kg/mol, MWD = 1.01, run 20, Table 3) were successfully synthesized. Overall, the copolymerization approach not only confirmed the living nature of the MMBL polymerization catalyzed by $^{i}Bu_3Si^+$, it also solved the insolubility and bimodality issue of PMBL thus successfully leading to the well-defined MBL-containing copolymers.

Thermal Properties of Polymers. We reported earlier that the atactic PMBL (M_n = 5.98 $\times 10^4$) and atactic PMMBL (M_n = 5.48 $\times 10^4$) produced by the decamethylsamarocene catalyst show narrow, one-step decomposition windows, with the initial (T_{ini}) and end (T_{end}) onset temperatures of PMMBL (T_{ini} = 356 °C, T_{end} = 441 °C) being 12 °C and 25 °C higher than those of PMBL (T_{ini} = 344 °C, T_{end} = 406 °C), both of which are higher than the onset decomposition

temperatures (T_{ini} = 340 °C, T_{end} = 399 °C) of the atactic PMMA with comparable MW.[16] Even more dramatically, the T_g's of the resulting atactic PMBL and PMMBL are 194 ºC and 227 ºC, respectively, which are ~90 °C and ~120 °C higher than the T_g (105 °C) of the typical atactic PMMA with comparable MW.[16] Consistent with these findings, the DSC analysis showed that the atactic PMBL (run 3, Table 1) and PMMBL (run 9, Table 1) produced by the current SKA + TTPB system also exhibit high T_g's of 194 and 225 °C, respectively (Figure 4). As anticipated, the block copolymer PMMBL-*b*-PMBL displays two T_g's of 212 °C and 197 °C, corresponding to the PMMBL and PMBL blocks, respectively, while the statistical copolymer PMMBL-*co*-PMBL shows only one T_g at 213 °C (Figure 4).

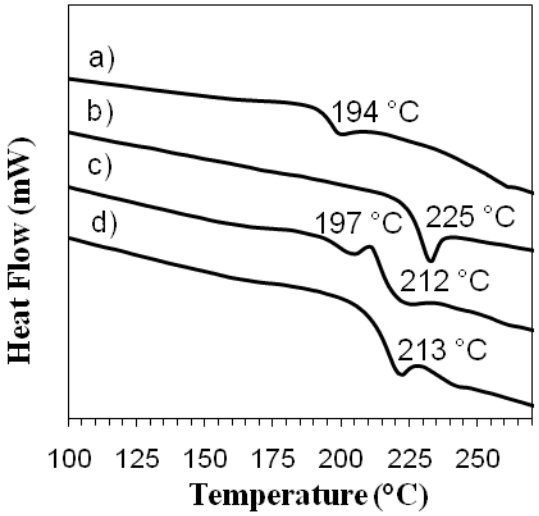

Figure 4. DSC of a) PMBL (run 3, Table 1); b) PMMBL (run 9, Table 1); c) PMMBL-*b*-PMBL (run 19, Table 3); and, d) PMMBL-*co*-PMBL (run 20, Table 3).

With a series of MMBL homopolymers having a wide range of MW's on hand, we also investigated the effect of M_n on the T_g of PMMBL (Figure 5). Specifically, PMMBLs with M_n = 2.64, 8.99, 17.8, 30.4, 92.3, and 543 kg/mol exhibited T_g = 210, 212, 214, 216, 220, and 225 °C, respectively. These results suggest that the critical MW of PMMBL (estimated off of leveling of T_g values) is rather high, over 40 (~47) kg/mol.

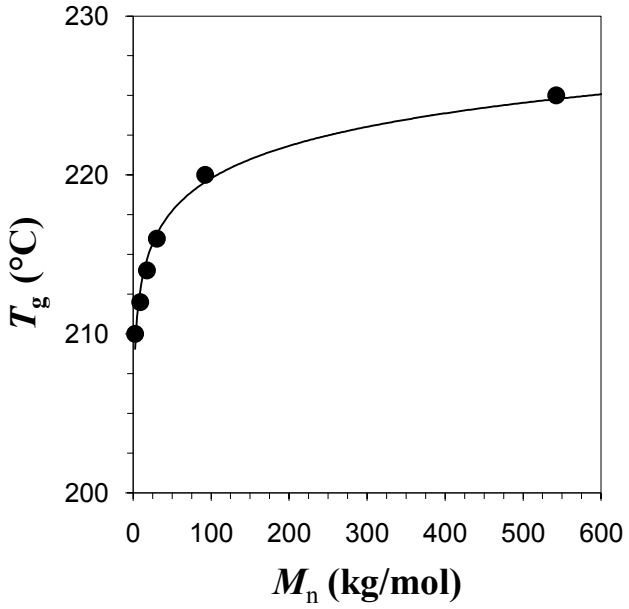

Figure 5. Plot of T_g vs M_n of atactic PMMBL.

Conclusions

Utilizing the recently developed unique polymerization system that employs the SKA + TTPB combination for in situ generation of the highly active *ambiphilic* propagating species containing both the nucleophilic SKA initiating moiety and the electrophilic silylium catalyst, this study has thoroughly investigated the characteristics of the polymerization of two naturally renewable butyrolactone-based vinylidene monomers, MBL and MMBL. Key findings of this study are summarized as follows.

First, while the polymerization of MBL in CH_2Cl_2 at ambient temperature is heterogeneous and achieves typically low yields of polymers that also exhibit bimodal MWD's, introduction of the γ-methyl group to the γ-butyrolactone ring (i.e., MMBL) enables a homogeneous reaction through completion in 10 min even with a low catalyst loading of 0.05 mol% (relative to monomer) and, more importantly, a rapid (up to 12,000 h^{-1} TOF) and living polymerization, thereby producing polymers with controlled low to high (M_n = 5.43 × 10^5 kg/mol) MW and narrow MWD's (1.01–1.06). Besides the high degree of control, the activity of the MMBL

polymerization by the current system is outstanding, typically achieving a complete monomer conversion within minutes of reaction at ambient temperature, as compared to the MMBL polymerization by conventional mechanisms, including radical, anionic, and group-transfer polymerization methods, which required many hours, often at low temperatures, achieving low to high, but never complete conversions.

Second, through investigations into effects of SKA (thus the resulting R_3Si^+ catalyst) and activator (thus the resulting counteranion) structures, we have found that the $Me_2C{=}C(OMe)OSi^iBu_3/Ph_3CB(C_6F_5)_4$ combination is the most active *and* controlled system for (M)MBL polymerizations. The resulting large $^iBu_3Si^+$ cation (relative to the smaller Me_3Si^+ cation), when paired with the weakly coordinating anion $[B(C_6F_5)_4]^-$, exhibits exceptional activity and control toward polymerization of sterically less demanding monomers such as (M)MBL (and acrylates). These results further highlight the importance of the cation–anion pairing in catalysis and of the good match between the catalyst and monomer structures in polymerization.

Third, the living nature of the current polymerization system catalyzed by $^iBu_3Si^+$ has been further confirmed by the synthesis of well-defined block copolymers of MBL and MMBL with MMA as well as block and statistical copolymers of MBL with MMBL. All copolymers produced herein exhibit unimodal and narrow MWD's of $\leq$1.03. As anticipated, the block copolymer PMMBL-*b*-PMBL displays two T_g's corresponding to the PMBL and PMMBL blocks, while the statistical copolymer PMMBL-*co*-PMBL shows only one T_g.

Fourth, the current system produces essentially atactic polymers exhibiting high T_g's of 194°C (PMBL) and 225 °C (PMMBL). These values represent T_g enhancements of ~90 °C (for PMBL) and ~120 °C (for PMMBL) over the T_g (105 °C) of the typical atactic PMMA. Also interestingly, the presence of the cyclic butyrolactone moiety in PMMBL considerably increases its estimated critical MW (~47 kg/mol) over that of PMMA (~28 kg/mol).

Acknowledgment. This work was supported by the National Science Foundation (NSF-0848845). We thank Boulder Scientific Co. for the research gift of $[Ph_3C][B(C_6F_5)_4]$. This

dissertation chapter contains the manuscript of the full paper published in *Macromolecules* [Miyake, G. M.; Zhang, Y.; Chen, E. Y.-X. *Macromolecules* **2010**, *43*, 4902-4908]. Y.Z. investigated the effects of the activator on the polymerization and polymer characteristics.

References

(1) Coates, G. W.; Hillmyer, M. A. A virtual issue on "Polymers from Renewable Resources", *Macromolecules* **2009**, *42*, 7987–7989.

(2) Gandini, A. Polymers from Renewable Resources: a Challenge for the Future of Macromolecular Materials. *Macromolecules* **2008**, *41*, 9491–9504.

(3) Tullo, A. H. Growing Plastics. *C&E News*, **2008**, *86* (39), 21–25.

(4) Williams, C. K.; Hillmyer, M. A. Polymers from Renewable Resources: A Perspective for a Special Issue of Polymer Reviews. *Polym. Rev.* **2008**, *48*, 1−10.

(5) Meier, M. A. R.; Metzger, J. O.; Schubert, S. Plant Oil Renewable Resources as Green alternatives in Polymer Science. *Chem. Soc. Rev.* **2007**, *36*, 1788−1802.

(6) Mullin, R. Sustainable Specialties. *C&E News*, **2004**, *82* (45), 29–37.

(7) Hoffman, H. M. R.; Rabe, J. *Angew. Chem. Int. Ed. Engl.* **1985**, *24*, 94–110.

(8) Manzer, L. E. *ACS Symp. Ser.* **2006**, *921*, 40–51.

(9) Manzer, L. E. *Appl. Catal. A: Gen.* **2004**, *272*, 249–256.

(10) Akkapeddi, M. K. *Polymer* **1979**, *20*, 1215–1216.

(11) Stansbury, J. W.; Antonucci, J. M. *Dent. Mater.* **1992**, *8*, 270–273.

(12) Akkapeddi, M. K. *Macromolecules* **1979**, *12*, 546–551.

(13) Kimura, Y.; Nakamura, S. JP 046560 A, **2009**.

(14) Pickett, J. E.; Ye, Q. U.S. Patent 2007/0122625, **2007**.

(15) Bandenburg, C. J. WO 069926, **2004**.

(16) Miyake, G. M.; Newton, S. E.; Mariott, W. R.; Chen, E. Y.-X. *Dalton Trans.* **2010**, DOI:10.1039/c001909g).

(17) Mosnáček, J.; Yoon, J. A.; Juhari, A.; Koynov, K.; Matyjaszewski, K. *Polymer* **2009**, *50*, 2087–2094.

(18) Mosnáček, J.; Matyjaszewski, K. *Macromolecules* **2008**, *41*, 5509–5511.

(19) Ueda, M.; Takahashi, M.; Imai, Y.; Pittman, C. U. Jr. *J. Polym. Sci.: Polym. Chem. Ed.* **1982**, *20*, 2819–2828.

(20) Gridnev, A. A.; Ittel, S. D. WO 035960 A2, **2000**.

(21) Sogah, D. Y.; Hertler, W. R.; Webster, O. W.; Cohen, G. M. *Macromolecules* **1987**, *20*, 1473–1488.

(22) van den Brink M.; Smulders, W.; van Herk, A. M.; German, A. L. *J. Polym. Sci.: Polym. Chem. Ed.* **1999**, *37*, 3804–3816.

(23) Koinuma, H.; Sato, K.; Hirai, H. *Makromol. Chem., Rapid Commun.* **1982**, *3*, 311–315.

(24) Lee, C.; Hall, H. K. Jr. *Macromolecules* **1989**, *22*, 21–25.

(25) Trumbo, D. L. *Polym. Bull.* **1991**, *26*, 271–275.

(26) Qi, G.; Nolan, M.; Schork, F. J.; Jones, C. W. *J. Polym. Sci.: Polym. Chem.* **2008**, *46*, 5929–5944.

(27) Bandenburg, C. J. U.S. Patent 6,841,627 B2, **2005**.

(28) Suenaga, J.; Sutherlin, D. M.; Stille, J. K. *Macromolecules* **1984**, *17*, 2913–2916.

(29) Chen, E. Y.-X. *Chem. Rev.* **2009**, *109*, 5157–5214.

(30) Zhang, Y.; Chen, E. Y.-X. *Macromolecules* **2008**, *41*, 36−42.

(31) Zhang, Y.; Chen, E. Y.-X. *Macromolecules* **2008**, *41*, 6353−6360.

(32) Kakuchi, R.; Chiba, K.; Fuchise, K.; Sakai, R.; Satoh, T.; Kakuchi, T. *Macromolecules* **2009**, *42*, 8747−8750.

(33) Ute, K.; Ohnuma, H.; Kitayama, T. *Polym. J.* **2000**, *32*, 1060–1062.

(34) Zhuang, R.; Müller, A. H. E. *Macromolecules* **1995**, *28*, 8035–8042; 8043–8050.

(35) Ute, K.; Ohnuma, H.; Shimizu, I.; Kitayama, T. *Polym. J.* **2006**, *38*, 999–1003.

(36) Allen, R. D.; Long, T. E.; McGrath, J. E. *Polym. Bull.* **1986**, *15*, 127−134.

(37) (a) Bochmann, M.; Lancaster, S. J. *J. Organomet. Chem.* **1992**, *434*, C1–C5. (b) Chien, J. C. W.; Tsai, W.-M.; Rausch, M. D. *J. Am. Chem. Soc.* **1991**, *113*, 8570–8571.

(38) Jutzi, P.; Müller, C.; Stammler, A.; Stammler, H. *Organometallics* **2000**, *19*, 1442–1444.

(39) (a) Favarger, F.; Ginglinger, C. G.; Monchaud, D.; Lacour, J. *J. Org. Chem.* **2004**, *69*, 8521–8524. (b) Lee, H. S.; Novak, B. *Polym. Prepr.* **2005**, *46*, 839–840.

Chapter 8

Summary

This work investigated polymerization catalysis for the synthesis of technologically important chiral and sustainable polymers. Chiral polymers are not only fundamentally interesting, due to the rich and complex architecture of macromolecular chirality as compared to that of small molecules, but also technologically important because their unique chiral arrays give rise to a number of potential, and in some cases commercially implemented, applications. As petroleum resources continue to be depleted, polymer chemists face the challenge of gradually replacing existing petroleum-based polymeric materials with those derived from naturally occurring, renewable resources in a technologically and economically competitive fashion.

Chiral zirconocenium catalysts, (*S,S*)-(EBI)Zr^{+}(THF)[OC(O^{i}Pr)=CMe_2][$MeB(C_6F_5)_3$]$^{-}$ [(*S,S*)-**1**, EBI = $C_2H_4(\eta^5\text{-Ind})_2$] and its enantiomer (*R,R*)-**1**, have been synthesized and employed in the asymmetric coordination polymerization of prochiral *N,N*-diaryl acrylamides to optically active, stereoregular polymers with solution-stable, single-handed helical secondary structures (Chart 1). The optical activity of the resulting poly(*N,N*-diaryl acrylamide)s is dictated by the chirality of the catalyst, such that *rac*-**1** produces optically inactive polymers, while (*S,S*)- and (*R,R*)-**1** produce polymers that have opposite optical rotations and nearly mirror image CD spectra.

Chart 1. Synthesis of Right- and Left-Handed Rigid Helical Poly(*N,N*-Diaryl Acrylamide)s.

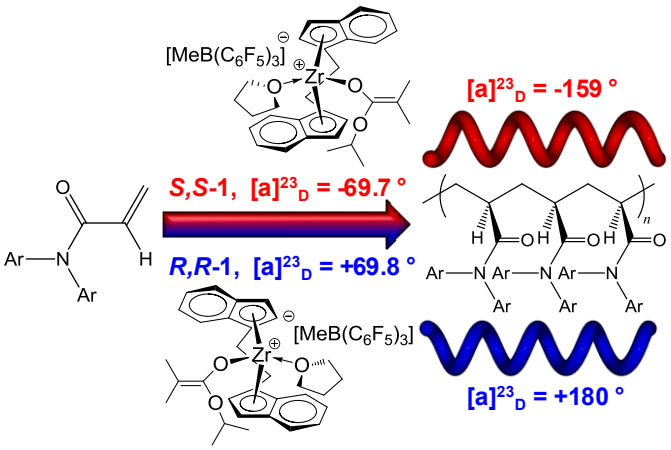

Kinetic studies show that the polymerization of *N,N*-diaryl acrylamides by **1** proceeds via a monometallic, coordination-conjugate addition mechanism. Investigation into polymer chain-length effects on optical activity of the chiral polymers reveals two opposite trends, depending on the polymer secondary structure (i.e., helical vs. random coil conformation). For helical polymers, as the chain-length increases, the optical activity increases as the helix becomes better defined. In contrast, for random-coil polymers, the optical activity quickly diminishes with an increase in chain-length. We have also examined the necessity of the diaryl side-groups to render a solution stable helix, and synthesized the first solution stable helical poly(*N,N*-dialkyl arylamide), poly(acryloyl piperidine).

These enantiomeric zirconocenium catalysts were utilized in the first successful metallocene-mediated coordination-addition polymerization of *N,N*-dialkyl methacrylamides, such as methacryloyl-2-methyl aziridine (MMAz). The polymerization of MMAz by **1**, is stereospecific, and provides a high degree of control of the polymerization, resulting in highly isotactic polymers with predicted molecular weights (MW's) and narrow molecular weight distributions (MWD's). The enantiomeric catalyst, (*S,S*)-**1**, demonstrated the ability to perform the kinetic resolution polymerization of MMAz, although the stereoselectivity was low, s = 1.8 (Scheme 1).

Scheme 1. Proposed kinetic resolution polymerization of MMAz by (*S,S*)-**1**.

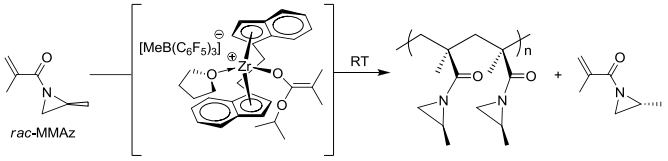

Interested in synthesizing chiral *N,O*-functionalized polar vinyl polymers as potential polymeric ligands/stabilizers for transition metal nanocluster catalysts, en route to asymmetric catalysis, we have explored the polymerization of acryloyl and vinyl substituted, chiral oxazolidinones. The polymerization of the acryloyl functionalized monomer, *N*-acryloyl-(*R* or *S*)-4-phenyl-2-oxazolidinone, by the enantiomeric zirconocenium catalysts is stereospecific, however, the chiral side-group is not sterically bulky enough and too far removed from the polymer main-chain to result in a solution stable helical conformation, and optical activity of the resulting isotactic polymers is solely due to the chirality of the side-group. The vinyl functionalized monomer, *N*-vinyl-(*R*)-4-phenyl-2-oxazolidinone [(*R*)-VOZ], was not polymerizable by similar metallocene catalysts, but we discovered a novel, chiral auxiliary controlled cationic polymerization, initiated by Lewis and BrØnsted acids, producing highly isotactic polymers (Scheme 2). In the case of (*R*)-PVOZ, the chiral side-group is brought closer to the polymer backbone, and it exhibits substantial chiral amplifications by virtue of adopting a solution-stable, one-handed helical conformation.

Scheme 2. Proposed chiral auxiliary-controlled isospecific cationic polymerization of (*R*)-VOZ.

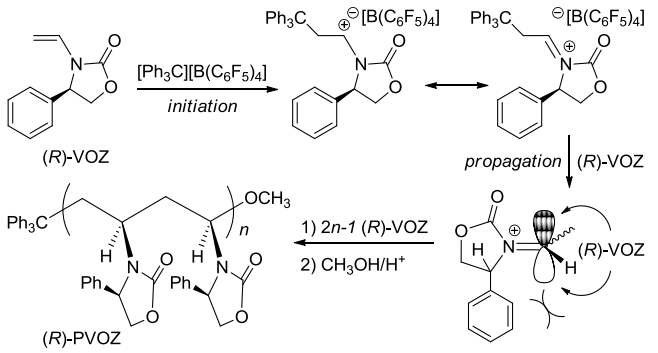

Towards utilizing helical polymers, two pseudo-enantiomeric poly(phenyl acetylene)s bearing cinchona alkaloid organocatalyst side-groups have been synthesized. These polymers not only assume excess one-handed helicity, but the handedness of these polymers can be controlled by interactions with different solvents. Thus, by changing the solvent, the same chiral organocatalyst can be supported on either a right- or left-handed helical polymer (Chart 2). The effects of helicity and helix-sense on the enantioselectivity of these supported organocatalysts was examined in the conjugate addition of 2-napthalenethiol to 2-cyclohexen-1-one. It was shown that one helix-sense increased the enantioselectivity of the organocatalyst (as compared to its monomeric form), while the other helix-sense was non-influential on the enantioselectivity of the organocatalyst.

Chart 2. Helix-Sense Control of Poly(Cinchona Phenyl Acetylene) and its Effect on Enantioselectivity.

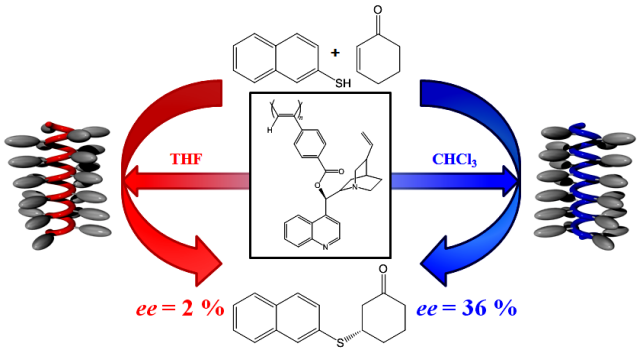

Renewable butyrolactone-based vinylidene monomers, such as MBL (α-methylene-γ-butyrolactone) and MMBL (γ-methyl-α-methylene-γ-butyrolactone), are of particular interest in exploring the prospects of substituting the petroleum-based methacrylate monomers for specialty chemicals production. The polymerization of such monomers by group 3 and 4 transition metal catalysts has been investigated. Unlike the poor results obtained with group 4 catalysts, the polymerization of MBL by group 3 catalysts, especially $Cp^*_2Sm(THF)_2$, is rapid, efficient, and controlled under ambient conditions, exhibiting a high TOF of 3000 h^{-1}, typically near

quantitative initiator efficiency, and the ability to control the polymer MW, while achieving quantitative monomer conversion. The polymerization of MMBL is as effective as that of MBL, and the resulting atactic PMBL and PMMBL have high T_g's of 194 ºC and 227 ºC, respectively; when compared to atactic PMMA having comparable MW, the T_g and onset decomposition temperatures of the PMMBL produced are substantially higher (by ~120 °C and 40 °C, respectively). Results of the kinetic and polymerization studies indicate that the true active species is the trivalent samarocene centers attached to the single growing polymer chain, derived presumably from a redox-then-radical-coupling process. Catalytic polymerization of MBL by $Cp^*_2Sm(THF)_2$ has also been realized in the presence of an enolizable organo acid as a suitable chain transfer agent (Scheme 3). When 3-methyl-2-butanone (MBO) is used as the chain transfer reagent, the initiator effiency reached 1060%, giving a turn over number of ~10.

Scheme 3. Chain transfer polymerization of MBL catalyzed by $Cp^*_2Sm(THF)_2$.

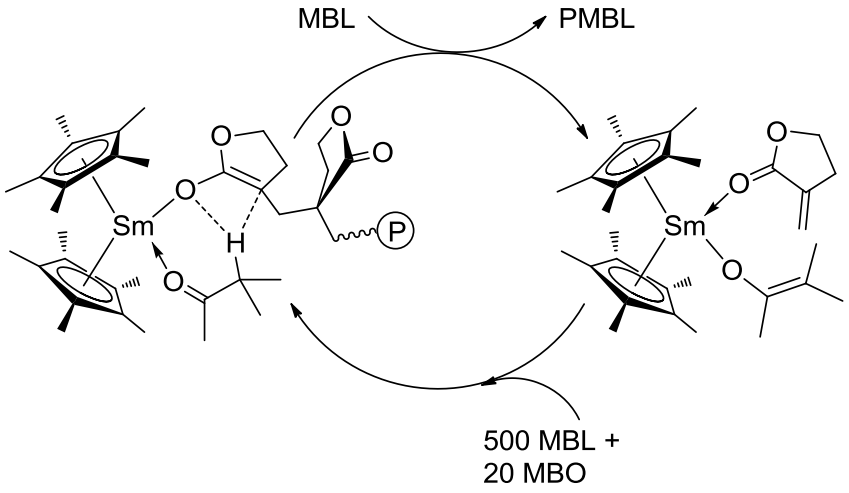

MBL and MMBL have also been polymerized in a rapid and living fashion, using an ambiphilic silicon propagating species consisting of both the nucleophilic silyl ketene acetal (SKA) initiating moiety and the electrophilic silylium catalyst. Due to the insolubility of the resulting PMBL in non-coordinating solvents, the polymers exhibit bimodal MWD's and incomplete monomer conversion at high monomer to catalyst feed ratios. The polymerization of MMBL remains homogenous throughout the course of polymerization, and under ambient conditions and with a low catalyst loading (0.05 mol% relative to monomer), this polymerization system rapidly (within 10 minutes) and completely converts MMBL to PMMBL with controlled low to high (M_n = 5.43 × 10^5 g/mol) MW's and narrow MWD's (1.01–1.06). Demonstrating the living nature of this polymerization system, and to overcome the insolubility of PMBL, well-defined block copolymers of MBL with MMA as well as block and statistical copolymers of MBL with MMBL have been synthesized (Chart 3).

Chart 3. Copolymerization of MBL and MMBL with MMA and With Each Other

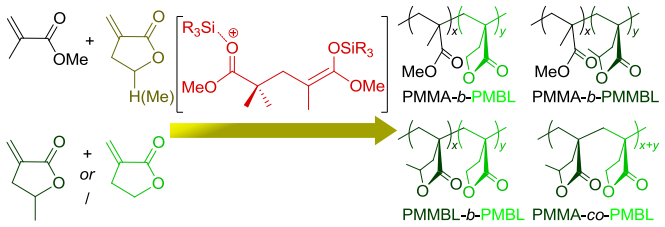

.

Appendix I

List of Publications by GMM

1) Zhang, Y.; Miyake, G. M.; Chen, E. Y.-X. "Alane-Based Classical and Frustrated Lewis Pairs in Polymer Synthesis: Rapid Polymerization of MMA and Naturally Renewable Methylene Butyrolactones into High-Molecular-Weight Polymers," *Angew. Chem. Int. Ed*., **2010**, *49*, 10158-10162.

2) Miyake, G. M.; DiRocco, D.; Liu, Q.; Oberg, K. M.; Bayram, E.; Finke, R. G.; Rovis, T.; Chen, E. Y.-X. "Stereospecific Polymerization of Chiral Oxazolidinone-Functionalized Alkenes," *Macromolecules* **2010**, *43*, 7504-7514.

3) Miyake, G. M.; Newton, S. E.; Mariott, W. R.; Chen, E. Y.-X. "Coordination Polymerization of Renewable Butyrolactone-Based Vinyl Monomers by Lanthanide and Early Metal Catalysts," *Dalton Trans.* **2010**, *39*, 6710-6718.

4) Miyake, G. M.; Zhang, Y.; Chen, E. Y.-X. "Living Polymerization of Naturally Renewable Butyrolactone-Based Vinylidene Monomers by Ambiphilic Silicon Propagators," *Macromolecules* **2010**, *43*, 4902-4908.

5) Del Villano, L.; Kelland, M. A.; Miyake, G. M.; Chen, E. Y.-X. "Effect of Polymer Tacticity on the Performance of Poly(*N,N*-dialkylacrylamide)s as Kinetic Hydrate Inhibitors," *Energy Fuels* **2010**, *24*, 2554-2562.

6) Miyake, G. M.; Caporaso, L.; Cavallo, L.; Chen, E. Y.-X. "Coordination-Addition Polymerization and Kinetic Resolution of Methacrylamides by Chiral Metallocene Catalysts," *Macromolecules* **2009**, *42*, 1462-1471.

7) Miyake, G. M.; Chen, E. Y.-X. "Metallocene-Mediated Asymmetric Coordination Polymerization of Polar Vinyl Monomers to Optically Active, Stereoregular Polymers," *Macromolecules* **2008**, *41*, 3405-3416.

8) Miyake, G. M.; Mariott, W. R.; Chen, E. Y.-X. "Asymmetric Coordination Polymerization of Acrylamides by Enantiomeric Metallocenium Ester Enolate Catalysts," *J. Am. Chem. Soc.* **2007**, *129*, 6724-6725.